

**Hydrodesulfurization and Hydrodenitrogenation of Model
Compounds Using *in-situ* Hydrogen over Nano-Dispersed
Mo Sulfide Based Catalysts**

By

Kun Liu

**A thesis
presented to the University of Waterloo
in fulfillment of the thesis
requirement for the degree of
Doctor of Philosophy
in
Chemical Engineering**

Waterloo, Ontario, Canada, 2010

© Kun Liu 2010

I hereby declare that I am the sole author of this thesis. This is a true copy of the thesis, including any required final revisions, as accepted by my examiners.

I understand that my thesis may be made electronically available to the public.

ABSTRACT

Heavy oil derived from oil sands is becoming an important resource of energy and transportation fuels due to the depletion of conventional oil resources. However, bitumen and heavy oils have a low hydrogen/carbon ratio and contain a large percentage of sulfur and nitrogen heterocyclic compounds. At the level of deep desulfurization, aromatic poly-nuclear molecules, especially nitrogen-containing heterocyclic compounds, exhibit strong inhibitive effect on hydrodesulfurization (HDS) due to competitive adsorption on catalytically active sites with sulfur-containing molecules. Therefore, it is necessary to study the HDS of refractory sulfur-containing compounds and also the effect of nitrogen-containing species on the deep HDS for achieving the ultra low sulfur specifications for transportation fuels. Additionally, the cost of H₂ increased in recent years and a bitumen emulsion upgrading technique using an alternative *in-situ* H₂ generated *via* the water gas shift (WGS) reaction during the hydro-treating was developed in our group. In the present study, a kind of nano-dispersed unsupported MoS_x based catalyst was developed and used for hydrodesulfurization, hydrodenitrogenation (HDN) and upgrading bitumen emulsions.

Objectives of this thesis were to (1) improve the catalytic activity of the nano-dispersed Mo based catalysts towards the HDS and HDN reactions of refractory sulfur-/nitrogen-containing compounds; and (2) compare the reactivity of *in-situ* hydrogen generated *via* the WGS reaction *versus* externally provided molecular hydrogen in HDS and HDN reactions to improve the efficiency of the bitumen emulsion upgrading technology developed by our group.

In the present study, to stimulate the reaction system of bitumen emulsion, water was added into the organic reaction system, so there are different phases in this reaction system. To investigate the activity of the catalyst, the catalyst particles dispersed in different phases were characterized separately *via* HRTEM-EDX. After HRTEM-EDX study, all phases were mixed up and dried for further characterizations, BET, SEM, and XRD. The catalyst prepared in *in-situ* hydrogen was found to have higher surface area and smaller particle size than the one made in molecular hydrogen. The presence of sulfur-/nitrogen-containing compounds in the preparation system caused significant changes in the morphology of dispersed Mo sulfide catalyst according to HRTEM observations.

Refractory sulfur-containing compounds of dibenzothiophene (DBT) and 4,6-dimethyldibenzothiophene (4,6-DMDBT) were used as model compounds in HDS studies. The simultaneous HDS of both model compounds was performed at different reaction temperatures from 330°C to 400°C. The effect of the reaction temperature on the WGS reaction in the presence of sulfur-containing model compounds was reported. A kinetic model for HDS reactions was proposed and used in discussing experiment results. The relative HDS reactivity of 4,6-DMDBT to DBT using dispersed Mo sulfide catalyst in *in-situ* hydrogen was found to be higher than the reported results which were obtained over supported catalysts. Nickel and potassium were introduced into Mo sulfide catalysts as promoters and their effect on the WGS reaction and the HDS reaction were discussed.

The simultaneous HDS was carried out in the two different hydrogen sources. The *in-situ* hydrogen reaction system showed higher conversion and desulfurization results of both

sulfur model compounds. This observation has been found to be mainly contributed by the higher activity of the Mo sulfide catalyst prepared in *in-situ* H₂.

Strong inhibitive effect of nitrogen-containing compounds, basic quinoline or non-basic carbazole, on the HDS of refractory sulfur model compounds was observed and discussed. Basic quinoline was a much stronger inhibitor than non-basic carbazole. The two HDS reaction pathways were affected by nitrogen-containing compounds to different extents.

The HDN of quinoline over the dispersed Mo sulfide catalyst using *in-situ* hydrogen had been studied extensively by a previous member in our group. In this thesis, the HDN of carbazole was studied. From the identification of HDN products of carbazole, a HDN reaction network was proposed. The HDN of carbazole was processed at different reaction temperatures. The WGS reaction was not inhibited in the presence of carbazole. Comparable reactivity of the two hydrogen sources towards the HDN of carbazole was observed. The presence of 4,6-DMDBT caused significant effect on the HDN of carbazole due to the competitive adsorption on the catalyst surface.

ACKNOWLEDGEMENTS

To achieve the Ph.D degree is my first important objective as I came to Canada. I was lucky to get the chance to accomplish my wish in the University of Waterloo. The Ph.D program is challenging both academically and personally. I would like to appreciate the encouragement, support, instruction, tutorial, and cooperation provided by the Department of Chemical Engineering and the University of Waterloo during the past five years. Without these help, my study pursuing this degree would be much more difficult.

First of all, I would express my sincere gratitude to my supervisor, Professor Flora T.T. Ng for her academic instruction, research guidance, continuous encouragement, and financial support. Her professional experience, active research attitude, and her keen judgement on the study direction are the guiding light in my study.

Secondly, I would extend my gratitude to the members in the Comprehensive Examination and the Oral Defence, Professor Jenő Sharer, Professor Ali Elkamel, Professor Mario Gauthier, and Professor Ajay Dalai for their constructive comments and contributions to this thesis. I would also show my gratitude to the lecturers of the three courses I took during my Ph.D program. They are Professor Garry Rempel, Professor Pu Chen, and Professor Thomas A. Duever. The study on these courses was very helpful with completing this thesis.

Next, financial support from the *Natural Sciences and Engineering Research Council* (NSERC) of Canada, Strategic Project Program is gratefully appreciated.

A great gratitude would be sent to Jennifer Moll, Roy Lee, and Annie Zhang, who gave me the training to start my research work. I would also appreciate all my colleagues and friends, Prem Pal, Christ Choy, Donghua Zuo, Abdulaziz Eidan Al-Ghamdi, Lei Jia, Kamalakar Gunda, Yinmei Ye, and Zhiwen Qi for their help and support throughout this work. I would acknowledge the kind assistance of Ralph Dickhout, Birt Habicher, Ravindra Singh and Rick Hecktus during my research. I am indebted to Professor Tong Leung and Nina Heinig for the SEM service and training provided by them. The service on HRTEM-EDX characterization provided by Fred Pearson in the Canadian Centre for Electron Microscopy (CCEM) was appreciated.

As a daughter, I would like to bow my deep gratitude and my love to my parents, Fengming Liu and Wenru Li. I appreciate them raising me up, providing me a comfortable growing up environment, supporting on my education, and giving me their great selfless love. I would like to send my appreciation to my sister, Hui Liu, who supported and took care of my mother all the time during my study.

Finally, I want to express my deep gratitude to my husband, Qing Chen, for his constant encouragement, understanding, and support throughout my study and my life. I also appreciate the birth of my daughter, who gave me a lot of happiness during my study.

To my parents, my husband, and my daughter, with LOVE.

Table of Contents

Table of Contents	xi
List of Figures	xvii
List of Tables	xxv
List of Abbreviations	xxx
Chapter 1 Introduction	1
Chapter 2 Literature Review	9
2.1 Dispersed Mo sulfide catalysts.....	9
2.2 HDS of refractory sulfur-containing compounds.....	11
2.3 Use in-situ hydrogen instead of molecular hydrogen.....	17
2.4 Inhibitive effect of N-containing species on HDS	18
2.5 HDN of carbazole.....	20
Chapter 3 Experimental and Characterization	23
3.1 Reactors	23
3.2 Reactants	26
3.3 Reaction procedure.....	27
3.3.1 Preparing feed stocks and sealing reactor vessel	27
3.3.2 Checking leakage and feeding reactant gases	28
3.3.3 Reacting, taking gas/liquid samples and stopping the reaction	31
3.4 Product analysis.....	33
3.4.1 Gas analysis	33
3.4.2 Liquid analysis	34
3.5 Characterization Techniques	35
Chapter 4.....	39
4.1 Introduction.....	39
4.2 <i>Ex-situ</i> preparation of catalysts.....	43
4.3 Characterization results.....	48
4.3.1 BET	48
4.3.2 XRD	49
4.3.3 HRTEM-EDX	50

4.3.3.1 HRTEM images of candidate catalyst samples prepared in <i>in-situ</i> H ₂ and molecular H ₂	51
4.3.3.2 HRTEM images of spent Mo sulfide catalysts in the presence of S-/N-species	62
4.3.4 SEM morphology of MoS ₂ particles	66
4.4 Discussion	68
4.4.1 Effect of H ₂ sources on the preparation of dispersed Mo sulfide catalyst	68
4.4.2 Effect of S-/N-containing compounds on the morphology of the dispersed Mo sulfide catalyst.....	70
4.4.3 Element distribution in different phases.....	72
4.5 Conclusions.....	74
Chapter 5 Simultaneous Hydrodesulfurization of Dibenzothiophene and 4,6-Dimethyldibenzothiophene	77
5.1 Introduction.....	77
5.2 Experimental.....	81
5.3 Identification of HDS products of 4,6-DMDBT.....	83
5.4 Results and discussion	86
5.4.1 Water gas shift reaction.....	87
5.4.2 HDS kinetics modeling	89
5.4.3 Simultaneous HDS of DBT and 4,6-DMDBT	94
5.4.4 Effect of Ni on the simultaneous HDS of DBT and 4,6-DMDBT using <i>in-situ</i> H ₂ . 100	
5.4.5 Effect of K on the simultaneous HDS of DBT and 4,6-DMDBT using <i>in-situ</i> H ₂ .. 107	
5.5 Conclusions.....	114
Chapter 6 Comparison between <i>in-situ</i> H ₂ and molecular H ₂ for Hydrodesulfurization.....	117
6.1 Introduction.....	117
6.2 Experimental.....	118
6.2.1 Simultaneous HDS of DBT and 4,6-DMDBT using two different hydrogen sources	118
6.2.2 HDS activity of <i>ex-situ</i> prepared dispersed Mo sulfide catalysts.....	119
6.2.3 Reactivity of the two hydrogen sources	121
6.3 Results and discussion	121
6.3.1 Characterization	121
6.3.2 <i>In-situ</i> hydrogen versus molecular hydrogen for HDS	124

6.3.2.1 Precursor of PMA	124
6.3.2.2 Precursor of ATTM	127
6.3.2.3 Discussion	129
6.3.3 HDS results using <i>ex-situ</i> prepared catalysts	134
6.3.4 Reactivity of <i>in-situ</i> H ₂ versus molecular H ₂	139
6.4 Conclusions	143
Chapter 7 Inhibitive Effect of N-Containing Compounds on Hydrodesulfurization Reactions	145
7.1 Introduction	145
7.2 Experimental	147
7.3 Results and discussion	148
7.3.1 HDS in the presence of N-containing compounds using <i>in-situ</i> H ₂	148
7.3.2 HDS in the presence of N-containing compounds using molecular H ₂	156
7.4 Conclusions	159
Chapter 8 Hydrodenitrogenation of Refractory Heterocyclic N-Containing Compound of Carbazole	161
8.1 Introduction	161
8.2 Experimental	167
8.3 Identification of HDN products of carbazole	168
8.4 Kinetics of the HDN of Carbazole	180
8.5 WGS reaction in the presence of carbazole	186
8.6 <i>In-situ</i> H ₂ versus molecular H ₂ in the HDN of carbazole over the dispersed Mo sulfide catalyst	187
8.7 HDN of carbazole versus HDN of quinoline	191
8.8 Effect of 4,6-DMDBT on the HDN of Carbazole	198
8.9 Conclusions	205
Chapter 9 Conclusions and Recommendations	207
9.1 Conclusions	207
9.1.1 <i>In-situ</i> H ₂ versus molecular H ₂ in the preparation of dispersed catalyst	207
9.1.2 Simultaneous HDS of DBT and 4,6-DMDBT using <i>in-situ</i> hydrogen	207
9.1.3 <i>In-situ</i> H ₂ versus molecular H ₂ in HDS	208
9.1.4 Effect of promoters on the simultaneous HDS of DBT and 4,6-DMDBT	208

9.1.5 Effect of nitrogen-containing compounds on HDS.....	209
9.1.6 HDN of carbazole.....	209
9.2 Recommendations.....	209
9.2.1 Optimizing the preparation conditions of dispersed catalyst	209
9.2.2 Extend the use of <i>ex-situ</i> prepared catalysts for hydro-treating gas oil and upgrading bitumen emulsions.....	210
9.2.3 Investigate the HDN activity of Ni promoted Mo sulfide catalysts	210
References.....	211
APPENDIX A --- Mass Balance Sample Calculations.....	223
A1. Concentrations of reactants (listed in Table 3-2)	223
A2. Mass balance of the gas phase (involved in a CO experiment).....	226
A3. Mass balance of <i>in situ</i> H ₂	228
A4. Mass balance of the aqueous phase	230
A5. Mass balance of the organic phase	231
APPENDIX B --- GC Analytic Methods.....	233
B-1 Liquid Sample Analysis – GC method	233
B-1.1 Control method:.....	233
B-1.2 Integration event.....	235
B-1.3 Calibration Method	235
B-2 GC Calculation Processes	237
B-3 RGA Analytic Method.....	239
B-3.1 Configuration of the RGA.....	239
B-4 Calculation of gas component concentrations based on GC analytic results.....	243
B-5 Compare of calculation methods for conversions.....	243
APPENDIX C --- HREM Statistic Results and EDX Spectra.....	249
C-1. EDX spectra for MoCO ₃ 40, MoH ₃ 40, and SMO ₃ 40.....	249
C-2. HRTEM statistic results.....	255
APPENDIX D --- Example Calculation of Average MoS ₂ Slab Length.....	267
APPENDIX E --- Experimental raw data for Chapter 5	271
E.1 Experimental data of HDS over Mo sulfide at different reaction temperatures and regression figures / ANOVA tables	271

E.2 Experiment data for HDS over promoted (Ni or K) Mo sulfide catalysts	287
E.3 EDX spectra for NiMo catalyst after consumed in HDS.....	289
APPENDIX F --- Experimental raw data for the Chapter 6	291
APPENDIX G --- Raw Data for Chapter 7.....	295
APPENDIX H --- Raw Data for Chapter 8.....	297

List of Figures

Fig. 1 - 1 The new one-step bitumen emulsion upgrading technology developed by Ng <i>et al</i> 2-3	2
Fig. 2 - 1 HDS reaction net work of DBT using <i>in-situ</i> H ₂ over dispersed Mo sulfide catalysts. DBT: dibenzothiophene, BP: biphenyl, TH-DBT: tetrahydrodibenzothiophene, CHB: cyclohexylbenzene, DCH: dicyclhexyl.....	14
Fig. 2 - 2 HDS reaction net work of 4,6-DMDBT using <i>in-situ</i> H ₂ over dispersed Mo sulfide catalysts. 4,6-DMDBT: 4,6-dimethyldibenzothiophene, 3,3'-DMBP: 3,3'-dimethylbiphenyl, DM-TH-DBT: dimethyl-tetrahydro-dibenzothiophene, DMCHB: dimethyl- cyclohexylbenzene.....	15
Fig. 2 - 3 GC chromatograph of HDS products of DBT and 4,6-DMDBT detected by FID and PFPD detectors.....	16
Fig. 3 - 1 Flow chart of the SS 300cc batch Autoclave reactor	24
Fig. 3 - 2 Flow chart of the HC batch Autoclave reactor.....	25
Fig. 3 - 3 Reaction temperature – pressure relationship in a typical HDS experiment from room temperature to 380°C, (590 psi of CO, 10 psi H ₂ S, 430 ppmw Mo, 100 ml toluene, 10 ml H ₂ O, DBT+4,6-DMDBT, SS reactor)	31
Fig. 3 - 4 Flowchart of product analysis after the hydro-treating process	35
Fig. 4 - 1 The “Rim-Edge” model of a MoS ₂ catalytic particle ³²	40
Fig. 4 - 2 Separate phases observed in the liquid product after hydro-treating reactions.....	43
Fig. 4 - 3 Vacuum drying system.....	46
Fig. 4 - 4 Experimental design on the catalyst preparation for characterization (detailed preparation conditions refer to Table 4-1)	47
Fig. 4 - 5 XRD spectra of candidate Mo sulfide catalyst prepared in <i>in-situ</i> H ₂ or molecular H ₂	50
Fig. 4 - 6 HRTEM images of MoS ₂ slabs collected from the organic phase, MoCO340.....	52
Fig. 4 - 7 HRTEM images of Wcat particles, MoCO340.	53

Fig. 4 - 8 HRTEM images of MoS ₂ slabs dispersed in phases of (A) O/W, (B) Aqu., and (C) Baq, MoCO340.....	54
Fig. 4 - 9 HRTEM images of the MoS ₂ slabs collected from the organic phase, MoH340....	55
Fig. 4 - 10 HRTEM images of Wcat particles, MoH340.....	56
Fig. 4 - 11 HRTEM images of MoS ₂ slabs dispersed in phases of (A) O/W, (B) Aqu., and (C) Baq, MoH340.....	57
Fig. 4 - 12 Crystalline size distribution of the MoS ₂ slabs dispersed in different phases (except the Baq phase) of the sample MoCO340, prepared at 340°C using <i>in situ</i> H ₂	60
Fig. 4 - 13 Crystalline size distribution of MoS ₂ slabs dispersed in different phases of the sample MoH340, prepared at 340°C using molecular H ₂	62
Fig. 4 - 14 HRTEM images of MoS ₂ slabs in all phases of SMOCO340. A. Org., B. Wcat, C. O/W, D. Aqu., E. Baq.	64
Fig. 4 - 15 HRTEM images of MoS ₂ slabs in all phases of NMOCO340. A. Org., B. Wcat, C. O/W, D. Aqu., E. Baq.	65
Fig. 4 - 16 SEM image of MoCO340 taken by the SE2 detector at the magnification of 100KX.....	66
Fig. 4 - 17 SEM image of MoH340 taken by the SE2 detector at the magnification of 100KX	67
Fig. 4 - 18 A typical EDX spectrum of a Mo sulfide sample, SMOCO340-Org.	72
Fig. 5 - 1 Atomic ball model showing a hypothetical, bulk-truncated MoS ₂ hexagon exposing the two types of low-index edges, the S edges and Mo edges ³⁴ (blue: Mo; yellow: S). License number for reusing this figure from Elsevier: 2531641409788.....	79
Fig. 5 - 2 Varian CO-3800 gas chromatograph of HDS products of DBT and 4,6-DMDBT, detected <i>via</i> FID and PFPD (GC method given in Appendix B).....	84
Fig. 5 - 3 Major WGS gas concentrations and the conversions of CO as a function of the reaction time at different reaction temperature: A: 330°C, B: 350°C, C: 380°C, D: 400°C. .	88
Fig. 5 - 4 Regression fitting points for <i>k'</i> _{HYDD} in the HDS of DBT over dispersed Mo sulfide catalyst using <i>in-situ</i> H ₂ at 380 °C using the proposed kinetics HDS model (experiment ID: DS0907).	93

Fig. 5 - 5 HDS product distribution of DBT over dispersed Mo sulfide catalyst using <i>in-situ</i> H ₂ at 380 ⁰ C (experiment ID: DS0907).	95
Fig. 5 - 6 HDS product distribution of 4,6-DMDBT over dispersed Mo sulfide catalyst using <i>in-situ</i> H ₂ at 380 ⁰ C (experiment ID: DS0907).	96
Fig. 5 - 7 Conversion and desulfurization results of DBT and 4,6-DMDBT over promoted Mo sulfide catalysts using <i>in-situ</i> H ₂ .	102
Fig. 5 - 8 HRTEM image of NiMo catalyst particles dispersed in the organic phase (A) and on the reactor vessel wall (B) collected after HDS experiment (EDX spectra given in Appendix E).	105
Fig. 5 - 9 HRTEM image of MoS ₂ slabs collected on the reactor vessel wall after the HDS experiment over NiMo catalyst.	106
Fig. 5 - 10 Conversion of CO <i>via</i> WGS reaction as a function of reaction time over different dispersed sulfided catalysts.	108
Fig. 5 - 11 XRD spectra of K promoted MoS ₂ catalyst particles prepared in CO at 340 ⁰ C (K:Mo=1:9 molar).	110
Fig. 5 - 12 HRTEM images of Wcat particles of K promoted Mo sulfide catalyst prepared in CO at 340 °C (K:Mo=1:9 molar).	112
Fig. 5 - 13 SEM images of K promoted Mo sulfide catalyst particles detected by SE2 (prepared in CO at 340 °C, K:Mo=1:9 molar).	113
Fig. 6 - 1 Peak fitting for the spectra of dispersed MoS catalysts prepared in <i>in-situ</i> H ₂ and molecular H ₂ .	123
Fig. 6 - 2 Simultaneous HDS of DBT and 4,6-DMDBT in <i>in-situ</i> hydrogen <i>versus</i> molecular hydrogen over dispersed Mo sulfide catalyst derived from PMA at 380 ⁰ C.	125
Fig. 6 - 3 Desulfurization of DBT and 4,6-DMDBT as a function of reaction time using <i>in-situ</i> hydrogen and molecular hydrogen, respectively, over dispersed Mo sulfide catalyst derived from PMA at 380 ⁰ C.	126
Fig. 6 - 4 Conversion and sulfur-removal of model sulfur-containing compounds obtained as a function of the gas composition of syngas.	128
Fig. 6 - 5 Simultaneous HDS of DBT and 4,6-DMDBT over dispersed Mo sulfide catalyst <i>ex-situ</i> prepared in CO or molecular H ₂ at 380 ⁰ C. A: HDS of DBT over ExCO-01, B: HDS of	

4,6-DMDBT over <i>Ex</i> CO-01, C: HDS of DBT over <i>Ex</i> H-01, D: HDS of 4,6-DMDBT over <i>Ex</i> H-01.....	137
Fig. 6 - 6 Sulfur-removal of DBT and 4,6-DMDBT over dispersed Mo sulfide catalyst <i>ex-situ</i> prepared in CO or molecular H ₂ at 380°C.....	138
Fig. 6 - 7 Simultaneous HDS of DBT and 4,6-DMDBT at 380°C over dispersed Mo sulfide catalyst <i>ex-situ</i> prepared in CO using <i>in-situ</i> hydrogen and molecular hydrogen. A: HDS of DBT in <i>in-situ</i> H ₂ , B: HDS of 4,6-DMDBT in <i>in-situ</i> H ₂ , C: HDS of DBT in molecular H ₂ , D: HDS of 4,6-DMDBT molecular H ₂ . Other conditions: 100ml toluene, 5ml H ₂ O, 595 psi H ₂ , 5 psi H ₂ S, 0.5g 4,6-DMDBT, 0.42g DBT, 600 ppmw Mo, HC reactor	141
Fig. 7 - 1 Effect of the nitrogen heterocyclic compounds on the S-removal from DBT (A) and 4,6-DMDBT (B) over a dispersed Mo sulfide catalyst using <i>in-situ</i> hydrogen. Equi-molar DBT and 4,6-DMDBT (1670 ppmw of S in total), 590 psi of CO and 10 psi of H ₂ S (at room temperature), 500 ppmw Mo, S:N=2:1 (molar), 380°C.....	151
Fig. 7 - 2 Effect of the basic quinoline and non-basic carbazole on the HDS reaction pathways of DBT and 4,6-DMDBT over the nano-dispersed Mo sulfide catalyst using <i>in-situ</i> hydrogen. Equi-molar DBT and 4,6-DMDBT (1670 ppmw of S in total), 590 psi of CO and 10 psi of H ₂ S (at room temperature), 500 ppmw Mo, S:N=2:1 (molar), 380°C.....	153
Fig. 7 - 3 Effect of the nitrogen-containing compounds on the hydrogenation of naphthalene over a dispersed Mo sulfide catalyst using <i>in-situ</i> hydrogen. 590 psi of CO and 10 psi of H ₂ S (at room temperature), 500 ppmw Mo, 380°C.....	155
Fig. 7 - 4 HDS of DBT and 4,6-DMDBT in over dispersed Mo sulfide catalyst obtained at different reaction conditions: <i>In-situ</i> H ₂ /molecular H ₂ , with/without quinoline or carbazole, 590 psi of CO(or H ₂) and 10 psi of H ₂ S (the pressure at room temperature), 400~500 ppmw Mo, 380°C, 3hr	158
Fig. 7 - 5 Selectivity between HDS reaction pathways of DBT and 4,6-DMDBT obtained at different reaction conditions: <i>In-situ</i> H ₂ /molecular H ₂ , with/without quinoline or carbazole, 590 psi of CO(or H ₂) and 10 psi of H ₂ S (the pressure at room temperature), 400~500 ppmw Mo, 380°C, 3hr	159

Fig. 8 - 1 HDN reaction network of quinoline ⁸⁹ . Where, Q is quinoline, THQ1, 1,2,3,4-tetrahydroquinoline, THQ5, 5,6,7,8-tetrahydroquinoline, DHQ, decahydroquinoline, OPA, ortho-propylaniline, PCHA, 2-propylcyclohexylamine, PCHE, propylcyclohexene, PCH, propylcyclohexane, PB, propylbenzen. License number for reusing this figure from Elsevier: 2531650864304.....	163
Fig. 8 - 2 HDN reaction network of carbazole presented by Szymanska <i>et al</i> ^{54a} over bulk β -Mo ₂ C.....	165
Fig. 8 - 3 HDN reaction network of carbazole suggested by F. Sanchez-Minero <i>et al</i> , ⁹²	165
Fig. 8 - 4 HDN reaction network of carbazole suggested in literatures ^{54c-49c}	166
Fig. 8 - 5 GC Chromatographs of carbazole HDN products obtained <i>via</i> FID and TSD detectors (Reaction conditions: 380 ⁰ C, <i>in situ</i> hydrogen, Mo sulfide catalyst)	169
Fig. 8 - 6 MS spectra of the N-removed products of carbazole with the GC retention times of 13.94 min and 14.24 min.	170
Fig. 8 - 7 HDN products distribution of carbazole (Cz0901-380 ⁰ C, <i>in situ</i> H ₂ , 180 min) ...	174
Fig. 8 - 8 Proposed HDN reaction network of carbazole over the dispersed Mo catalyst using <i>in situ</i> H ₂ (the products blanketed were not detected by GC).....	176
Fig. 8 - 9 Bond length and bond order of C-C, C-N/C-S bonds in molecules of intermediates of DBT and carbazole (MM2 calculation results). L: bond length, O: bond order.	179
Fig. 8 - 10 Distribution of HDN products of carbazole over dispersed Mo sulfide catalyst using <i>in situ</i> H ₂	180
Fig. 8 - 11 Pseudo first order plots of carbazole at 380 ⁰ C.....	182
Fig. 8 - 12 Repeatability of the experiment, Cz0901, (380 ⁰ C, <i>in situ</i> hydrogen). A: N-containing species, including carbazole and TH-carbazole; B: Two-ring and ring-opened products; C: Isomers of HCHE.....	184
Fig. 8 - 13 Concentrations of carbazole and TH-Cz as a function of reaction time at different reaction temperatures, 340~380 ⁰ C.....	185
Fig. 8 - 14 Denitrogenation of carbazole as a function of reaction time at different reaction temperatures, 340~380 ⁰ C.	185
Fig. 8 - 15 CO conversions <i>via</i> the WGS reaction and the concentrations of <i>in situ</i> H ₂ generated as a function of reaction time.	187

Fig. 8 - 16 Distribution of HDN products of carbazole over dispersed Mo sulfide catalyst using molecular H ₂	188
Fig. 8 - 17 Values of α as a function of reaction time obtained under different reaction conditions, using in situ H ₂ or molecular H ₂	190
Fig. 8 - 18 HDN product distribution of quinoline and carbazole obtained in separate runs.	194
Fig. 8 - 19 Length of C-C and C-N bonds in molecules of Quinoline and carbazole (Molecular Mechanics (<i>MM2</i>) Calculations, MINIMIZED ENERGY, CHEM OFFICE)..	197
Fig. 8 - 20 Distribution of HDN products of carbazole under different reaction conditions over dispersed Mo sulfide catalyst with adding 4,6-DMDBT.	201
Fig. 8 - 21 Values of α as a function of reaction time obtained under different reaction conditions, (A) without the addition of 4,6-DMDBT, or (B) with adding 4,6-DMDBT.....	202
Fig. 8 - 22 Conversions of DBT, 4,6-DMDBT, quinoline, carbazole and naphthalene over dispersed Mo sulfide catalyst in in-situ hydrogen at 380°C.	204
Fig. B - 1 GC calibration curves of starting reactants, DBT, 4,6-DMDBT, and carbazole.	236
Fig. C - 1 EDX spectra of MoCO340-org.....	249
Fig. C - 2 EDX spectra of MoCO340-Baq	250
Fig. C - 3 EDX spectra of MoH340-org	250
Fig. C - 4 EDX spectra of MoH340-Aqu.....	251
Fig. C - 5 EDX spectra of MoH340-Baq	251
Fig. C - 6 EDX spectra of MoH340-O/W.....	252
Fig. C - 7 EDX spectra of MoH340-Wcat	252
Fig. C - 8 EDX spectra of SMOCO340-O/W	253
Fig. C - 9 EDX spectra of SMOCO340-Baq	253
Fig. C - 10 EDX spectra of sMOCO340-org.....	254
Fig. C - 11 EDX spectra of SMOCO340-Aqu.....	254
Fig. C - 12 Distribution of MoS ₂ slab length, catalyst sample of MoCO340, prepared at 340 C in CO derived from PMA.....	256

Fig. C - 13 Distribution of MoS ₂ slab stacking degree, catalyst sample of MoCO340, prepared at 340 C in CO derived from PMA	257
Fig. C - 14 Distribution of MoS ₂ slabs, catalyst sample of MoH340, prepared at 340 C in H ₂ derived from PMA	259
Fig. C - 15 Distribution of MoS ₂ slab stacking degree, catalyst sample of MoH340, prepared at 340 C in H ₂ derived from PMA	260
Fig. C - 16 Distribution of MoS ₂ slabs, catalyst sample of SMOCO340, prepared at 340 C in CO derived from PMA.....	262
Fig. C - 17 Distribution of MoS ₂ slab stacking degree, catalyst sample of SMOCO340, prepared at 340 C in CO derived from PMA	263
Fig. C - 18 Distribution of MoS ₂ slabs, catalyst sample of NMOCO340, prepared at 340 C in CO derived from PMA.....	265
Fig. C - 19 Distribution of MoS ₂ slab stacking degree, catalyst sample of NMOCO340, prepared at 340 C in CO derived from PMA	266
Fig. D - 1 An HRTEM picture of the catalyst sample, SMOCO340, with measurement marked.....	268
Fig. D - 2 Distribution of MoS ₂ slab length.....	270
Fig. E - 1 Pseudo-first –order plots for the conversions of DBT and 4,6-DMDBT in HDS, DS0905, 330°C	272
Fig. E - 2 Regression for $kDDS'$ in the HDS of DBT, DS0905, 330°C	272
Fig. E - 3 Regression for $kHYDD'$ in the HDS of DBT, DS0905, 330°C	273
Fig. E - 4 Regression for $kDDS'$ in the HDS of 4,6-DMDBT, DS0905, 330°C.....	274
Fig. E - 5 Regression for $kHYDD'$ in the HDS of 4,6-DMDBT, DS0905, 330°C.....	274
Fig. E - 6 Pseudo-first –order plots for the conversions of DBT and 4,6-DMDBT in HDS, DS0906, 355°C	276
Fig. E - 7 Regression for $kDDS'$ in the HDS of DBT, DS0906, 355°C.....	276
Fig. E - 8 Regression for $kHYDD'$ in the HDS of DBT, DS0906, 355°C	277
Fig. E - 9 Regression for $kDDS'$ in the HDS of 4,6-DMDBT, DS0906, 355°C.....	278

Fig. E - 10 Regression for k_{HYDD}' of 4,6-DMDBT, DS0906, 355C	278
Fig. E - 11 Pseudo-first –order plots for the conversions of DBT and 4,6-DMDBT in HDS, DS0907, 380°C	280
Fig. E - 12 Regression for k_{DDS}' in the HDS of DBT, DS0907, 380°C.....	280
Fig. E - 13 Regression for k_{HYDD}' in the HDS of DBT, DS0907, 380°C, ... k_{HYDD}	281
Fig. E - 14 Regression for k_{DDS}' in the HDS of 4,6-DMDBT, DS0907, 380°C.....	282
Fig. E - 15 Regression of k_{HYDD}' of 4,6-DMDBT, DS0907, 380C	282
Fig. E - 16 Pseudo-first –order plots for the conversions of DBT and 4,6-DMDBT in HDS, DS0908, 400°C	284
Fig. E - 17 Regression for k_{DDS}' in the HDS of DBT, DS0908, 400°C.....	284
Fig. E - 18 Regression for k_{HYDD}' in the HDS of DBT, DS0908, 400°C	285
Fig. E - 19 Regression for k_{DDS}' in the HDS of 4,6-DMDBT, DS0908, 400°C.....	286
Fig. E - 20 Regression for k_{HYDD}' of 4,6-DMDBT, DS0908, 400 C	286
Fig. E - 21 EDX of NiMo(after HDS) sulfide, organic phase	289
Fig. E - 22 EDX of NiMo(after HDS) sulfide, Wcat phase Sp1-Fig. 5-12.....	289
Fig. E - 23 EDX of NiMo(after HDS) sulfide, Wcat phase Sp2-Fig. 5-12.....	290
Fig. E - 24 EDX of NiMo(after HDS) sulfide, Wcat phase Sp3-Fig. 5-12.....	290

List of Tables

Table 3 - 1 Reactants, catalyst precursors, solvents, and gases used in experiments	26
Table 3 - 2 Typical experimental conditions, including amounts and concentrations of solvents, reagents, and gases in a typical HDS experiment [†]	28
Table 3 - 3 Configuration and gas separation of RGA	34
Table 4 - 1 Dispersed molybdenum sulfide catalysts preparation conditions, 340 °C, 1hr	47
Table 4 - 2 BET surface area and average pore size of dispersed Mo sulfide particles prepared under different conditions (detailed preparation conditions refer to Table 4-1).....	49
Table 4 - 3 Average crystalline length and average stacking degree of MoS ₂ slabs dispersed in different phases of samples MoCO340 and MoH340*.	59
Table 4 - 4 Distribution of the length of MoS ₂ slabs which dispersed in Org. and Wcat phases, catalyst samples of MoCO340 and MoH340 (more details available in Appendix C).	61
Table 4 - 5 Average crystalline length and stacking number of the MoS ₂ slabs dispersed in different phases of samples MoCO340, SMOCO340 and NMOCO340*	63
Table 4 - 6 Elements detected <i>via</i> EDX from different phases (SMoCO340)*.....	73
Table 5 - 1 Detail reaction conditions of the experiments involved in Chapter 4 [†]	82
Table 5 - 2 GC retention time of HDS products of DBT and 4,6-DMDBT (Varian CP-3800) [†]	86
Table 5 -3 Pseudo-first-order rate constants involved in HDS reactions of DBT and 4,6-DMDBT as a function of reaction temperature over dispersed Mo sulfide catalyst using <i>in-situ</i> H ₂ *.....	94
Table 5 - 4 Selectivity of HDS pathways observed over sulfided Mo & NiMo catalysts*. 103	103
Table 5 - 5 HDS results of DBT and 4,6-DMDBT over KMo catalyst using <i>in-situ</i> H ₂	109
Table 6 - 1 Two-step experimental design.....	118

Table 6 - 2 Detail reaction conditions of the experiments to study HDS in the two different hydrogen sources [†]	119
Table 6 - 3 Experimental conditions for preparing <i>ex-situ</i> catalysts and for investigating their HDS activities	120
Table 6 - 4 Experimental conditions for comparing the reactivity of two hydrogen sources*	121
Table 6 - 5 Particle size obtained from the Scherrer equation and peak fitting of the XRD spectra for each MoS ₂ particles prepared in different H ₂ atmospheres	124
Table 6 - 6 Pseudo-first-order rates constants in the simultaneous HDS of DBT and 4,6-DMDBT at 380°C over dispersed Mo sulfide catalyst prepared from PMA in the two hydrogen sources (other detailed conditions refer to Table 6-2)	130
Table 6 - 7 Selectivity between two HDS reaction pathways observed using syngas with different CO/H ₂ ratio over dispersed Mo sulfide catalyst derived from ATTM at 380°C (detailed experimental conditions refer to Table 6-2).....	133
Table 6 - 8 Pseudo-first-order rate constants in the simultaneous HDS of DBT and 4,6-DMDBT at 380°C over <i>ex-situ</i> prepared dispersed Mo sulfide catalyst (other detailed conditions refer to Table 6-3)	136
Table 6 - 9 Pseudo-first-order rate constants in the HDS of DBT at 340°C over <i>ex-situ</i> prepared dispersed Mo sulfide catalysts (other detailed conditions refer to Table 6-3).....	136
Table 6 - 10 Pseudo-first-order rates constants in the simultaneous HDS of DBT and 4,6-DMDBT at 380°C in the two hydrogen sources over the <i>ExCO-01</i> catalyst (other detailed conditions refer to Table 6-4)	142
Table 7 - 1 Detailed reaction conditions of the experiments involved in Chapter 6*	147
Table 7 - 2 Conversions and product distributions for the HDS of DBT and 4,6-DMDBT in the presence of nitrogen heterocyclic compounds over a dispersed Mo sulfide catalyst using <i>in-situ</i> hydrogen*	149
Table 8 - 1 Detailed reaction conditions of the experiments involved in Chapter 8*	167

Table 8 - 2 Suggested molecular structures (GC-MS results) of the N-removed product at the retention time of 13.94 min.....	171
Table 8 - 3 Suggested molecular structures (GC-MS results) of the N-removed product at the retention time of 14.24 min.....	172
Table 8 - 4 GC retention time and identification of hydrotreating products derived from HDN of carbazole.....	175
Table 8 - 5 HDN product distribution of quinoline and carbazole over nano-dispersed Mo sulfide catalyst in <i>in-situ</i> H ₂ at 380°C for 1 hr (2.2 mmol N, 350 ppmw N, 430-500 ppmw Mo, SS reactor, 60min, 590 psi CO, 10 psi H ₂ S).....	192
Table 8 - 6 Pseudo first order rate constants for the conversion of carbazole and 4,6-DMDBT under different experimental conditions: (a) using <i>in-situ</i> H ₂ , without the addition of 4,6-DMDBT, or (b) using <i>in-situ</i> H ₂ ,with adding 4,6-DMDBT*.....	200
Table 8 - 7 Pseudo-first-order rate constant of each component in the hydro-treating reaction of the mixture*.....	205
Table A - 1 Composition of WGS gases in the final gas sample in the experiment DM-65 (590 psi CO, 10 psi H ₂ S, 380°C, 1hr)	226
Table A - 2 Concentrations of HDS products and the amount of consumed hydrogen in the experiment DM-65 (590 psi CO, 10 psi H ₂ S, 380°C, 1hr)	229
Table C - 1 Distribution of MoS ₂ slab length, catalyst sample of MoCO340	255
Table C - 2 Stacking degree distribution of MoCO340.....	256
Table C - 3 Distribution of MoS ₂ slab length, catalyst sample of MoH340.....	258
Table C - 4 Stacking degree distribution of MoH340.....	259
Table C - 5 Distribution of MoS ₂ slab length, catalyst sample of SMOCO340	261
Table C - 6 Stacking degree distribution of SMOCO340.....	263
Table C - 7 Distribution of MoS ₂ slab length, catalyst sample of NMOCO340	264
Table C - 8 Stacking degree distribution of NMOCO340	265

Table D - 1 Table of MoS ₂ slab length and distribution (sorted from maximum to minimum)	269
Table E - 2 Experiment DS0905, 330 °C	271
Table E - 3 ANOVA table of $k(DBT\ HYDD)'$, DS0905, 330°C	273
Table E - 4 ANOVA table of $k(4,6DMDBT\ HYDD)'$, DS0905, 330°C	274
Table E - 5 Experiment DS0906, 355 °C	275
Table E - 6 ANOVA table of $kDBT\ HYDD'$ at 355°C	277
Table E - 7 ANOVA $k4,6DMDBT\ HYDD'$ at 355°C	278
Table E - 8 Experiment DS0907, 380C	279
Table E - 9 ANOVA $k(DBT\ HYDD)'$, 380°C	281
Table E - 10 ANOVA $k(4,6DMDBT\ HYDD)'$, 380°C	282
Table E - 11 Experiment DS0908, 400 C	283
Table E - 12 ANOVA $k(DBT\ HYDD)'$, 400°C	285
Table E - 13 ANOVA $k(4,6DMDBT\ HYDD)'$, 400°C	286
Table E - 14 HDS of DBT and 4,6-DMDBT over the dispersed MoNi catalysts	287
Table E - 15 HDS results of DBT and 4,6-DMDBT over KMo catalyst using <i>in-situ</i> H ₂ .	288
Table F - 1 Experiment raw data of DS1001-PMA, H ₂	291
Table F - 2 Experiment raw data of DS1002-PMA, CO	291
Table F - 3 Experiment raw data of ATTM, syngas	292
Table F - 4 Experiment raw data of ExCO0901	292
Table F - 5 Experiment raw data of ExH0901	293
Table F - 6 Experiment raw data of ExCO1001	293
Table F - 7 Experiment raw data of ExH1001	293
Table F - 8 Experiment raw data of ExCO0902	294
Table F - 9 Experiment raw data of ExCO0903	294

Table G - 1 HDS of DBT and 4,6-DMDBT with the presence of N-containing compounds	295
Table H - 1 HDN carbazole at 380 °C, Cz0901.....	297

List of Abbreviations

Instruments

HRTEM	High-Resolution Transmission Electron Microscopy	EDX	Energy-Dispersive X-ray analyzer
GC	Gas Chromatograph	XRF	<i>X-Ray Fluorescence</i>
XRD	X-Ray Diffraction	AA	Atomic Adsorption
RGA	Refinery Gas Analyzer	FID	Flame Ionization Detector
ICP	Inductively Coupled Plasma spectrometer	PFPD	pulsed flame photometric detector
DFT	Density Functional Theory	TSD	Thermionic Specific Dectector
STM	Scanning Tunnelling Microscopy	HAADF-STEM	High-Angle Annular Dark-Field Scanning Transmission Electron Microscopy
TCD	Thermal Conductive Detector	SEM	Scanning Electron Microscope
PDF	Photo-Deflection Spectroscopy	EXAFS	Extended X-ray absorption fine structure
MS	Mass Spectroscopy		

Reagents

PMA	PhosphoMolybdic acid		
ATTM	Ammonium TetraThioMolybdate	4,6-DMDBT	4,6-DiMethyl-DiBenzoThiophene
DBT	DiBenzoThiophene	DMBP	DiMethylBiPhenyl
DCH	DiCycloHexane	Iso-	Isomers of
CHB	CycloHexylBenzene	BP	BiPhenyl
TH-	TetroHydro-	Q	Quinoline
DH-	DiHydro-	Cz	Carbazole
HH-	HexaHydro-	Naph	Naphthalene
T	Toluene	4-MDBT	4-MethylDibenzoThiophene
1-MN	1-Methyl-Naphthalene	THQ1	1,2,3,4-TetroHydroQuinoline
THQ5	5,6,7,8-TetraHydroQuinoline	DHQ	DecaHydroQuinoline
OPA	Ortho-PropylAniline	PCHA	2-PropylCycloHezylAmine
PCHE	PropylCycloHexEne	PCH	PropylCycloHexane
PB	PropylBenzene	CHCHE	CycloHexylCycloHexEne
HCHA	HexylCycloHexAne	PHA	PhenylHexAne

Reactions

HDS	Hydrodesulfurization	WGS	Water Gas Shift reaction
HDN	Hydrodenitrogenation	AGO	Atmospheric Gas Oil
DDS	Direct DeSulfurization	LGO	Light Gas Oil
HYD	HYDrogenation	HDM	Hydrodemetallization
HYDD	HYDrogenation Desulfurization	HY	Hydrogenation

Units

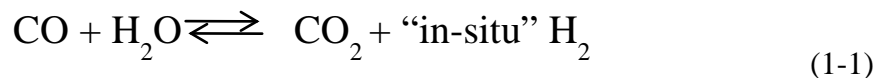
Psi	Pound per square inch	hr	Hour
MPa	Mega Pascal	rpm	Round of minute
MI	Milliliter	wt%	Weight percent
Ppmw	Part per millium by weight		

Others

DI	De-Ionized	SS	Stainless Steel
HC	Hastalloy C		

Chapter 1 Introduction

Canada's oil sands deposits contain as much as 173 billion barrels of economically viable oil, second only in size to Saudi Arabia¹. To recover deep buried oils, techniques such as steam injection or hot water extraction are applied and result in forming heavy oil/bitumen emulsions. As an inhibitor for hydro-treating reactions, the water present in heavy oil/bitumen emulsions has to be removed from the reaction system by adding surfactants before upgrading. To solve this problem, a novel heavy oil/bitumen emulsion upgrading process was developed in our group, wherein both water-removal and upgrading were encompassed in a single-step process^{2,3,4}, as shown in Fig. 1-1. This process is based on the activation of water present *via* water gas shift reaction (as shown in Eq.(1-1)) to generate reactive hydrogen *in-situ* for upgrading. The previous work done in our lab^{5,6} has demonstrated that *in-situ* H₂ is more effective than molecular H₂ for upgrading Cold Lake bitumen emulsions (22wt% H₂O, 4.4 wt% S dry, 8780 CP@40°C). Therefore, *in situ* H₂ is a promising and economical alternative source of molecular hydrogen for industrial upgrading processes.



Besides the WGS reaction, reactions involved in the new one-step upgrading process include hydrodesulfurization (HDS), hydrodenitrogenation (HDN), hydrodemetallization (HDM), hydrogenation, and hydrocracking. The present study is focused on HDS and HDN

reactions using model compounds to understand these fundamental reactions occurring during the upgrading process.

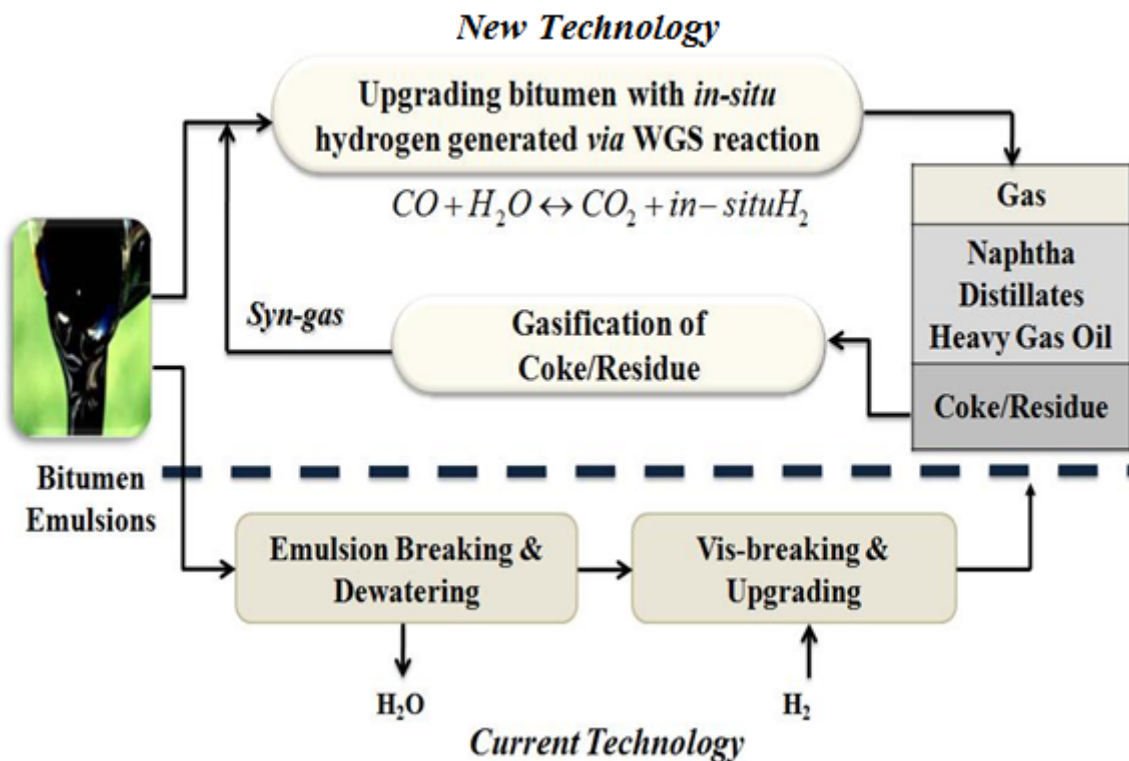


Fig. 1 - 1 The new one-step bitumen emulsion upgrading technology developed by Ng *et al*²⁻³

It is well known that environmental concerns result in more rigorous legislation specifications for petroleum products, including fuel oils. These specifications emphasize the importance of the conversion of heavy oil/bitumen into lighter and more valuable clean products⁷ with ultra-low sulfur concentration. The maximum amount of sulfur allowed in gasoline and diesel fuel was reduced to 50 ppm in 2005 and would probably be reduced even further by 2010⁸. Deep hydrodesulfurization technology must be implemented to attain this low level limitation on sulphur content . At the level of deep desulfurization, aromatic polynuclear molecules, especially nitrogen-containing heterocyclic compounds, exhibit

strong inhibitive effect on HDS⁹. The negative effect of nitrogen-containing compounds on HDS is very strong, even at concentrations as low as 5 ppm of nitrogen in the form of quinoline or carbazole¹⁰. The nitrogen-containing compounds are more difficult to be removed than sulfur-containing species. Therefore, it is necessary to study the effect of nitrogen-containing compounds on the deep HDS of refractory sulfur-containing species for achieving the recent ultra-low sulfur specifications for gasoline and diesel fuels. If most of sulfur- and nitrogen-containing compounds could be removed from heavy oils/bitumen emulsions in the preliminary upgrading process, the burden of sulfur removal in the downstream treatments would be greatly alleviated. Therefore, one of major objectives of this thesis is to investigate (1) the catalytic HDS and HDN activities of candidate catalysts, (2) HDS and HDN reaction mechanisms and kinetics using model compounds, and (3) mutual effects between HDS and HDN reactions.

Dibenzothiophene and 4,6-dimethyldibenzothiophene are typical refractory sulfur species present in heavy oil/bitumen and they will be used as sulfur-containing model compounds in the present study. Carbazole and its derivatives have been reported as predominant nitrogen-containing compounds in an atmospheric gas oil (AGO)¹¹. They were also identified as the most refractory organic nitrogen-containing species towards HDN in a blended gas oil¹². Therefore, carbazole will be used as one of nitrogen-containing compounds to study HDN reactions in this thesis. Besides non-basic carbazole, basic quinoline will also be used as a basic nitrogen-containing model compound in the chapter studying the effect of nitrogen-containing compounds on the HDS activity of the catalyst since it has been considered as one of the strongest HDS inhibitors due to the strong adsorption on active sites *via* the

donation of their unpaired electrons to the Lewis sites or by the interaction with the protons of the Brønsted acid sites^{9, 13}.

The other major objective of this thesis is to develop high effective catalysts for upgrading bitumen emulsions. Unsupported dispersed Mo sulfide based catalysts were found to be more efficient in hydro-treating than traditional supported catalysts. According to experimental results of Aldridge and Bearden¹⁴, an unsupported M-Coke catalytic system provided several orders of magnitude more catalyst particles per cm³ of oil in the reactor, even though the amount of M-Coke catalyst in the reactor was only a fraction of that used in an expanded bed. Compared with supported catalysts, unsupported dispersed catalysts have a number of advantages such that^{15,16}: (1) deactivation problems could be reduced by the use of once-through dispersed catalysts; (2) a high degree of catalytic metal utilization results from the absence of diffusional limitations; (3) well-dispersed small particles provide a high surface area for maximum interaction of feed, oil and hydrogen.

As well accepted, nickel has a significant promotional effect on the HDS/HDN reactions after being introduced into the MoS based catalyst. It was proposed that the promoter (Ni) weakened the metal-sulfur bond in the MoS itself, and increased the electronic density on the sulfur atoms, which could also be interpreted in terms of an enhancement of the basicity of the S²⁻ centers¹⁷. Furthermore, the positive effect of Ni on the WGS reaction was also reported¹⁸. Potassium is a well-accepted effective promoter for the WGS reaction^{19,18,20}. Therefore, in this thesis, to develop more effective nano-dispersed molybdenum catalysts for upgrading bitumen and heavy oils by using syngas, nickel and potassium promoters will be

introduced into the catalyst to improve the activity for both the WGS reaction and the bitumen upgrading reactions.

To achieve these two major objectives, developing high active catalysts and investigating HDS/HDN reaction mechanisms and kinetics, experiments will be carried out in a batch reactor using CO to provide *in-situ* generated hydrogen over dispersed Mo sulfide based catalysts. The HDS activity of unpromoted and promoted dispersed Mo sulfide catalysts will be investigated first. The HDS of sulfur-containing model compounds obtained using *in-situ* hydrogen will be compared with that using molecular hydrogen to evaluate the efficiency of the CO reaction system towards HDS reactions with the presence of water over dispersed catalysts. Continuously, the effect of the two nitrogen-containing model compounds on HDS will be compared and discussed. Finally, the catalyst activity towards the HDN of carbazole and HDN reaction mechanism and kinetics will be studied in both hydrogen sources. To explain the experimental results, morphology and physical properties of candidate catalysts are characterized *via* HRTEM, SEM, XRD, and BET.

There are 9 chapters in this thesis. Chapter 1 and Chapter 2 introduce the background and objectives of the present study. Chapter 3 describes experimental and characterization conditions, including flow charts for reactors, experimental procedures, methodology for analyzing products, and characterization techniques.

Chapter 4 is an important chapter in this thesis. It extends the characterization to the catalyst particles dispersed in different phases involved in hydro-treating reactions *via* high-resolution transmission electron microscopy (HRTEM) combined with energy-dispersed X-ray analyzer

(EDX). This technique could provide an insight into the morphology of Mo sulfide slabs and the atomic composition of the observed catalyst particles. Additionally, the BET, XRD, and SEM techniques are also applied to analyze the surface area, pore size, crystal diameter, and dispersion of catalysts. The characterization results will be used to understand and explain experiment results.

From Chapter 5, experimental results will be reported and discussed. First of all, simultaneous HDS of DBT and 4,6-DMDBT over *in-situ* prepared dispersed Mo sulfide catalyst is described in Chapter 5. After introducing the identification of their HDS products, kinetics modeling and calculation, the effect of reaction temperature, and the effect of promoters on HDS reactions are studied.

At the beginning of Chapter 6, the simultaneous HDS results of DBT and 4,6-DMDBT are compared *via* using different hydrogen sources, CO, syngas, and molecular hydrogen. Continuously, the effect of hydrogen sources on the HDS activity of the dispersed Mo sulfide catalyst is identified *via ex-situ* preparing the nano-dispersed catalysts in CO or hydrogen. The reactivity of the two hydrogen sources in the simultaneous HDS of DBT and 4,6-DMDBT is also compared in this chapter.

The strong inhibitive effect of N-containing compounds on HDS has been observed by many researchers^{21,22,23}. To reach deep HDS, this effect has to be studied. In Chapter 7, the inhibitive effect of carbazole and quinoline on the simultaneous HDS of DBT and 4,6-DMDBT is investigated and discussed.

Chapter 8 is focused on the HDN of carbazole. An HDN reaction network of carbazole is proposed in this chapter. Kinetic modeling of pseudo-first-order rate constant for the conversion of carbazole is introduced and applied in HDN studies. HDN results of carbazole obtained using the two sources of hydrogen are compared and discussed. In the last section of this chapter, the effect of a sulfur-containing compound, 4,6-DMDBT, on the HDN of carbazole is investigated and discussed.

Chapter 9, the last chapter, is devoted to summarize major conclusions and to list the recommendations for future studies.

Chapter 2 Literature Review

2.1 Dispersed Mo sulfide catalysts

Traditional hydro-treating catalyst usually contains sulfided molybdenum promoted by cobalt and/or nickel and is supported on porous alumina with high surface area. In recent years, the application of unsupported dispersed molybdenum sulfide based catalysts for deep HDS and upgrading of heavy oils is studied intensively^{24,25,26,27,28,29,30}. The use of unsupported catalysts, which could be dispersed in a heavy feedstock, is considered to be a promising way to improve the efficiency of HDS/hydro-treating processes. Unsupported catalyst provides very high density of active sites for hydro processing reactions³¹, reaches high degree of catalytic metal utilization due to the absence of diffusion limitation, and reduces deactivation problems by the once-through use of dispersed catalysts¹⁵⁻¹⁶. These advantages lead to more efficient activation of hydrogen molecules, and hence, high suppressibility of coke formation. For this reason, hydro-refining processes utilizing dispersed catalysts are particularly suited for upgrading heavy oils. Furthermore, unsupported dispersed catalysts are more suitable for specific studies *via* advanced analytical techniques than their supported counterparts to understand reaction mechanisms and find out active sites because the interference with support has been eliminated^{31,32,33,34,35}.

Dispersed catalysts can be *in-situ* generated in the feed of heavy oil as finely dispersed powders *via* thermal or hydrothermal decomposition of water-soluble or oil-soluble catalyst

precursors^{36,37,38}. The term of hydrothermal decomposition preparation method is a process of thermal decomposing the catalyst precursor in the presence of water and this process is also called as aqueous preparation. This technique is suited for preparing dispersed catalysts from water soluble precursors. E. Devers *et al*³⁸ compared the methods of hydrothermal decomposition with traditional thermal decomposition, in which there was no water involved, and they found the hydrothermal samples had higher activity towards the HDS of thiophene.

It is well known that the presence of water has significant inhibitive effect on hydro-treating reactions because of its high oxygen content and its competitive adsorption on the catalyst surface. Therefore, the effect of water on hydro-treating reactions is important in the application of hydrothermal synthesis of highly active catalysts. It is believed that the inhibitive effect of water could be diminished by maintaining the pressure of H₂S at a desirable level so that the catalyst can be kept in sulfided state³⁹. Satterfield *et al*⁴⁰ observed a promotion effect of water on the HDN of quinoline and they reported the enhancing effect of water increased in the presence of H₂S. Song *et al*^{25, 41} dissolved molybdenum precursor in water when they studied on the liquefaction of coal over dispersed MoS₂ catalyst and they discovered a surprisingly strong promotion effect of water addition on the catalytic conversion of coals. They found that: (1) water addition was effective for the generation of active Mo sulfide from ammonium tetrathiomolybdate (ATTM); but when the active catalyst had been generated, the water had an inhibitive effect on the C-O bond cleavage or the hydrogenation of aromatic rings; (2) the surface area of MoS₂ generated from ATTM with added water was much higher (>300 m²/g for the sample prepared at 375C) than that from ATTM alone (<300 m²/g for the sample prepared at 375C). They explained that the added

water could dissolve ATTM, and the presence of the organic solvent helped to disperse ATTM-containing water droplets during agitation, which gave rise to finely dispersed precursor molecules isolated by organic solvent prior to and during their decomposition and hydrogen reduction^{25, 41}.

Our group has used dispersed MoS₂ based catalysts prepared *via* the hydrothermal synthesis method for upgrading heavy oils and HDS for years. The ratio between water to reacting reagents was optimized^{36, 42}. Based on our study, water had a positive effect on HDS and upgrading at low concentrations and inhibitive effect was observed when increasing water concentration beyond the optimum ratio.

2.2 HDS of refractory sulfur-containing compounds

To understand basic HDS reaction mechanisms in the present reaction system, *in-situ* H₂ with *in-situ* prepared dispersed Mo sulfide catalyst, model sulfur-containing compounds was used in this thesis to investigate the HDS activity of candidate catalysts and study the application of *in-situ* H₂ for HDS.

As reported, the size and the type of sulfur-containing compounds present in major transportation fuels, gasoline, jet fuels, and diesel fuels, have a relationship to the boiling range of each distillate fuel fraction⁴³. In the middle distillates, alkylated benzothiophene, dibenzothiophene, and alkylated dibenzothiophene are major sulfur-containing species, and in heavy oils, more than or equal to three-polycyclic sulfur-containing compounds are predominant, such as DBT and benzonaphthothiophene. The reactivity of sulfur-containing

compounds in HDS reactions is mainly determined by molecular size and structure, and also is affected by the number and the location of alkyl-substituents to the molecule. For example, among the isomers of dimethyl-benzothiophene, the one with methyl substituents at 4- and 6-positions, which are adjacent to the sulfur atom, has the lowest HDS reactivity due to the highest steric hindrance of the methyl substituents at these locations to the access of the molecule to the catalyst surface.

Bataille *et al*¹⁷ reported that 4,6-DMDBT had similar adsorption coefficient as DBT on Mo sulfide surface and they attributed the much lower reactivity of 4,6-DMDBT to (1) the fact that only one β -H available for the elimination step, (2) a steric hindrance caused by the methyl groups during the E₂ elimination step of the dihydrointermediates, and (3) an effect of the methyl group on the acidity of the H atom at positions 4 and/or 6.

Therefore, to achieve deep HDS, the conversion and the removal of these key substituted DBT to a large extent determine the required HDS conditions. In this thesis, the HDS of 4,6-DMDBT in a mixture with one of the typical sulfur-containing compounds present in heavy oils, DBT, will be studied over the dispersed Mo sulfide catalyst using *in-situ* H₂.

It is well known, the HDS reaction of refractory sulfur-containing compounds proceeds in two reaction pathways, direct desulfurization route (DDS) and hydrogenation desulfurization route (HYD). The HDS reaction networks of DBT and 4,6-DMDBT were proposed in Fig. 2-1 and Fig. 2-2 based on the HDS products detected in the present study⁴⁴ (the identification of HDS products refers to the section of 5.3) and also based on the comparison with literatures^{13c}.

In the HDS of DBT, biphenyl (BP) is the DDS product obtained *via* the direct sulfur removal from the molecule, whereas, cyclohexylbenzene (CHB) and dicyclhexyl (DCH) are sulfur-removed products obtained in the HYD route with hydrogenated aromatic rings. The product of tetrahydro-DBT (TH-DBT) is the partially hydrogenated benzenic ring(s) and it is an intermediate in the HYD pathway. The sulfur-removed products obtained *via* the HYD route are called as HYDD products (as illustrated in Fig. 2-1) in this thesis. Similarly, the HDS products of 4,6-DMDBT could be divided to DDS and HYDD products as shown in Fig. 2-2. However, the HDS of 4,6-DMDBT is more complicated than that of DBT due to the presence of the methyl substituents in the molecule, whose positions change during the HDS reactions due to isomerization. As a result, many isomers of DDS and HYDD products were detected in the HDS of 4,6-DMDBT (Fig. 2-3). Actually, the isomerization of 4,6-DMDBT occurred during the HDS is beneficial for the HDS of 4,6-DMDBT by transforming the molecule into more reactive isomers^{45,46}.

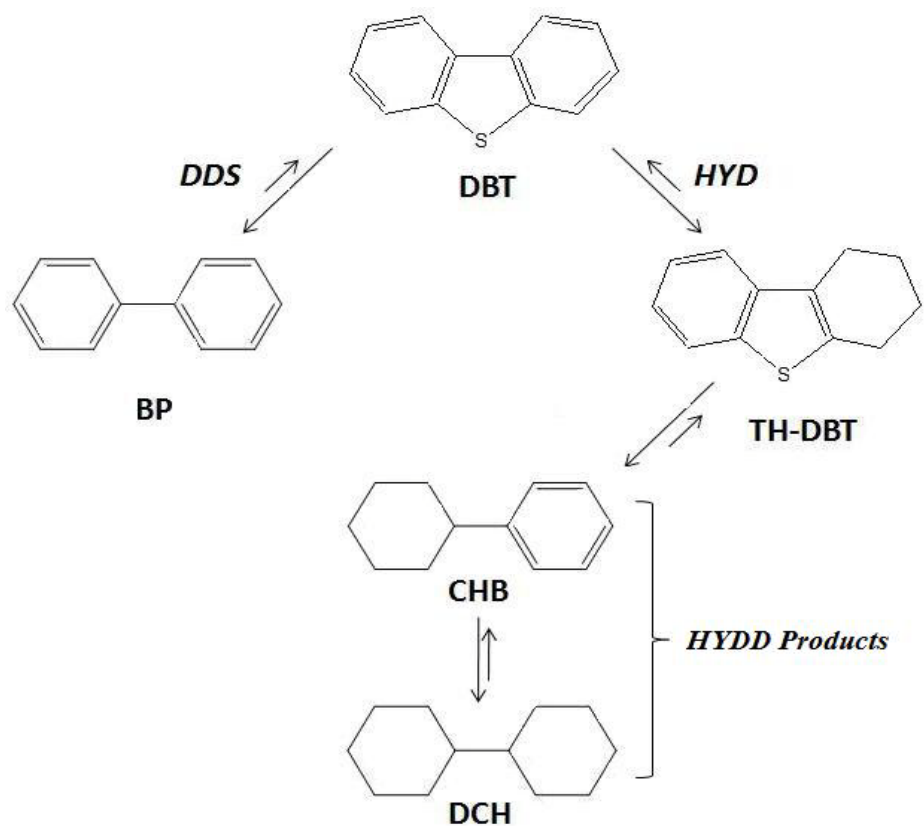


Fig. 2 - 1 HDS reaction net work of DBT using *in-situ* H₂ over dispersed Mo sulfide catalysts. DBT: dibenzothiophene, BP: biphenyl, TH-DBT: tetrahydrodibenzothiophene, CHB: cyclohexylbenzene, DCH: dicyclohexyl

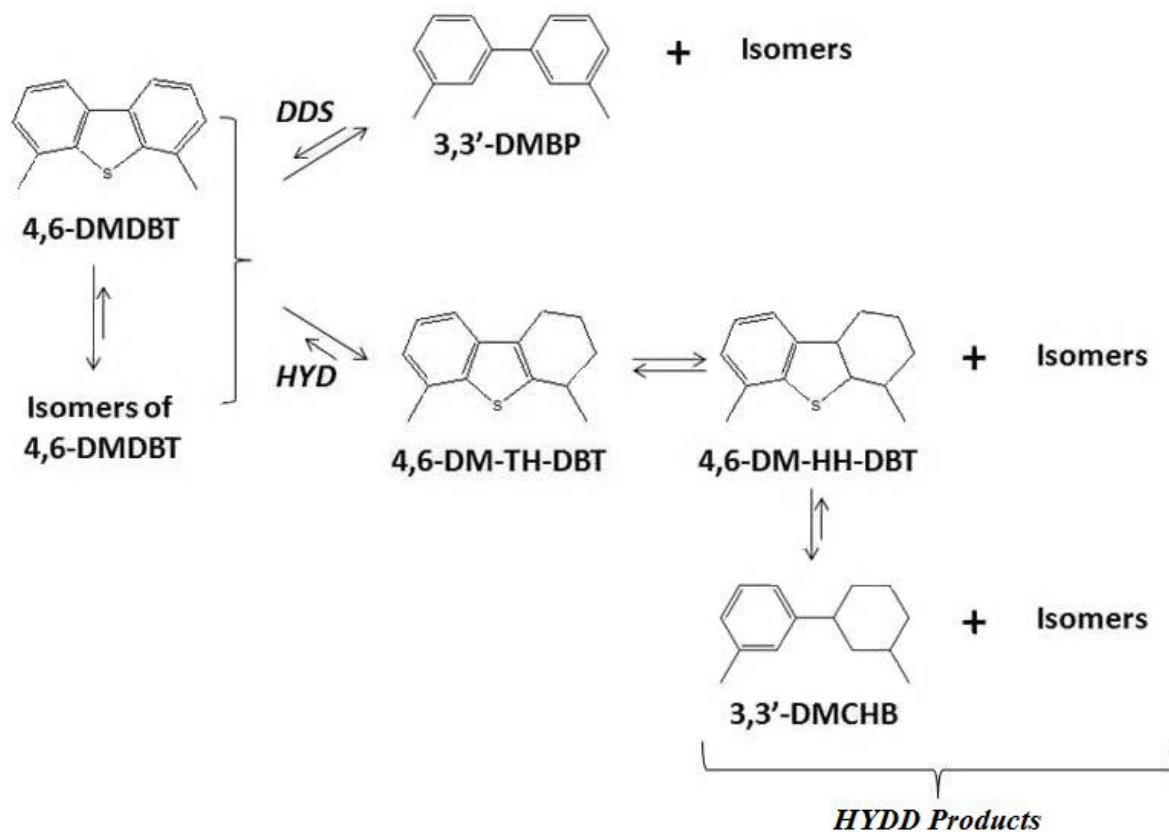


Fig. 2 - 2 HDS reaction network of 4,6-DMDBT using *in-situ* H₂ over dispersed Mo sulfide catalysts. 4,6-DMDBT: 4,6-dimethyldibenzothiophene, 3,3'-DMBP: 3,3'-dimethylbiphenyl, DM-TH-DBT: dimethyl-tetrahydro-dibenzothiophene, DM-HH-DBT: dimethyl-hexahydro-dibenzothiophene, DMCHB: dimethyl-cyclohexylbenzene

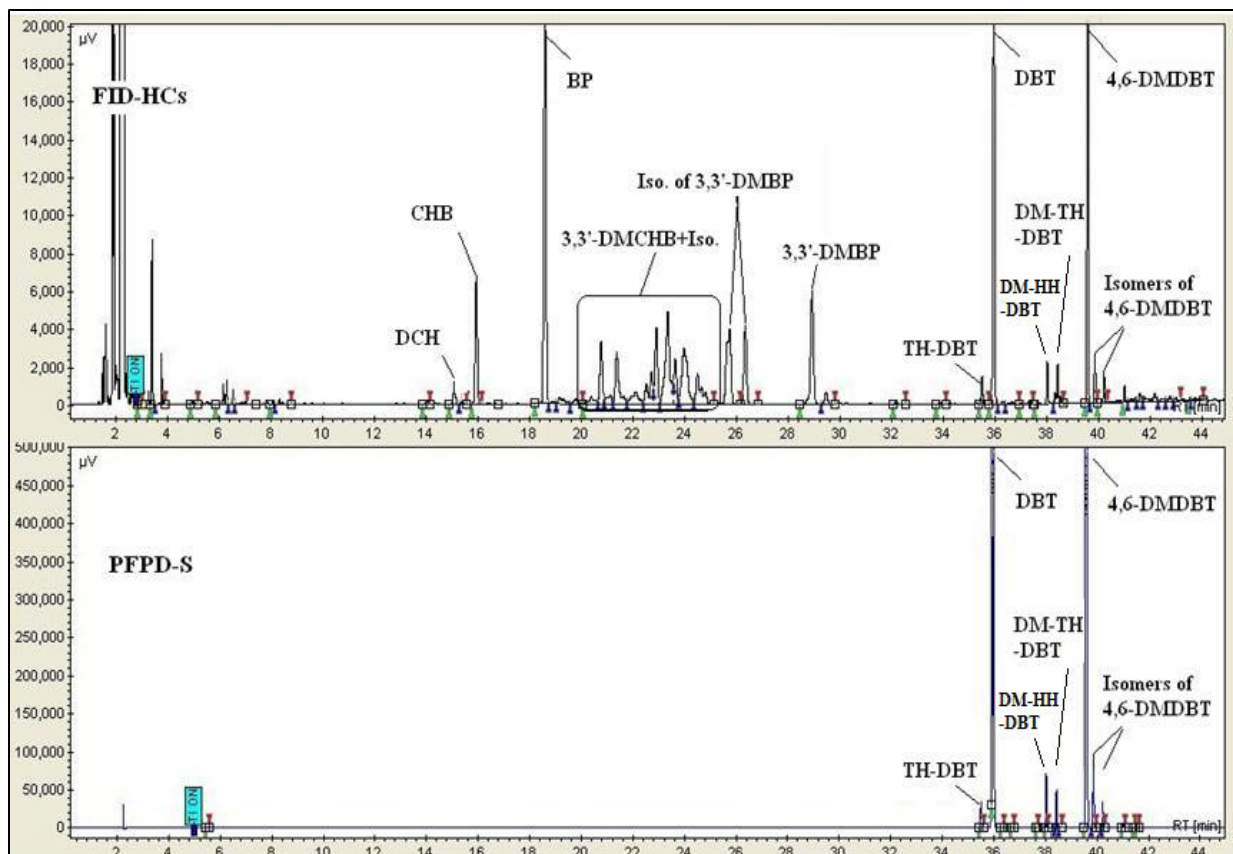


Fig. 2 - 3 GC chromatograph of HDS products of DBT and 4,6-DMDBT detected by FID and PFPD detectors.

The selectivity of the two reaction pathways is a key point in the HDS study. It is determined by many factors, such as the sulfur-containing molecular structure, feedstock composition, catalyst morphology and composition, and experimental conditions^{32,13c,47,8}. It has been widely observed that DDS is the dominant reaction route in the HDS of DBT^{13c,48}, while conversely, HYD is the major reaction pathway in the HDS of 4,6-DMDBT^{13c}. The high selectivity towards the HYD route is attributed to the steric hindrance of the adsorption of the sulfur atom on the catalyst surface caused by the presence of methyl groups at positions of 4 and 6 in the 4,6-DMDBT molecule⁴⁸. This thesis would be the first to study the effects of

reaction conditions, such as the use of different hydrogen sources, catalyst morphology, and the addition of nitrogen-containing species, on the selectivity between the two HDS reaction pathways in the HDS of each sulfur-containing model compound over dispersed Mo sulfide catalyst using *in-situ* hydrogen.

2.3 Use *in-situ* hydrogen instead of molecular hydrogen

The comparison between *in-situ* H₂ versus molecular H₂ in HDS reactions was discussed in literatures^{36, 49}, but contradicting results were observed. As reported by Ng^{49a} and Liu^{49b}, *in-situ* H₂ was superior to molecular H₂ in the HDS of benzothiophene (BT) and DBT, while Takemura *et al*^{49d} observed that molecular H₂ was more effective than *in-situ* H₂ in the HDS of Khafji residual oil over supported CoMo/Al₂O₃. Comparative reactivity of both of them in the HDS of BT and DBT over commercial CoMo(NiMo)/Al₂O₃ catalysts was reported by Kumar *et al*^{49c}. Lee *et al*³⁶ attributed these reported contradicting results to the different proportions of H₂O to CO used in the hydro-treating reactions. In the present reaction system, water has two functions of (1) participating the WGS reaction to generate *in-situ* H₂, and (2) inhibiting the hydrotreating reactions. Therefore, by changing the ratio between H₂O to CO, higher reactivity of *in-situ* H₂ than molecular H₂ in the HDS of DBT could be obtained as seen by Lee's results^{36, 42}.

The application of *in-situ* H₂ in the HDS of DBT and the HDN of quinoline has been studied intensively by Lee⁴². Comparable and even more effective hydro-treating results were observed when using *in-situ* H₂ instead of molecular H₂. Besides the model compounds study,

the efficiency of the *in-situ* H₂ reaction system in bitumen upgrading was also investigated by using a Cold Lake bitumen emulsion provided by Imperial Oil in our group⁶. In this real feedstock study, *in-situ* H₂ was more active than molecular H₂. So, the application of *in-situ* H₂ as an additional effective H₂ source is a promising process for upgrading bitumen emulsions. In this thesis, the comparison of the reactivity of two hydrogen resources will be extended in the simultaneous HDS of DBT and 4,6-DMDBT and also in the HDN of carbazole.

2.4 Inhibitive effect of N-containing species on HDS

In the petroleum industry, the long-term trend is towards processing heavier feed stocks containing large quantities of sulfur and nitrogen. The problem in deep removal of sulfur has become more serious due to the lower and lower legislation limit of sulfur content in finished gasoline and diesel fuel products, and the higher and higher sulfur and nitrogen contents in the crude oils. As summarized by Song⁴³, the majority of sulfur-containing compounds present in heavy oils are greater than or equal to three-ring polycyclic sulfur compounds, including DBT, benzonaphthothiophene, phenanthro[4,5-b,c,d]thiophene and their alkylated derivatives. These multi-ring polycyclic sulfur species have low reactivity in HDS and they are the sulfur-containing compounds detected in the finished commercial transportation fuel product of diesel. The removal of such low reactive sulfur species is a challenge to the present technique. Moreover, the inhibition effect on the deep HDS of heavy oils becomes more severe due to the competitive adsorption of nitrogen-containing compounds on the catalytically active sites of the catalyst.

Most of the nitrogen in petroleum is in the form of 5- and 6-membered heteroatom rings and anilines. The 6-membered rings and anilines are the most basic, accounting for about one third of the total nitrogen. Usually, basic nitrogen-containing compounds, such as quinoline, were considered as stronger inhibitors for HDS than non-basic nitrogen-containing species, such as carbazole³⁹. The inhibiting behaviour of nitrogen-containing compounds on hydro-treating reactions was described using Langmuir-Hinshelwood rate equations⁵⁰. For six-membered heterocyclic nitrogen-containing species, a good correlation between adsorption equilibrium constants and proton affinities, except for sterically hindered nitrogen-containing compounds, was observed by LaVopa *et al*^{50a} and Nagai *et al*^{50b}. They have found that the adsorption strength of the inhibitors increased in the order of ammonia < aniline < pyridine < quinoline. This order was in accordance with the order of inhibition strength on the poisoning of hydroprocessing catalysts by these nitrogen species^{50a}. The initial adsorption of six-membered heterocyclic nitrogen compounds, such as quinoline and pyridine, was proposed to be through the nitrogen heteroatom, either by donating its un-paired electron to a Lewis site or by the interaction with the proton of a Brønsted site^{8, 50a, b}.

As the major nitrogen-containing compounds present in many hard-to-desulfurize middle distillates^{10-11, 51}, the effect of five-membered heterocyclic nitrogen-containing compounds, such as carbazole and its derivatives, on HDS reactions are also studied intensively, and they are normally considered as less poisoning than basic species. However, the inhibitive strength of the non-basic carbazole on the HDS of model sulfur-containing compounds is not conclusive. As reported by Nagai and Kabe^{50c}, strong inhibitive effect on the HDS of DBT was caused by the presence of carbazole. As observed by Laredo *et al*¹⁰, non-basic carbazole had comparable negative effect as the basic quinoline on the HDS of DBT over a commercial

CoMo/ γ -Al₂O₃ catalyst. The different observed inhibitive strength of five-membered heterocyclic carbazole on HDS reactions may be due to the nature of the active catalysts as suggested by the experimental results obtained by Turaga *et al.*, who observed that carbazole had little effect on the HDS of 4,6-DMDBT over a commercial γ -Al₂O₃-supported CoMo sulfide catalyst, while it significantly inhibited the HDS activity of a CoMo/MCM-41 catalyst^{13b}. Their results indicated that the effect of carbazole on HDS could be affected by the physical property of catalyst. The effect of carbazole on HDS has been rarely studied over dispersed Mo sulfide catalysts, and this would be investigated in Chapter 7 of present thesis.

2.5 HDN of carbazole

Carbazole (Cz) and alkylcarbazoles are predominate nitrogen-containing species present in refractory raw distillates, and they were identified as the most refractory organic nitrogen-containing compounds in the feed stocks towards HDN reactions^{11-12, 52}. The lone pair of electrons of the nitrogen atom in the carbazole molecule are conjugated with the π electrons of aromatic rings, so the five-membered heterocyclic carbazoles are non-basic nitrogen-containing compounds with the pKa value of -6.0²¹. The carbazole molecule favours to adsorb on the catalytic active sites *via* aromatic rings in a parallel way because the lone pair of electrons in the nitrogen atom are not available in the end-on adsorption on the catalyst surface⁵³. This is also the predominant adsorption pattern of 4,6-DMDBT, one of the most refractory sulfur-containing compounds, and polycyclic aromatic hydrocarbons in the hydrogenation reactions^{8, 13c, 53}. The presence of carbazole and its derivatives may influence the HDS of sulfur-containing compounds and became a barrier to reach the more and more

strict legislation on the sulfur content in fuel products. Therefore, the HDN of carbazole should be carefully studied.

The HDN of carbazole caused less attention than the HDS of DBT and 4,6-DMDBT and there is not a well accepted reaction mechanism as reported in literatures⁵⁴. It is well known that nitrogen removal requires ring hydrogenation prior to C-N bond cleavage⁵⁵. As assumed by Perot⁵⁶ that three types of reactions would be involved in HDN leading to the hydrogenolysis of nitrogen-containing compounds: (1) hydrogenation of nitrogen-containing heterocycles, (2) hydrogenation of benzenic cycles, and (3) C-N bond cleavage. So an effective HDN catalyst should have both hydrogenation activity and hydrogenolysis activity. Additionally, the reaction of cracking has been observed during HDN as indicated by Ledoux et al⁵⁷.

Chapter 8 of this thesis would be the first to investigate the HDN of carbazole over dispersed Mo sulfide catalyst using *in-situ* hydrogen compared *versus* molecular hydrogen and an HDN reaction network will be proposed on the basis of product distribution of carbazole.

Chapter 3 Experimental and Characterization

Before reporting and discussing experiment results, it is necessary to introduce experimental system, product analysis, and catalyst characterization. Reactors, reactants, experimental operation procedure, product analysis methodology, and characterization techniques will be introduced in this chapter.

3.1 Reactors

Experiments were carried out in two separate 300 ml Autoclave high temperature and high pressure bolted closure laboratory batch reactors. One is an AISI 316 stainless steel (SS) batch reactor and the other one is a Hastelloy C (HC) batch reactor. The working volume of the SS batch reactor is 249 ml and that of the HC batch reactor is 300 ml. Both reactors are equipped, respectively, with a Magnedrive II assembly stirrer and a 45° pitch impeller. The two reactors and their accessories (valves, fittings and tubing) are designed to be capable of 5,000 psi at up to 510 °C. Flowcharts of the two batch reactors are given in Fig.3-1 and Fig.3-2, respectively.

As drawn in Fig.3-2, the HC batch reactor is composed by three systems as shown in squares with broken lines: gas supply, reactor, and sampling system. The SS batch reactor has the same gas supply and reactor system as the HC reactor, while it does not have the liquid-sampling system. Therefore, in the experiments using the SS batch reactor, only the final

liquid product is available for analysis, while in the experiments using the HC batch reactor, liquid products at different reaction times could be sampled for analysis during running reactions.

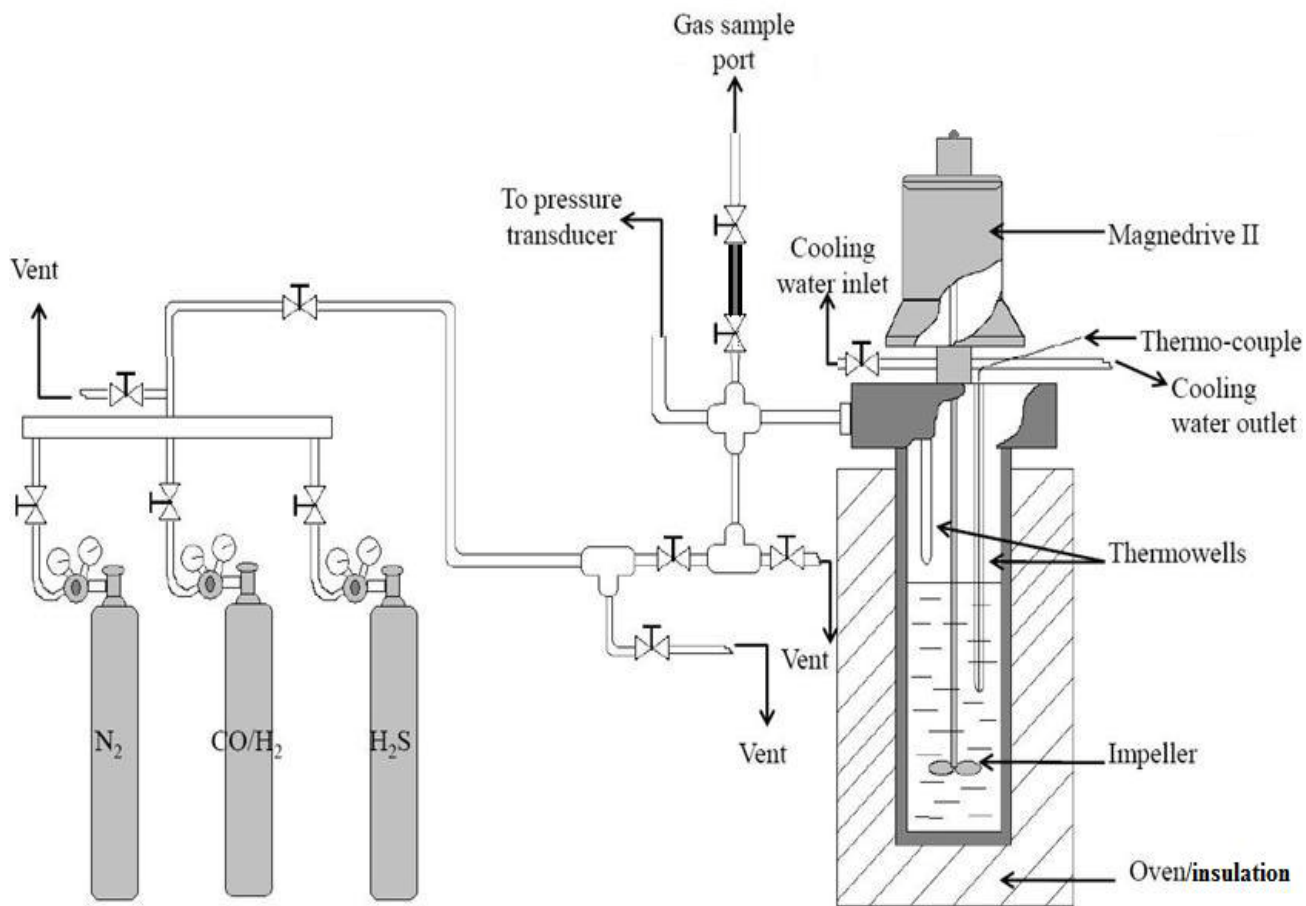


Fig. 3 - 1 Flow chart of the SS 300cc batch Autoclave reactor

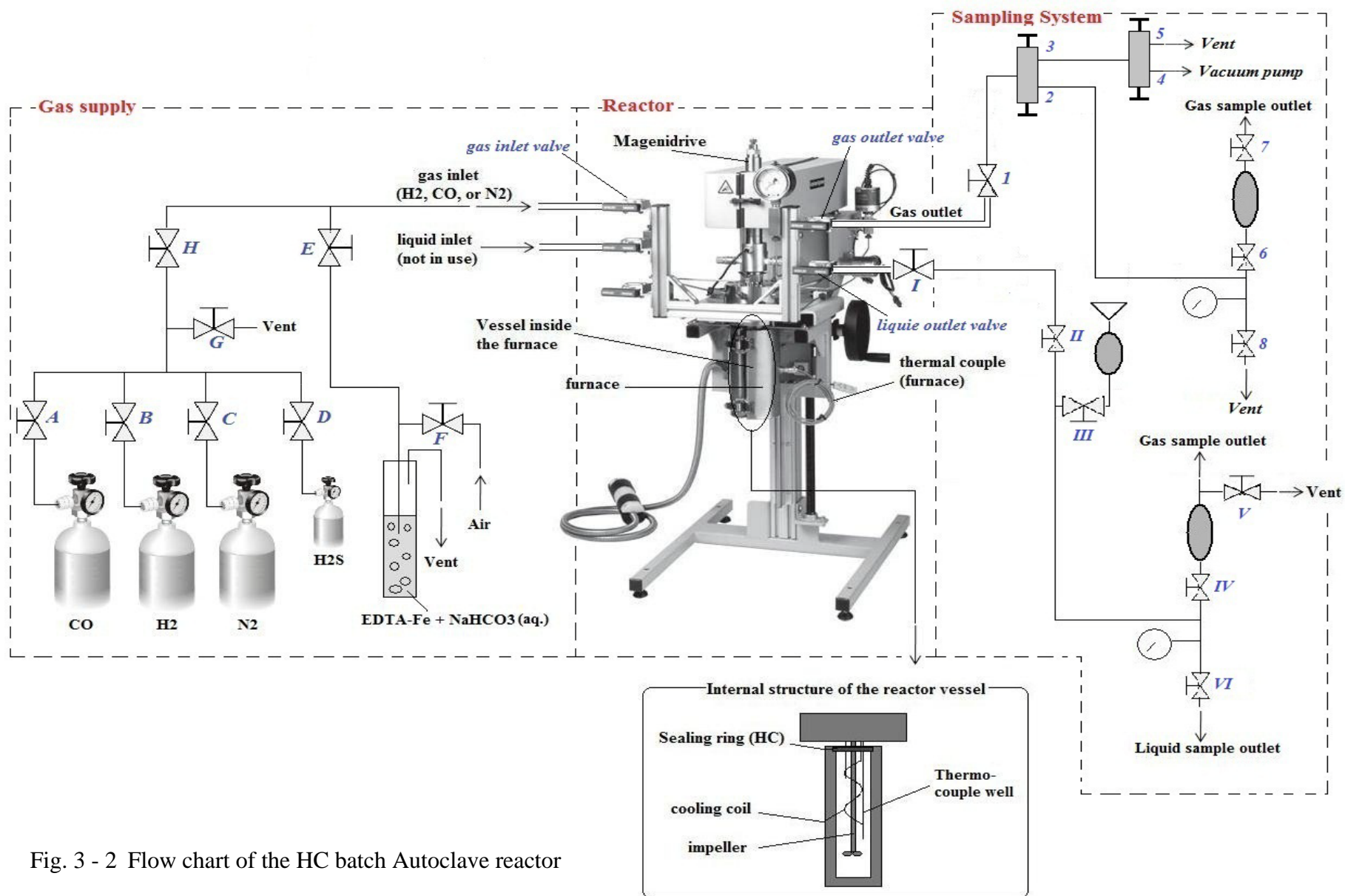


Fig. 3 - 2 Flow chart of the HC batch Autoclave reactor

3.2 Reactants

Model S-/N-containing compounds and catalyst precursors used in this thesis were purchased from Sigma-Aldrich without further purification. Gases used for checking sealing and reactions were all provided by Praxair. Detailed information of reactants is listed in Table 3-1.

Table 3 - 1 Reactants, catalyst precursors, solvents, and gases used in experiments

	Supplier	Purity	Product No.	Usage
Catalyst precursors				
Phosphomolybdic acid hydrate (PMA)	Aldrich	ACS reagent	221856	Mo precursor
Ammonium Tetrathiomolybdate (ATTM)	Aldrich	≥ 99.97%	323446	
Nickel (II) sulfate hexahydrate	Aldrich	> 99%	22767-6	Ni precursor
Potassium carbonate	Aldrich	≥ 99%	209613	K precursor
S-containing model compounds				
Dibenzothiophene (DBT)	Aldrich	≥ 98%	D32202	
4,6-dimethyldibenzothiophene (4,6-DMDBT)	Aldrich	≥ 97%	479411	
N-containing model compounds				
Quinoline (Q)	Aldrich	≥ 98%	241571	
Carbazole (Cz)	Aldrich	≥ 95%	C5132	
Solvent				
Toluene (T)	OmniSolv	99.99%	TX0737-1	Solvent for model compounds
De-ionized (DI) water	Departmental	-	-	WGS reactant and the solvent for cat. precursor
Gases				
CO	Praxair	2.4	CO-2.4T	WGS reactant gas
H ₂		5.0	HY5.0UH-T	Reactant gas
N ₂		4.5	N2-4.5T	Sealing check
H ₂ S		2.6	HS2.6-Q	Sulfidation reagent

3.3 Reaction procedure

A hydro-treating experiment in a batch reactor involves the following major steps:

- (1) preparing feed stocks and sealing reactor vessel
- (2) checking leakage and feeding reactant gases
- (3) reacting, taking gas/liquid samples and stopping the reaction

3.3.1 Preparing feed stocks and sealing reactor vessel

In a typical experiment, model S-/N-containing compound(s) is (are) dissolved in 100 ml of toluene. Catalyst precursor is dissolved in deionized (DI) water. Amount of each reagent in a typical HDS experiment is listed in Table 3-2. Detailed reaction conditions of each experiment will be listed in the chapters where the experiment results are reported and discussed.

The sealing of Autoclave batch reactors was accomplished *via* a sealing O-ring. Before each usage, each side of the sealing O-ring was coated with a thin layer of Dow MolyKote[®] lubricant. This lubricant layer could promote sealing and make the sealing O-ring easily to be removed from the top of the vessel after high-pressure/temperature reactions. After the sealing O-ring was totally dry, transferred the organic model compound(s) solution and the aqueous catalyst precursor solution into the reactor vessel. Put on the sealing O-ring, set up the Magedriver II, covered the lid and then sealed the reactor vessel. Finally assembled cooling water line (for cooling down the Magedrive II) and thermocouples.

Table 3 - 2 Experiment conditions, including amounts and concentrations of solvents, reagents, and gases in a typical HDS experiment[†]

	Amount	Concentration	S/Mo
Organic phase			
Solvent-toluene	100 ml	---	S*/Mo ≈ 12 (molar) *S: as in the S-model compounds
Model compounds			
DBT	0.42g	0.022 mol/l	
4,6-DMDBT	0.50g	0.023 mol/l	
		S: 1647 ppmw, 0.045 mol/l	
Aqueous phase			
Solvent-DI water	10ml	---	
Precursor-PMA	0.07~0.075g	Mo* : 0.4 mmol, 430 ppmw	
Gases (pressure at room temperature)			
CO	590 psi	Mol of CO: 0.227 mol	H₂S/Mo=10 (molar)
H ₂ S	10 psi	Mol of H ₂ S: 0.004 mol	
Reaction temperature		380 °C	
Reaction time		1~3 hr	
Catalyst		Dispersed Mo sulfide	

[†] Detailed composition of starting materials in each experiment will be given in separate chapters. Calculation involved in this table is given in Appendix A1.

* Mo concentration in the aq. phase was determined by ICP

3.3.2 Checking leakage and feeding reactant gases

Author checked the leakage of the reactor vessel by pressurizing the vessel with N₂ to 1200~1500 psi. This action was completed in following steps (refer to Fig. 3-2):

- (1-1) Made sure that gas/liquid inlet valves and gas/liquid outlet valves were closed well;

- (1-2) Opened valves C, H and G to release the pressure in gas lines and then closed them;
- (1-3) Opened N₂ cylinder and adjusted the regulator to around 1500 psi;
- (1-4) Opened valve C, valve H and gas inlet valve, allowing N₂ fed into the reactor vessel;
- (1-5) When N₂ pressure of the reactor vessel reached to 1200-1500 psi, closed gas inlet valve;
- (1-6) Closed N₂ gas cylinder;
- (1-7) Released the pressure left in the gas line by opening valve G;
- (1-8) Closed valves G, H, and C.

Left pressurized reactor vessel for 15-20 min, and recorded the vessel pressure every 5-10 min. The reactor was sealed successfully if the pressure did not drop down. To vent gas from the vessel, opened valves 5 (valve 4 closed), 3 (valve 2 closed), 1 and finally opened gas outlet valve. All valves should be closed after gas pressure decreased down to atmospheric pressure.

Before charging reactant gases, H₂S and CO (or H₂), the reactor should be purged with CO (or H₂) three times to remove un-wanted gases from the reactor, such as O₂ and N₂. Reactant gas charging procedure was done as follows (refer to Fig. 3-2):

- (2-1) Made sure that gas/liquid inlet valves and gas/liquid outlet valves were closed well;

- (2-2) Opened valves A (or B), H and G to release the pressure in gas lines and then closed them;
- (2-3) Opened CO (or H₂) cylinder and adjusted its regulator to a little higher than 600 psi;
- (2-4) Opened valves A (or B) and H, then gas inlet valve;
- (2-5) Closed gas inlet valve when reactor pressure reached to 300-400 psi;
- (2-6) Opened cooling water and turned on Magedrive II, stirring at 400-600 rpm for 1-2 min;
- (2-7) Stopped stirring, and vented CO (or H₂) from the reactor vessel;
- (2-8) Repeated steps (2-4) to (2-7) to purge two more times;
- (2-9) Had valve A closed, opened valves D, H and G, venting CO (or H₂) from gas lines;
- (2-10) Closed valves D, H and G;
- (2-11) Opened H₂S cylinder and regulator;
- (2-12) Had valves D and H open, opened valve E (making sure valve F closed) for several seconds to flush the gas line with H₂S;
- (2-13) Closed valve E;
- (2-14) Slowly opened gas inlet valve, charging H₂S into the reactor;
- (2-15) Closed gas inlet valve and closed H₂S cylinder;
- (2-16) Opened valve E to vent out H₂S and then closed it. Opened valve F, allowing air flow into the H₂S treaters;
- (2-17) Closed valve D, and opened valve A (or B) allowing CO to fill gas lines;
- (2-18) Opened gas inlet valve, pressurized the reactor to designated pressure;

(2-19) Closed gas inlet valve and CO cylinder;

(2-20) Opened valve G, venting CO out of gas lines, and then closed all valves.

The most commonly used molar ratio between CO and H₂S was 590:10. H₂S was introduced to sulfide and to form active MoS₂ catalyst. At this time, the reactor was ready to be used for running one experiment.

3.3.3 Reacting, taking gas/liquid samples and stopping the reaction

The reactor was heated up to the designated reaction temperature at the rate of 4-6°C/min and was kept at the reaction temperature for 1-3 hrs with stirring at 900-950 rpm (1000-1100 rpm for the HC batch reactor). At 380°C, the pressure would be around 2800-2900 psi (19-20MPa). The relationship between pressure and temperature in a typical HDS reaction using *in-situ* H₂ is shown in Fig. 3-3.

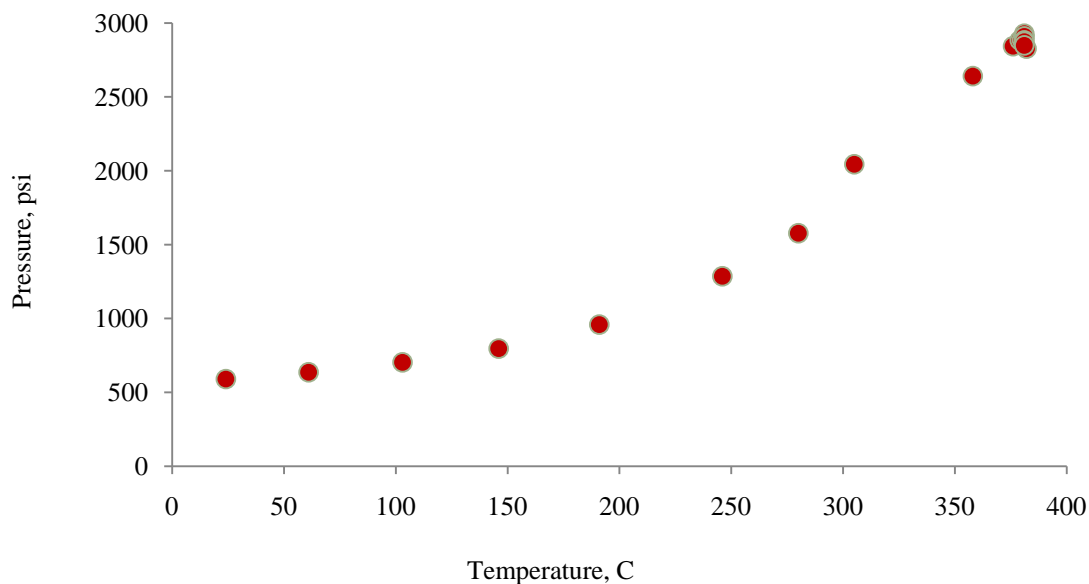


Fig. 3 - 3 Reaction temperature – pressure relationship in a typical HDS experiment from room temperature to 380°C, (590 psi of CO, 10 psi H₂S, 430 ppmw Mo, 100 ml toluene, 10 ml H₂O, DBT+4,6-DMDBT, SS reactor)

When using the HC batch reactor, gas and liquid samples could be taken during the reaction.

Liquid samples were taken according to the following procedure (refer to Fig. 3-2):

- (3-1) Opened valves I to VI to vent gas and liquid left from previous experiment from sampling system;
- (3-2) Closed valves I to VI;
- (3-3) Opened liquid outlet valve, and some liquid moved into the sampling tubing by high pressure inside the reactor. **Valve I must be closed firmly in this step, or a large amount of liquid would come out of the reactor;**
- (3-4) Closed liquid outlet valve quickly. Liquid sample stayed in the tubing between the liquid outlet valve and valve I at high pressure. The temperature of the liquid sample cooled down to room temperature quickly;
- (3-5) Opened valves II and IV (making sure valve III closed well) having liquid sample expand to downstream sampling tubing. Gases came out with the liquid sample separated at the tee between valves IV and VI. The small Swagelok sample cylinder connected between valves IV and V had two functions: condensing liquid phase evaporated in the gas phase and decreasing the pressure;
- (3-6) Took gas sample at gas sample outlet, after that opened valve V to vent;
- (3-7) Put one vial directly under liquid sample outlet, and opened valve VI to collect liquid sample.

In a normal liquid product sampling procedure, the sampling system was flushed two times. Namely steps (3-3) to (3-7) were repeated three times. Gas and liquid collected at the last time were analyzed.

When the reaction completed, stopped stirring, turned off the furnace, and shut down the cooling water. After the reactor cooled down to room temperature, picked up final gas sample, opened the reactor vessel, and took liquid product. Next, analyzed gas and liquid products.

3.4 Product analysis

Compositions of gas and liquid products were very important to calculate the conversion of CO *via* the WGS reaction, the conversion and the desulfurization of S-containing compounds *via* the HDS reaction, and the selectivity between HDS reaction pathways. Hence, gas and liquid samples were identified and quantitatively analyzed.

3.4.1 Gas analysis

Gas samples were analyzed by two gas chromatographs. Early samples (before 2008) were analyzed on a Perkin Elmer Model 8500 gas chromatograph equipped with one thermal conductivity detector (TCD) and two packed columns: 80/100 mesh Haysep C and 80/100 mesh Molecular Sieve 5A. Gases, containing H₂, O₂, H₂S, CO, and CO₂, were separated on the 5A molecular sieve column, whereas CO₂ and H₂S were separated on the Haysep C column because CO₂ and H₂S would poison the molecular sieve. The gas mixture was switched between the two columns by a 10-port valve.

After 2008, an Agilent Refinery Gas Analyzer (RGA, 3000 Micro C) was purchased and used in gas analysis. Injected gas samples are delivered to the sample inlet of the RGA after

passing through a sample conditioning system, which selectively removes any liquid fractions from the sample. Then an internal vacuum pump draws the conditioned samples into four independent GC modules simultaneously. Table 3-3 lists detailed configuration and separation of gases on RGA. Each GC module houses a silicon micro injector, a temperature-controlled capillary column, and a micro thermal conductivity detector (TCD). This RGA could finish one analysis in 4 minutes, so it is useful in the study on the WGS reaction.

Table 3 - 3 Configuration and gas separation of RGA

Channels	A	B	C	D
Injector Type	Backflush	Backflush	Backflush	Firmed volume
Carrier Gas	Argon	Helium	Helium	Helium
Column Type	Molecular Sieve	Plot U	Alumina	OV-1
Detector Type	TCD	TCD	TCD	TCD
Inlet Type	Heated	Heated	Heated	Heated
Gas separated	H ₂ , O ₂ , N ₂ , CH ₄ , CO	CO ₂ , C ₂ , H ₂ S, COS	C ₃ , C ₄ , C ₅	i-C ₄ , C ₆

3.4.2 Liquid analysis

Liquid products were analyzed on a Varian CP-3800 gas chromatograph, which is configured with a VF-05MS capillary column, connected to three different detectors: flame ionization detector (FID), thermionic specific detector (TSD, <1 ppmw of N), and pulsed flame photometric detector (PFPD, <1 ppmw of S). Three detectors of this GC can simultaneously implement semi-identification and quantitative analysis of sulfur-containing compounds (by PFPD), nitrogen-containing compounds (by TSD), and hydrocarbons (by FID) present in the

liquid sample. Conversions of model compounds in hydro-treating reactions and distribution of their products were calculated based on the results obtained from this GC. The flowchart of the product analysis is shown in Fig. 3-4. Detailed calculation process and GC running methods are given in Appendix B.

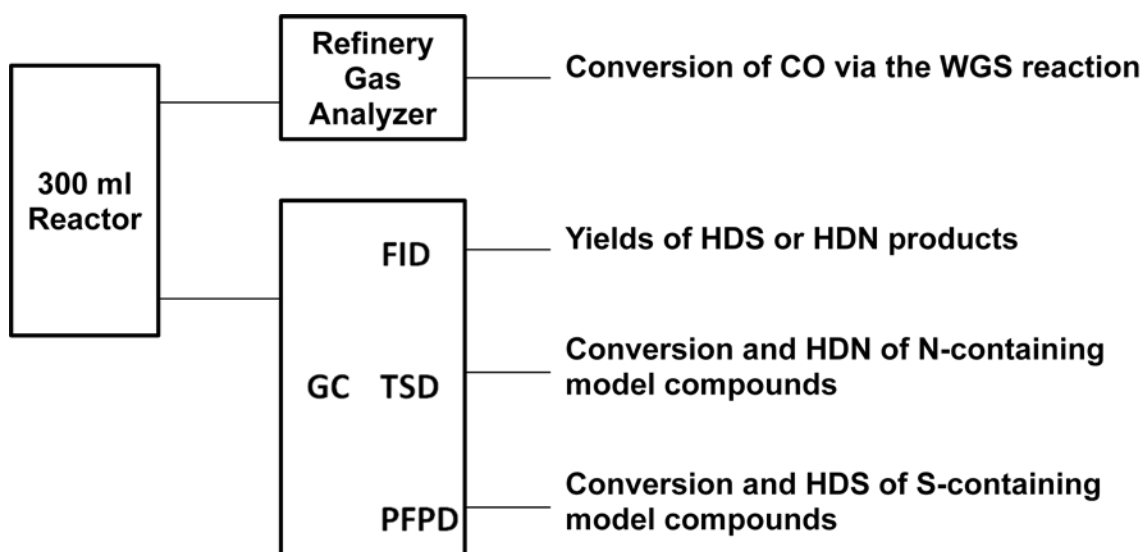


Fig. 3 - 4 Flowchart of product analysis after the hydro-treating process

3.5 Characterization Techniques

Physical property and morphology of candidate catalysts were characterized *via* X-ray diffraction (XRD), BET, HRTEM, and scanning electron microscope (SEM). From these characterization techniques, following information could be obtained:

XRD – crystalline identification

BET – surface area and pore size

HRTEM-EDX – crystal size, stacking degree, and morphology; atomic composition of a specific area of catalyst particles

SEM-EDX – particle morphology and dispersion; atomic composition of a specific area of catalyst particles

XRD: XRD measurement was performed on a Burker UXS D8 Focus X-ray Diffractometer with a Cu source of X-ray. The measuring wave length was 0.15406 nm. The survey measurement was scanned from 10 degree to 70 degree with 0.02 degree increment at the scanning speed of 1 sec/step.

BET: BET surface area measurement was carried out on a Micromeritics Gemini 2375 surface area analyzer. Catalyst samples were dried in N₂ at 110°C overnight and cooled down to room temperature before BET analysis.

HRTEM-EDX: Catalyst powders dispersed in different phases were diluted by ethanol and sonicated to disperse well. One drop of the solution was deposited on a holey-carbon film supported on Cu grids. Details of TEM sample preparation is described in the following Chapter. Specimens were examined using a JEOL 2010 TEM operated at an accelerating voltage of 200keV. Interested particles were chosen for energy dispersive X-ray spectrometer analysis.

SEM-EDX: An LEO 1530 Field Emission Scanning Electron Microscope equipped with SE2 and BSD detectors was used. Specimens were characterized at 5kV or 25kV. A high voltage of 25kV was selected to complete the EDX analysis of Mo, whose identification peaks appear in the range of 16-21kV. Catalyst powders were loaded on a sample holder,

surface of which was covered with a black sticky tape. Then the sample holder was dropped into a gold coating machine (Desk II Gold Sputter/Etch Unit, Denton Vacuum, LLC). Coating chamber was evacuated and the sample surface was coated with a 3-10 nm gold film to increase the conductivity. Gold-coated specimen was then transferred into SEM sample chamber and the SEM analysis was processed under high vacuum conditions (lower than 1.5×10^{-5} mBar).

Chapter 4

Catalyst Preparation and Characterization

4.1 Introduction

Key factors in the application of dispersed catalysts for hydro-treating are particle size and the population of catalyst particles obtained per unit volume of reactants. The activity of catalyst is controlled by the degree of dispersion and the composition of catalyst under a given set of reaction conditions. The term of dispersion on supported catalyst is defined as “the ratio of the number of active metal atoms on the surface of a catalyst to the total number of active phase atoms in it”⁵⁸. Therefore, the size of catalyst particles and stacking degree of molybdenum sulfide slabs are important to improve the dispersion and further increase the catalyst activity. Roxlo *et al*⁵⁹ studied the infrared optical absorption on edge planes in single MoS₂ crystal platelets using photo-deflection spectroscopy (PDF). They estimated that a fundamental turnover frequency in the HDS of dibenzothiophene for edge-like defects was $7.9 \times 10^{-2} \text{ molecules/EdgeSite} \cdot \text{s}^{-1}$ under reaction conditions.

It was found that, on unsupported Mo catalysts, active metals were present in MoS₂-like phases⁶⁰. MoS₂ has a layer structure. Within one layer, its structure can be viewed as a two-dimensional macromolecule with each Mo ion surrounded by six sulfur anions in a trigonal prismatic arrangement. In this configuration, each sulfur ion is bound to three Mo ions,

which results in a weak interaction with the next layer. A main theme in many structure-activity studies of molybdenum catalysts has been to establish whether different hydro-treating reactions are catalyzed predominately by sites along MoS₂ edge-surfaces or sites associated with basal planes^{26-27, 32, 60}.

Daage and Chianelli³² proposed rim sites of Mo sulfide crystals and edges of top and bottom layers were where hydrogenation reaction of large molecules, like DBT, took place; while edge sites of “sandwiched” layers catalyzed sulfur removal reactions. This was called as “Rim-Edge” model as shown in Fig. 4-1. Based on this model, selectivity between HDS reaction pathways was determined by the stacking number of MoS₂ slabs.

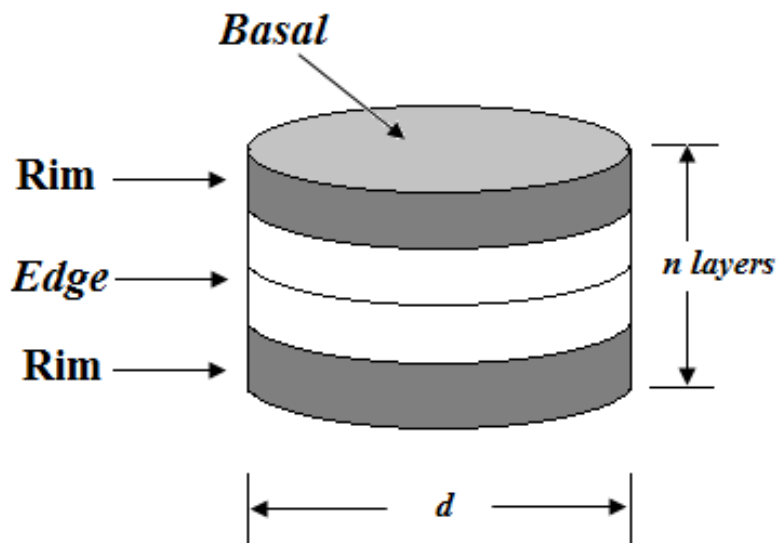


Fig. 4 - 1 The “Rim-Edge” model of a MoS₂ catalytic particle³²

Iwata *et al*²⁶⁻²⁷ extended the use of the “rim-edge” model in their study of hydro-treating heavy oils. They suggested that hydrogenation reactions could be catalyzed on all NO adsorption sites which were likely located on all edge sites. Their results also indicated that the number of HYD active sites increased with decreasing the number of stacked slabs in each MoS₂ particles.

High-resolution transmission electron microscopy is a widely used technique to study the length and stacking degree of MoS₂ slabs. Iwata²⁷ prepared unsupported molybdenum sulfide *via* different methods and compared their catalytic activity towards the HDS of DBT and the hydrogenation (HY) of 1-methyl-naphthalene (1-MN). *Via* HRTEM and XRD images, they found that the catalyst with a poorly crystallized bent and folded multi-layered MoS₂ exhibited higher activity than the one with a well crystallized multi-layered MoS₂. Highly bent sites may lead to sulfur vacancies during reactions, where were considered as the active sites for desulfurization reactions. They concluded that active sites were located on the curvature of basal planes in addition to edge planes.

Roy Lee, a previous member of our group, prepared dispersed molybdenum sulfide catalysts *via* the hydrothermal decomposition of phosphomolybdate acid (PMA) at 150 °C, 250 °C, and 340°C using *in-situ* H₂ and molecular H₂, respectively, and characterized candidate catalysts using SEM, XRD, BET, XPS, and Raman⁴². His characterization results indicated that nano-sized MoS₂ particles with high surface area, 120-360 m²/g, were prepared. SEM images showed that the catalyst prepared in *in-situ* H₂ had significantly smaller particle size than the one made in molecular H₂. With increasing preparation temperature using *in-situ* H₂, MoS₂ crystals were detected in Raman spectrum from 250°C and molybdenum oxides

disappeared at 340°C. XPS study confirmed that Mo ions at the outer surface of catalyst particles were completely reduced to Mo⁴⁺ at 340°C when prepared in *in-situ* H₂. Therefore, Lee's characterization results suggested that in the present reaction system, *in-situ* H₂ was an effective atmosphere for preparing active molybdenum sulfide catalyst and the catalyst should be prepared at the temperature higher than 340°C.

With the presence of water, our reaction system is a multi-phase reaction system. During hydro-treating reactions, molybdenum precursor, which was pre-dissolved in aqueous phase, was decomposed, reduced and sulfided to black insoluble molybdenum sulfide. Liquid product and catalyst particles were collected after the reaction. The black dispersed molybdenum sulfide particles were found to be dispersed in different phases: organic phase (Org.), aqueous phase (Aqu.), oil/water interface (O/W) and at the bottom of the aqueous phase (Baq.), as shown in Fig. 4-2. Besides these phases in the liquid product, lots of black catalyst particles left on reactor vessel wall, which were collected and analyzed as the phase of wall catalyst (Wcat.). Among these phases, the organic phase is where hydro-treating reactions occurred and the Wcat phase contains most of the catalyst particles.

A question was asked: if the catalyst particles collected from different phases have the same morphology? Since in the previous study⁴² the catalyst particles were not separated from different phases and were not characterized as in different phases, this question could not be answered. In this work, catalyst particles from different phases were collected and characterized. The crystal slab length and the stacking degree of the dispersed Mo sulfide

particles collected from different phases were analyzed using HRTEM-EDX. Characterization techniques of SEM, XRD and BET will also be used in this chapter.

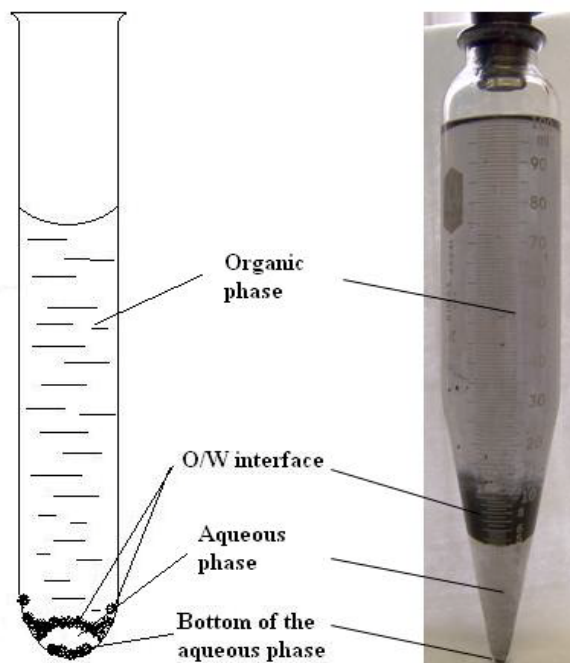


Fig. 4 - 2 Separate phases observed in the liquid product after hydro-treating reactions

4.2 *Ex-situ* preparation of catalysts

As discussed in the previous section, the dispersed molybdenum sulfide catalyst was *in-situ* prepared *via* the hydrothermal decomposition, the reduction, and the sulfidation of water-soluble molybdenum precursors in the HDS/HDN reaction system. After reaction, solid catalyst particles were observed to disperse in separate phases: Org., Aqu., O/W, Baq., and Wcat as shown in Fig. 4-2.

The morphology of catalyst particles was characterized on a JEOL 2010 HRTEM combined with EDX at an accelerating voltage of 200keV. Freshly prepared catalyst powders were

diluted and ultrasonically dispersed in ethanol at room temperature. Suspended catalyst particles in clear ethanol solution were dropped onto a carbon coated copper grid. HRTEM samples were prepared in a glove bag, which was filled with N₂, to prevent the contact with air. A detailed procedure for preparing HRTEM samples was described as follows:

- (1) Purged reagent alcohol with N₂ for 1hr to remove dissolved oxygen, and kept the de-aired reagent alcohol in a sealed container.
- (2) Purged an empty and clean separate sealed container with N₂ for longer than 10 min to replace the air inside, and then sealed the container.
- (3) Released the pressure of the reactor and opened the reactor with N₂ flowing to PROTECT the liquid product from air.
- (4) Collected liquid product (all phases) and transferred it into the N₂-filled container (step (2)) and sealed well.
- (5) Transferred the liquid product, the reactor vessel (covered with a rubber stopper), and the de-aired reagent alcohol into a glove bag, and sealed the glove bag well.
- (6) Vacuumed the glove bag and filled it with N₂, repeated 3 times.
- (7) In the N₂-filled glove bag, opened the container with the liquid product, and separated the organic phase from others (phases of O/W, Aqu. and Baq.). Rinsed the reactor vessel with de-aired reagent alcohol, and then collected Wcat powders.
- (8) Transferred some black particles from each phase to an empty vial, and then added some de-aired reagent alcohol (2-3 ml) to dilute and allowed the black powders to disperse.

(9) Sealed all vials and sample containers, and opened the glove bag.

(10) Transferred the sealed vials of diluted solutions out of the glove bag and sonicated for 3-5 min.

(11) Returned these vials back into the glove bag, and repeated step (6).

(12) Prepared HRTEM samples by dropping 1 drop of the clear phase of ethanol diluted solution of each phase on separate Cu grid (200 mesh carbon coated Cu grid), and allowed the grid to dry.

(13) Kept HRTEM samples in a N₂-filled glove bag.

After HRTEM analysis, samples from all phases were mixed and dried *via* a vacuum drying system, as illustrated in Fig. 4-3. The dried catalyst powders were kept in a N₂ filled glove bag and catalyst powders were characterized using BET, XRD and SEM. Experimental design for catalyst characterization and detailed catalyst preparation conditions are given in Fig. 4-4 and Table 4-1, respectively. Dispersed molybdenum sulfide based catalysts were prepared under different conditions to investigate the effect of hydrogen sources and S-/N-containing species on the physical properties and the morphology of candidate dispersed Mo sulfide catalysts.

It is important to note that the catalysts were prepared at 340 °C instead of the temperature for hydro-treating at 380 °C in this research. There are two concerns: (1) to compare the characterization results with previous results³⁹; and (2) to run catalyst preparation

experiments under the safe pressure limit of the reactor (if the reaction was carried out at 380°C, the pressure would be over 4000 psi).

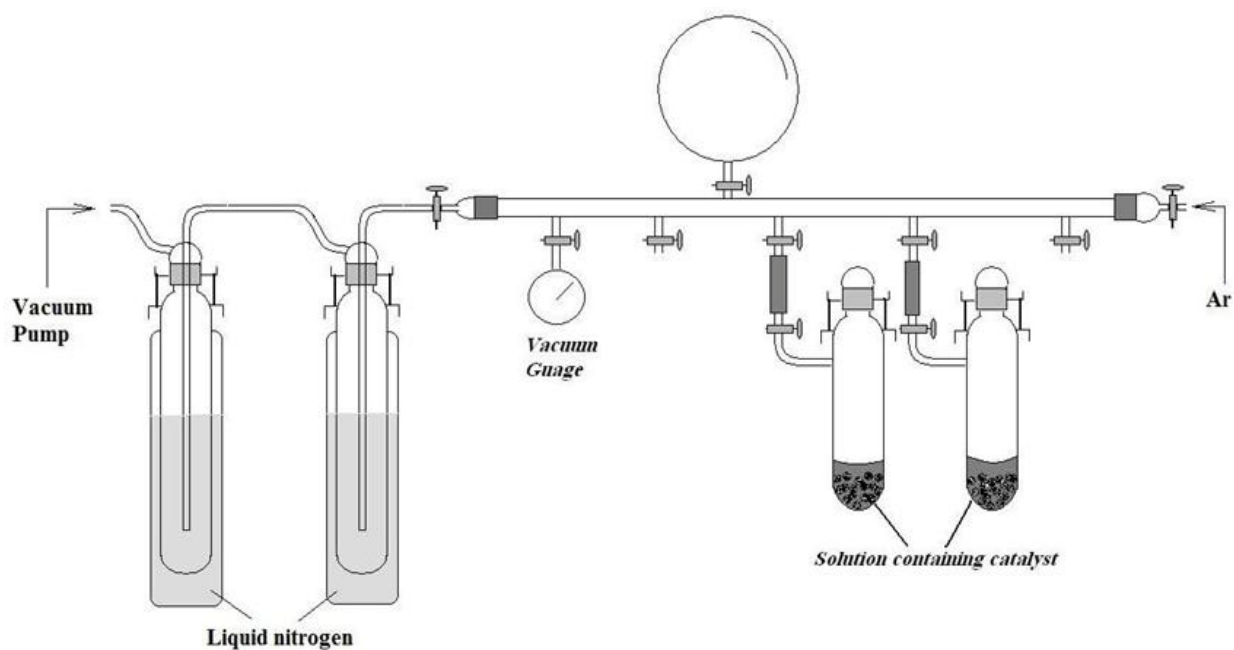


Fig. 4 - 3 Vacuum drying system

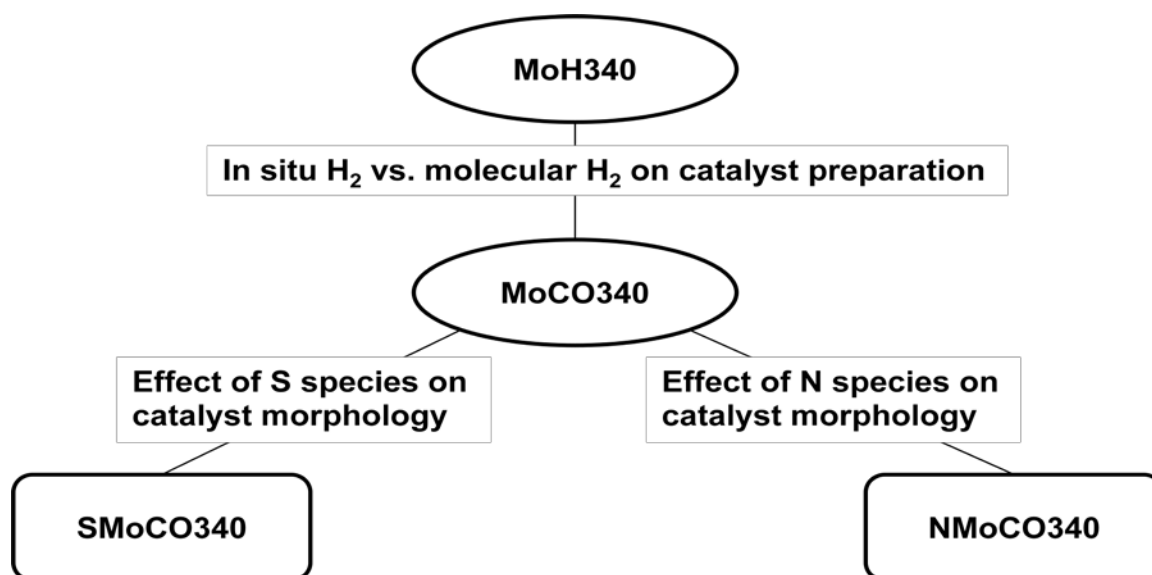


Fig. 4 - 4 Experimental design on the catalyst preparation for characterization (detailed preparation conditions refer to Table 4-1)

Table 4 - 1 Dispersed molybdenum sulfide catalysts preparation conditions, 340 °C, 1hr

Run No.		MoCO340	MoH340	SMoCO340	NMoCO340
Aqueous phase	PMA, g	3.86	4.09	3.99	3.99
	H ₂ O, ml	25	25	25	25
Organic phase	Toluene, ml	100	100	100	100
	DBT, g	-	-	0.42	-
	4,6-DMDBT, g	-	-	0.50	-
	Quinoline, g	-	-	-	0.36
Gases*	H ₂ S, psi	200	200	200	200
	CO, psi	500	-	500	500
	H ₂ , psi	-	500	-	-

* Total pressure at room temperature was around 600 psi due to the solubility of H₂S in solution.

4.3 Characterization results

4.3.1 BET

The surface area and the pore size of dispersed Mo sulfide catalyst particles prepared under different conditions at 340 °C were characterized by BET (Micromeritics Gemini 3243) and the results are shown in Table 4-2. In this section, catalyst particles were not analyzed by phases. They were a mixture of particles collected from all phases and dried *via* vacuum drying (Fig. 4-3). The Mo sulfide catalyst sample prepared in *in-situ* hydrogen was found to have the highest BET surface area, 266 m²/g, among all candidate catalyst samples. Surface areas of all dispersed Mo sulfide samples were higher or close to 200 m²/g, including the samples prepared in the presence of S-/N-containing compounds.

The surface area higher than 200 m²/g was lower than normal supported hydrotreating catalysts, wherein high surface area materials were used as carriers, but it was significantly higher than the value of around 10 m²/g surface area of unsupported MoS catalysts prepared and reported by Iwata *et al*²⁷ *via* traditional thermal decomposition method. Hence, the hydrothermal decomposition method is an effective way to prepare dispersed Mo sulfide catalysts with high surface areas. This is in agreement with what was reported by Dever³⁸ and Song^{25, 41}. During the hydrothermal preparation process, the presence of water favored the dispersion of the aqueous Mo precursor in the organic phase in small water droplets and resulted in smaller MoS₂ particles with higher surface area.

Table 4 - 2 BET surface area and average pore size of dispersed Mo sulfide particles prepared under different conditions (detailed preparation conditions refer to Table 4-1)

Sample	MoCO340	MoH340	SMoCO340	NMoCO340
BET surface area, m ² /g	266	205	207	198
Pore volume, cm ³ /g	0.13	0.10	0.10	0.10
Adsorption average pore diameter (4V/A by BET), nm	1.96	1.95	-	1.97

4.3.2 XRD

X-Ray Diffraction measurements were performed on a Burker UXS D8 Focus X-ray Diffractometer with a Cu source of X-ray. The measuring wave length was 0.15406 nm. The survey measurement (2θ) was scanned from 10 degree to 70 degree with 0.02 degree increment at the scanning speed of 1 sec/step.

XRD spectra of the samples prepared in CO and molecular H₂ are shown in Fig. 4-5. Wide peaks at the diffraction angles (2θ) of 13-14, 33-34, 39-40, and 59-60 were observed in XRD chromatographs of tested dispersed Mo sulfide catalysts. These XRD peaks were corresponding to the diffraction bands of MoS₂ crystallites, i.e. (002), (100), (103), and (110)⁶¹. XRD patterns of the candidate dispersed Mo sulfide catalysts confirmed the generation of MoS₂ under different preparation conditions. MoS₂ was widely accepted as the active phase for hydrotreating reactions. Wide peaks shown in XRD spectra indicated that the prepared unsupported MoS₂ particles had poor crystal structures and dispersed in small crystalline size.

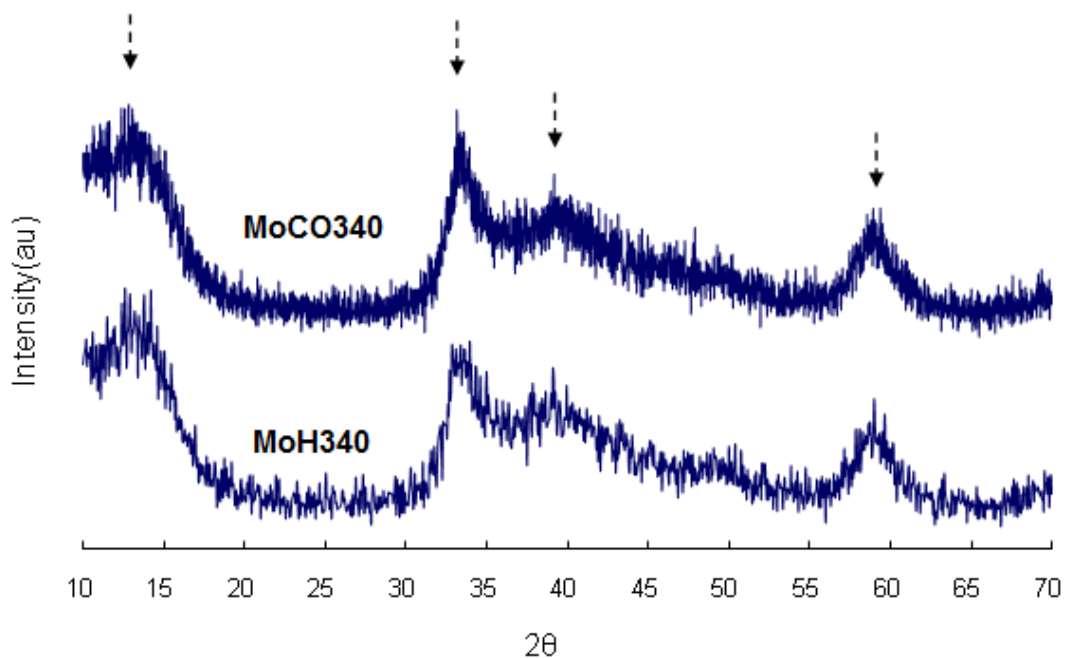


Fig. 4 - 5 XRD spectra of candidate Mo sulfide catalyst prepared in *in-situ* H₂ or molecular H₂.

Other conditions: 3.9-4.0g PMA, 25ml H₂O, 100ml toluene, no S-/N-containing compounds, 200psi H₂S, 500psi CO or H₂.

4.3.3 HRTEM-EDX

Via using HRTEM and EDX, the catalyst morphology and the semi-quantitative elemental composition of the candidate dispersed Mo sulfide catalysts were obtained. HRTEM-EDX results could be used to explain the experimental results and provide suggestions for future experimental design.

4.3.3.1 HRTEM images of candidate catalyst samples prepared in in-situ H₂ and molecular H₂

HRTEM images of each phase of candidate catalysts *ex-situ* prepared in *in-situ* H₂ (MoCO340) and in externally supplied molecular H₂ (MoH340) are shown in Fig. 4-6 to Fig. 4-11. The black bent thread-like fringes correspond to MoS₂ slabs. MoS₂ has an identical structure based on trigonal prisms structure of sulfur coordinated to Mo. The trigonal prisms are strongly bonded in two dimensions forming the S-Mo-S sandwiches, which can stack to form three-dimensional crystals of varying stacking arrangements. MoS₂ usually found in 2H (hexagonal) form indicating that the unit cell repeats along the hexagonal c-axis after two layers. The MoS₂ slabs perpendicular to the (002) planes are easily observed *via* HRTEM, whereas basal planes tend to be unobservable, especially in low-stacked solids⁶². That is why the morphology of MoS₂ slabs observed in HRTEM images is in thread-like shapes. Stacked MoS₂ layers are bonded *via* weak Van der Waals forces and the spacing between stacked MoS₂ layers is an identical parameter. The spacing measured from the fringes of both candidate catalyst samples was in the range of 6.1-6.5 Å, close to the d₀₀₂ of MoS₂ (6.15Å). EDX analysis of the HRTEM observed slabs also confirmed the presence of sulfided Mo in all phases of both candidate catalysts. EDX spectra are listed in Appendix C.

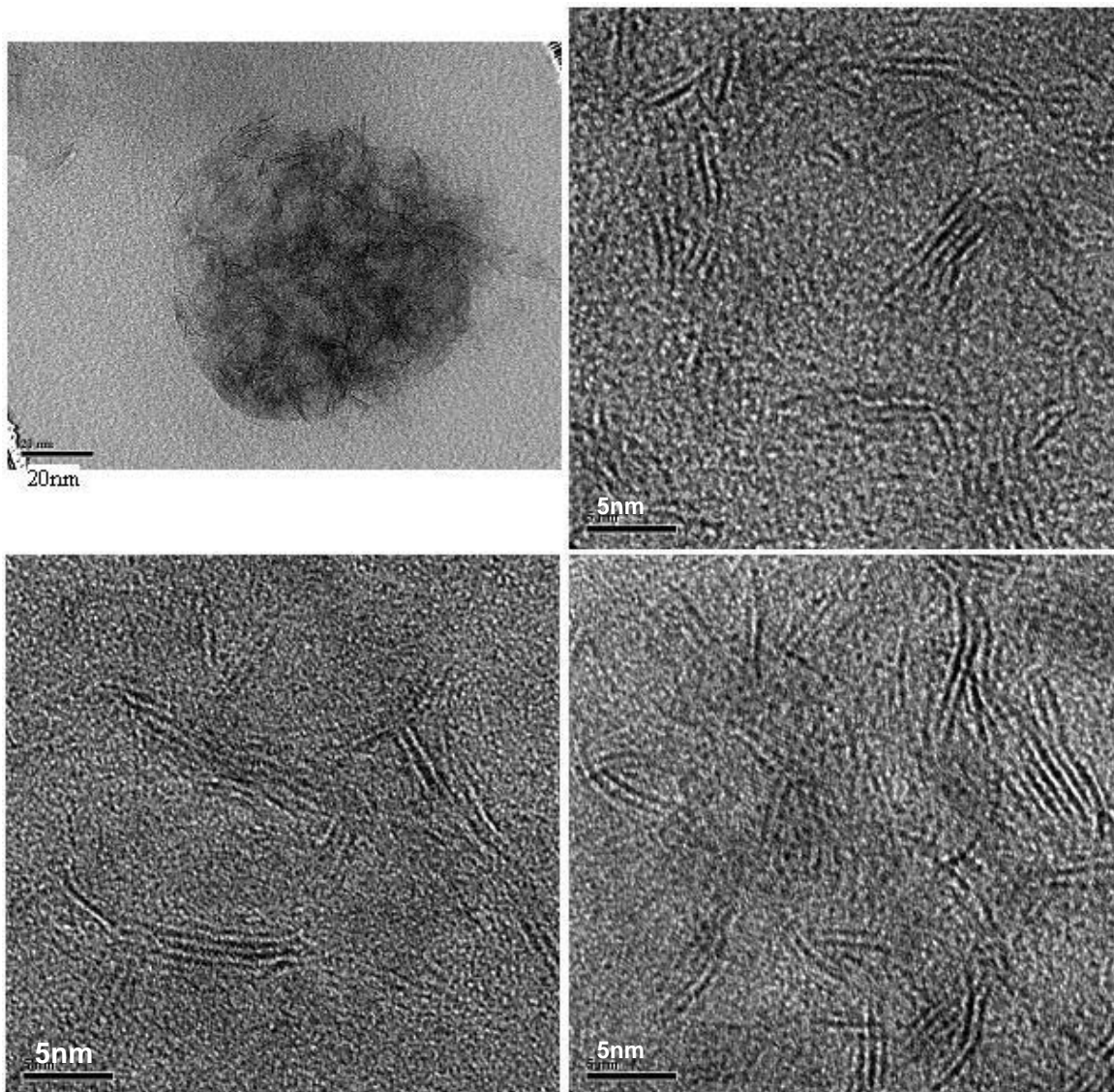


Fig. 4 - 6 HRTEM images of MoS₂ slabs collected from the organic phase, MoCO340.

Other conditions: 3.9-4.0g PMA, 25ml H₂O, 100ml toluene, no S-/N-containing compounds, 340°C, 200psi H₂S, 500psi CO.

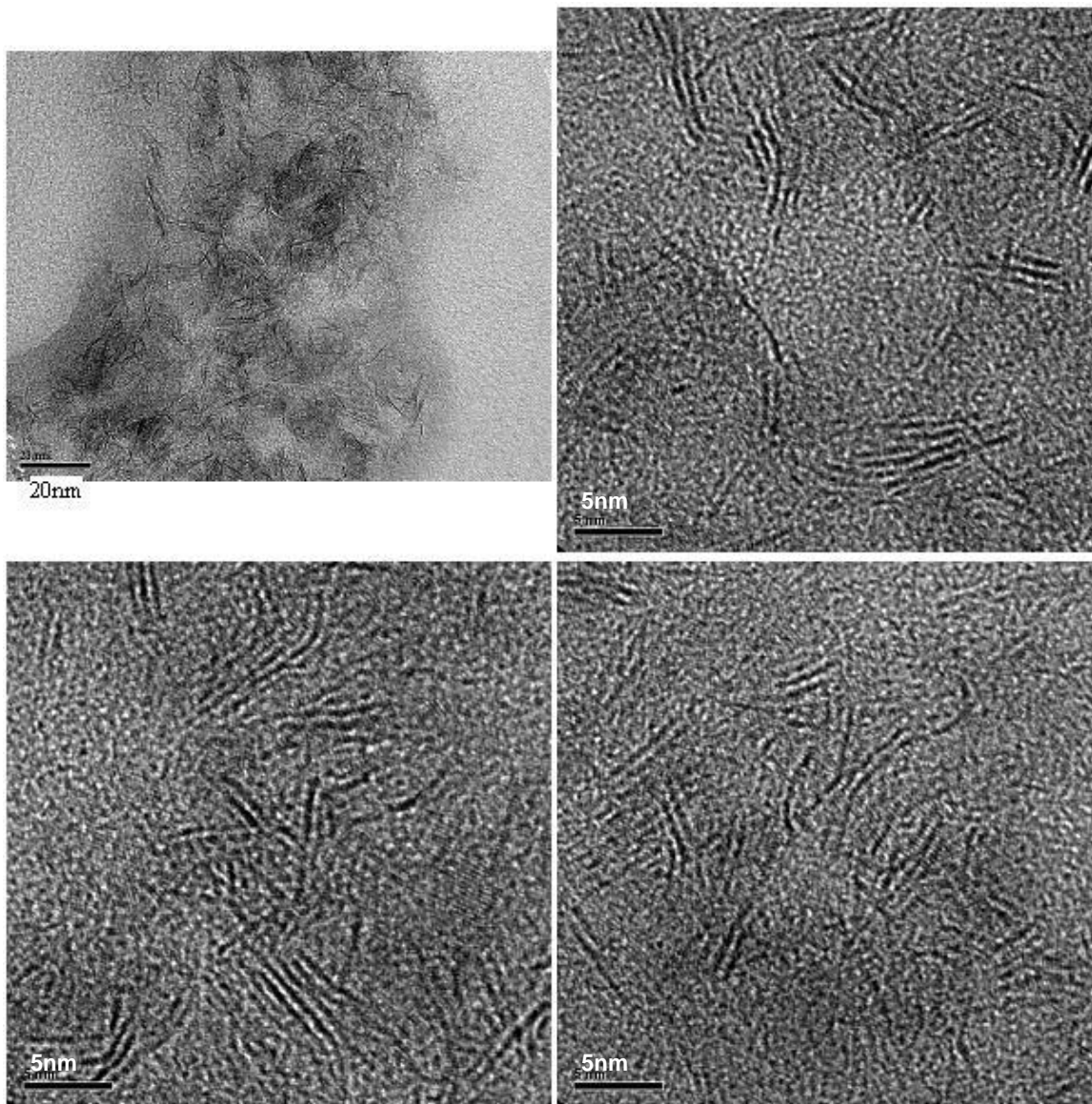


Fig. 4 - 7 HRTEM images of Wcat particles, MoCO340.

Other conditions: 3.9-4.0g PMA, 25ml H₂O, 100ml toluene, no S-/N-containing compounds, 340°C, 200psi H₂S, 500psi CO.

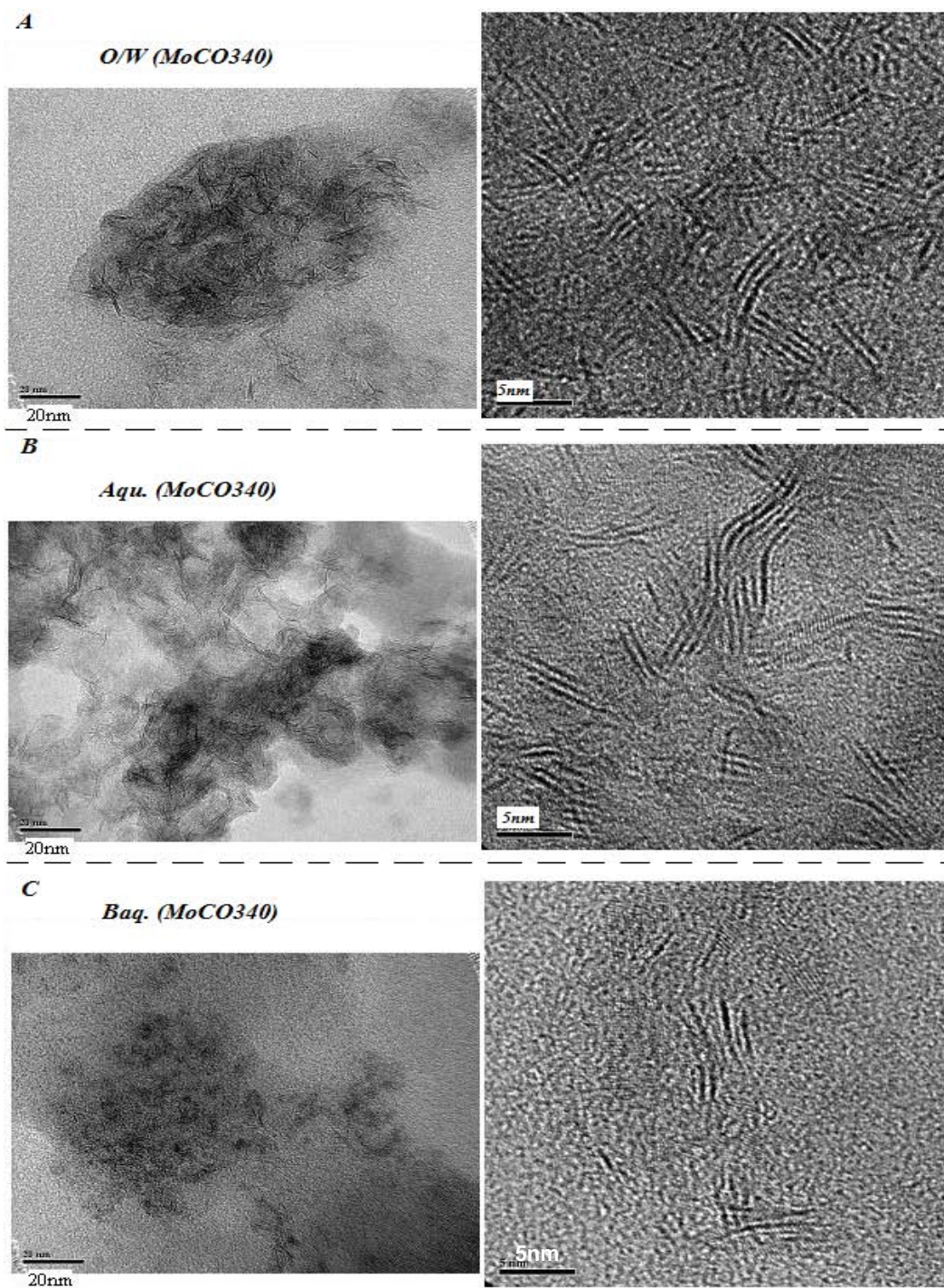


Fig. 4 - 8 HRTEM images of MoS₂ slabs dispersed in phases of (A) O/W, (B) Aqu., and (C) Baq, MoCO340.

Other conditions: 3.9-4.0g PMA, 25ml H₂O, 100ml toluene, no S-/N-containing compounds, 340°C, 200psi H₂S, 500psi CO.

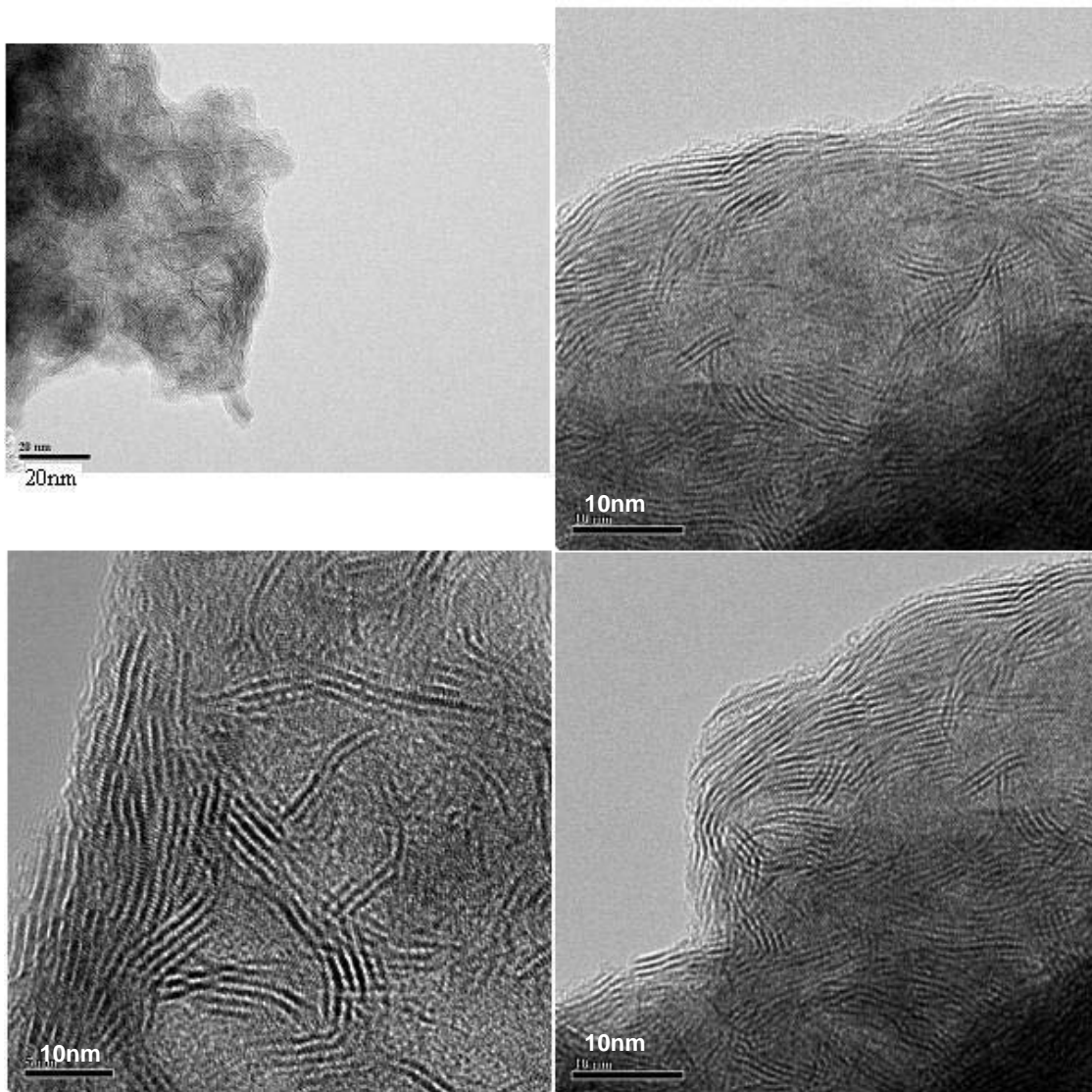


Fig. 4 - 9 HRTEM images of the MoS₂ slabs collected from the organic phase, MoH340.

Other conditions: 3.9-4.0g PMA, 25ml H₂O, 100ml toluene, no S-/N-containing compounds, 340°C, 200psi H₂S, 500psi H₂.

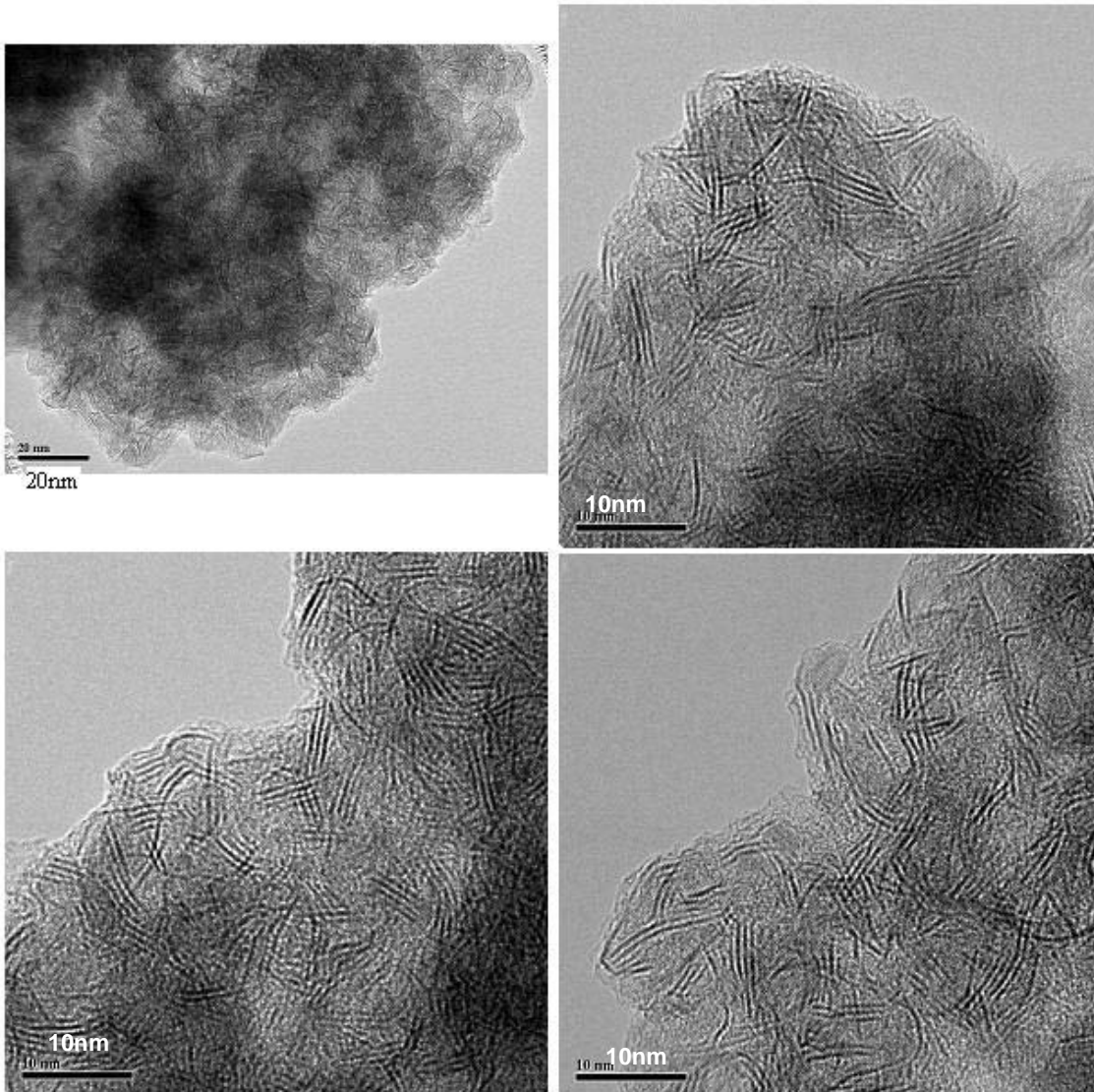


Fig. 4 - 10 HRTEM images of Wcat particles, MoH340.

Other conditions: 3.9-4.0g PMA, 25ml H₂O, 100ml toluene, no S-/N-containing compounds, 340°C, 200psi H₂S, 500psi H₂.

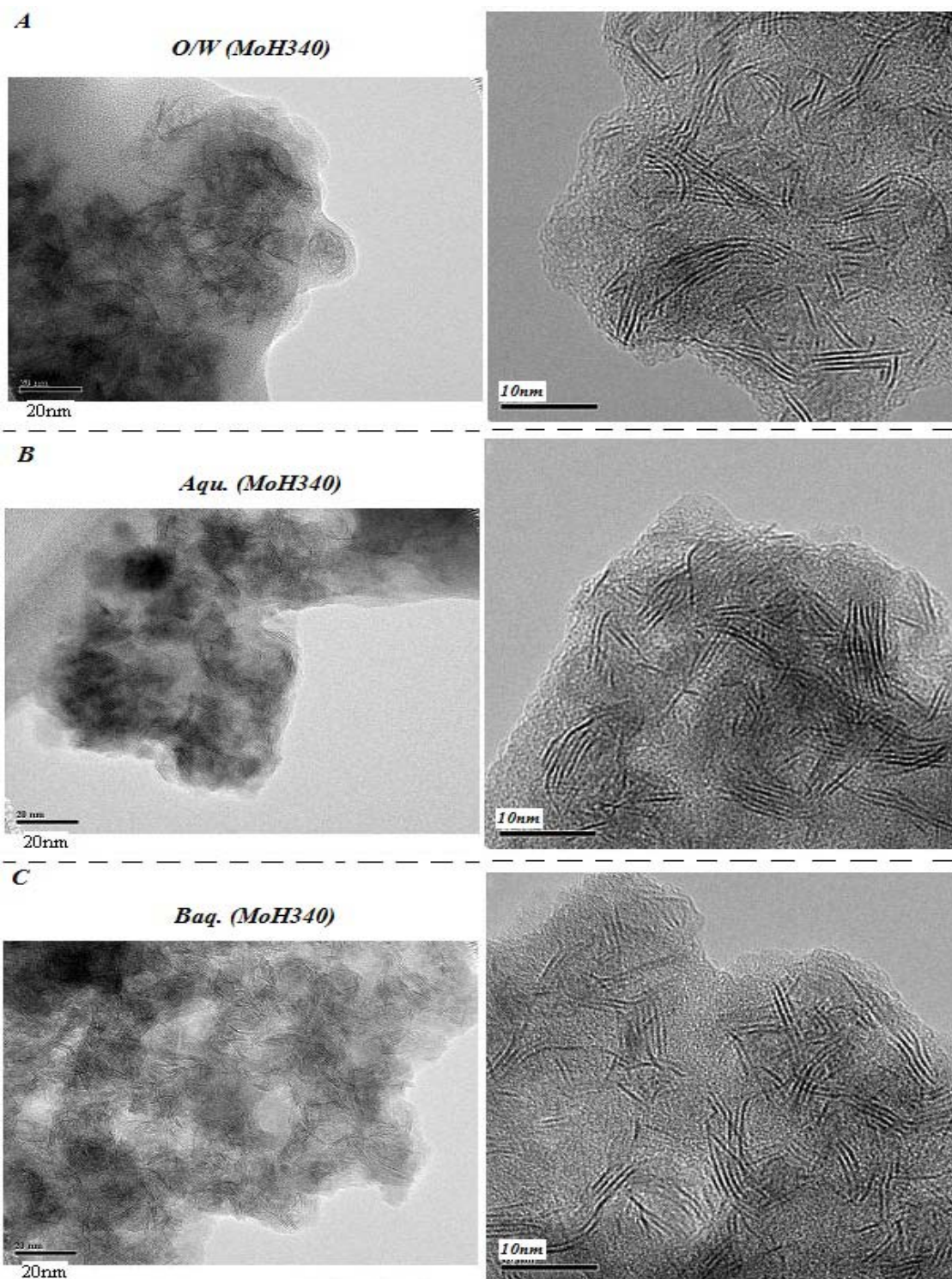


Fig. 4 - 11 HRTEM images of MoS₂ slabs dispersed in phases of (A) O/W, (B) Aqu., and (C) Baq, MoH340.

Other conditions: 3.9-4.0g PMA, 25ml H₂O, 100ml toluene, no S-/N-containing compounds, 340°C, 200psi H₂S, 500psi H₂.

MoS₂ slab length and stacking degree were determined *via* statistical analysis by measuring 480-650 MoS₂ slabs of each sample in HRTEM images. Average Mo sulfide crystalline slab length, \bar{L} , and average stacking number, \bar{N} , were calculated according to equations (4-1) and (4-2).

$$\bar{L} = \frac{\sum_{i=1}^n n_i L_i}{\sum_{i=1}^n n_i}, \quad (4-1)$$

wherein:

\bar{L} --- average length of the MoS slabs

L_i --- length of the i^{th} MoS slab

n_i --- number of the slabs with the length of L_i

$$\bar{N} = \frac{\sum_{i=1}^n n_i N_i}{\sum_{i=1}^n n_i}, \quad (4-2)$$

wherein:

\bar{N} --- average stacking number of the stacked MoS slab groups

N_i --- stacking number, equals to 1,2,3,...,n

n_i --- number of the stacked MoS slab groups with the stacking number of n_i

The average length and the average stacking degree of MoS₂ slabs dispersed in the five phases of the two candidate catalysts, MoCO340 and MoH340, are listed in Table 4-3. An example of the measurement and the calculation process of average MoS₂ slab length are given in Appendix D.

Table 4 - 3 Average crystalline length and average stacking degree of MoS₂ slabs dispersed in different phases of samples MoCO340 and MoH340*.

Phase**		Org.	Wcat.	Aqu.	O/W	Baq.
Average length, nm	MoCO340	4.5	4.7	5.4	3.9	4.3 [†]
	MoH340	8.2	5.8	6.1	6.7	5.8
Average stacking degree layers/group	MoCO340	2.7	2.9	3.0	2.8	2.4
	MoH340	5.8	4.4	4.4	4.4	4.3

*: Preparation conditions: 3.9-4.0g PMA, 25ml H₂O, 100ml toluene, no S-/N-containing compounds, 340°C, 200psi H₂S, 500psi CO (MoCO340) or H₂ (MoH340).

** : Average length and average stacking degree were calculated according to equations (4-1) and (4-2), respectively.

†: few MoS₂ slabs found in this phase (as shown in Fig. 4-8C)

For the sample of MoCO340 which was made using *in-situ* hydrogen, the statistic average length of MoS₂ slabs in each phase was in the range of 3.9-5.4 nm. Most MoS₂ crystal groups had 2-4 layers in each phase. It is worth to note that there were too few MoS₂ slabs observed *via* HRTEM in the Baq phase (Fig. 4-8C), hence, the statistic average numbers of this phase were not representative and they were listed just for reference. The order of the average MoS₂ slab length is listed as below:

$$\text{O/W (3.9 nm)} < \text{Org. (4.5nm)} \sim \text{Wcat. (4.7 nm)} < \text{Aqu. (5.4 nm)}$$

The distribution of counted MoS₂ sheets as a function of slab length with a one nanometer increment is illustrated in Fig. 4-12. In the organic phase, wherein hydro-treating reactions took place, there were 61% counted MoS₂ slabs distributed in the range of (2.0nm–4.9nm, Table 4-4). There were no slabs observed longer than 9.0 nm and more than 93% were shorter than 7.0 nm. The average MoS₂ slab length of Wcat particles was close to that of the MoS₂ sheets dispersed in the organic phase, while the slab length distributions in the two phases were different. Among Wcat particles, about 55% MoS₂ slabs had a length in the range of (2.0nm-4.9nm). There was about 1% longer than 14nm and less than 84% shorter than 7.0 nm. The latter number was almost 10% lower than that obtained in the organic phase. Therefore, when preparing dispersed Mo sulfide in *in-situ* H₂, the MoS₂ particles were dispersed in smaller sizes in the organic phase than those collected from the reactor vessel wall (Wcat).

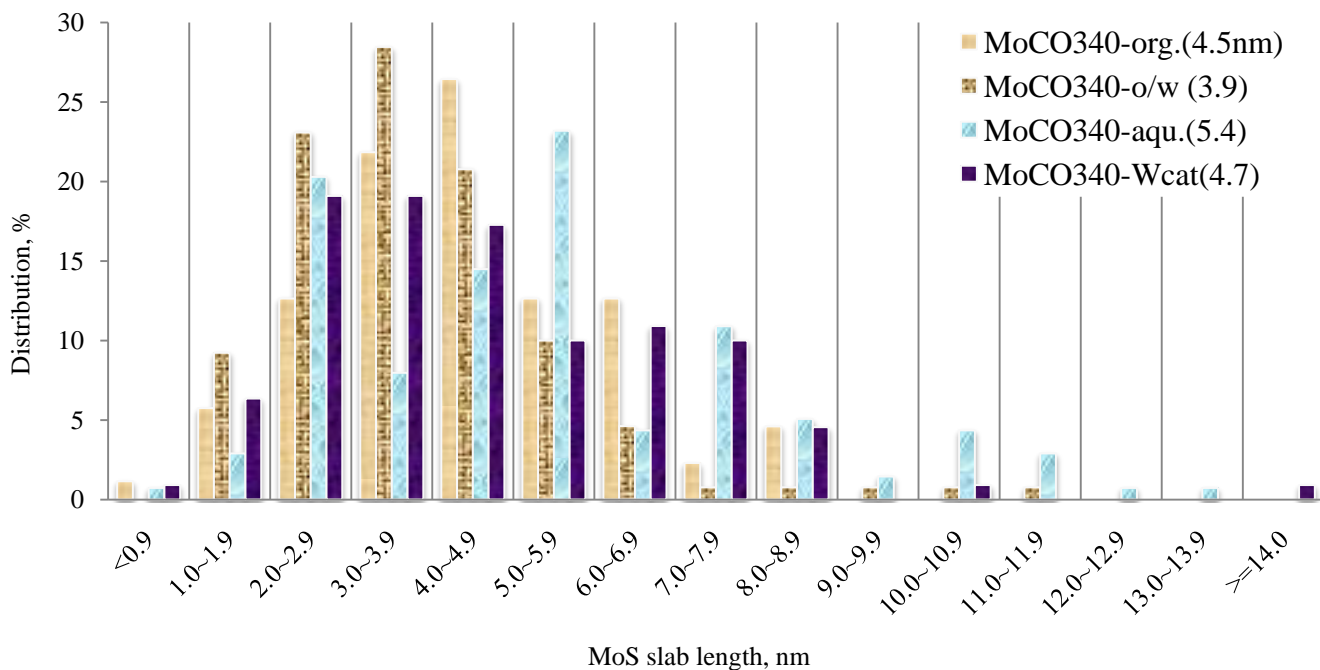


Fig. 4 - 12 Crystalline size distribution of the MoS₂ slabs dispersed in different phases (except the Baq phase) of the sample MoCO340, prepared at 340°C using *in situ* H₂

Table 4 - 4 Distribution of the length of MoS₂ slabs which dispersed in Org. and Wcat phases, catalyst samples of MoCO340 and MoH340 (more details available in Appendix C).

Length, nm	MoCO340		MoH340	
	Org.	Wcat	Org.	Wcat
<2.00	6.9%	7.3%	0.0%	0.0%
2.00-5.00	60.9%	55.5%	28.3%	48.2%
<7.00	93.1%	83.6%	56.5%	75.0%
<10.00	100.0%	98.2%	71.7%	94.1%
≥10.00	0.0%	1.8%	28.3%	6.0%

For the sample of MoH340 which was prepared in molecular hydrogen, the statistic average length and the statistic average crystalline stacking number of MoS₂ slabs in each phase were in the range of 5.8-8.2 nm and 4.3-5.8 layers/group, respectively. The average slab length of each phase (Table 4-3) increased in the order of:

$$\text{Wcat. (5.8 nm)} \sim \text{Baq. (5.8 nm)} < \text{Aqu. (6.1 nm)} < \text{O/W (6.7 nm)} < \text{Org. (8.2 nm)}$$

The MoS₂ slabs in the organic phase of MoH340 were much longer, straighter, and dispersed in larger stacking groups than those observed in the other four phases. In this phase, all MoS₂ slabs were longer than 2.0nm (Fig. 4-13). The MoS₂ sheets in the length range of (0-7.0nm) occupied 56% and there were more than 13% sheets longer than 14nm. In the phase of Wcat, 75% MoS₂ slabs were shorter than 7.0nm and 94% distributed in the range of (0-10.0nm). Hence, when preparing the catalyst in external supplied molecular hydrogen, the MoS₂ particles collected from reactor vessel wall, where most catalyst powders located, were shorter than those dispersed in the organic phase.

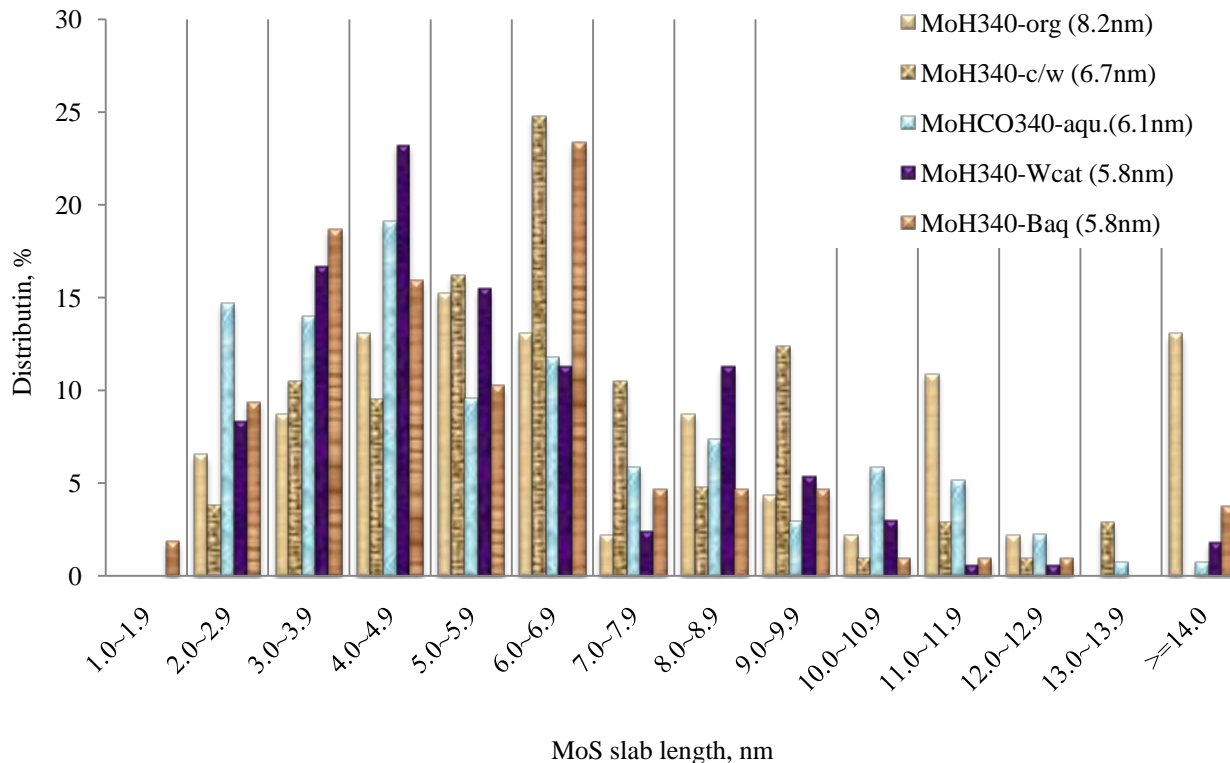


Fig. 4 - 13 Crystalline size distribution of MoS₂ slabs dispersed in different phases of the sample MoH340, prepared at 340°C using molecular H₂

4.3.3.2 HRTEM images of spent Mo sulfide catalysts in the presence of S-/N-species

The morphology of *in-situ* prepared dispersed Mo sulfide catalyst in *in-situ* H₂ in the presence of S-/N-species was characterized *via* HRTEM. The HRTEM images of these two samples are shown in Fig.4-14 and Fig.4-15. Compared to the HRTEM images of fresh prepared dispersed Mo sulfide catalyst, MoCO340, MoS₂ slabs were significantly longer and straighter after introducing S-/N-containing model compounds into the system. This observation was confirmed from statistic analysis results listed in Table 4-5. Both average slab length and stacking degree increased to different extents in all phases. Although the average MoS₂ slab length in the organic phase of SMOCO340 was the same as that of the

fresh catalyst, MoCO340, the average stacking degree increased by 0.6 layer/ group. The presence of nitrogen-containing compound, quinoline, led to more severe aging effect on the catalyst morphology than sulfur-containing compounds.

Table 4 - 5 Average crystalline length and stacking number of the MoS₂ slabs dispersed in different phases of samples MoCO340, SMOCO340 and NMOCO340*

Phase		Org.	Wcat.	Aqu.	O/W	Baq.
Average length, nm	MoCO340	4.5	4.7	5.4	3.9	4.3 [†]
	SMoCO340	4.5	5.5	7.3	5.6	4.6
	NMoCO340	6.0	5.8	6.1	6.5	5.2
Average stacking degree layers/group	MoCO340	2.7	2.9	3.0	2.8	2.4
	SMoCO340	3.3	3.7	4.0	3.3	3.2
	NMoCO340	3.8	3.8	3.3	3.3	3.8

*: Cat. preparation conditions: 3.9-4.0g PMA, 25ml H₂O, 100ml toluene, 200psi H₂S, 500psi CO, 340°C, 0.42g DBT and 0.50g 4,6-DMDBT for SMOCO340, 0.36g quinolone for NMOCO340, no S-/N-containing compounds for MoCO340.

[†]: few MoS₂ slabs found in this phase (as shown in Fig. 4-8C)

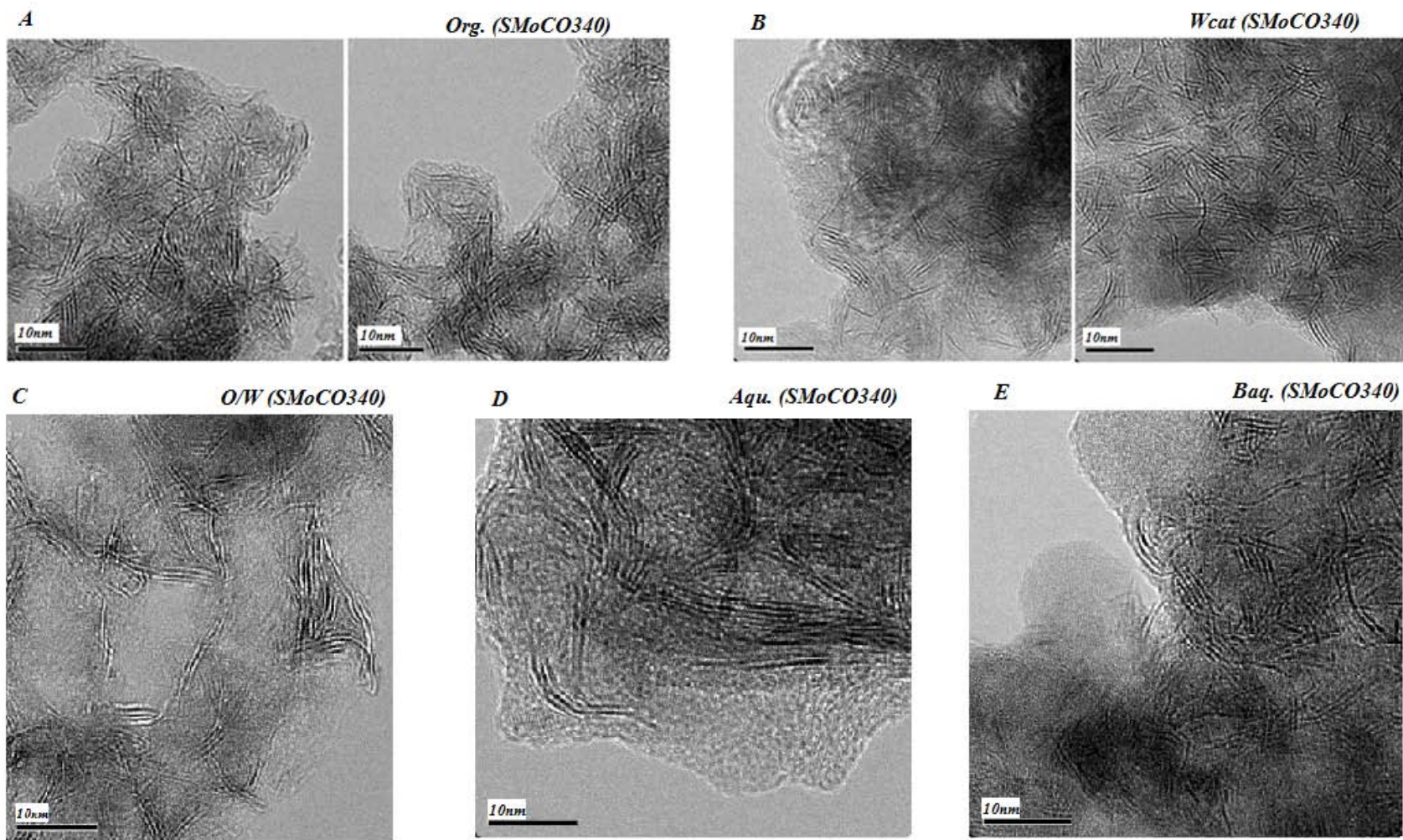


Fig. 4 - 14 HRTEM images of MoS₂ slabs in all phases of SMOCO340. A. Org., B. Wcat, C. O/W, D. Aqu., E. Baq.
 Preparation conditions: 3.9-4.0g PMA, 25ml H₂O, 100ml toluene, 200psi H₂S, 500psi CO, 340°C, 0.42g DBT and 0.50g 4,6-DMDBT.

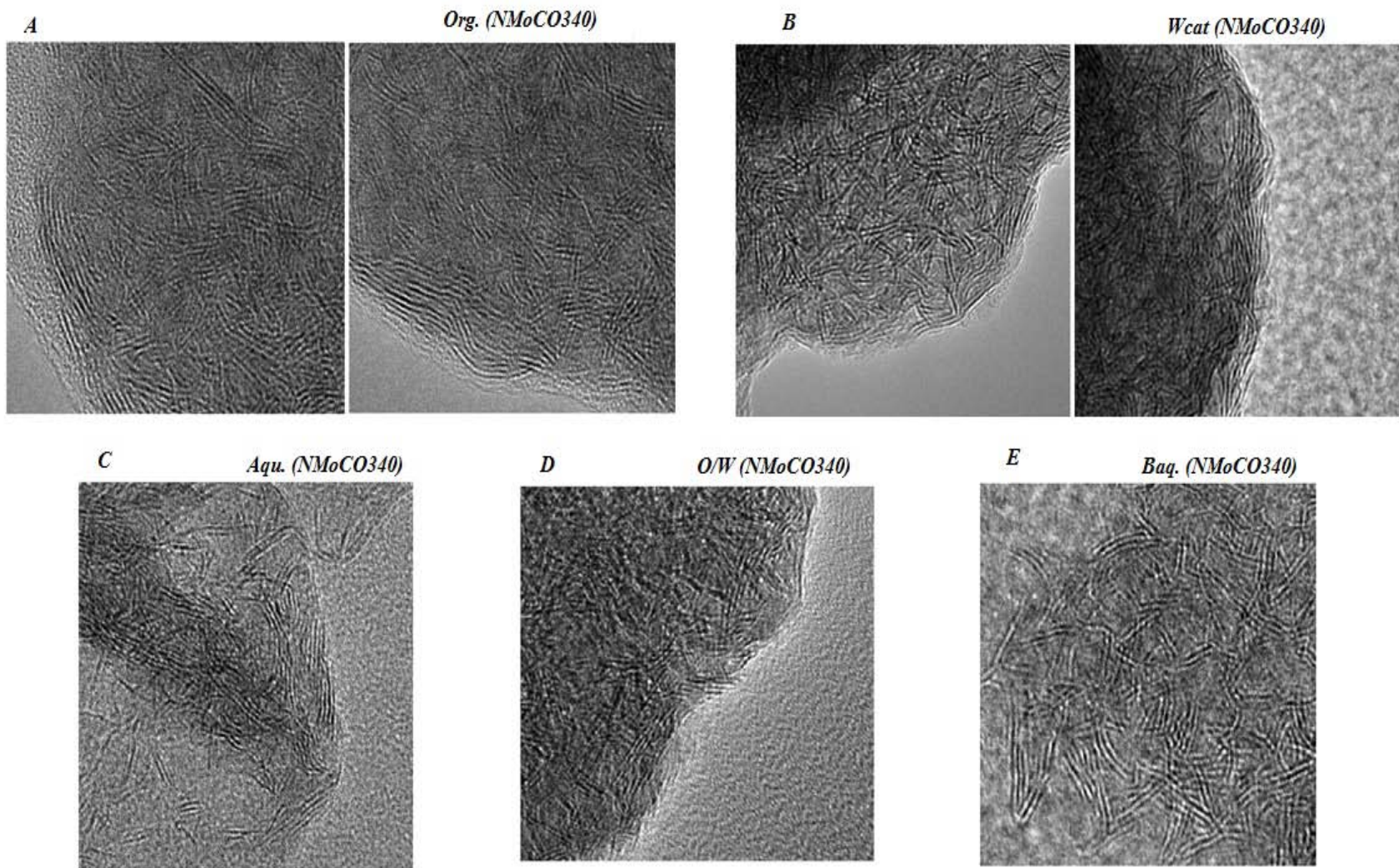


Fig. 4 - 15 HRTEM images of MoS₂ slabs in all phases of NMoCO₃₄₀. A. Org., B. Wcat, C. O/W, D. Aqu., E. Baq. Preparation conditions: 3.9-4.0g PMA, 25ml H₂O, 100ml toluene, 200psi H₂S, 500psi CO, 340°C, 0.36g quinolone

4.3.4 SEM morphology of MoS₂ particles

The stacked three-dimensional MoS₂ structure as shown in HRTEM images is composed by repeating the unit cell of two-dimensional trigonal prisms of S-Mo-S sandwiches along the hexagonal c-axis. However, such staked slab structure is not the final structure in which MoS₂ is present in the reaction system. The use of SEM could provide an insight into the real morphology of dispersed Mo sulfide catalyst. Most unsupported MoS₂ particles have been found to disperse in sphere shape and in uniform sizes as shown in SEM pictures (Fig. 4-16 and Fig. 4-17).

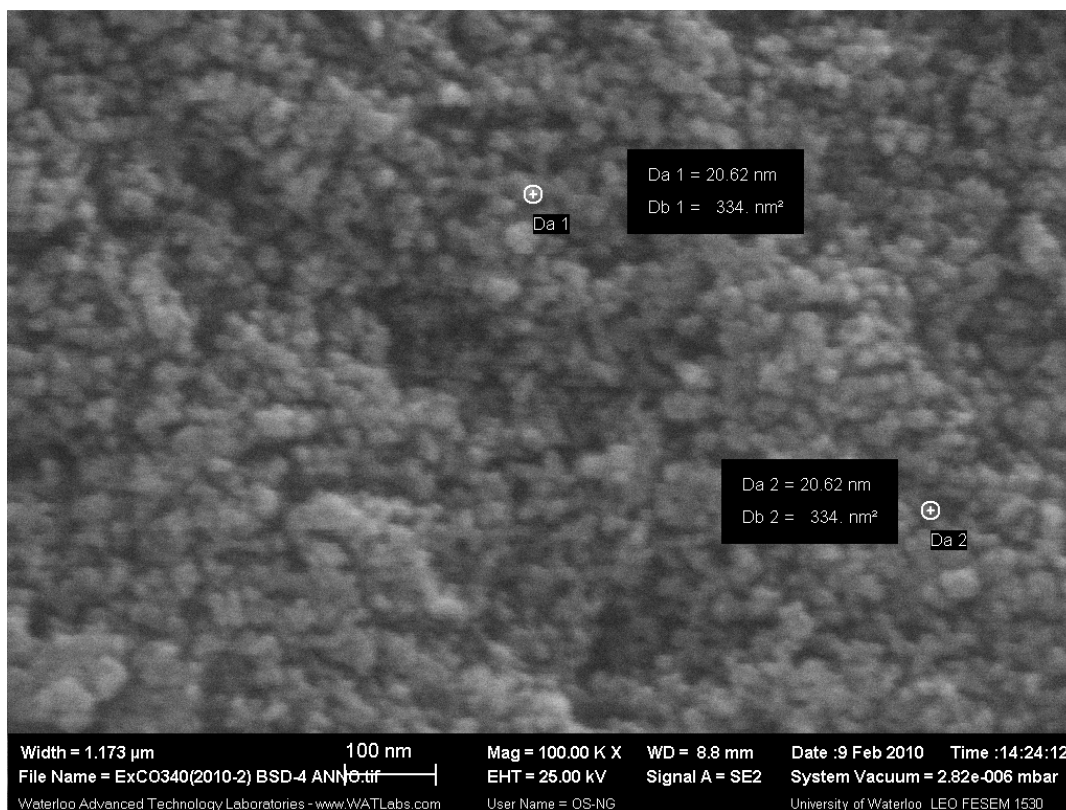


Fig. 4 - 16 SEM image of MoCO340 taken by the SE2 detector at the magnification of 100KX

The diameter of the dispersed Mo sulfide prepared in *in-situ* H₂ is about 20 nm (Fig.4-16), and the MoS₂ particle diameter of the sample prepared in molecular H₂ is around 30-40 nm (Fig.4-17). The larger SEM size than HRTEM statistic sizes indicated that MoS₂ particles were polycrystallines and were composed *via* the aggregation of small crystals.

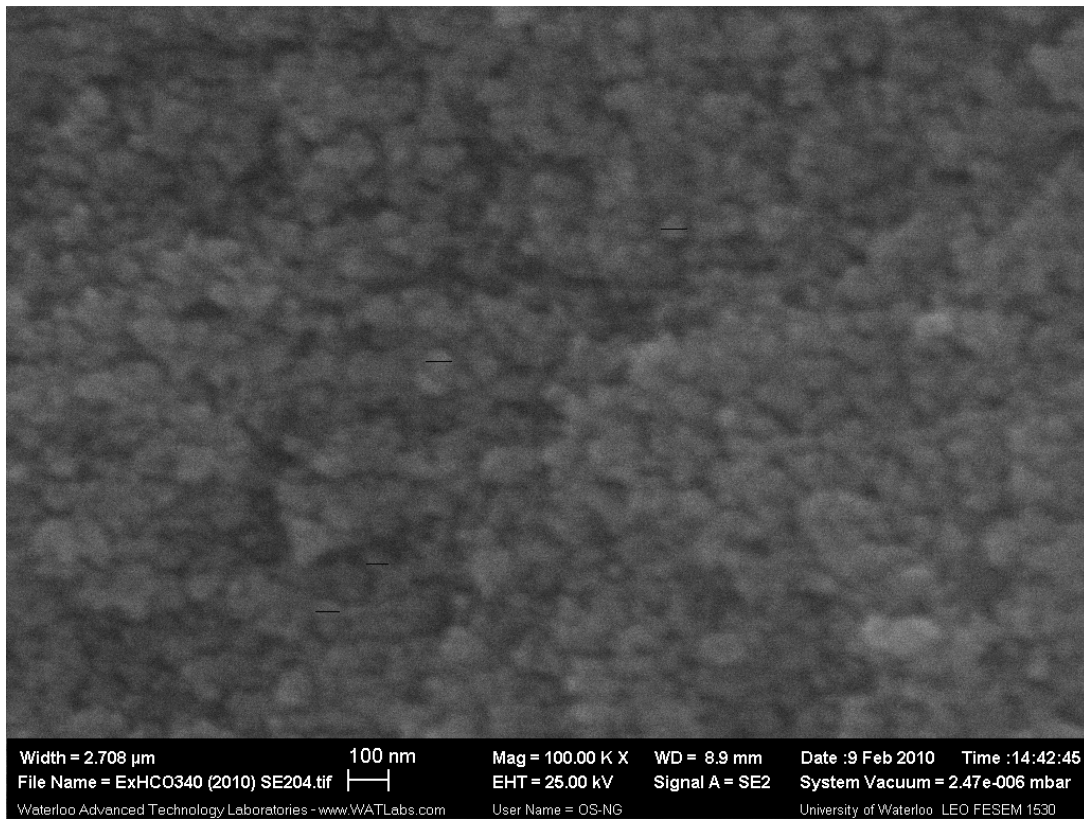


Fig. 4 - 17 SEM image of MoH340 taken by the SE2 detector at the magnification of 100KX

4.4 Discussion

4.4.1 Effect of H₂ sources on the preparation of dispersed Mo sulfide catalyst

As introduced previous chapters, CO was used as a new source of H₂ for hydro-treating reactions instead of expensive molecular hydrogen in our new bitumen upgrading technology. The *in-situ* hydrogen produced from CO *via* the water gas shift reaction was used in most reactions. To study the efficiency of *in-situ* hydrogen, molecular hydrogen was also used for comparison in the present study. Therefore, there are two hydrogen sources, *in-situ* hydrogen generated from CO and externally supplied molecular hydrogen. In this section, the effect of hydrogen sources on the physical properties of dispersed Mo sulfide catalyst will be discussed.

The BET surface area of the dispersed Mo sulfide catalyst prepared in molecular hydrogen was 60 m²/g lower than that made in CO. The BJH pore volume was also lower. This was attributed to the longer MoS₂ slab length and the higher stacking degree of MoH340 as shown in HRTEM images. It should be noted that in the organic phase of MoH340, the MoS₂ slabs were in high crystallinity with long, straight, and parallel crystal sheets, whereas the MoS₂ slabs of MoCO340-Org were short, curved and disordered. It has been concluded that well-crystallized MoS₂ particles do not have the necessary activity for hydro-treating reactions⁶³. Therefore, the bent and disordered morphology of MoS₂ slabs observed on HRTEM images would be more beneficial for high activity towards hydro-treating reactions. As modeled by Johnson D.C. *et al* *via* their correlation of NMR and ESR studies on HDS activities^{64,65}, pairing of Mo atoms were located at edge sites and single Mo atoms provide unpaired spins at the corners of particles. As a result, the catalyst particles were electronically conducting at the edges, which were considered

as active sites on MoS₂ slabs. This model has been demonstrated by Topsøe in their STM studies^{66,67}. Shorter MoS₂ length and smaller MoS₂ crystal stacks provide more corner and edge positions on the active phase. It was also recognized that these edge and corners were the active sites on the surface of MoS₂ particles for HDS and HDN reactions^{27, 68}. According to this model, the activity of the MoS₂ particles prepared using *in-situ* H₂ should have higher activity towards HDS reactions. The comparison between the HDS activities of the dispersed Mo sulfide catalysts prepared in the two hydrogen sources will be discussed in chapter 6.

However, the reason for the smaller MoS₂ clusters obtained in the case of CO is not clear. Mo (VI) in the precursor of PMA is reduced firstly to Mo (IV) and then activated *via* sulfidation. In the CO system, reductive hydrogen was *in-situ* generated *via* the water gas shift reaction, while, in the H₂ system, reductive hydrogen was externally supplied. The concentration of the reduction gas, hydrogen, in the H₂ system was much higher than that in the CO system. Therefore, the molecular H₂ reaction system provided a more constant reaction atmosphere for generating MoS₂ crystals and promoted the growth of the MoS₂ crystals, while in the CO system, the occurrence of water gas shift reaction and the low concentration of hydrogen may influence the growth of MoS₂ crystals. This may be one reason for the short, disordered, and bent MoS₂ slabs prepared in CO system. Although the amount of hydrogen in the CO system was lower than in the system with molecular H₂, it was enough to reduce Mo (VI) to Mo (IV).

D. Genuit *et al*⁶⁹, prepared unsupported sulfided molybdenum sulfided at 450°C *via* the solution decomposition of ammonium thiodimolybdate and they observed black MoS₂ slabs with 11 nm and 7 layers. The unsupported sulfided molybdenum catalyst prepared at 330°C by Iwata *et al*²⁶

dispersed as highly folded and bent MoS₂ slabs with the length longer than 10nm. These reported MoS₂ slabs were significantly longer than what obtained in the present study.

4.4.2 Effect of S-/N-containing compounds on the morphology of the dispersed Mo sulfide catalyst

In the presence of S-/N-containing compounds during the preparation of dispersed Mo sulfide catalyst, the BET surface area of the catalyst decreased significantly by 22% and 25% (Table 4-2), respectively. The statistical average MoS₂ slab length and the average stacking degree also increased significantly in all tested phases after consumed in HDS/HDN reactions. Therefore, we may expect the deactivation of the dispersed Mo sulfide catalyst after hydro-treating runs.

Generally, there are four main reasons for catalyst deactivation⁷⁰ during the hydro-treating of heavy oils:

- Sintering of the active phase at high reaction temperature leading to a decrease in dispersion;
- Active sites poisoned or blocked by strongly adsorbed species, such as coke;
- The pore structure of the catalyst blocked by coke deposition, resulting in the loss of pore volume and surface area;
- Metal decomposition on the catalyst surface.

The last possibility is not likely because we are using model compounds dissolved in toluene and water. Therefore, the adsorption of reactants on the catalyst surface and the deposit of coke produced from model compounds are the most possible reasons for the observed changes in the

morphology of dispersed Mo sulfide catalyst. As a result of coking, the catalyst sample NMoCO340 would have smaller catalyst surface area, which had been observed in the BET surface area characterization results as shown in Table 4-2.

It has been reported that adsorbed nitrogen-containing compounds may act as coke precursors⁷¹. Furimsky noted a marked increase in C/N ratio in the coke deposits compared to the feedstock, indicating preferential adsorption of nitrogen-containing species on the catalyst surface⁷². Satterfield *et al* observed that intermediates formed during the HDN of quinoline left some deposit on the catalyst surface⁷³. Hence, the nitrogen-containing compound, quinoline, caused more severe change in the morphology of the dispersed Mo sulfide catalyst than sulfur-containing compounds. This coke formation should be one reason for the inhibitive effect of nitrogen-containing compounds on HDS reactions, which will be reported and discussed later in Chapter 7.

As suggested by Daage and Chianelli³², the rim sites of the MoS₂ crystallines were the hydrogenation active sites, while the edge sites of “sandwiched” layers catalyzed the sulfur removal step. Therefore, the selectivity between the two reaction pathways, DDS over HYD, in HDS reactions should increase when using the catalyst with higher stacking degree. The HRTEM results obtained in the present study showed that the stacking degree of the MoS₂ crystalline slabs was different when prepared in different gas atmospheres, *in-situ* hydrogen and molecular hydrogen. Therefore, based on using the Daage and Chianelli proposal, the molar ratio of DDS/HYD in HDS reactions should be higher when using molecular hydrogen.

4.4.3 Element distribution in different phases

The application of EDX with HRTEM makes it possible to obtain information on elemental composition of a certain area of the catalyst sample, so that we could learn about elemental distribution and atomic composition of specific slab groups. Fig.4-18 is a typical EDX spectrum of a molybdenum sulfide sample. Besides sulfur and molybdenum, elements of copper and carbon derived from the carbon coated copper grid were detected. These four elements were expected to occur in EDX spectrum. However, some unexpected atoms were detected and the elemental distribution in different phases was found to be different.

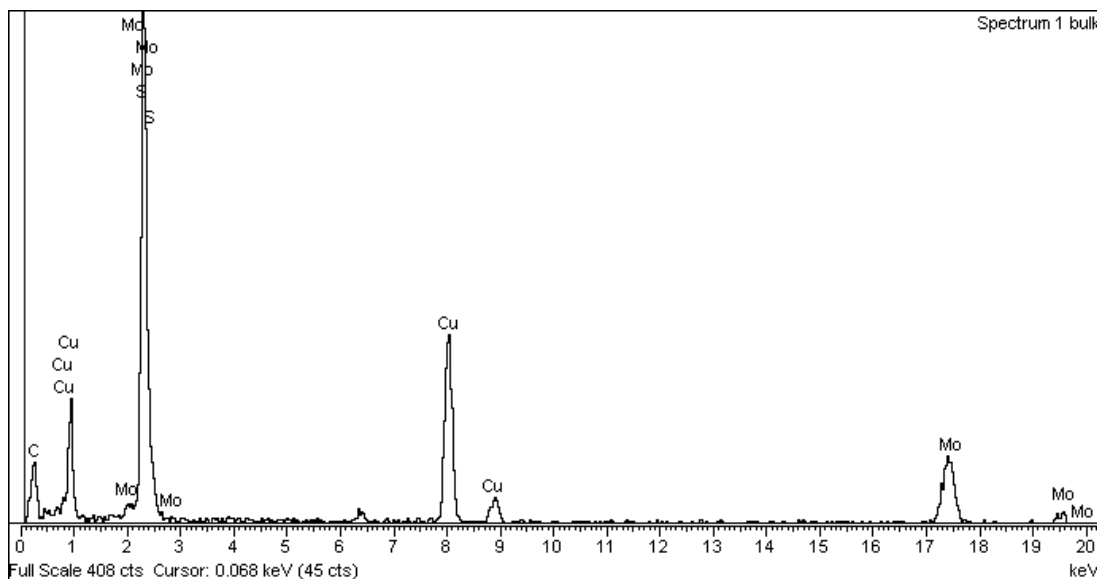


Fig. 4 - 18 A typical EDX spectrum of a Mo sulfide sample, SMOCO340-Org.

Cat. preparation conditions: 3.9-4.0g PMA, 25ml H₂O, 100ml toluene, 200psi H₂S, 500psi CO, 340°C, 0.42g DBT and 0.50g 4,6-DMDBT.

Elements detected by EDX in each phase of SMOCO340 are listed in Table 4-6 as an example. The EDX spectra of all characterized samples are given in Appendix D. Besides S, Mo, P, O, Cu, and C, Ni, Ca, K, Fe, and Si were also detected. Oxygen was considered to be derived from the air absorbed on the grid or on the catalyst surface. Phosphorus came from the molybdenum precursor, PMA. Ni, Ca, and K may be from the DI water or the contaminants left in the reactor vessel from previous experiments. The signal of Fe might be resulted from the corrosion of the reactor vessel. Si might derive from Moly-Kote[®]. It is interestingly to note that the black particles present at the bottom of the aqueous phase, the Baq phase, contained more elements than the other phases, and the catalyst particles in the organic phase and the Wcat particles were much cleaner. Since the organic phase is where HDS/HDN occurred, the unwanted contaminant elements would not cause significant effect on the experiment results. This also applies to the Wcat phase, which contained most catalyst particles.

Table 4 - 6 Elements detected *via* EDX from different phases (SMOCO340)*

Phase		Org.	Aqu.	O/W	Wcat.	Baq.
Elements contained (EDX characterization)		Cu,C,S, Mo	Cu,C,S, Mo,Fe,Co, O,Ca,Ni,Si, Os	Cu,S, Mo,Fe,O, P,Ca	Cu,C,S, Mo,Fe, O,P	Cu,S, Mo,Fe,O,P,Mn, Ni, Mg, Ca,K,Ti, Si, Cl
Atomic composition (EDX semi-quantitative analysis)	Mo	1	1	1	1	1
	S	1.29	2.16	1.59	1.69	1.81
	O	0.12	0.26	0.51	0.02	1.27
	(S+O)/Mo	< 2	> 2	< 2	< 2	> 2

*: Cat. preparation conditions: 3.9-4.0g PMA, 25ml H₂O, 100ml toluene, 200psi H₂S, 500psi CO, 340°C, 0.42g DBT and 0.50g 4,6-DMDBT.

If we set the atomic concentration of Mo as 1, the relative atomic concentration of S is listed in Table 4-6. As observed from HRTEM images, MoS₂ was found as the major component of the catalyst particles. Therefore, the atomic ratio of S/Mo should be around 2.0, but the data listed in the Table 4-6 showed that the S/Mo ratios in the Org., O/W, Wcat, and Baq phases were lower than 2.0. The highest S/Mo ratio, which was the only one higher than 2, was obtained in the aqueous phase, wherein the sulfidation reagent of H₂S present. This indicated that there was some Mo atom present in the catalyst system in a form other than MoS₂. This may be attributed to incomplete sulfidation of Mo during the preparation and partial oxidation of MoS₂ when preparing HRTEM samples. After adding sulfur and oxygen and then compared with Mo, it was found that still some excess Mo not in the form of sulfide or oxide in the phases except Aqu and Baq phases. Therefore, based on the EDX semi-quantitative analysis, some Mo was present in the form of atomic Mo in the organic phase and on the wall catalyst particles.

4.5 Conclusions

The characterization of the morphology of nano-sized catalyst particles dispersed in separate phases using HRTEM-EDX is an important contribution of this thesis. Combined with other characterization results, we may draw conclusions as follows:

- (1) As observed from HRTEM-EDX and XRD, MoS₂ was generated after the hydro-thermal decomposition of the Mo precursor in the presence of the sulfidation gas, H₂S.
- (2) MoS₂ with high surface area (>200 m²/g) was prepared in the present study. The sample made in the molecular hydrogen had lower surface area than the one prepared in *in-situ* hydrogen.

- (3) XRD spectra indicated that the MoS₂ prepared had low degree of crystallinity.
- (4) Smaller BET catalyst surface areas, longer MoS₂ sheets, and higher MoS₂ stacking degree were observed for the catalysts prepared in the presence of S- or N-species, probably due to the adsorption of reactants/products and the formation of coke on the catalyst surface. The deactivation of the dispersed catalyst in long-term HDS/HDN experiments is expected and basic quinoline may cause more severe deactivation than the refractory sulfur-containing compounds.
- (5) HRTEM images suggested that the morphology of the MoS₂ particles prepared in CO would be more active for hydro-treating reactions than that made in molecular H₂.
- (6) More contaminant elements were detected *via* EDX in the Baq phase, while in phases of Org. and Wcat, the element composition indicated that there were less metallic species.

Chapter 5 Simultaneous Hydrodesulfurization of Dibenzothiophene and 4,6-Dimethyldibenzothiophene

5.1 Introduction

There are two major adsorption modes of sulfur-containing model compounds on the catalyst surface in HDS reactions. One is σ -adsorption mode, wherein the molecule stands on the catalyst surface *via* the sulfur atom adsorbing on the active site. σ -adsorption is the predominant adsorption way of DBT molecules on the catalytically active sites and results in the direct desulfurization from the molecules and hence, DDS route is the major reaction pathway in the HDS of DBT⁸. The presence of the two methyl substituents at 4 and 6 positions adjacent to the heteroatom inhibits the access of the sulfur atom to the catalyst surface sites, so the adsorption of 4,6-DMDBT in the σ -mode is much weaker than that of DBT and direct sulfur-removal from the 4,6-DMDBT molecule is strongly suppressed.

The other adsorption mode is π -adsorption mode. During HDS, the flat 4,6-DMDBT molecule has more possibility to be adsorbed on the active sites with the aromatic rings parallel to the catalyst surface, in which way the π -electron clouds of aromatic rings binding to the active sites and results in the hydrogenation of the sulfur-containing molecule. The hydrogenation of aromatic rings leads to a flexible cyclohexyl ring, and then the sulfur atom has more access to the σ -bonding of sulfur atom to the active sites. Therefore, the HYD pathway is the major route in

the HDS of 4,6-DMDBT. The electron-donating effect of the two methyl groups makes the hydrogenation reaction in the HDS of 4,6-DMDBT even faster than that of DBT⁸.

It should be noted that Koltai *et al*⁷⁴ suggested a dihydro-intermediate of DBT or 4,6-DMDBT was produced as the first step in HDS reactions. This dihydro-intermediate was unstable and could be transformed *via* the two pathways, DDS and HYD, on similar catalytic sites by further hydrogenation to produce tetrahydro- and hexahydro- intermediates or by desulfurization according to an elimination mechanism resulting in biphenyl derivatives.

To elucidate the HDS reaction mechanism and the two different reaction pathways in details, Topsøe's group^{33-35, 75,66,76} characterized the active nanostructures and tried to identify the specific active sites involved in HYD and DDS pathways using scanning tunnelling microscopy (STM), density functional theory (DFT), and high-angle annular dark-field scanning transmission electron microscopy (HAADF-STEM). The morphology of single-layer MoS₂ nanoclusters weakly supported on a Au(111) surface was observed in large-scale STM images under different sulfidation gas atmospheres³⁴. It was found that under highly sulfiding conditions (H₂S:H₂=500), a triangular shape was the stable form of MoS₂ nanoclusters, while when using more reducing conditions (H₂S:H₂=0.07), a hexagonal morphology emerged instead of the triangular shape. Therefore, the stable shape of MoS₂ clusters seemed sensitive to the sulfidation gas atmosphere. They also found that truncated hexagons had an edge elimination (the sulfur edge), which was completely absent in the triangular MoS₂ structure (as shown in Fig. 5-1). Namely, the triangular MoS₂ nanoclusters generated under highly-sulfiding conditions were terminated by fully saturated Mo edges, whereas the hexagonal clusters exposed two types of

edges, Mo edges covered with S monomers and fully S-saturated sulfur edges with H atoms adsorbed (S-H groups), which was believed to be important in HDS as a source of reactive hydrogen atoms. The sulfur vacancies on the catalyst surface are considered as the active sites for sulfur removal, which is an important reaction step in the DDS pathway and is the final step in the HYD reaction route.

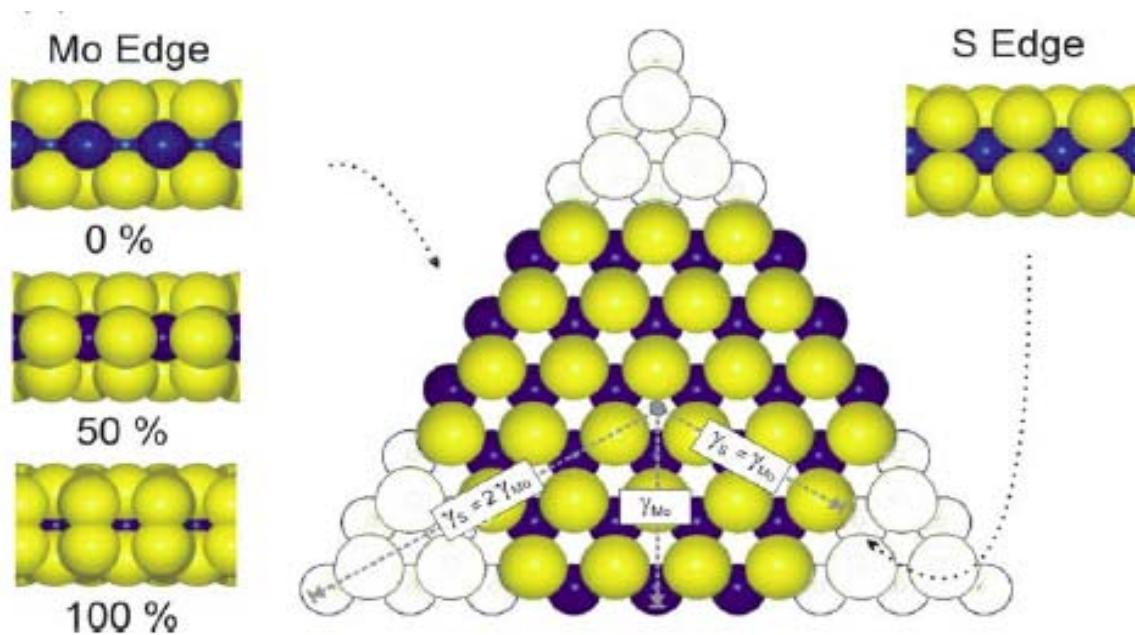


Fig. 5 - 1 Atomic ball model showing a hypothetical, bulk-truncated MoS₂ hexagon exposing the two types of low-index edges, the S edges and Mo edges³⁴ (blue: Mo; yellow: S). License number for reusing this figure from Elsevier: 2531641409788.

It is well known that the addition of Ni and/or Co into the MoS₂ would increase the reactivity of the catalysts. As a promoter, only a small fraction of Co or Ni relative to Mo is needed. A key discovery in the study of Co/Ni promoted Mo catalysts was reported by Topsøe *et al*⁶⁰ who proposed and identified the CoMoS/NiMoS structures, when they applied *in-situ* Mössbauer Emission Spectroscopy technique in the study of supported/unsupported Mo sulfide catalysts.

Via extended X-ray adsorption fine structure study (EXAFS), they observed Co atoms located in the same plane as Mo atoms with shorter Co-S distance than Mo-S in the MoS₂ phase. The presence of Ni/Co enhanced the C-S bond cleavage activity of the catalyst *via* weakening the metal-sulfur bond and increased the electronic density on the sulfur atoms¹⁷.

In the previous work of our group⁴², Co and Ni was added into the dispersed Mo sulfide catalysts, respectively. The characterization of the promoted Mo catalysts has shown that Co/Ni existed not only on the outer surfaces of the catalysts, but also in the bulk phase. The catalytic activity towards the HDS of DBT was enhanced significantly with the presence of Ni, while the selectivity between the two HDS pathways kept at a similar level. However, the promotional effect of Co on the HDS of DBT using *in-situ* hydrogen was not as significant as Ni, and the conversion of DBT was even a little lower than using MoS₂.

The traditional and currently commercially used WGS catalyst is CuO-ZnO-Al₂O₃ catalyst, which has high activity towards WGS at low reaction temperatures²⁰. However, it is not tolerant to sulphur or oxygen and so it could not be applied in treating oil fuel feed stocks. Many researcher have found that potassium promoted sulfided (Ni)Mo catalyst has high activity towards the WGS reaction and is active in the presence of sulfur and oxygen^{18, 20, 77}.

In the present chapter, the reaction pathways for the HDS of 4,6-DMDBT in a mixture with DBT will be studied. The effect of Ni and K on HDS will also be studied. The following topics will be discussed:

- WGS reaction in the presence of S model compounds at different reaction temperature
- Identification of HDS products of 4,6-DMDBT
- Kinetics calculation
- The effect of Ni and K on WGS and HDS

5.2 Experimental

Detailed experiment process has been described in Chapter 2 and will not be repeated here. The experimental conditions are listed in Table 5-1.

Table 5 - 1 Detail reaction conditions of the experiments involved in Chapter 5[†]

Experiment ID		Reaction temp., °C	Reactant gases, psi			Reaction time, min	Active metal precursor	$\frac{Ni}{Mo}$ molar
			CO	H ₂	H ₂ S			
Reaction temperature	DS0905*	330	590	0	10	180	PMA	---
	DS0906*	350	590	0	10	180	PMA	---
	DS0907*	380	590	0	10	180	PMA	---
	DS0908*	400	590	0	10	180	PMA	---
Effect of Ni on HDS [‡]	NiS-01	380	590	0	10	60	Mo: PMA Ni: NiSO ₄	0.5
	NiS-02	380	585	0	15	60	Mo: PMA Ni: NiSO ₄	0.5
	DM-65	380	590	0	10	60	PMA	---
Effect of K on HDS	WG-08	380	590	0	10	250	PMA	---
	WG-09	380	590	0	10	270	PMA K ₂ CO ₃	0.4 ^{††}
	WG-10 ^{‡‡}	380	590	0	10	195	K ₂ CO ₃	---
	DSK-01	380	590	0	10	60	PMA K ₂ CO ₃	0.4 ^{††}

[†]: other common conditions: 10 ml H₂O, 100ml toluene, 0.5g 4,6-DMDBT, 0.42g DBT, 430-500ppmw Mo (0.4 mmol Mo)

* run in the HC reactor, others (not starred) were run in the SS reactor

[‡]: Ni+Mo=0.4 mmol

^{††}: K/Mo=0.4, K+Mo=0.4mmol, no S-containing compounds present

^{‡‡}: K=0.4mmol, no S-containing compounds present

5.3 Identification of HDS products of 4,6-DMDBT

The identification of HDS products derived from the HDS of DBT was reported in the previous work done by Lee⁴², hence, in this thesis, the identification of products was focused on the HDS of 4,6-DMDBT. The Varian CP-3800 GC, which was configured with three detectors, can be used to help identify HDS products. The peaks present on the FID chromatographs but not on the PFPD chromatograph are sulfur-removed products of DBT/4,6-DMDBT. GC chromatographs obtained by FID and PFPD are shown in Fig. 5-2.

Reagents of 4,6-DMDBT, 2,8-DMDBT, and 3,3'-DMBP were purchased from Sigma-Aldrich, so these three peaks were identified simply by the injection of standards. The sulfur-removed products were initially separated from the sulfur-containing products *via* comparing FID *versus* PFPD chromatographs (Fig. 5-2). Further identification of unknown products was completed using a gas chromatography-mass spectroscopy (GC-MS) system (Varian GC-CP3800/MS-Saturn 2000).

It was reported that the isomerization of 4,6-DMDBT occurred before the HDS step and the peaks of its isomers, such as 2,4-DMDBT and 1,4-DMDBT, were located after that of 4,6-DMDBT in the GC chromatograph⁶⁹. One (39.9 min) of the two peaks after 4,6-DMDBT merged on the PFPD chromatograph (Fig. 5-2), had been identified as 2,8-DMDBT *via* standard reagent. The other peak (40.2 min) was indicated to have the same molecular weight and similar molecular structure as 4,6-DMDBT as suggested by GC-MS. Hence, it was identified to be another isomer of 4,6-DMDBT. Due to the isomerisation of 4,6-DMDBT, many isomers of the downstream products *via* the both reaction pathways had been observed.

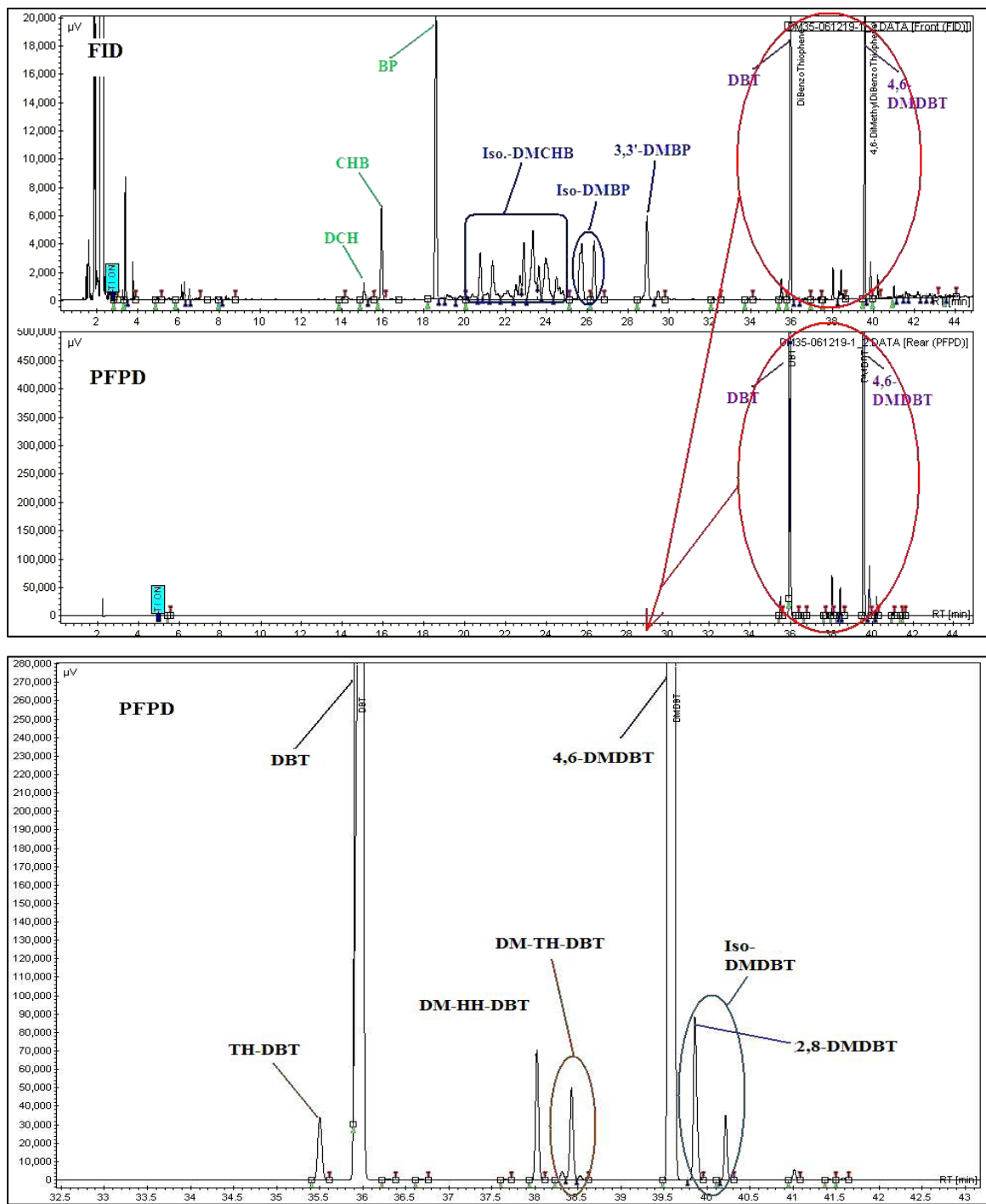


Fig. 5 - 2 Varian CO-3800 gas chromatograph of HDS products of DBT and 4,6-DMDBT, detected *via* FID and PFPD (GC method given in Appendix B).

Besides 4,6-DMDBT and its isomers present in the PFPD chromatograph, more peaks were detected between the retention times of DBT and 4,6-DMDBT. As suggested by GC-MS, the three peaks closer to 4,6-DMDBT at 38.35 min, 38.46 min, and 38.56 min were dimethyl-tetrahydro-dibenzothiophene (DM-TH-DBT) and the peaks before (including) 38.06 min were 4,6-dimethyl-hexahydro-dibenzothiophene (DM-HH-DBT). Detailed GC retention time of each component is listed in Table 5-2.

These identification results indicated that the same HDS products of DBT and 4,6-DMDBT were obtained in the present study using *in-situ* H₂ over dispersed Mo sulfide catalyst as those reported using supported catalysts^{8, 78}.

The determination of concentrations of HDS products was carried out *via* external calibration of each component detected in products. The GC response factors of the peaks whose standards available from markets were calculated from the slopes of external calibration curves. Iso-DMDBT and iso-DMBP were assumed to have the same GC response factors as 4,6-DMDBT and 3,3'-DMBP, respectively. The calibration curves and detailed component concentration calculation process are given in Appendix B.

Table 5 - 2 GC retention time of HDS products of DBT and 4,6-DMDBT (Varian CP-3800)[†]

Group	Component	Detector	Retention time, min	Identified by
Starting model compounds	DBT	FID/PFPD	35.85	Standard
	4,6-DMDBT	FID/PFPD	39.50	Standard
HDS products of DBT	DCH	FID	15.46	Standard
	CHB	FID	15.80	Standard
	BP	FID	18.46	Standard
	TH-DBT	FID/PFPD	35.50	GC-MS
HDS products of 4,6-DMDBT	DMCHB	FID	20.70-24.74	GC-MS
	3,3'-DMBP	FID	28.90	Standard
	Iso-DMBP	FID	25.65, 26.25, 29.37	GC-MS
	DM-HH-DBT	FID/PFPD	32.11, 34.18, 36.24-38.05	GC-MS
	DM-TH-DBT	FID/PFPD	38.27, 38.39, 38.48	GC-MS
	Iso-DMDBT	FID/PFPD	39.90, 40.14	Standard/GC-MS

[†]: each component has the same retention time ($\pm 2\%$) on the chromatographs obtained via different detectors.

5.4 Results and discussion

In this section, experimental results will be reported. A kinetics model will be proposed and used to calculate pseudo-first-order reaction rate constants for the conversion of starting materials and for the two reaction pathways. Then, the simultaneous HDS of DBT and 4,6-DMDBT over the dispersed Mo sulfide catalyst using *in-situ* H₂ under different reaction temperature will be

discussed. Additionally, the effect of promoters, Ni and K, on the HDS activity of both model sulfur-containing compounds will also be investigated in this chapter.

5.4.1 Water gas shift reaction

Since the *in-situ* hydrogen is produced *via* the WGS reaction from CO, the effect of reaction temperature on the WGS reaction is studied firstly before discussing the HDS of DBT and 4,6-DMDBT. Concentrations of WGS gases, CO, CO₂ and *in-situ* H₂, at different reaction temperatures are shown in Fig. 5-6.

As the heating rate in all experiments was the same, the heating time was longer in the experiment running at higher temperature. Hence, at higher reaction temperatures, there was more time allowing CO be converted to *in-situ* hydrogen *via* the WGS reaction, resulted in less initial concentration of CO and more initial amount of H₂ as shown in Fig. 5-3.

The concentration of *in-situ* hydrogen increased initially and stayed in the range of 30-40mol%. At high reaction temperature of 380°C and 400°C, the concentration of *in-situ* hydrogen decreased slightly at the end of the reaction while the amount of CO₂ kept increasing due to the consumption of hydrogen in HDS reactions. This is also the reason for lower concentration of *in-situ* hydrogen than that of CO₂ during the reaction.

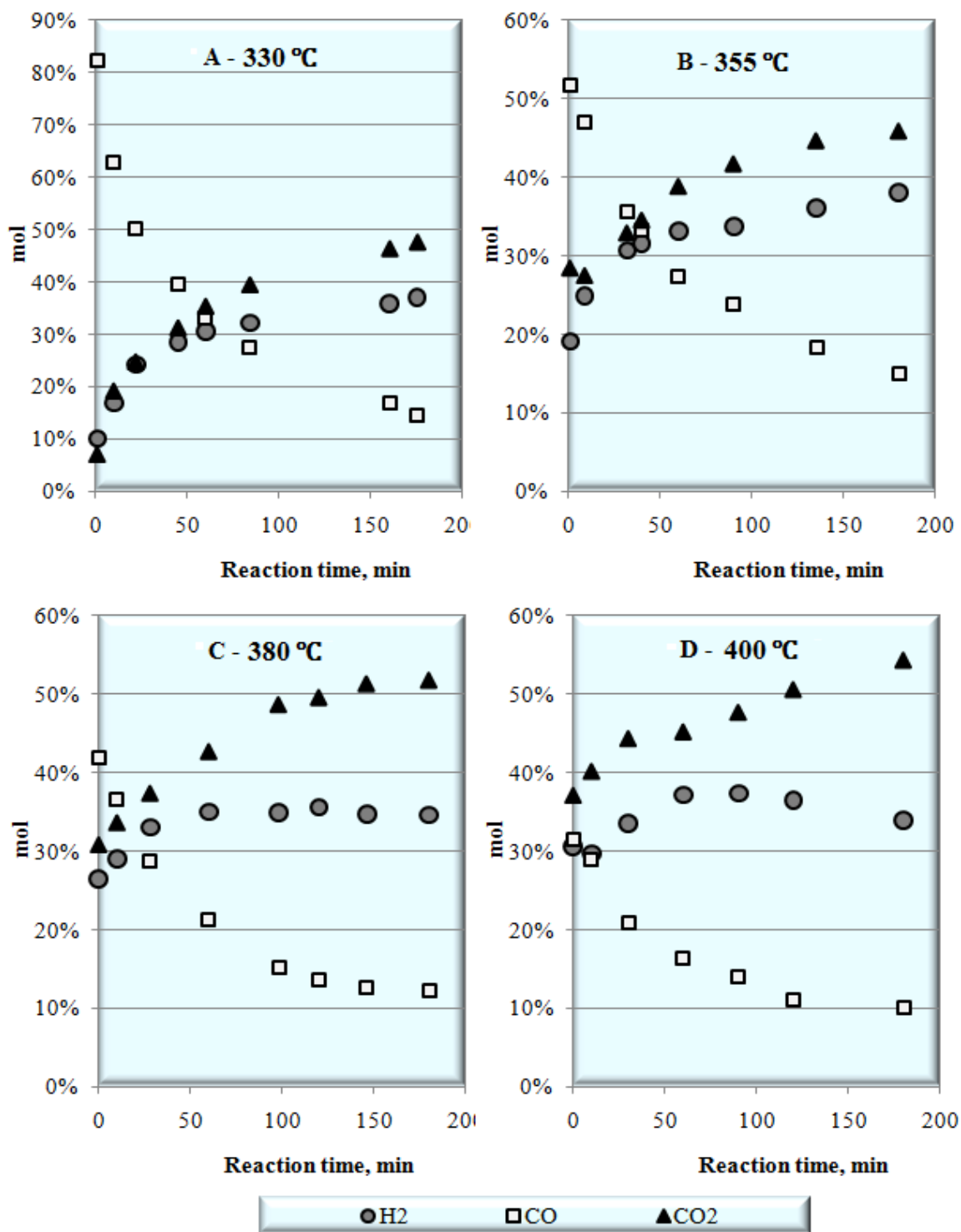


Fig. 5 - 3 Major WGS gas concentrations and the conversions of CO as a function of the reaction time at different reaction temperature: A: 330°C, B: 350°C, C: 380°C, D: 400°C.

Other conditions: HC reactor, equi-molar DBT and 4,6-DMDBT, 1600~1800 ppmw S in total, 400~450 ppmw Mo, S/Mo~10/1, 10 ml H₂O, 100 ml toluene, 590 psi CO mixed with 10 psi H₂S.

As suggested by Newsome¹⁹, water gas shift reaction was an exothermic reaction and the equilibrium constant K_{eq} could be estimated *via* equation (5-1), which could be used in the temperature range of 315 °C to 480 °C. According to this proposal, when running HDS reactions at different temperature, the equilibrium concentration of *in-situ* H₂ should be lower at higher reaction temperature.

$$K_{eq} = \exp\left(\frac{4577.8}{T} - 4.33\right) \quad (5-1)$$

However, the gas composition observed in the present study at different reaction temperature had shown that the concentration of *in-situ* hydrogen was stable in the range of 30-40mol% at all reaction temperatures except the lowest one, 330°C. This is not in accordance with the estimation (Eq. (5-1)), probably due to the higher consumption of *in-situ* H₂ in the simultaneous HDS reactions of DBT and 4,6-DMDBT at higher reaction temperature, which pushed the equilibrium to the right side of Eq.(1-1) and resulted in a higher CO conversion in the WGS reaction. The slow reaction rate, low consumption of *in-situ* hydrogen and shorter heating time at the lowest reaction temperature, 330°C, contributed to the low concentration and slow increasing of *in-situ* hydrogen with extending the reaction time.

5.4.2 HDS kinetics modeling

The equation of the HDS reaction of DBT is given in Eq.(5-2).



The rate constant of the HDS of DBT is determined by the concentration of DBT and the partial pressure of hydrogen as shown in Eq.(5-3):

$$r_{DBT} = k_{(DBT\ Conv.)} \cdot C_{DBT} \cdot p_{H_2} \quad (5-3)$$

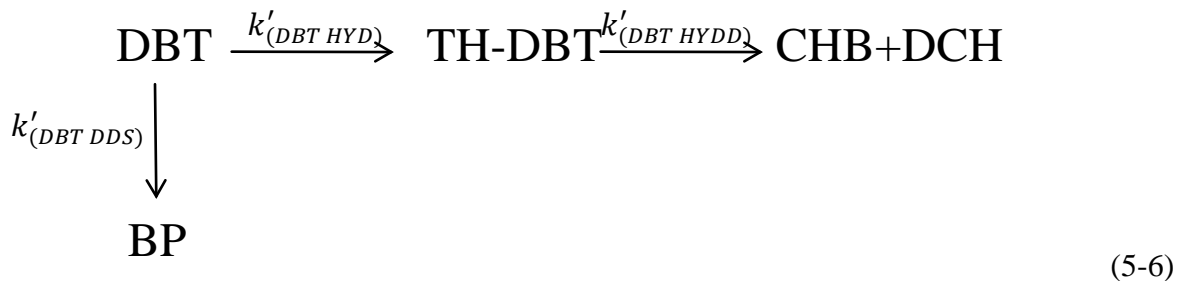
Since the concentration of *in-situ* hydrogen in the gas mixture was found to be apparently constant at 35mol% (Fig. 5-3), the concentration of hydrogen was assumed constant in the present kinetic model. Hence, a rate constant of k' is defined as:

$$k'_{(DBT\ Conv.)} = k_{(DBT\ Conv.)} \cdot p_{H_2} \quad (5-4)$$

So:

$$r_{DBT} = k'_{(DBT\ Conv.)} \cdot C_{DBT} \quad (5-5)$$

As introduced in section 5.1, HDS reaction processes in two pathways, DDS and HYD. Therefore, we simplified the HDS reaction network as shown in equation (5-6) (using DBT as an example, the same model also used for the HDS of 4,6-DMDBT).



Reaction rates of each reaction pathway could be impressed in Eqs.(5-7) to (5-9).

$$\left\{ \begin{array}{l} r_{DBT} = d[DBT]/dt = -k'_{(DBT\ Conv.)} \cdot C_{DBT} = -(k'_{(DBT\ HYD)} + k'_{(DBT\ DDS)}) \cdot C_{DBT} \quad (5-7) \\ r_{THDBT} = d[THDBT]/dt = k'_{(DBT\ HYD)} \cdot C_{DBT}^t - k'_{(DBT\ HYDD)} \cdot C_{THDBT}^t \quad (5-8) \\ r_{BP} = d[BP]/dt = k'_{(DBT\ DDS)} \cdot C_{BP}^t \quad (5-9) \end{array} \right.$$

Upon integrating:

$$\left\{ \begin{array}{l} C_{DBT}^t = C_{DBT}^0 \times e^{-(k'_{(DBT\ HYD)} + k'_{(DBT\ DDS)}) \cdot t} \\ \Rightarrow \ln \left(\frac{C_{DBT}^t}{C_{DBT}^0} \right) = -(k'_{(DBT\ HYD)} + k'_{(DBT\ DDS)}) \cdot t \quad (5-10) \end{array} \right.$$

$$\left\{ \begin{array}{l} C_{BP}^t = -\frac{C_{DBT}^t \times k'_{(DBT\ DDS)}}{k'_{(DBT\ HYD)} + k'_{(DBT\ DDS)}} \times (e^{-(k'_{(DBT\ HYD)} + k'_{(DBT\ DDS)}) \cdot t} - 1) \quad (5-11) \end{array} \right.$$

$$\left\{ \begin{array}{l} C_{THDBT}^t = \frac{C_{DBT}^t k'_{(DBT\ HYD)}}{(k'_{(DBT\ HYDD)} - k'_{(DBT\ HYD)} - k'_{(DBT\ DDS)})} \\ \times (e^{-(k'_{(DBT\ HYD)} + k'_{(DBT\ DDS)}) \cdot t} - e^{-k'_{(DBT\ HYDD)} \cdot t}) \quad (5-12) \end{array} \right.$$

The value of $k'_{(DBT\ Conv.)}$ is the pseudo-first-order rate constant for the conversion of starting sulfur-containing compounds in HDS reactions. According to Eq.(5-10), this number can be obtained via plotting $\ln \frac{C_{DBT}^t}{C_{DBT}^0}$ versus t . The slope is $-(k'_{(DBT\ HYD)} + k'_{(DBT\ DDS)})$, eg. $-k'_{(DBT\ Conv.)}$.

According to Eq.(5-11), if plot $\frac{C_{BP}^t}{C_{DBT}^t}$ versus $(e^{-(k'_{(DBT\ HYD)} + k'_{(DBT\ DDS)}) \cdot t} - 1)$, the slope would be

$\frac{-k'_{(DBT\ DDS)}}{k'_{(DBT\ HYD)} + k'_{(DBT\ DDS)}}$, wherein $-(k'_{(DBT\ HYD)} + k'_{(DBT\ DDS)})$ has been obtained from Eq.(5-10), so the values of $k'_{(DBT\ HYD)}$ and $k'_{(DBT\ DDS)}$ can be calculated, respectively. Eq.(5-12) is more complicated than the other two. The value of $k'_{(DBT\ HYDD)}$ can not be calculated *via* simply plotting. Non-linear regression is required and this is the most difficult part in this kinetic model, therefore, the significance of the regression involved in $k'_{(DBT\ HYDD)}$ was tested, which can be evaluated *via* comparing F values. If the observed F value (F_{OBS}) is bigger than the tabulated F value, the regression using the estimated k_{HYDD} is significant. In the present study, at the 95% confidence level, the tabulated F value is 5.99. Therefore, if the F_{OBS} is higher than 5.99, the regression should be significant. All regression curves and ANOVA (Analysis Of Variance) tables of $k'_{(DBT\ HYDD)}$ estimation have been given in Appendix E.

For example, the F_{OBS} values for the HYDD pathway reaction constant in the HDS of DBT and 4,6-DMDBT at 380 °C were 533 (fitting points shown in Fig. 5-4) and 16, respectively. Both of them are higher than the tabulated F value of 5.99, and hence the calculated $k'_{(DBT\ HYDD)}$ values are acceptable. Additionally, the regression for $k'_{(DBT\ HYDD)}$ in the HDS of DBT was better fitting than in the HDS of 4,6-DMDBT, indicating that this kinetics model (Eq.(5-6)) is more appropriate for the HDS of DBT than that of 4,6DMDBT.

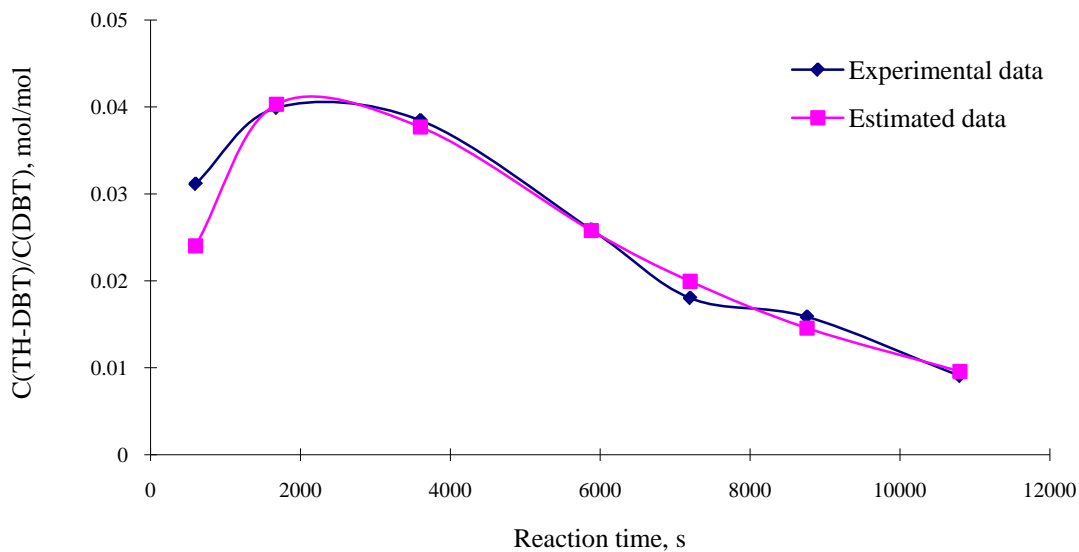


Fig. 5 - 4 Regression fitting points for k'_{HYDD} in the HDS of DBT over dispersed Mo sulfide catalyst using *in-situ* H_2 at $380\ ^\circ C$ using the proposed kinetics HDS model (experiment ID: DS0907).

Other conditions: HC reactor, equi-molar DBT and 4,6-DMDBT, 1600-1800 ppmw S in total, 400-450 ppmw Mo, S/Mo: $\sim 10/1$, 10 ml H_2O , 100 ml toluene, 590 psi CO mixed with 10 psi H_2S

Calculated pseudo-first-order rate constant of each single HDS reaction step for the HDS of DBT and 4,6DMDBT are listed in Table 5-3.

Table 5 -3 Pseudo-first-order rate constants involved in HDS reactions of DBT and 4,6-DMDBT as a function of reaction temperature over dispersed Mo sulfide catalyst using *in-situ* H₂*.

Reaction temp., °C		$k'_{Conv.} \times 10^5$ (Conversion) [†]	$k'_{DDS} \times 10^5$	$k'_{HYD} \times 10^5$	$k'_{HYDD} \times 10^5$	Selectivity [‡]	$\frac{k'_{(DBT\ Conv.)}}{k'_{(DMDBT\ Conv.)}}$
DBT	330 (DS0905)	4.2	2.5	1.7	26.5	1.5	1.7
	355 (DS0906)	10.3	7.1	3.2	51.0	2.2	2.8
	380 (DS0907)	20.7	15.3	5.4	80.9	2.8	2.8
	400 (DS0908)	31.3	23.7	7.6	149	3.1	2.5
4,6- DMDBT	330 (DS0905)	2.5	---	1.6	12	---	---
	355 (DS0906)	4.6	0.8	3.9	61	0.21	---
	380 (DS0907)	7.3	1.5	5.8	70	0.26	---
	400 (DS0908)	12.3	4.7	7.6	75	0.62	---

*: Other conditions: HC reactor, equi-molar DBT and 4,6-DMDBT, 1600-1800 ppmw S in total, 400-450 ppmw Mo, S/Mo: ~10/1, 10 ml H₂O, 100 ml toluene, 590 psi CO mixed with 10 psi H₂S

†: $k'_{Conv.} = k'_{DDS} + k'_{HYD}$

‡: $selectivity = k'_{DDS}/k'_{HYD}$

5.4.3 Simultaneous HDS of DBT and 4,6-DMDBT

Fig. 5-5 represents the HDS product distribution in the HDS of DBT over the dispersed Mo sulfide catalyst using *in-situ* hydrogen at 380°C. Four products were observed: biphenyl (BP), the product of the DDS pathway, tetrahydro-DBT (TH-DBT), the intermediate of the HYD pathway, and cyclohexylbenzene (CHB) and dicyclohexyl (DCH), the HYDD products of DBT which are final products of the HYD route. The contribution of BP in all sulfur-removed products was higher than 80% at 380°C during the reaction. This showed that the DDS route was

much faster than the HYD route in the HDS of DBT. The concentration of TH-DBT decreased with extending the reaction time, indicating that this intermediate was consumed quickly to generate further sulfur-removed products, CHB and DCH.

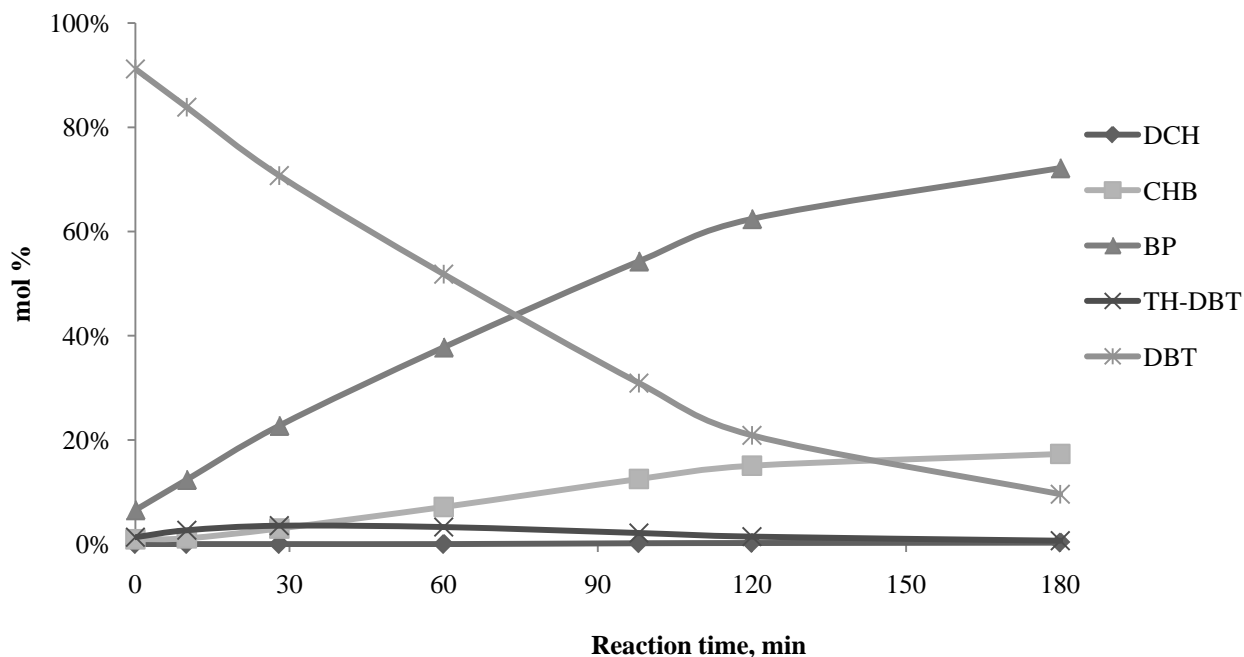


Fig. 5 - 5 HDS product distribution of DBT over dispersed Mo sulfide catalyst using *in-situ* H₂ at 380°C (experiment ID: DS0907).

Other conditions: HC reactor, equi-molar DBT and 4,6-DMDBT, 1600~1800 ppmw S in total, 400~450 ppmw Mo, S/Mo~10/1, 10 ml H₂O, 100 ml toluene, 590 psi CO mixed with 10 psi H₂S

Fig. 5-6 shows the HDS product distribution in the HDS of 4,6-DMDBT over the dispersed Mo sulfide catalyst in *in-situ* hydrogen at 380°C. Low concentrations of intermediates, DM-TH-DBT and DM-HH-DBT, suggested fast C-S bond cleavage from partially hydrogenated sulfur-containing products of 4,6-DMDBT. Desulfurized molecules DMCHB were final products of the HYD pathway and DMBPs were products of the DDS route. The higher concentration of

DMCHB indicated higher selectivity towards to the HYD pathway in the HDS of 4,6-DMDBT. Hence, DBT and 4,6-DMDBT have different predominant reaction pathway during HDS reactions. This is in accordance with what was reported using supported Mo sulfide catalysts^{48,79,80}.

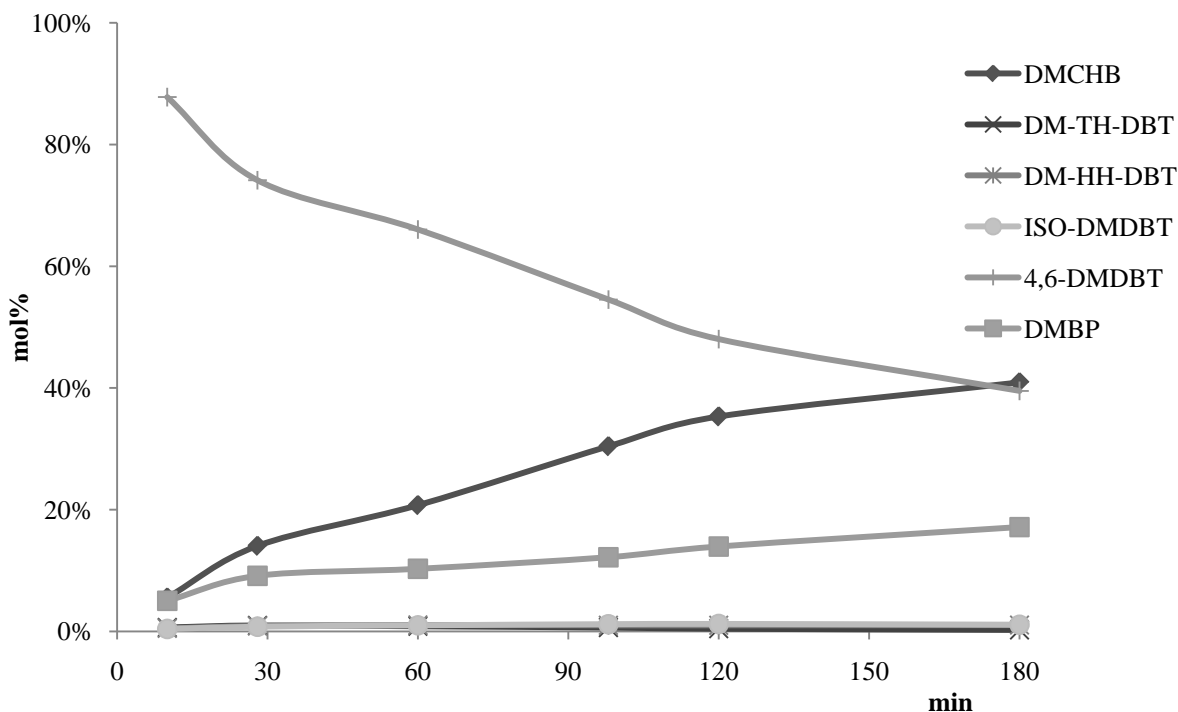


Fig. 5 - 6 HDS product distribution of 4,6-DMDBT over dispersed Mo sulfide catalyst using *in-situ* H₂ at 380°C (experiment ID: DS0907).

Other conditions: HC reactor, equi-molar DBT and 4,6-DMDBT, 1600~1800 ppmw S in total, 400~450 ppmw Mo, S/Mo~10/1, 10 ml H₂O, 100 ml toluene, 590 psi CO mixed with 10 psi H₂S

Pseudo-first-order rate constants were determined according to the HDS kinetic model shown in Eq. (5-6). The selectivity between the two routes, k'_{DDS}/k'_{HYD} , was 1.5 to 3.1 in the HDS of DBT, while 0.2 to 0.6 in the HDS of 4,6-DMDBT from 330°C to 380°C. Low rate constants for the

direct sulfur removal from 4,6-DMDBT molecules showed that 4,6-DMDBT was extremely difficult to desulfurize directly. In the flat 4,6-DMDBT molecule, the methyl groups and the sulfur atom are in the same plane of the molecule. The adsorption of 4,6-DMDBT in the π mode with the molecule flat on the catalyst surface allow benzene rings, both methyl groups and the sulfur atom have access to active sites, and have the hydrogenation of 4,6-DMDBT occur. However, as the spacious methyl groups adjacent to the sulfur atom in the 4,6-DMDBT molecule, they hinder the molecule from binding on the catalyst surface on the catalyst surface *via* the sulfur atom in the σ mode with the molecule perpendicular to the catalyst surface. Therefore, the adsorption of 4,6-DMDBT in the σ mode is much weaker than that of DBT, and the DDS pathway in the HDS of 4,6-DMDBT was strongly suppressed.

It is interesting to observe that the rate constant of the HYD pathway, k_{HYD} , in the HDS of 4,6-DMDBT was close to the one in the HDS of DBT, Table 5-3. This trend did not change with increasing the reaction temperature from 330°C to 400°C. This indicated that the presence of methyl groups did not affect the π adsorption of 4,6-DMDBT on the catalyst surface. Additionally, the electron-donating effect of the two methyl groups in the 4,6-DMDBT molecule may even make the HYD faster than in the HDS of DBT⁸. Differently, the rate constant of the DDS route, k'_{DDS} , in the HDS of 4,6-DMDBT was found to be much lower than that in the HDS of DBT. Therefore, the lower reactivity of substituted DBT molecules over the dispersed Mo sulfide catalyst was primly attributed from the extremely slow direct desulfurization in the HDS of 4,6-DMDBT.

The pseudo-first-order rate constant of the sulfur-removal step in the HYD route, k_{HYDD} , was observed to be much higher (> 10 times) than k'_{HYD} and k'_{DDS} , and even higher than the pseudo-first-order rate constant for the conversion of the starting material, k'_{Conv} . The higher rate constant in the HYDD step than HYD was also observed by Wang and Prins⁸¹. This indicates that the sulfur-removal from sulfur-containing partially hydrogenated molecules, such as TH-DBT in the HDS of DBT and DM-TH-DBT, DM-HH-DBT in the HDS of 4,6-DMDBT, was much faster than the first hydrogenation step to generate hydrogenated intermediates. Therefore, these sulfur-containing partially hydrogenated products were considered as intermediate in the HYD route. As a result, the concentrations of these intermediates increased initially and decreased with extending the reaction time to generate further sulfur-removed products.

The HDS reactivity of DBT over the dispersed Mo sulfide catalyst using *in-situ* H₂ was found to be 2.8 times as high as that of 4,6-DMDBT at 355°C (Table 5-3). The low reactivity of 4,6-DMDBT was previously expected as it is one of the most refractory sulfur compounds present in oil fuels, and its HDS reactivity was around 10 times lower than that of DBT in the HDS of a diesel fuel at 360°C over a traditional supported CoMo catalyst⁴⁶. More recently, Wang and Prins⁸¹ reported that 4,6-DMDBT was 7 times less reactive than DBT at 300°C over a NiMoS₂/γ-Al₂O₃ catalyst. So, the relative reactivity of 4,6-DMDBT to that of DBT was much higher in our catalytic reaction system using dispersed MoS₂ catalyst with *in-situ* H₂. It is interesting to note that Yoosuk *et al*⁷⁸ reported the ratio of the HDS rate constants for the conversions of DBT and 4,6-DMDBT to be 1.4 at 300°C using an unsupported sulfide NiMo catalyst, and an unsupported MoS₂ was even more active towards the HDS of 4,6-DMDBT where the ratio of the HDS rate constants for the conversions of DBT and 4,6-DMDBT was 0.55. Hence, dispersed unsupported

Mo sulfide based catalysts apparently have a higher relative activity towards the HDS of 4,6-DMDBT than the traditional supported catalysts. Yoosuk *et al*⁷⁸ attributed the higher activity of unsupported catalysts to their higher hydrogenation activities. Another possible explanation is that the dispersed unsupported catalyst provides more effective surface area for the π -adsorption of the 4,6-DMDBT and hence more effective for the HDS of the bulky refractory sulfur-containing compounds. Additionally, the interaction between the catalytically active phases and the carrier of the supported catalysts is eliminated. The unsupported catalyst may provide a higher surface area for the interaction with refractory sulfur-containing compounds. This may also contribute to the higher efficiency of the catalyst in the HDS reactions of highly refractory sulfur-containing compounds. Therefore, the unsupported finely dispersed Mo sulfide based catalyst system is more appropriate than the supported catalysts in hydro-treating heavy feed stocks.

The ratio between the reactivity of DBT and 4,6-DMDBT in the simultaneous HDS reactions over dispersed Mo sulfide catalyst using *in-situ* H₂ was almost constant within the temperature range of 355 °C to 400 °C. This means that the pseudo-first-rate constants for the conversions of both sulfur-containing model compounds increased to the same extent under the present experimental conditions when the reaction temperature was increased from 355°C to 400°C.

However, running HDS at different reaction temperature resulted in the change of the selectivity between two reaction pathways. The selectivity between the two reaction pathways (Table 5-3), k'_{DDS}/k'_{HYD} , in the HDS of both sulfur-containing model compounds increased with increasing the reaction temperature, namely, the DDS route was more favored. Especially, in the HDS of

4,6-DMDBT, at 400 °C, the selectivity towards DDS increased by almost 2 times compared to at 355 °C. At 400 °C, when the simultaneous HDS reaction proceeded for 180 min, the sulfur-removed products obtained *via* the DDS reaction route contributed 86% and 44% to the total sulfur-removal of DBT and 4,6-DMDBT, respectively, while, DDS only contributed around 30% to the sulfur-removal of 4,6-DMDBT at 380 °C. Hence, for HDS reactions at high temperature over the dispersed Mo sulfide catalyst using *in-situ* hydrogen, sulfur could be removed at a lower consumption of hydrogen due to the higher selectivity towards the direct desulfurization pathway.

5.4.4 Effect of Ni on the simultaneous HDS of DBT and 4,6-DMDBT using *in-situ* H₂

Nickel is a well-accepted promoter for Mo sulfide based catalysts for hydro-treating reactions. In the present section, Ni was added with a molar ratio of Ni/Mo as 0.5 with a constant total metal concentration used in the experiment. Such an atomic ratio between Ni and Mo was optimized by Lee⁴² previously in our group. The effect of Ni on the HDS of DBT was also studied previously by Lee, and his results indicated that the conversion and the sulfur-removal of DBT was enhanced significantly with the presence of Ni⁴².

In this chapter, we extended the use of Ni in the HDS of 4,6-DMDBT in a mixture with DBT. There were two experiments using Ni-promoted catalyst, NiMo-1 and NiMo-2. In the experiment of NiMo-2, the partial pressure of pre-sulfurization gas, H₂S, was 50% higher than that in the NiMo-1 run. The experiment using un-promoted catalyst, Mo, was run under the exact same conditions as the NiMo-1 run. In all these three experiments, the total molar amount of active metals, Mo and Ni, was kept constant. The data illustrated in Fig. 5-7 suggest that:

- The addition of Ni into the dispersed Mo sulfide catalyst promoted the HDS of DBT significantly. Conversion and desulfurization of DBT increased by 60% and 88%, respectively (Mo vs. NiMo-1). When increasing the partial pressure of H₂S, the HDS results of DBT were further promoted over the NiMo catalyst (NiMo-1 vs. NiMo-2).
- Differently, the HDS of 4,6-DMDBT was not promoted significantly with the presence of Ni under experimental conditions (Mo vs. NiMo-1). Significantly higher conversion of 4,6-DMDBT was observed after increasing the partial pressure of H₂S over Ni-promoted catalyst, however, the sulfur-removal did not increase significantly (NiMo-1 vs. NiMo-2). The different promotional effect of Ni on the HDS of DBT and 4,6-DMDBT was also observed in the LGO studies carried out in our group⁸².

In Yoosuk's study on the HDS of DBT and 4,6-DMDBT over dispersed Mo and NiMo catalysts⁷⁸, conversions of DBT and 4,6-DMDBT were also observed to be promoted to different extents too, by 8 times and 3 times, respectively. Compared to their HDS results over Ni promoted Mo sulfide catalysts, the HDS results obtained in the present study were much lower.

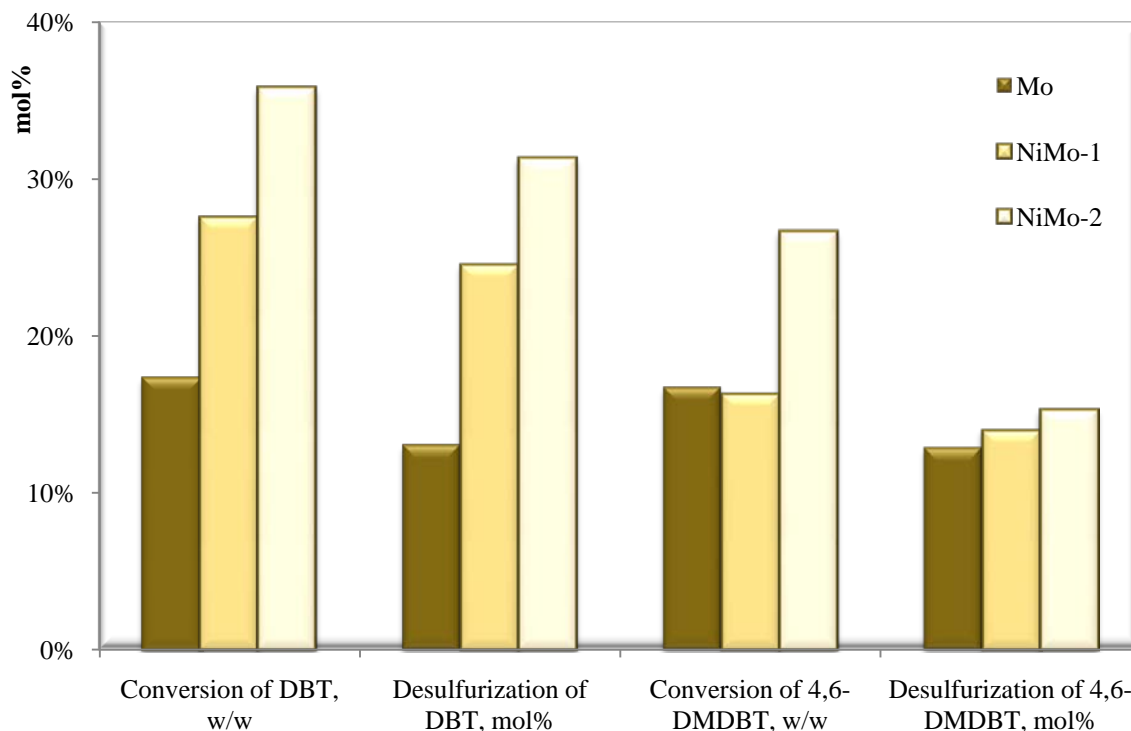


Fig. 5 - 7 Conversion and desulfurization results of DBT and 4,6-DMDBT over promoted Mo sulfide catalysts using *in-situ* H₂.

Other conditions: Ni/Mo: ~0.5, 380^oC, equi-molar DBT+4,6-DMDBT, 1670 ppmw S, S/(Ni+Mo): ~10/1, 1hr, 100 ml toluene, 10 ml PMA aqueous solution, 590 psi CO + 10 psi H₂S (585 psi CO + 15 psi H₂S in the NiMo-2 run)

Due to the same amount of metals was used in the experiments using dispersed Mo and NiMo catalysts, less Mo was used in the experiment in the NiMo runs than in the Mo run. Hence, although similar HDS results of 4,6-DMDBT were obtained over the two different catalysts, it may lead to the conclusion that Ni had shown promotional effect on the HDS of 4,6-DMDBT due to the lower amount of the active Mo used. Also it could be expected that when the amount of Mo was kept constant in experiments, the HDS activity of the NiMo sulfide catalysts would be promoted more significantly.

The higher conversion of 4,6-DMDBT obtained in the experiment under higher partial pressure of H₂S indicated that the sulfidation of the NiMo catalyst was not completed. 10 psi of H₂S was an optimized pre-sulfidation condition in our preliminary experiments to generate highly active dispersed Mo sulfide catalyst for the simultaneous HDS of DBT and 4,6-DMDBT⁸³. However, this optimized amount of H₂S does not seem to be high enough for the pre-sulfidation of NiMo catalyst. Therefore, the dispersed Ni-promoted Mo catalyst was more difficult to be sulfided and activated than the unpromoted Mo catalyst, hence, more severe pre-sulfidation condition is required when using Ni-promoted catalysts. On the other hand, the increased H₂S partial pressure resulted in a positive effect on the conversion of 4,6-DMDBT, but did not promote the desulfurization of the sulfur-containing compound. This is probably due to the inhibitive effect of excess H₂S on the C-S cleavage step. Such inhibitive effect of excess H₂S also explained the lower selectivity on the DDS pathway in the 15 psi H₂S experiment (Table 5-4).

Table 5 - 4 Selectivity of HDS pathways observed over sulfided Mo & NiMo catalysts*

		NiMo-1 (10 psi H₂S)	NiMo-2 (15 psi H₂S)
DBT	<i>DDS/HYDD</i>	5.7	4.6
	<i>DDS/HYD</i>	3.1	2.6
4,6-DMDBT	<i>DDS/HYDD</i>	0.84	0.77
	<i>DDS/HYD</i>	0.69	0.64

*: Other conditions: Ni/Mo: ~0.5, 380⁰C, equi-molar DBT+4,6-DMDBT, 1670 ppmw S, S/(Ni+Mo) or S/Mo: ~10/1, 1hr, 100 ml toluene, 10 ml PMA aqueous solution, 590 psi CO + 10 psi H₂S (585 psi CO + 15 psi H₂S in the NiMo-2 run)

Although promotional effect of Ni on the HDS activity of Mo sulfide catalyst was observed, it was much lower than expected. The morphology of NiMo catalyst was characterized *via* HRTEM-EDX after consumed in an HDS experiment. The characterized NiMo catalyst particles were collected from both the organic phase and the Wcat phase. Interestingly, the black particles present in the organic phase was identified to be sulfided Ni by EDX and the molar ratio between the two elements, S:Ni, equaled to 1:9 (Fig. 5-8A). This observation suggested that little Mo was present in the organic phase and Ni was not completely sulfided. The latter observation was in agreement with previous conclusion that NiMo catalyst requires more severe sulfidation conditions. The absence of Mo sulfide in the organic phase may be another important reason for the low promotional effect of Ni on the HDS activity of Mo sulfide catalyst.

Element of Mo was detected by EDX in the catalyst particles collected on the reactor vessel wall as shown in Fig. 5-8B. However, the particles detected in the Wcat sample had two different phases: Mo-abundant phase (areas sp2 and sp3 in Fig. 5-8B) and Ni-abundant phase (area sp1 in Fig. 5-8B). The distance between layers (Fig. 5-9) was measured to be around 0.64nm, which was the identified spacing of MoS₂ slabs. This indicated that NiS and MoS₂ slabs were present as separate phases. Hence the Ni was not playing a role in promoting the MoS₂ activity for HDS.

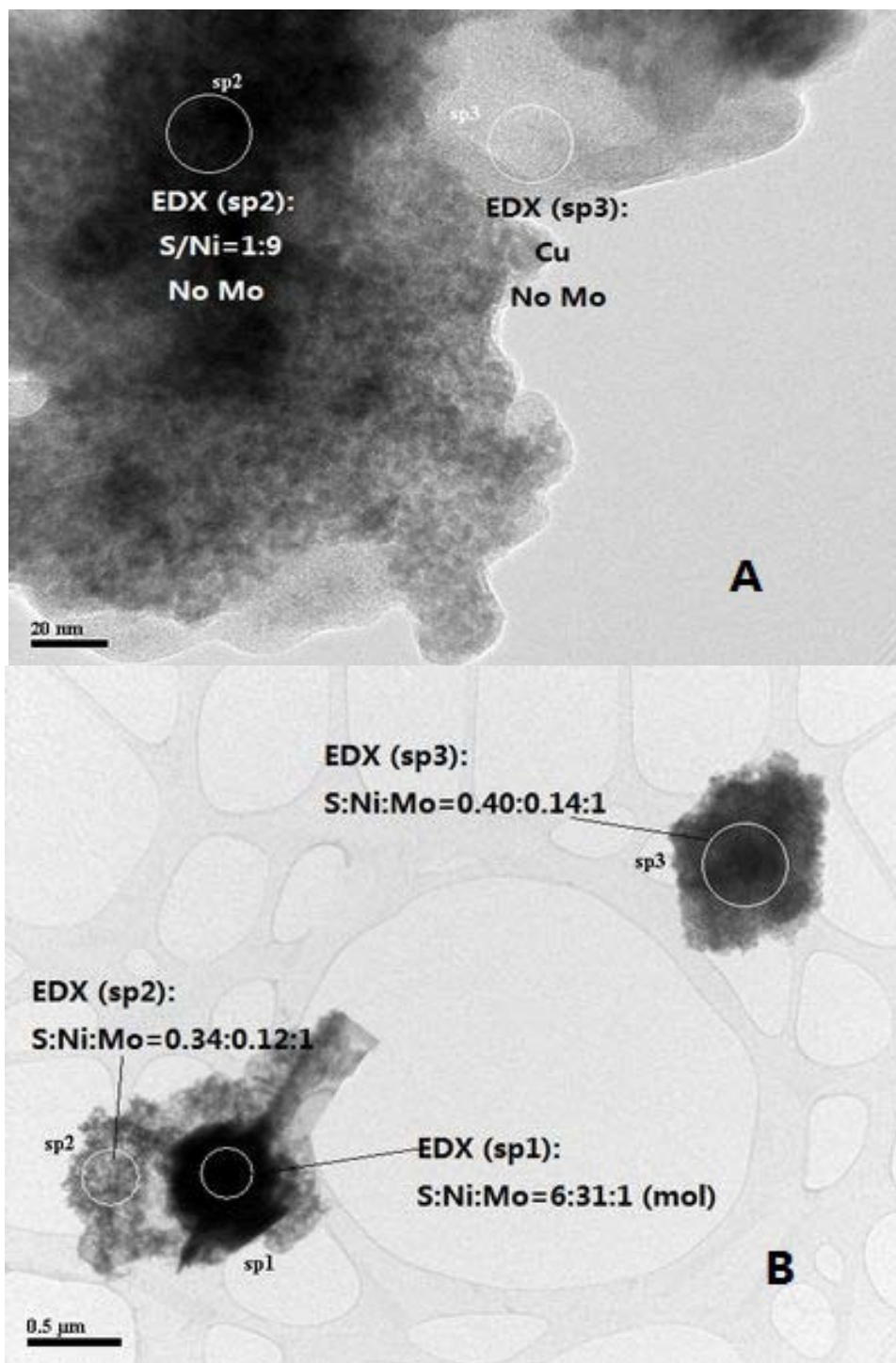


Fig. 5 - 8 HRTEM image of NiMo catalyst particles dispersed in the organic phase (A) and on the reactor vessel wall (B) collected after HDS experiment (EDX spectra given in Appendix E). HDS conditions: 0.42g DBT+0.5g DMDBT, 380°C, 590psi CO+10psi H₂S, S/(Ni+Mo): ~10:1, 2hr

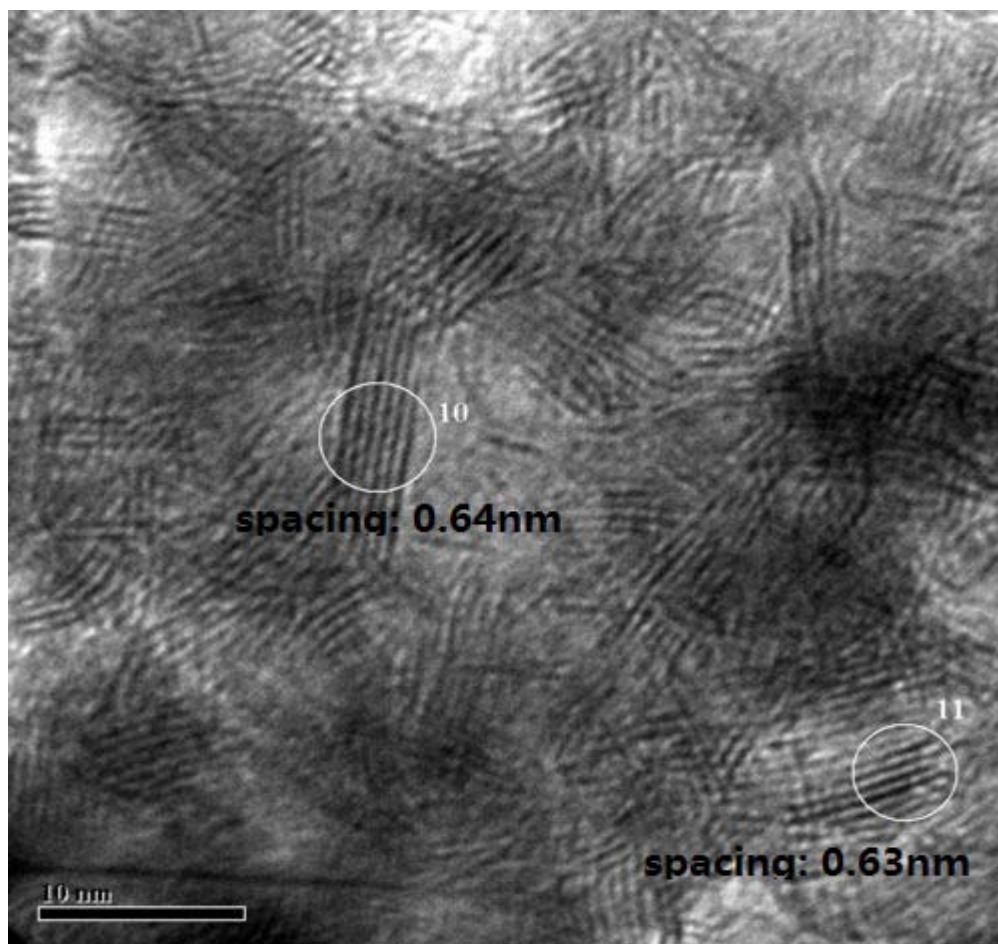


Fig. 5 - 9 HRTEM image of MoS₂ slabs collected on the reactor vessel wall after the HDS experiment over NiMo catalyst.

5.4.5 Effect of K on the simultaneous HDS of DBT and 4,6-DMDBT using *in-situ* H₂

Water gas shift reaction is applied in the present study to provide *in-situ* H₂ for hydro-treating reactions. High conversion of CO *via* the WGS reaction is pursued in the present study for providing as much *in-situ* H₂ as possible for hydro-treating reactions. As potassium was found to have effective promotional effect on the WGS reaction^{20, 77a, 84}, potassium was added into the dispersed Mo sulfide based catalyst as a promoter for providing more *in-situ* H₂ for further HDS reactions.

Before studying the effect of potassium on HDS reactions, the effect of potassium on the WGS reaction was investigated first. In this study, potassium was introduced into the dispersed Mo sulfide catalyst as the ratio of K/Mo was 0.4 and the total amount of active metals was a constant in all experiments. Fig. 5-10 illustrated the conversion of CO *via* the WGS reaction as a factor of reaction time over different dispersed sulfide catalysts.

As shown in Fig. 5-10, in the experiment using un-promoted Mo sulfide catalyst (WG-08), the conversion of CO *via* the WGS reaction reached 71.2% at the end of the reaction (250 min), while this level of CO conversion was observed at 30 min when using potassium promoted Mo sulfide catalyst. After adding K into the Mo sulfide catalyst (WG-09), much higher conversion of CO was observed. In the experiment of WG-08, the conversion of CO increased from 25.4% to 71.2% in the first 250 min of the reaction time. After introducing potassium (K/Mo=0.4, molar) into sulfided molybdenum, the conversion of CO *via* the water gas shift reaction increased from 44.4% at 0 min to 90.6% at 260 min under the same reaction conditions. The conversion of CO

was 90% at 130 min and then stayed at this level. This indicated that the equilibrium conversion of CO under the present reaction conditions (380°C, 590psi CO, 10ml DI H₂O) was around 90%~91%, which was a little lower than calculated equilibrium CO conversion of 96.8%. The promotional effect of potassium on the activity towards WGS reaction was significant. Therefore, more hydrogen could be generated during the reaction when using potassium promoted molybdenum sulfide catalyst for HDS reactions and modified HDS result was expected.

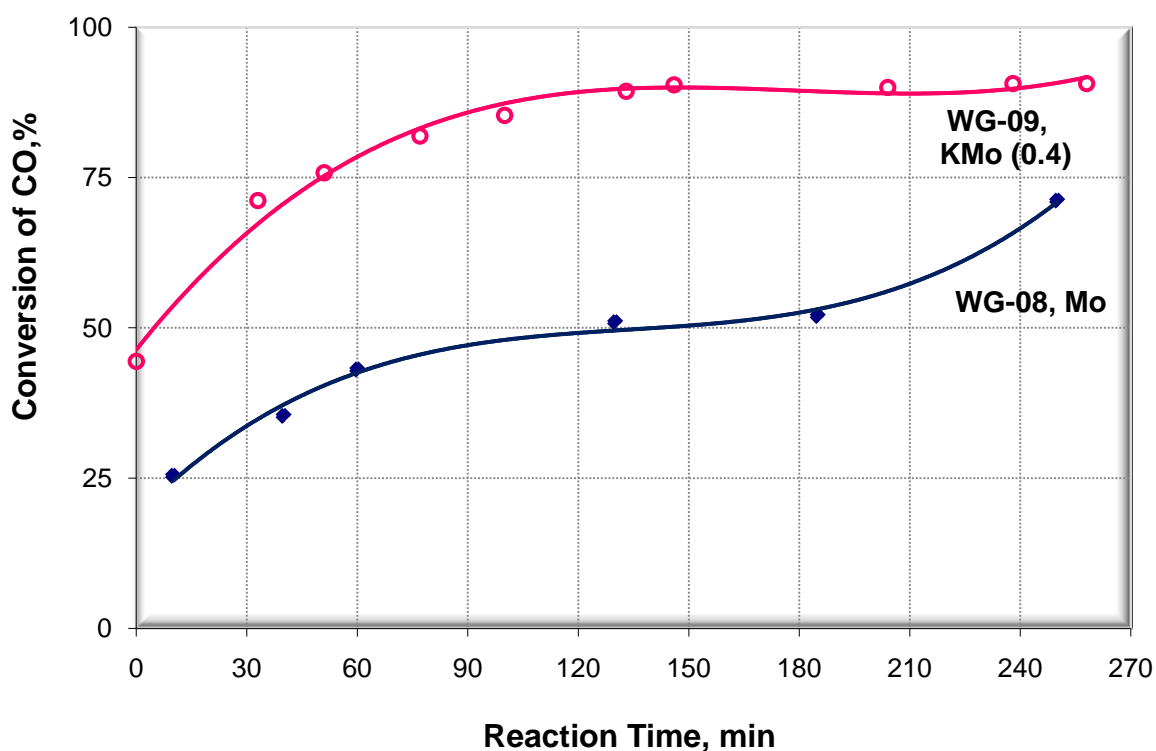


Fig. 5 - 10 Conversion of CO *via* WGS reaction as a function of reaction time over different dispersed sulfided catalysts.

Other conditions: SS reactor, 0.4 mmol active metals (Mo in WG-08 or Mo+K in WG-09), K/Mo=0.4 (WG-09), 10 ml H₂O, 100 ml toluene, 590 psi CO mixed with 10 psi H₂S, Perkin-Elmer GC

The use of potassium promoted Mo sulfide catalyst was extended in HDS studies. Experiment results are listed in Table 5-5. Potassium showed strong inhibitive effect on the HDS of DBT and 4,6-DMDBT. Especially in the HDS of DBT, very little DBT was converted over the KMo sulfide catalyst. The negative effect of potassium on the HDS of 4,6-DMDBT seemed to be smaller than on the HDS of DBT, but the desulfurization of 4,6-DMDBT was still lower than that of DBT.

Table 5 - 5 HDS results of DBT and 4,6-DMDBT over KMo catalyst using *in-situ* H₂.

		K/Mo=0.4	Mo
Feed	DBT	95.9%	68.6%
Intermediate	TH-DBT	0.6%	8.9%
DDS	BP	3.2%	16.7%
HYDD	CHB	0.3%	4.9%
	DCH	0	0.9%
Feed	4,6-DMDBT	91.0%	69.7%
Intermediate	ISO-DMDBT	1.4%	2.5%
	HH-DMDBT	2.2%	2.3%
	TH-DMDBT	1.5%	2.4%
DDS	DMBP	1.9%	2.6%
HYDD	DMCHB	2.0%	20.5%

Kantschewa *et al*^{77a} studied the nature and properties of a potassium-promoted NiMo-Al₂O₃ WGS catalyst. They observed significant enhancement in the WGS activity, but reduced activity towards the HDS of thiophene. They explained the low HDS activity of KNiMo catalyst as follows:

- Mo was coordinated octahedrally in NiMo/Al₂O₃, while it was coordinated tetrahedrally in KNiMo/Al₂O₃.
- Addition of potassium destroyed the surface heteropolymolybdate phase, which was the precursor for the active phase of a sulfided NiMo/Al₂O₃ catalyst; hence the NiMoS phase could not sufficiently be developed with the presence of potassium.
- Mo⁵⁺ was the stable oxidation state in the sulfided KNiMo catalyst, while Mo⁴⁺ was considered as the really active phase for HDS.

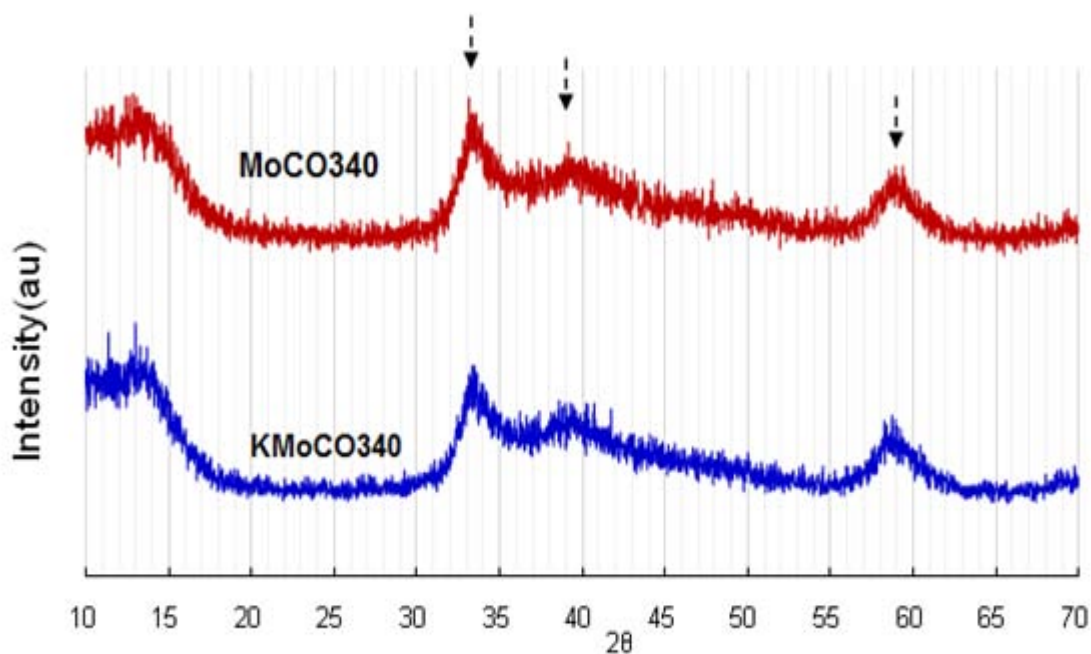


Fig. 5 - 11 XRD spectra of K promoted MoS₂ catalyst particles prepared in CO at 340°C (K:Mo=1:9 molar)

Identified peaks of MoS₂ were observed in the XRD spectrum of K promoted Mo catalyst prepared in CO at 340°C (Fig 5-11), indicating the generation of active MoS₂ in the presence of potassium. The typical thread-shaped MoS₂ slabs with similar statistic average slab length were

also observed in the HRTEM images of the KMo catalyst. However, HRTEM (Fig. 5-12) and SEM images (Fig. 5-13) showed that the surface morphology of the dispersed Mo sulfide catalyst changed after introducing potassium. This change is much clearer as shown in the SEM image, wherein the sphere shape of Mo sulfide disappeared and was replaced by a kind of stacked plate structure. The change in the morphology of the catalyst surface structure may play an important role in the significant decrease in the HDS activity of KMo sulfide catalyst. Therefore, potassium did not exhibit a promotional effect on the HDS activity of dispersed Mo sulfide based catalyst.

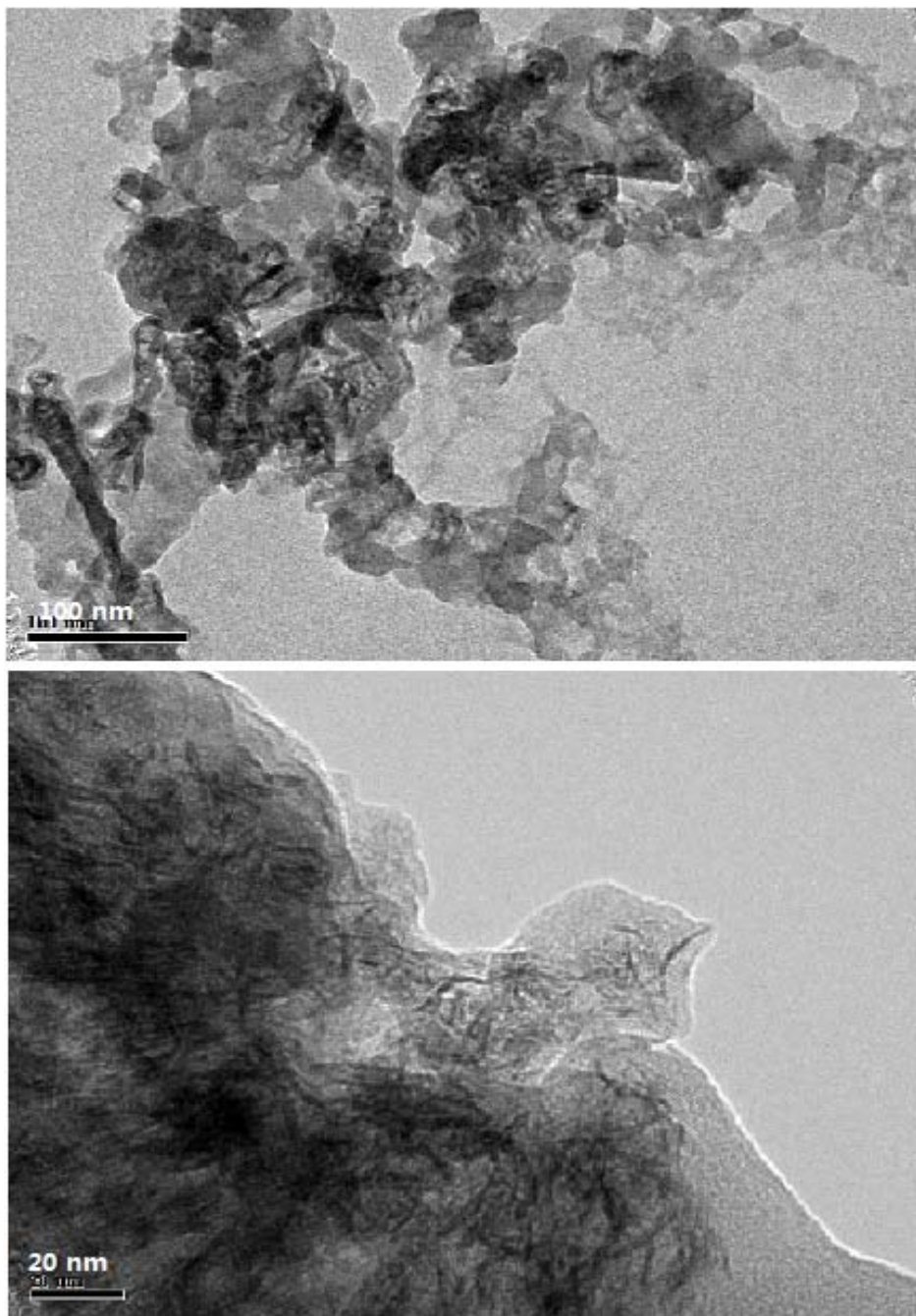


Fig. 5 - 12 HRTEM images of Wcat particles of K promoted Mo sulfide catalyst prepared in CO at 340 °C (K:Mo=1:9 molar)

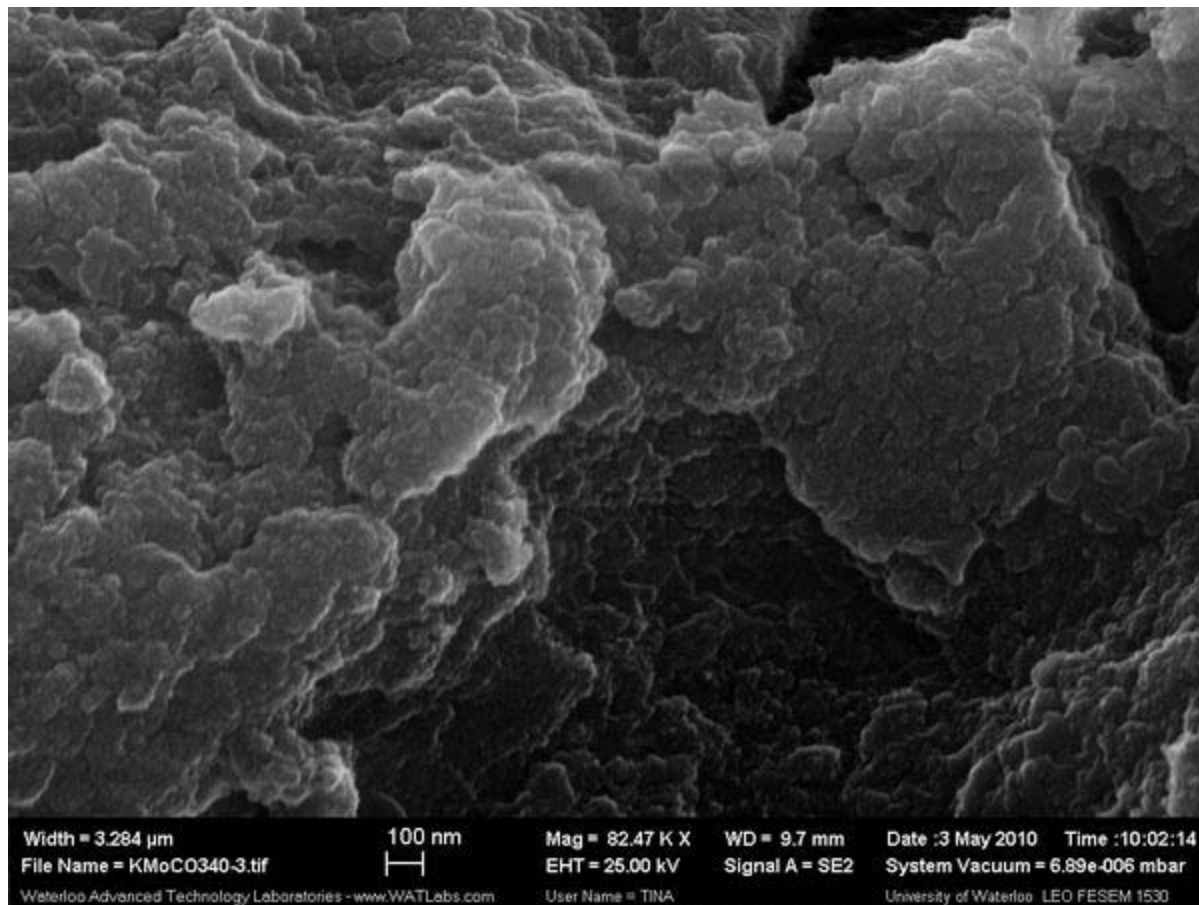


Fig. 5 - 13 SEM images of K promoted Mo sulfide catalyst particles detected by SE2 (prepared in CO at 340 °C, K:Mo=1:9 molar)

5.5 Conclusions

Although the HDS of refractory sulfur-containing compounds has been studied intensively, this thesis would be the first to investigate the simultaneous HDS of DBT and 4,6-DMDBT over nano-dispersed Mo sulfide based catalysts using *in-situ* H₂ generated from CO and H₂O *via* the WGS reaction. Our experimental results indicated that:

- (1) The concentration of hydrogen generated from CO *via* the WGS reaction stayed in the range of 30-40mol% in the WGS gas mixture at different reaction temperatures changing from 350°C to 400°C. Hence, the concentration of hydrogen was assumed as a constant in the HDS kinetic model proposed in the present study.
- (2) The reactivity (based on the conversion) of DBT in HDS over dispersed Mo sulfide catalyst was found to be 2.8 times as high as that of 4,6-DMDBT in the mixture with DBT. This number was much lower than what was observed over supported Mo catalysts for the HDS of DBT and 4,6-DMDBT mixture reported in literatures probably mainly due to more effective surface area provided for π -adsorption of 4,6-DMDBT molecules. Therefore, the unsupported Mo sulfide catalyst is relatively more active towards the HDS of refractory sulfur-containing compound.
- (3) The pseudo-first-rate constant of the HYD route in the HDS of 4,6-DMDBT was comparable to that in the HDS of DBT. The lower reactivity of 4,6-DMDBT than DBT was mainly due to the inhibition of the DDS pathway caused by the two methyl groups adjacent to the sulfur atom.
- (4) HDS product distribution of each sulfur model compound has shown that DDS was the major desulfurization pathway in the HDS of DBT, while HYD was the predominant way

in the HDS of 4,6-DMDBT. This is in accordance to the reported results using supported catalysts.

- (5) Within the reaction temperature range of 330~380°C, the reaction pathway of DDS was more favoured with increasing the temperature in the simultaneous HDS of DBT and 4,6-DMDBT.
- (6) Significant promotion effect of Ni on the HDS of DBT was observed after introducing Ni into the nano-dispersed Mo sulfide catalyst, while the HDS of 4,6-DMDBT was not enhanced by Ni.
- (7) More severe sulfidation condition is required in the preparation of Ni promoted Mo catalyst.
- (8) The absence of Mo sulfide in the organic phase and the separate presence of NiS from MoS₂ in the reaction system may contribute to the low promotional effect of Ni on the HDS activity of Mo sulfide catalyst.
- (9) Potassium had shown positive effect on improving WGS activity of the dispersed Mo sulfide catalyst, but strongly inhibited the HDS activity. The morphology of Mo sulfide catalyst changed significantly after added potassium. Therefore, although more *in-situ* H₂ was generated over a KMo sulfide catalyst, potassium could not be used as an effective promoter for HDS reactions.

Chapter 6 Comparison between *in-situ* H₂ and molecular H₂ for Hydrodesulfurization

6.1 Introduction

The *in-situ* H₂ reaction system used in our study is a process with water present. The catalyst used was an unsupported dispersed Mo sulfide based catalyst, which was prepared *in-situ* during the reactions. Hence, there are two factors involved in affecting the efficiency of the *in-situ* H₂ reaction system for hydro-treating reactions: (1) the activity of the *in-situ* prepared dispersed MoS catalyst and (2) the reactivity of *in-situ* H₂. Namely, the better bitumen upgrading results obtained using *in-situ* H₂ may be due to two reasons: (1) the dispersed MoS catalyst prepared in *in-situ* H₂ has higher activity, and (2) *in-situ* H₂ is more reactive than molecular H₂. If this assumption is true, what is the contribution of each factor to the higher efficiency of the *in-situ* H₂ reaction system? Therefore, in this chapter, the dispersed Mo sulfide catalysts were firstly prepared *ex-situ* in the two different H₂ resources. Hence, the question whether the catalyst prepared in *in-situ* H₂ has higher activity for hydro-treating reactions could be answered *via* investigating the HDS activity of the two *ex-situ* prepared dispersed MoS catalysts using molecular hydrogen. On the other hand, the question whether the *in-situ* H₂ is more reactive than molecular H₂ in hydro-treating could be answered *via* comparing the HDS results using the two different H₂ atmospheres over the same type of catalyst. The experiments involved in this study are two-step experiments and the catalysts prepared are marked as ‘*Ex*’ catalysts. The experimental design is given in Table 6-1.

Table 6 - 1 Two-step experimental design

	Step 1(catalyst preparation)			Step 2 (HDS activity study)	
	Catalyst ID	Gas atmosphere	Temp.	Gas atmosphere	H ₂ O
A [†]	<i>ExCO-01</i>	CO (H ₂ O present)	340 °C	590 psi H ₂ + 10 psi H ₂ S	0
	<i>ExH-01</i>	H ₂ (H ₂ O present)	340 °C	590 psi H ₂ + 10 psi H ₂ S	0
B [‡]	Use the catalyst of <i>ExCO-01</i>			595 psi CO + 5 psi H ₂ S	5 ml
				595 psi H ₂ + 5 psi H ₂ S	5 ml

[†] investigating the activity of the catalysts prepared in different gas atmosphere

[‡] comparing the reactivity of the two H₂ atmospheres over *ExCO-01*

6.2 Experimental

Experiments carried out in this chapter were designed to:

- (1) study the simultaneous HDS of DBT and 4,6-DMDBT using the two different hydrogen atmospheres;
- (2) determine the HDS activity of the two types of *ex-situ* prepared dispersed Mo sulfide catalysts;
- (3) compare the reactivity of *in-situ* hydrogen *versus* external supplied molecular hydrogen in HDS reactions over the same type of *ex-situ* prepared Mo sulfide catalyst.

6.2.1 Simultaneous HDS of DBT and 4,6-DMDBT using two different hydrogen sources

In this section, PMA and ammonia tetrathiomolybdate (ATTM) were used as molybdenum precursors to compare the simultaneous HDS results of DBT and 4,6-DMDBT using *in-situ* generated hydrogen *versus* using molecular hydrogen. Detailed experimental conditions have been listed in Table 6-2.

Table 6 - 2 Detail reaction conditions of the experiments to study HDS in the two different hydrogen sources[†]

Experiment ID	Reactant gases, psi			Reaction time, min	Active metal precursor
	CO	H ₂	H ₂ S		
DS1001*	0	600	10	150	PMA
DS1002*	600	0	10	150	PMA
DM-54	0	600	0	180	ATTM
DM-57	600	0	0	180	ATTM
DM-60	300	300	0	180	ATTM

[†]: other common conditions: 10 ml H₂O, 100ml toluene, 0.5g 4,6-DMDBT, 0.42g DBT, 430~500ppmw Mo (0.4 mmol Mo), 380°C

* run in the HC reactor, others (not starred) were run in the SS reactor

6.2.2 HDS activity of *ex-situ* prepared dispersed Mo sulfide catalysts

As designed in Table 6-1, *ex-situ* catalysts were prepared separately prior to running HDS reactions. 2g of PMA was dissolved in 20 ml DI water, 100 ml toluene was added, 200 psi H₂S was purged into the reactor for sulfidation, 500 psi of reactant gas (CO or H₂) was introduced and pressurized the reactor to 600 psi (at room temperature). The catalysts were prepared at 340°C. The prepared catalyst was then collected in N₂ and dried under vacuum. The *ex-situ* catalyst prepared in CO was named as *ExCO-01*, and the one prepared in molecular hydrogen

was marked as *ExH-01*. As designed in Table 6-1, the HDS activities of the two candidate *ex-situ* catalysts were investigated and compared under normal reaction conditions, which are listed in Table 6-3.

Table 6 - 3 Experimental conditions for preparing *ex-situ* catalysts and for investigating their HDS activities

Catalyst preparation					
Catalyst ID	Gas atmosphere	H₂S	H₂O	Temperature	
<i>ExCO-01</i>	CO (500 psi)	200 psi	20 ml	340 °C	
<i>ExH-01</i>	H ₂ (500 psi)	200 psi	20 ml	340 °C	

HDS activity investigation					
Experiment ID	Gas atmosphere	H₂S	H₂O	Temperature	Model compounds
<i>ExCO0901</i>	H ₂ (590 psi)	10 psi	0	380 °C	DBT+4,6-DMDBT*
<i>ExH0901</i>	H ₂ (590 psi)	10 psi	0	380 °C	
<i>ExCO1001</i>	H ₂ (600 psi)	0	0	340 °C	DBT**
<i>ExH1001</i>	H ₂ (600 psi)	0	0	340 °C	

* 0.5g 4,6-DMDBT and 0.42g DBT dissolved in 100 ml toluene, 0.09g *ex-situ* catalyst used (about 600 ppm Mo), S/Mo≈10 (molar)

** 2.1g DBT dissolved in 100 ml toluene (4100-4200 ppmw S, 11mmol Mo), 0.09g *ex-situ* catalyst used (about 600 ppm Mo), S/Mo≈22 (molar)

The activity of the two candidate *ex-situ* catalysts was firstly investigated *via* the simultaneous HDS of DBT and 4,6-DMDBT using molecular hydrogen. In these two experiments, 10 psi H₂S was fed into the reaction system to keep the *ex-situ* catalyst in the sulfidation status. And then,

two more repeating experiments were carried out by using DBT as the model compound and eliminate the influence of H₂S on HDS reactions. H₂S was not used in these experiments to test whether the catalyst activity lost after exposed in the air during experimental operations. Since DBT has much higher reactivity than 4,6-DMDBT, the HDS of DBT was processed at lower reaction temperature with higher concentration of the sulfur-containing compound in the feedstock.

6.2.3 Reactivity of the two hydrogen sources

The reactivity of the two hydrogen sources in the simultaneous HDS of DBT and 4,6-DMDBT was compared over *ex-situ* prepared dispersed Mo sulfide catalyst, ExCO-01. Detailed experimental conditions are listed in Table 6-4.

Table 6 - 4 Experimental conditions for comparing the reactivity of two hydrogen sources*

Catalyst ID	Gas atmosphere	H ₂ S	H ₂ O	Temperature
ExCO0902	CO (590 psi)	5 psi	5 ml	380 °C
ExCO0903	H ₂ (590 psi)	5 psi	5 ml	380 °C

* 0.5g 4,6-DMDBT and 0.42g DBT dissolved in 100 ml toluene, 0.09g *ex-situ* catalyst used (about 600 ppm Mo)

6.3 Results and discussion

6.3.1 Characterization

Characterization results of the catalysts prepared in *in-situ* H₂ and molecular H₂ have been reported and discussed in Chapter 4. BET and HRTEM results had shown that the dispersed Mo sulfide catalyst had higher surface area and dispersed in smaller particles.

In the XRD spectra, width of peaks increases when crystal size become smaller and particle size can be calculated from the peak width at half height of each characteristic peak according to Scherrer equation (Eq.(6-1)). Here the width at half height of peak at 59° was chosen to calculate D.

$$D = \frac{0.89 \cdot \lambda}{W \cdot \cos \theta} \quad (6-1)$$

where: D is the particle diameter, λ the wave length of the X-ray, W the full width at half maximum, θ the diffraction angle.

From the standard spectra of MoS₂ it is known that the peak at 59° is constituted and overlapped by two peaks at 58.5° and 60.2°. Assuming the MoS₂ catalysts particle are small enough and are able to be treated as small spheres, the particle size from different peaks can be the same. The peak at 59° can be fitted into two peaks based on Gaussian Function. Applying a limitation for the peak fitting (Eq.(6-2)):

$$\frac{W_1}{W_2} = \frac{\cos \theta_2}{\cos \theta_1} \quad (6-2)$$

With the peak center and width ratio, the wide peak at 59° was fitted as show in Fig.6-1. The MoS₂ particle diameters calculated according to each split peak of each MoS sample are listed in

Table 6-5. Calculated MoS₂ particle diameters prepared in *in-situ* H₂ and molecular H₂ were 3.6 nm and 3.4 nm, respectively, where the numbers were averaged from ones obtained at the split peaks of 58.5° and 60.2°. Larger MoS₂ particle size observed in SEM images, 20-40 nm, suggested dispersed Mo sulfide particles were dispersed as polycrystallines composed from the aggregation of small nano-sized crystals. Although the MoS₂ crystal diameters of the two *ex-situ* catalysts determined from XRD observation were almost the same, the morphology of MoS₂ slabs and the size of aggregated MoS₂ particles have been found to be different significantly *via* HRTEM and SEM characterization. As reported and discussed in Chapter 4, dispersed Mo sulfide catalyst prepared in *in-situ* hydrogen had higher surface area, larger pore volume, shorter MoS₂ sheets, lower stacking degree, and smaller particle size than the one prepared in molecular hydrogen.

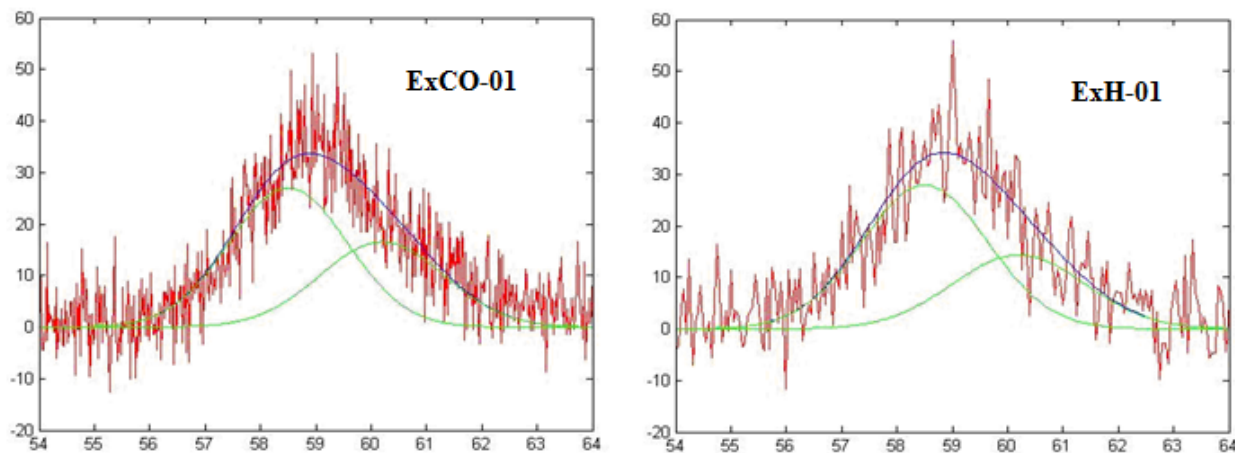


Fig. 6 - 1 Peak fitting for XRD spectra of dispersed MoS catalysts prepared in *in-situ* H₂ and molecular H₂.

Table 6 - 5 Particle size obtained from the Scherrer equation and peak fitting of the XRD spectra for each MoS₂ particles prepared in different H₂ atmospheres

Samples	2θ	W	D/nm	\bar{D} /nm
MoCO340 [†]	58.5	2.52	3.57	3.6
	60.2	2.55	3.57	
MoH340 [‡]	58.5	2.68	3.36	3.4
	60.2	2.71	3.35	

[†] The catalyst sample MoCO340 was previously prepared for HRTEM analysis under almost the same preparation conditions as the catalysts sample of ExCO-01. The characterization results (XRD, and HRTEM) of MoCO340 were reported in this section as the dispersed catalyst prepared *ex-situ* in *in-situ* H₂.

[‡] The catalyst sample MoH340 was previously prepared for HRTEM analysis under almost the same preparation conditions as the catalysts sample of ExH-01. The characterization results (XRD, and HRTEM) of MoH340 were reported in this section as the dispersed catalyst prepared *ex situ* in molecular H₂.

6.3.2 *In-situ* hydrogen versus molecular hydrogen for HDS

6.3.2.1 Precursor of PMA

The use of H₂ *in-situ* generated *via* the WGS reaction in hydro-treating reactions is a key point in the novel one-step bitumen upgrading technique developed by our group. The previous work in our group done by Moll⁶ has found that *in-situ* H₂ was more reactive in upgrading bitumen emulsions than molecular H₂. The upgraded bitumen obtained in the *in-situ* H₂ experiments had lower viscosity, lower gravity, and much less asphaltenes. In the present study, the reactivity of *in-situ* H₂ will be compared with molecular H₂ in the HDS reactions to investigate the effect of hydrogen atmosphere on HDS reactions occurring in upgrading processes.

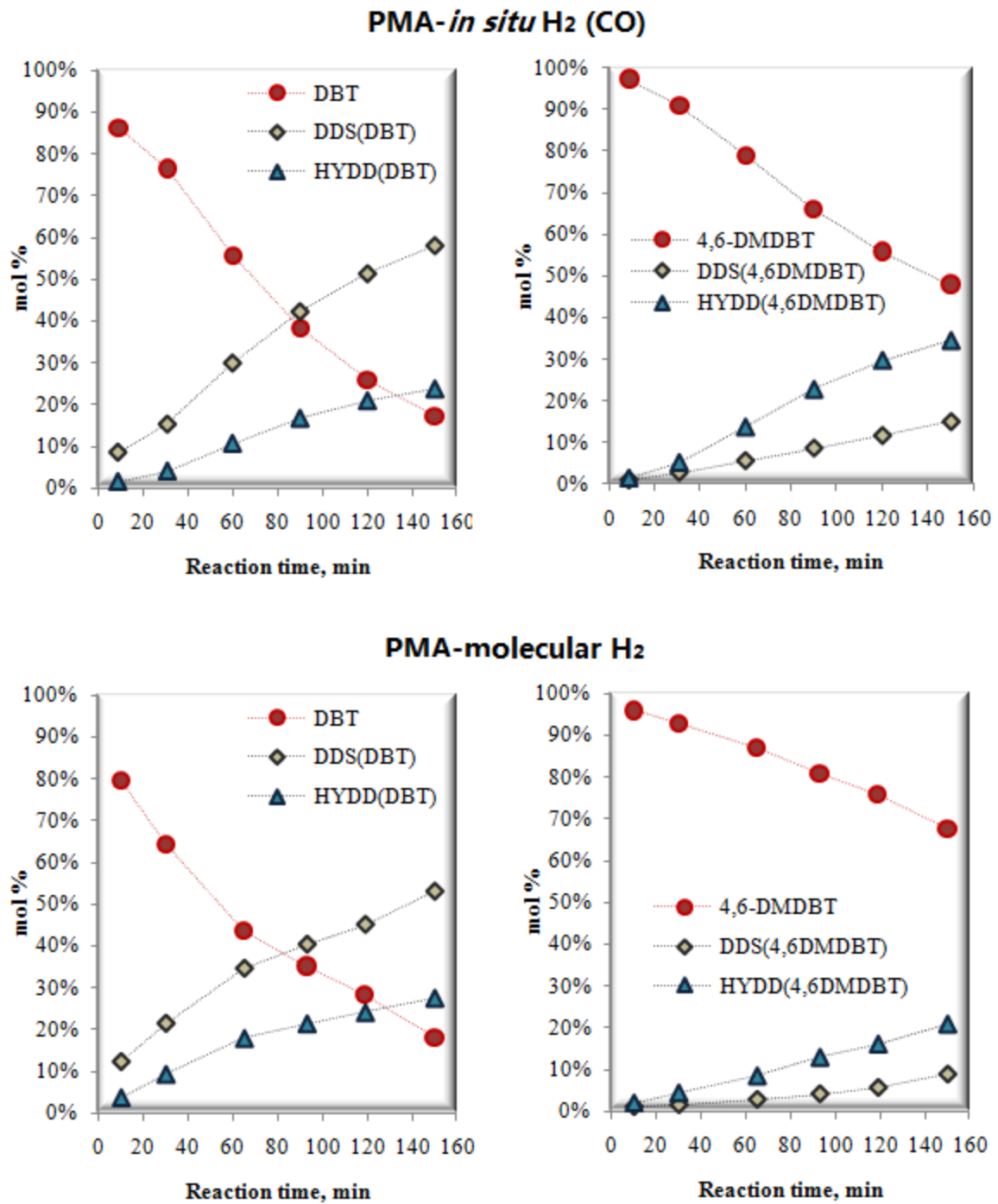


Fig. 6 - 2 Simultaneous HDS of DBT and 4,6-DMDBT in *in-situ* hydrogen versus molecular hydrogen over dispersed Mo sulfide catalyst derived from PMA at 380°C. Other conditions: 590 psi CO or H₂, 10 psi H₂S, 10 ml H₂O, 100 ml toluene, 0.5g 4,6-DMDBT, 0.42g DBT, 400-500 ppmw Mo, 150 min, HC reactor

Fig. 6-2 shows the simultaneous HDS of DBT and 4,6-DMDBT over *in-situ* prepared Mo sulfide catalyst derived from the precursor of PMA using the two different hydrogen sources. In the HDS of DBT with the presence of 4,6-DMDBT, the concentration of DBT changed in the same range under both reaction conditions, decreasing from 80-85 mol% to around 15 mol%. When using *in-situ* hydrogen (PMA-CO in Fig. 6-3), the sulfur removal from DBT was slightly lower than in the other reaction run in molecular hydrogen (PMA-H₂ in Fig. 6-3), while with extending the reaction time, the percent of desulfurization of DBT in the two experiments became very similar.

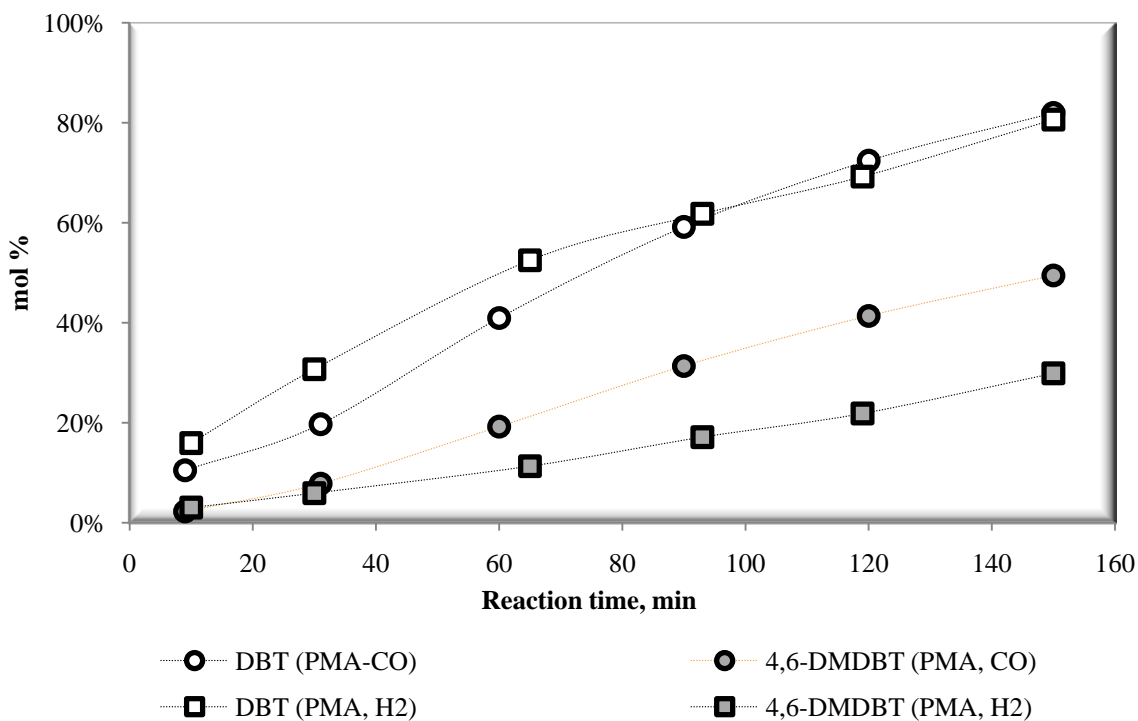


Fig. 6 - 3 Desulfurization of DBT and 4,6-DMDBT as a function of reaction time using *in-situ* hydrogen and molecular hydrogen, respectively, over dispersed Mo sulfide catalyst derived from PMA at 380°C.

Other conditions: 590 psi CO or H₂, 10 psi H₂S, 10 ml H₂O, 100 ml toluene, 0.5g 4,6-DMDBT, 0.42g DBT, 400-500 ppmw Mo, 150 min, HC reactor.

In the HDS of 4,6-DMDBT, the conversion of the starting material decreased from 97mol% to lower than 50mol% within 150min using *in-situ* hydrogen and changed from 97mol% to around 70mol% in the molecular hydrogen experiment (Fig. 6-2). The percentage of sulfur-removed products in the HDS product mixture obtained in the *in-situ* hydrogen run was found to be significantly higher than the number obtained in the molecular hydrogen run (Fig. 6-3).

6.3.2.2 Precursor of ATTM

Ammonium tetrathiomolybdate is an already sulfided Mo precursor. Mo sulfide catalysts can be synthesized directly *via* the thermal decomposition of ATTM and do not need further presulfidation. Song's group has done a lot of HDS study using Mo sulfide catalysts derived from ATTM^{13b, 78}. The unsupported Mo sulfide catalysts they prepared from ATTM *via* hydrothermal decomposition had a specific surface area of 320m²/g, which is higher than the one prepared from PMA in the present study. They have found that ATTM is an effective precursor for HDS reactions. In this section, ATTM was used instead of PMA to investigate the effect of hydrogen source on the simultaneous HDS of DBT and 4,6-DMDBT.

The simultaneous HDS of DBT and 4,6-DMDBT was carried out using 100% CO, 100% H₂, 50% CO with 50% H₂, respectively. The conversion of model compounds and the sulfur-removal results are charted in Fig.6-4. It was interesting to find that *in-situ* H₂ had significant advantages over molecular H₂ in the HDS of both sulfur-containing compounds. The conversion of starting materials and the sulfur-removal results increased with increasing the ratio of CO/H₂ in the reacting gas atmosphere.

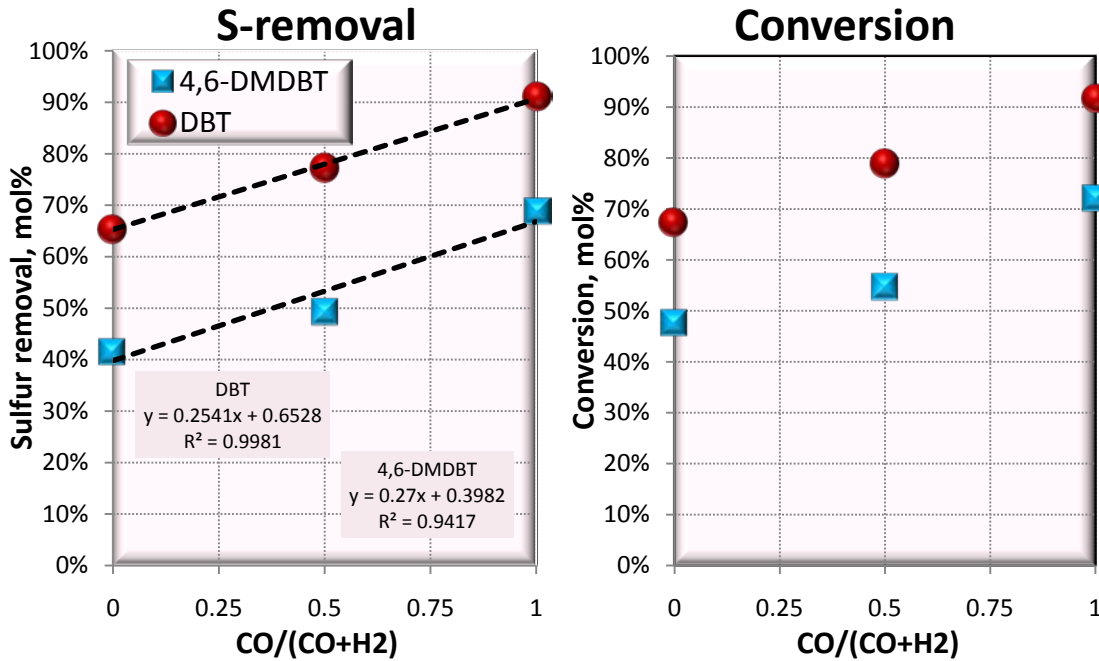


Fig. 6 - 4 Conversion and sulfur-removal of model sulfur-containing compounds obtained as a function of the gas composition of syngas.

Other conditions: 380⁰C, equi-molar DBT+4,6-DMDBT, 1670 ppmw S, 430 ppmw Mo, 3hr, 100 ml toluene, 10 ml ATTMM aqueous solution, S/Mo~10/1, 600 psi syngas.

Interestingly, when we illustrated the relationship of the sulfur-removal of DBT and 4,6-

DMDBT with the syn-gas composition, $\gamma = \frac{P_{CO}}{P_{CO} + P_{H_2}}$ (Fig. 6-4), we found that the

desulfurization percent (molar) of each model S compound could be linearly related to the value of γ (Eq. (6-3&6-4)). Therefore, if we know the molar composition of syn-gas, we may predict

HDS results of DBT and 4,6-DMDBT by using these equations.

$$D_{DBT}, \% = 0.25 \times \gamma + 0.65 \quad R^2 = 0.99 \quad (6-3)$$

$$D_{4,6-DMDBT}, \% = 0.27 \times \gamma + 0.40 \quad R^2 = 0.94 \quad (6-4)$$

Where,

$D_{DBT,\%}$: *S*-removal of DBT

$D_{4,6-DMDBT,\%}$: *S*-removal of 4,6-DMDBT

6.3.2.3 Discussion

The efficiency of the reaction system using two different hydrogen sources towards the simultaneous HDS of DBT and 4,6-DMDBT can be investigated *via* comparing the pseudo-first-order rate constant for the conversion of starting sulfur model compounds. In the PMA study, the rate constant for the conversion of DBT, Table 6-6, in the *in-situ* H₂ run was 1.2 times as high as that in the molecular hydrogen run. This promotional effect of *in-situ* H₂ in HDS was stronger in the HDS of the more refractory sulfur-containing compound, 4,6-DMDBT. Over the catalyst prepared from ATTM, the higher efficiency to the simultaneous HDS of DBT and 4,6-DMDBT obtained using the *in-situ* H₂ was even more significant than what have observed in the PMA study, and the desulfurization percentage could be correlated to the molar composition of the gas mixture of CO and hydrogen according to Eq. (6-3) and Eq. (6-4). Therefore, CO is a promising hydrogen source for hydrodesulfurization of refractory sulfur-containing species in the presence of water.

The higher desulfurization results obtained using *in-situ* H₂ may be due to the reduction of the water content during the reactions *via* being consumed in the WGS reaction to generate *in-situ* H₂ in the 100% CO experiment. Water is an important and special reactant in the present reaction system. Firstly, water reacts with CO to provide *in-situ* H₂ for hydro-treating reactions. Secondly, water is the phase where the catalyst precursor is present initially, and is involved in the

hydrothermal decomposition of the precursor to prepare the catalyst. The presence of water was reported to have positive effect on producing MoS₂ with higher surface area and smaller particle size, and also have promotional effect on the fine-dispersion of catalyst particles in the reaction system^{38, 41}. Thirdly, the adsorption of water molecules on the catalyst surface has inhibitive effect on hydro-treating reactions. This inhibitive effect should be minimized in the presence of WGS reaction to provide *in-situ* H₂ for hydro-treating reactions. Therefore, the consumption of water in the 100% CO experiment reduced the adsorption of water molecules on the active sites and resulted in higher conversion and sulfur-removal of DBT and 4,6-DMDBT.

Table 6 - 6 Pseudo-first-order rates constants in the simultaneous HDS of DBT and 4,6-DMDBT at 380°C over dispersed Mo sulfide catalyst prepared from PMA in the two hydrogen sources (other detailed conditions refer to Table 6-2)

	PMA, CO		PMA, H ₂	
	DBT	4,6-DMDBT	DBT	4,6-DMDBT
$k'_{Conv.}$	19.5×10^{-5}	8.8×10^{-5}	16.7×10^{-5}	4.1×10^{-5}
k'_{DDS}	13.6×10^{-5}	2.5×10^{-5}	10.0×10^{-5}	1.1×10^{-5}
k'_{HYD}	5.9×10^{-5}	6.3×10^{-5}	6.7×10^{-5}	3.0×10^{-5}
k'_{DDS}/k'_{HYD}	2.3	0.4	1.5	0.4
HDS of DBT: $k'_{Conv., CO}/k'_{Conv., H_2}$	1.2			
HDS of 4,6-DMDBT: $k'_{Conv., CO}/k'_{Conv., H_2}$	2.1			

Additionally, according to HRTEM and SEM characterization results, the dispersed Mo sulfide catalyst prepared in *in-situ* hydrogen derived from PMA had shorter curved MoS₂ slabs with lower stacking degree and dispersed in smaller polycrystalline particles. The BET specific area

of the catalyst prepared in *in-situ* H₂ is also higher than the other one. Hence, the catalyst prepared in *in-situ* H₂ may provide more edge and corner active sites exposed for HDS reactions. This may be another important reason contributing for the higher efficiency of *in-situ* H₂ reaction system towards the HDS of refractory sulfur-containing compounds.

The selectivity between the two HDS pathways was considered to depend on the coexistence of the two different active sites for DDS and HYD reactions. Tanaka^{74b} cut MoS₂ single crystals into several pieces perpendicularly to basal planes to increase the area of edge planes with the basal plane area constant. This cut resulted in the increase of hydrogenation activity of the catalyst. According to the “Rim-Edge” model³¹, increasing the amount of rim sites would improve the selectivity for hydrogenation reactions. According to the insightful study into the micro-structure of MoS₂ slabs by Topsøe group³⁴⁻³⁵, a kind of metallic-like brim sites, which located adjacent to the edge of MoS₂ slabs, existed and they played an important role in hydrogenation reactions. According to these advanced MoS₂ structure-activity correlations, the catalyst with a low stacking degree would have a greater selectivity to hydrogenated products. Our HRTEM results have shown that the stacking degree of the catalyst prepared in *in-situ* hydrogen (MoCO340) is much lower than the one made in molecular hydrogen (MoH340). Hence, based on the reported correlation of the MoS₂ structure to the catalyst activity, the catalyst generated in *in-situ* hydrogen should have higher selectivity for the HYD pathway. As the predominant reaction pathway in the HDS of 4,6-DMDBT, the higher concentration of HYD active sites on the catalyst surface would result in higher conversion and desulfurization of 4,6-DMDBT. This is in agreement with the higher pseudo-first-order rate constant for the conversion of 4,6-DMDBT obtained in the experiment using *in-situ* hydrogen.

However, the ratio between the pseudo-first-order rate constants of DDS and HYD routes in the HDS of DBT in the PMA study decreased from 2.3 to 1.5 when using *in-situ* hydrogen instead of molecular hydrogen, namely, the pathway of direct desulfurization in the HDS of DBT was more favored in the *in-situ* hydrogen reaction system. This observation was not in agreement with the correlation of the MoS₂ structure to the selectivity. Molecules of 4,6-DMDBT preferred to adsorb on the HYD sites rather than DDS sites because of the steric hindrance of the two methyl groups adjacent to the sulfur atom on the DDS active sites. Therefore, in the HDS of DBT in the mixture with 4,6-DMDBT, the competitive adsorption of the two sulfur-containing compounds on the HYD active sites may contribute to the lower selectivity towards HYD in the HDS of DBT. Additionally, the higher amount of hydrogen in the experiment using external provided molecular hydrogen may be another reason for the higher selectivity of HYD in the HDS of DBT.

The experiments using ATTM were carried out in the SS reactor, which is not equipped with a liquid sampling line. Only the final HDS products were available for the analysis. So the ratio between the concentrations of DDS and HYD products was used instead of pseudo-first-order rate constants in the discussion on the selectivity between the two reaction pathways. The numbers are listed in Table 6-7. The direct desulfurization pathway was more favored in the HDS of both DBT and 4,6-DMDBT when increasing the concentration of molecular H₂ in the syngas. Hydrogenation reaction occurred at the sites composing of a vacancy associated with a S-H group and with a hydrogen atom adsorbed on a molybdenum atom¹⁷. Therefore, the availability of adsorbed hydrogen is important in hydrogenation steps. The higher selectivity on HYD observed when using CO instead of molecular H₂ as the reaction atmosphere indicated that

the *in-situ* H₂ generated *via* the WGS reaction had provided at least comparable amount of adsorbed S-H for HYD reactions.

Table 6 - 7 Selectivity between two HDS reaction pathways observed using syngas with different CO/H₂ ratio over dispersed Mo sulfide catalyst derived from ATTM at 380°C (detailed experimental conditions refer to Table 6-2)

		CO	CO+H ₂	H ₂
$\frac{DDS^*}{HYD}$	DBT	2.5	2.4	3.5
	4,6-DMDBT	0.46	0.56	0.59

$$* \frac{DDS}{HYD} = \frac{DDS \text{ product}(s)}{\text{Intermediate}(s)+HYDD \text{ products}}$$

The relationship between the selectivity and the source of hydrogen obtained in the ATTM study was different from that observed in the PMA study. This probably depended on the morphology of the dispersed Mo sulfide catalysts derived from the two Mo precursors. Due to the absence of the characterization of the catalyst prepared from ATTM, it is not precise to discuss the details.

As discussed in this part, both the structure of the catalyst and the reactivity of the different sources of hydrogen may affect HDS and the selectivity between the two HDS pathways. However, the catalysts used in this section were *in-situ* prepared during hydro-treating reactions, so it is difficult to tell which factor plays a more important role in HDS reactions. Therefore, in the next section, the dispersed Mo sulfide catalysts would be *ex-situ* prepared and the simultaneous HDS of DBT and 4,6-DMDBT will be studied over *ex-situ* catalysts in the same

source of hydrogen, namely, molecular hydrogen. Such experimental design allows us to investigate the effect of the hydrogen sources on the catalyst activity towards HDS reactions.

6.3.3 HDS results using *ex-situ* prepared catalysts

In this section, catalytic activities of the two *ex-situ* prepared dispersed MoS₂ catalysts, *ExCO-01* and *ExH-01*, towards HDS were studied and compared. Pseudo-first-order rate constants for the conversion of starting materials and for the two reaction pathways over the two *ex-situ* catalysts are listed in Table 6-8 and the product distribution is shown in Fig. 6-5. The R^2 values of these rate constants were higher than 0.95, indicating that the pseudo-first-order rate constants were applicable. Comparing the HDS results of DBT and 4,6-DMDBT over *ExCO-01* to those obtained using *ExH-01*, we may find that:

- Rate constants for the conversion of the two sulfur model compounds increased by 50%;
- Selectivity towards the DDS route decreased from 1.2 to 0.9 in the HDS of DBT;
- Selectivity between the two route did not change significantly in the HDS of 4,6-DMDBT.
- Higher sulfur-removal was obtained (Fig.6-6).

Hence, the catalyst, *ExCO-01*, which was prepared in *in-situ* hydrogen exhibited higher HDS activity than the other one generated in molecular hydrogen, *ExH-01*. It is interesting to observe that the catalyst prepared in *in-situ* hydrogen had a higher selectivity towards DDS in the HDS of DBT in the mixture of 4,6-DMDBT, similar to the experimental results observed in the previous section wherein *in-situ* hydrogen was used instead of molecular hydrogen (Table 6-6, PMA as precursor). As discussed in the PMA study in the section 6.3.2.3, the lower selectivity of HYD

route over the lower stacked Mo sulfide catalyst prepared in *in-situ* hydrogen (*ExCO-01*) was due to the competitive adsorption of DBT and 4,6-DMDBT on the HYD active sites. To verify this proposal and repeat the comparison on the HDS activity of the two *ex-situ* catalysts, the HDS of DBT was carried out. The results are listed in Table 6-9.

Table 6 - 8 Pseudo-first-order rate constants in the simultaneous HDS of DBT and 4,6-DMDBT at 380°C over *ex-situ* prepared dispersed Mo sulfide catalyst (other detailed conditions refer to Table 6-3)

	Cat. of <i>ExCO</i> -01 (Exp. ID <i>ExCO</i> 0901)		Cat. of <i>ExH</i> -01 (Exp. ID <i>ExH</i> 0901)	
	DBT	4,6-DMDBT	DBT	4,6-DMDBT
$k'_{Conv.}$	36.0×10^{-5}	14.9×10^{-5}	24.7×10^{-5}	9.77×10^{-5}
k'_{DDS}	19.4×10^{-5}	3.96×10^{-5}	11.5×10^{-5}	2.69×10^{-5}
k'_{HYD}	16.6×10^{-5}	10.9×10^{-5}	13.2×10^{-5}	7.08×10^{-5}
k'_{DDS}/k'_{HYD}	1.2	0.4	0.9	0.4
HDS of DBT: $k'_{Conv., ExCO}/k'_{Conv., ExH}$			1.5	
HDS of 4,6-DMDBT: $k'_{Conv., ExCO}/k'_{Conv., ExH}$			1.5	

Table 6 - 9 Pseudo-first-order rate constants in the HDS of DBT at 340°C over *ex-situ* prepared dispersed Mo sulfide catalysts (other detailed conditions refer to Table 6-3)

	Cat. of <i>ExCO</i> -01 (Exp. ID <i>ExCO</i> 1001)	Cat. of <i>ExH</i> -01 (Exp. ID <i>ExH</i> 1001)
	DBT	DBT
$k'_{Conv.}$	11.0×10^{-5}	7.0×10^{-5}
k'_{DDS}	4.6×10^{-5}	4.2×10^{-5}
k'_{HYD}	6.4×10^{-5}	2.8×10^{-5}
k'_{DDS}/k'_{HYD}	0.7	1.5
HDS of DBT: $k'_{Conv., ExCO}/k'_{Conv., ExH}$	1.6	

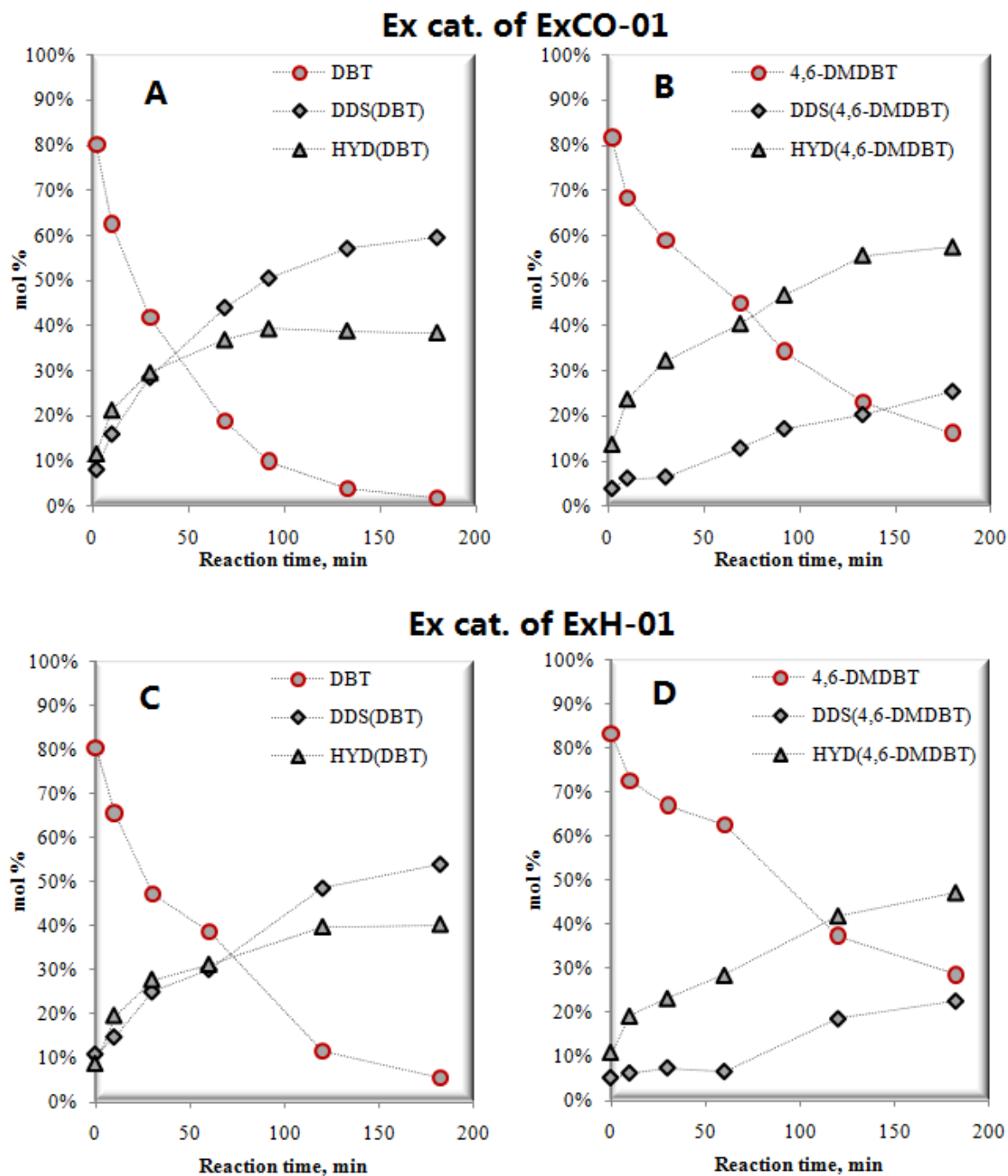


Fig. 6 - 5 Simultaneous HDS of DBT and 4,6-DMDBT over dispersed Mo sulfide catalyst *ex-situ* prepared in CO or molecular H₂ at 380°C. **A:** HDS of DBT over *ExCO-01*, **B:** HDS of 4,6-DMDBT over *ExCO-01*, **C:** HDS of DBT over *ExH-01*, **D:** HDS of 4,6-DMDBT over *ExH-01*. Other conditions: 100ml toluene, no H₂O, 590 psi H₂, 10 psi H₂S, 0.5g 4,6-DMDBT, 0.42g DBT, 600 ppmw Mo, HC reactor

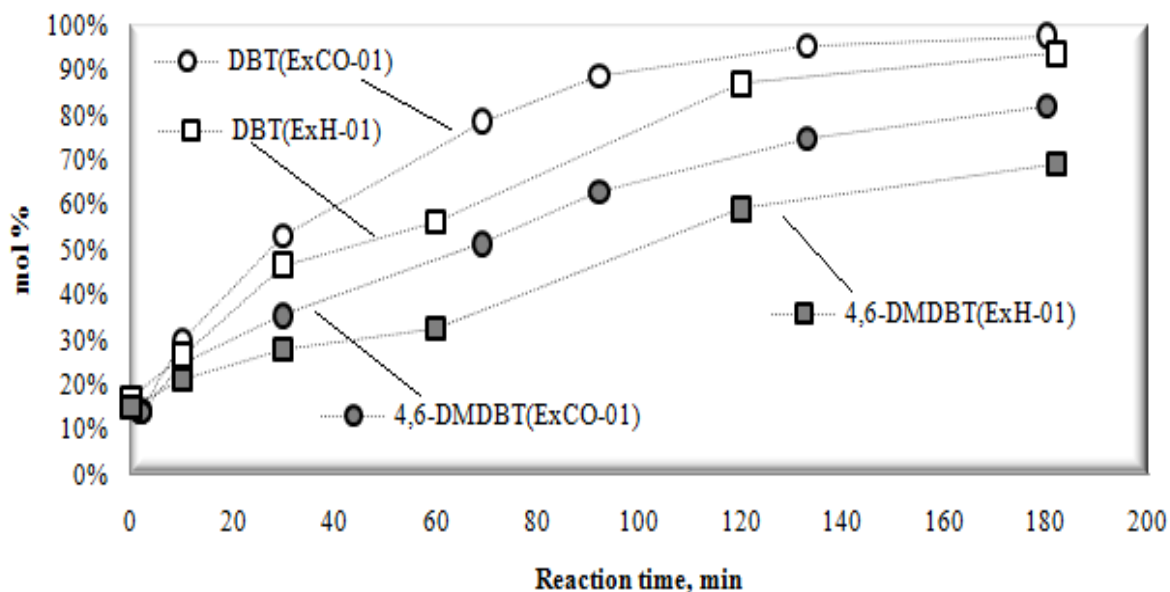


Fig. 6 - 6 Sulfur-removal of DBT and 4,6-DMDBT over dispersed Mo sulfide catalyst *ex-situ* prepared in CO or molecular H₂ at 380°C.

Other conditions: 100ml toluene, no H₂O, 590 psi H₂, 10 psi H₂S, 0.5g 4,6-DMDBT, 0.42g DBT, 600 ppmw Mo, HC reactor

At 340°C, the pseudo-first-order rate constant for the conversion of DBT obtained over the *ExCO-01* catalyst was found to be 1.6 times as high as that observed over the *ExH-01* catalyst. This number is almost the same as the ratio observed in the HDS of DBT in the mixture with 4,6-DMDBT. Therefore, the atmosphere of *in-situ* hydrogen has advantages over molecular hydrogen in generating highly active Mo sulfide catalyst for HDS reactions (Table 6-8 and Table 6-9).

The higher HDS activity of the *ExCO-01* catalyst may be due to its physical morphology more appropriate for HDS reactions. Higher BET surface area would provide more access for sulfur-

containing molecules to adsorb on active sites. Shorter MoS₂ length and smaller MoS₂ crystal stacks would have more active corner and edge positions exposed to reactants^{26-27, 61}.

Regarding the HDS of DBT in the mixture with 4,6-DMDBT, the reaction pathway of DDS was more favored over the *ExCO-01* catalyst, namely, the HYD route was more preferred over the *ExH-01* catalyst (Table 6-8). However, in the HDS of DBT alone, the pseudo-first-rate constant of the HYD pathway was even higher than the one of the DDS route over the *ExCO-01* and the selectivity for the DDS route was less favored. These observations indicated the *ExCO-01* catalyst had very high hydrogenation activity. Such catalyst with high hydrogenation activity would have advantages in reducing the yield of coke during upgrading heavy feed stocks. Moreover, the higher selectivity towards HYD over the *ExCO-01* catalyst was in accordance with the correlation of HDS selectivity to MoS₂ structures as discussed in the last section, and it also supported the proposal of the competitive adsorption of the two sulfur-containing compounds on HYD active sites.

6.3.4 Reactivity of *in-situ* H₂ versus molecular H₂

To compare the reactivity of *in-situ* H₂ versus molecular H₂ in the presence of water, simultaneous HDS of DBT and 4,6-DMDBT was studied in the two different hydrogen atmospheres over the same *ex-situ* catalyst, *ExCO-01*. Fig. 6-7 shows the HDS product distribution of DBT and 4,6-DMDBT obtained using *in-situ* hydrogen and molecular hydrogen. Concentrations of DBT were similar in the two experimental conditions, namely the conversion of DBT was similar when using the two different reactant hydrogen atmospheres. This is also

reflected from the pseudo-first-order rate constants for the conversions of DBT as listed in Table 6-10. The same situation was also observed in the HDS of 4,6-DMDBT. This indicated that the hydrogen generated *in-situ* via the WGS reaction had similar reactivity to molecular hydrogen towards the conversion of sulfur model compounds with the presence of water over the dispersed Mo sulfide catalyst. Therefore, the question asked in the introduction section was answered. The catalyst prepared in *in-situ* H₂ had higher activity towards HDS than the one prepared in molecular H₂; *in-situ* H₂ had similar reactivity as molecular H₂ in HDS reactions with the presence of water. The better hydro-treating results obtained in our previous studies^{5-6, 42, 49a, b} should be mostly attributed to the higher activity of the catalyst *in-situ* generated in CO.

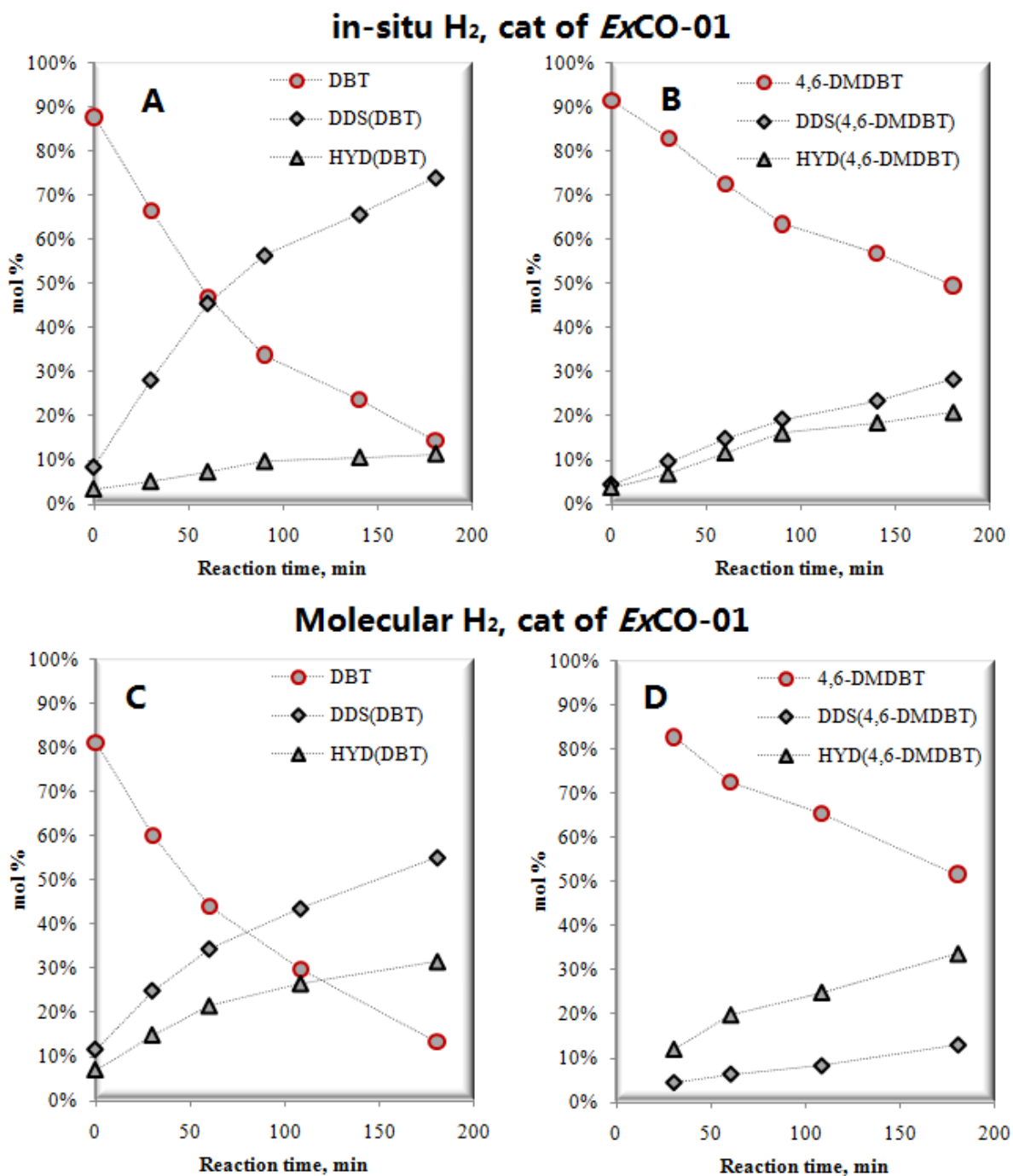


Fig. 6 - 7 Simultaneous HDS of DBT and 4,6-DMDBT at 380°C over dispersed Mo sulfide catalyst *ex-situ* prepared in CO using *in-situ* hydrogen and molecular hydrogen. A: HDS of DBT in *in-situ* H₂, B: HDS of 4,6-DMDBT in *in-situ* H₂, C: HDS of DBT in molecular H₂, D: HDS of 4,6-DMDBT molecular H₂. Other conditions: 100ml toluene, 5ml H₂O, 595 psi H₂, 5 psi H₂S, 0.5g 4,6-DMDBT, 0.42g DBT, 600 ppmw Mo, HC reactor

Table 6 - 10 Pseudo-first-order rates constants in the simultaneous HDS of DBT and 4,6-DMDBT at 380°C in the two hydrogen sources over the ExCO-01 catalyst (other detailed conditions refer to Table 6-4)

	CO (<i>In-situ</i> H ₂) (Exp. ID: ExCO0902)		Molecular H ₂ (Exp. ID: ExCO0903)	
	DBT	4,6-DMDBT	DBT	4,6-DMDBT
$k'_{Conv.}$	16.3×10^{-5}	5.7×10^{-5}	16.5×10^{-5}	5.1×10^{-5}
k'_{DDS}	12.8×10^{-5}	2.9×10^{-5}	8.4×10^{-5}	1.5×10^{-5}
k'_{HYD}	3.5×10^{-5}	2.8×10^{-5}	8.1×10^{-5}	3.6×10^{-5}
k'_{DDS}/k'_{HYD}	3.7	1.0	1.0	0.4
HDS of DBT: $k'_{Conv, CO}/k'_{Conv, H_2}$	1.0			
HDS of 4,6-DMDBT: $k'_{Conv, CO}/k'_{Conv, H_2}$	1.1			

Although the similar reactivity of the two kinds of hydrogen in the conversions of DBT and 4,6-DMDBT was observed, the selectivity between the two HDS reaction pathways, DDS *versus* HYD, was dramatically different. When using *in-situ* hydrogen instead of molecular hydrogen, the ratio of k'_{DDS}/k'_{HYD} increased from 1.0 to 3.7 in the HDS of DBT and from 0.4 to 1.0 in the HDS of 4,6-DMDBT, suggesting the HYD pathway was more favoured in the experiment using molecular hydrogen. Since these two experiments were carried out over the same *ex-situ* prepared catalyst, the source of hydrogen used in the experiments was the main reason causing the difference in the selectivity of HDS pathways. In the molecular hydrogen experiment, the concentration of reactive hydrogen is significantly higher than that in the CO run. Therefore, the

higher selectivity towards the HYD route was attributed from the high concentration of hydrogen in the molecular hydrogen experiment.

6.4 Conclusions

In the present chapter, better HDS results were obtained using *in-situ* hydrogen compared *versus* using molecular hydrogen. The higher efficiency of the *in-situ* hydrogen reaction system for upgrading bitumen emulsions and for HDS/HDN reactions were also observed previously^{5-6, 42}. The major reason for this phenomenon was figured out in this chapter *via* separating the preparation of dispersed catalyst from HDS reactions. From this study, following conclusions may be obtained:

- (1) The *in-situ* hydrogen reaction system is more effective than the molecular hydrogen reaction system in the simultaneous HDS of DBT and 4,6-DMDBT over the dispersed Mo sulfide catalyst prepared from PMA.
- (2) When using ATTM as the Mo precursor, conversions and desulfurizations of DBT and 4,6-DMDBT could be linearly correlated to the molar composition of syngas.
- (3) *In-situ* H₂ is a more effective hydrogen atmosphere than molecular H₂ for preparing more active dispersed Mo sulfide catalyst with higher BET surface area and smaller size MoS₂ particles.
- (4) In the HDS reactions, *in-situ* H₂ has similar reactivity to molecular H₂. Molecular hydrogen showed higher selectivity towards the HYD reaction pathway than *in-situ* hydrogen.

- (5) The higher activity of the catalyst prepared in the *in-situ* H₂ was the major contribution to the previously observed promising experimental results using the *in-situ* reaction system.
- (6) The dispersed Mo sulfide catalyst prepared in *in-situ* H₂ had high hydrogenation activities.

Chapter 7 Inhibitive Effect of N-Containing Compounds on Hydrodesulfurization Reactions

7.1 Introduction

Based on model compound studies, basic nitrogen-containing compounds have been considered as one of the strongest HDS inhibitors due to the strong adsorption of the basic nitrogen-containing compounds on active sites on catalyst surface *via* the donation of their unpaired electron to Lewis acid sites or by the interaction with protons of the Brønsted acid sites^{8, 13c, 47, 22-85}. Unlike basic nitrogen-containing compounds, the effect of non-basic nitrogen-containing compounds on HDS was less intensively studied previously. Since carbazole and its derivatives are the major nitrogen-containing compounds in many hard-to-desulfurize middle distillates^{11-12, 51a}, the effect of carbazoles on HDS has attracted more attention recently^{12, 13b, 86}.

The inhibitive effect of quinoline, indole and carbazole on the HDS of DBT was studied by Laredo et al, and a relationship between the HDS rate constant and the concentration of nitrogen-containing compounds was given in Eq.(6-1). In this equation, K_N is the apparent nitrogen-containing compound adsorption equilibrium constant (l/mmol) and represents the behaviour of all the nitrogen-containing compounds that contribute to the inhibition; C_N the initial nitrogen-containing compound concentration (mmol/l) and n the fitting exponent. Therefore, according to

Eq.(7-1), the inhibition effect of nitrogen species depends on their adsorption strength on the catalyst surface and their concentration in the reaction system.

$$r_{HDS} = k_{DBT}C_{DBT}/(1 + K_N^n C_N^n) \quad (7 - 1)$$

The inhibitive effect of non-basic nitrogen-containing compounds, such as carbazole, on HDS was attributed to the hydrogenation reactions converting the non-basic nitrogen-containing compounds into basic compounds, as suggested by Ho^{21, 71}, or due to their polymerization on the catalyst surface¹⁴. The competitive adsorption with sulfur species on active sites on the catalyst surface was also regarded to as a major contribution to the inhibitive effect of non-basic N-containing compounds on HDS reactions²². The initial contact of carbazoles on the catalyst surface is considered most likely as a side-on configuration involving the aromatic ring (parallel to the catalyst surface) rather than an end-on adsorption *via* the nitrogen heteroatom. The adsorption mode of five-membered heterocyclic nitrogen species on catalytically active sites is similar to that of polynuclear aromatics, such as naphthalene^{86a}. According to this adsorption mode proposal, the reaction pathway of HYD in the HDS of sulfur-containing model compounds would be affected more severely than that of DDS.

During HDN, ammonia is produced and released to the gas phase in the reaction system. A part of ammonia will strongly adsorb on the catalyst surface. This may also contribute to the inhibitive effect of nitrogen-containing species on deep HDS. The adsorption of ammonia was found to be weaker than nitrogen-heterocyclic compounds, and was generally treated as a reversible inhibition^{50a}.

This chapter would be the first study on the effect of basic quinoline and non-basic carbazole on the simultaneous HDS of DBT and 4,6-DMDBT using *in-situ* hydrogen over the nano-dispersed Mo sulfide catalyst.

7.2 Experimental

The experiment process has been described in Chapter 2 and will not be repeated here. Detailed conditions of experiments involved in this chapter are listed in Table 7-1. The two The SS Auto-clave batch reactors was used in this serial of experiments to study the effect of nitrogen-containing compounds on the HDS of DBT and 4,6-DMDBT.

Table 7 - 1 Detailed reaction conditions of the experiments involved in Chapter 7*

Experiment ID	Ratio between model compounds				Reaction time, hr	Reaction gas
	DBT	4,6-DMDBT	Quinoline	Carbazole		
NS-18	1	1	0	1	3	H ₂
NS-19	1	1	0	1	3	CO
NS-20	1	1	1	0	3	CO
NS-21	1	1	1	0	3	H ₂
DM-90	1	1	0	0	3	CO
NA-01	Naph: 2		0	0	3	CO
NA-02	Naph: 2		1	0	3	CO
NA-03	Naph: 2		0	1	3	CO

* Other conditions: 10 ml H₂O, 100ml toluene, 380°C, 10 psi H₂S, 590 psi CO or H₂, molar amount of 430~500ppmw Mo (PMA as the precursor)

7.3 Results and discussion

The experimental results on the effect of nitrogen-containing compounds on the HDS of DBT and 4,6-DMDBT are listed in Table 7-2. Molecular H₂ was also used as the reaction gas atmosphere to compare with *in-situ* H₂ to investigate the efficiency of the use of *in-situ* H₂ for HDS in the presence of nitrogen-containing compounds.

7.3.1 HDS in the presence of N-containing compounds using *in-situ* H₂

The simultaneous HDS of DBT and 4,6-DMDBT involved in this section were carried out in the presence of one nitrogen-containing compound, quinoline or carbazole. The nitrogen-containing compound was introduced into the feedstock according to the ratio of S:N equaling to 2:1. The experiment results are listed in Table 7-2.

Table 7 - 2 Conversions and product distributions for the HDS of DBT and 4,6-DMDBT in the presence of nitrogen heterocyclic compounds over a dispersed Mo sulfide catalyst using *in-situ* hydrogen*.

	No N-containing compounds (DM-90)		Quinoline present (NS-20)		Carbazole present (NS-19)	
	DBT	4,6-DMDBT	DBT	4,6-DMDBT	DBT	4,6-DMDBT
Conversion ^a , %	45.7	44.3	18.7	8.5	32.2	19.6
S-removal ^b , mol%	40.9	37.9	16.5	3.7	28.4	11.3
Via DDS ^c , %	71.8	42.7	95.2	73.0		63.2
Via HYD ^d , %	28.2	57.3	4.8	27.0		36.8
Conversion decreased by ^e	---	---	59%	81%	30%	56%
S-removal decreased by ^f	---	---	60%	90%	31%	70%
Relative reactivity ^g		1.03		2.20		1.64
Conversion of N-comp., %		---		99		60
N-removal, mol%		---		66		52

*: Equi-molar DBT and 4,6-DMDBT (1670 ppmw of S in total), 590 psi of CO and 10 psi of H₂S (at room temperature), 500 ppmw Mo, S:N=2:1 (molar), 380°C, 3hr

a: Conversion=(Starting conc. of S comp. - Final conc. of S-comp.)/Starting conc. of S comp.

b: S-removal=sum concentration of S-removed products.

c: S-removal *via* DDS=100% × DDS/(DDS + HYDD)

d: S-removal *via* HYD=100% × HYDD/(DDS + HYDD)

e: equals to $\frac{\text{Conversion of S comp. (No N)} - \text{Conversion of S comp. (Q or Cz)}}{\text{Conversion of S comp. (No N)}}$

f: equals to $\frac{\text{S removal of S comp. (No N)} - \text{S removal of S comp. (Q or Cz)}}{\text{S removal of S comp. (No N)}}$

g: equals to $\frac{\text{Conversion of DBT}}{\text{Conversion of 4,6DMDBT}}$

In the presence of basic quinoline, the conversion and the desulfurization (S-removal) of DBT decreased to the same extent, 60% (Table 7-2). The conversion and desulfurization of 4,6-DMDBT decreased by 81% and 90%, respectively. Considering the sulfur-removal percentages of the two sulfur-containing compounds, the contribution from the HYD pathway decreased more than from the DDS route. In the HDS of DBT, only 5% removed sulfur was obtained from the hydrogenation desulfurization pathway. In the presence of non-basic nitrogen-containing compound carbazole, the conversion of DBT and 4,6-DMDBT decreased by 30% and 56%, respectively, and the sulfur-removal of both S-containing compounds decreased by 31% and 70%, respectively. Similar to the experiments with quinoline, the conversion and the desulfurization of DBT were influenced by carbazole to the same extent, and the negative effect of carbazole on the sulfur-removal of 4,6-DMDBT was stronger than on the conversion.

Comparing the two sulfur-containing model species, the HDS of the more refractory 4,6-DMDBT was inhibited to a higher degree by the presence of basic or non-basic nitrogen-containing compounds than that of DBT over the nano-dispersed Mo sulfide catalyst using *in-situ* H₂. This was reflected from the relative HDS reactivity of the two sulfur-containing compounds as listed in Table 7-2, which was expressed as the ratio between the conversions of DBT to 4,6-DMDBT. Lower relative reactivity means higher reactivity of 4,6-DMDBT related to that of DBT in HDS reactions. The lowest number was obtained in the HDS reaction without the presence of any nitrogen-containing compound and the highest was obtained in the experiment in the presence of quinoline. After introducing basic quinoline into the reaction system, the catalytic activity towards the HDS of 4,6-DMDBT was almost completely inhibited

and the conversion was as low as 8.5%, (Table 7-2 and Fig. 7-1 B). Interestingly, the conversion of quinoline was as high as 99% and the nitrogen-removal of quinoline reached 66 mol%.

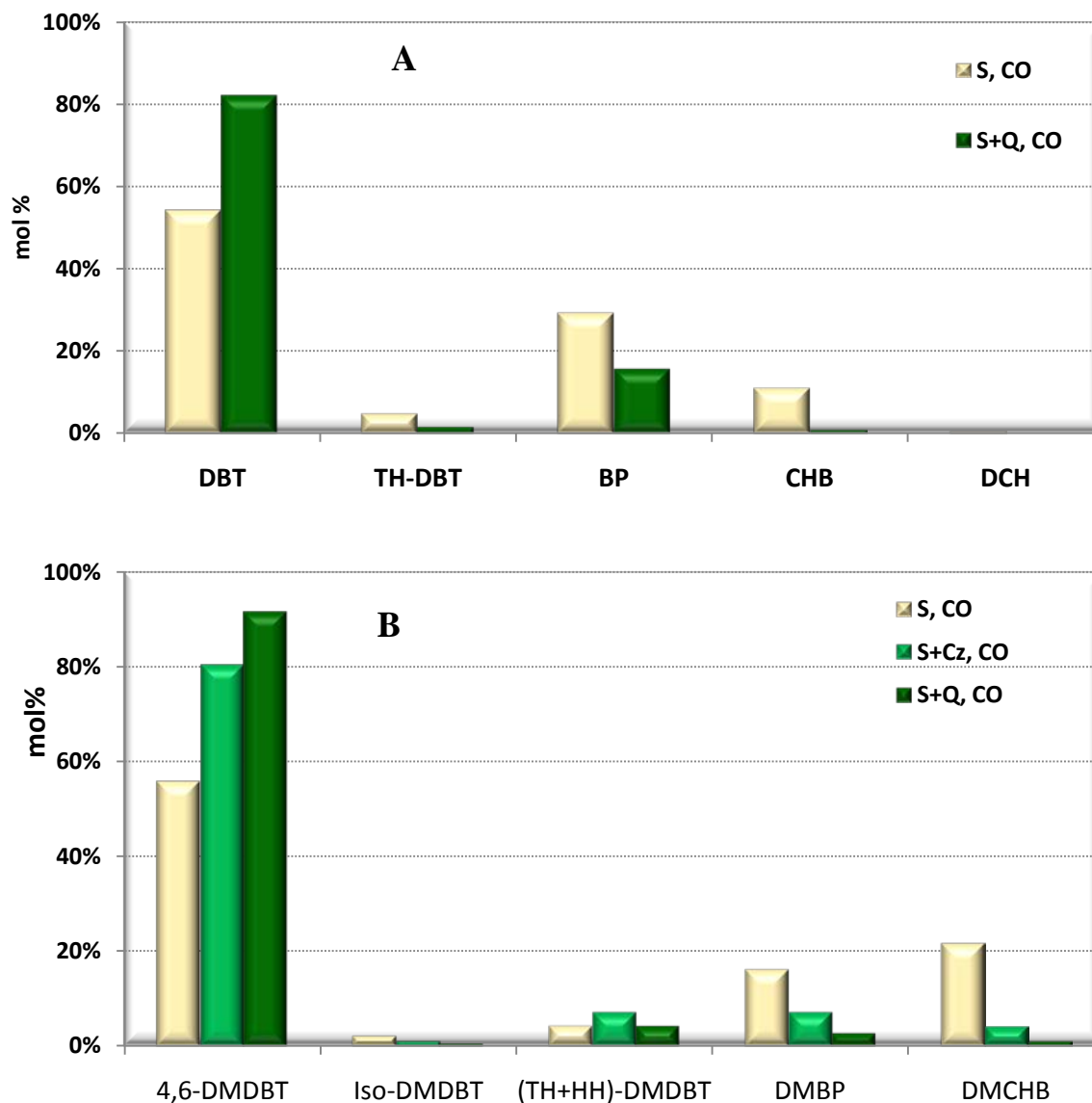


Fig. 7 - 1 Effect of the nitrogen heterocyclic compounds on the S-removal from DBT (A) and 4,6-DMDBT (B) over a dispersed Mo sulfide catalyst using *in-situ* hydrogen. Equi-molar DBT and 4,6-DMDBT (1670 ppmw of S in total), 590 psi of CO and 10 psi of H₂S (at room temperature), 500 ppmw Mo, S:N=2:1 (molar), 380°C

The conversion of CO *via* the WGS reaction obtained in the quinoline present experiment was even higher than that observed in the other two experiments; therefore, the presence of the nitrogen-containing species did not show inhibition on the WGS reaction. This demonstrated that the inhibitive effect of the nitrogen-containing compounds on the HDS reactions was not resulted from the inhibition of the WGS reaction to produce *in-situ* hydrogen. Hence, the major contribution of the strong inhibitive effect of nitrogen species on HDS was resulted from the competitive adsorption of model compounds on the catalytically active sites.

Because the HDN of carbazole and the HDS of DBT have common products, i.e. CHB, DCH, and BP, the effect of carbazole on the reaction pathways in the HDS of DBT could not be distinguished based on the product analysis from our experiments. Fig. 7-2 shows the effect of quinoline on HYDD and DDS products for the HDS of both sulfur-containing model compounds. In the presence of quinoline, the HYDD and DDS reaction products of DBT were reduced by 93% and 46%, respectively. Cyclohexylbenzene was the only desulfurized product obtained *via* the HYD route in the presence of quinoline, while both cyclohexylbenzene and saturated dicyclohexyl were observed in the HDS of DBT without added quinoline. Hence, basic quinoline had a more severe inhibitive effect on the HYD reaction pathway for the HDS of DBT than on the DDS route over the dispersed unsupported Mo sulfide catalyst.

For the HDS of 4,6-DMDBT, after adding carbazole, the concentration of the DDS products of 4,6-DMDBT was reduced by 56%, and the concentration of HYDD products was decreased by 81%. In the presence of quinoline, concentrations of DDS and HYDD products were decreased by 83% and 95%, respectively. Similar to the HDS of DBT, the desulfurization *via* the HYD

reaction pathway for the HDS of 4,6-DMDBT was more inhibited by the nitrogen heterocyclic compounds. As a result, interestingly, the DDS route became the major reaction pathway instead of the HYD pathway contributing for the sulfur-removal from 4,6-DMDBT due to the stronger inhibitive effect of the nitrogen heterocyclic compounds on the HYD route.

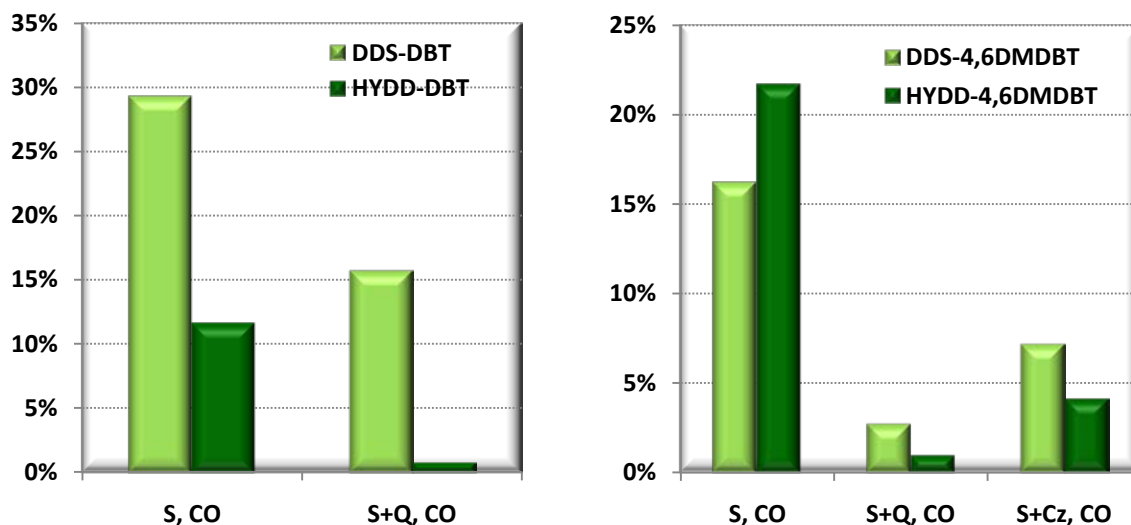


Fig. 7 - 2 Effect of the basic quinoline and non-basic carbazole on the HDS reaction pathways of DBT and 4,6-DMDBT over the nano-dispersed Mo sulfide catalyst using *in-situ* hydrogen. Equimolar DBT and 4,6-DMDBT (1670 ppmw of S in total), 590 psi of CO and 10 psi of H₂S (at room temperature), 500 ppmw Mo, S:N=2:1 (molar), 380°C

The different inhibitive effects of the nitrogen-containing compounds on the two reaction pathways suggested that the DDS and HYD reactions took place on different active sites. This assumption has also been proposed by other research groups for the supported Mo catalysts^{13a, 50a}. Egorova and Prins studied the nature of active HDS sites and they suggested that the DDS and HYD reaction pathways occurred over separate active sites due to the different adsorption

modes on the catalyst surface⁸⁰. The adsorption mode of the nitrogen-containing compounds on the unsupported MoS₂ catalyst probably plays an important role in the observed inhibition effect on HDS. The strong adsorption of the nitrogen heterocyclic compounds, quinoline and carbazole parallel to the catalyst surface *via* a π interaction of the aromatic ring would have a severe inhibition effect on the HYD route in the HDS of DBT and 4,6-DMDBT.

Logadóttir *et al* studied the inhibition of aromatics and N-containing species on the HYD route over MoS₂ catalyst *via* density functional theory (DFT) calculations⁸⁷. They have found that the preference adsorption site of the model compound of aromatics, benzene, located at Mo-edge rather than on the basal plane. Also, the Mo-edge was found to be the preference adsorption site for the N-containing heterocyclic molecule, pyridine, and the Mo-edge was where pyridinium ion generated and adsorbed stably. The production of pyridinium ions was a key reaction step involved in the hydrogenation of pyridine molecules. Both benzene and pyridine/pyridinium ion preferably adsorb at the Mo-edge, indicating the active site for hydrogenation was located at the Mo-edge. Additionally, they suggested that the inhibition of basic N-containing compound on hydrogenation reactions may also be due to the consumption of H from the Brønsted acid sites in the protonation of basic nitrogen species and thereby reduced the number of H atoms available for hydrogenation.

The preferable adsorption of nitrogen-containing species on HYD active sites was confirmed *via* the experiment results of the hydrogenation of an aromatic model compound, naphthalene, with/without the presence of quinoline or carbazole (Fig. 7-3). Similarly to the effect of nitrogen-containing compounds on the HDS of sulfur compounds, both quinoline and carbazole had a

significant inhibitive effect on the hydrogenation of naphthalene, and the effect caused by quinoline was stronger than carbazole.

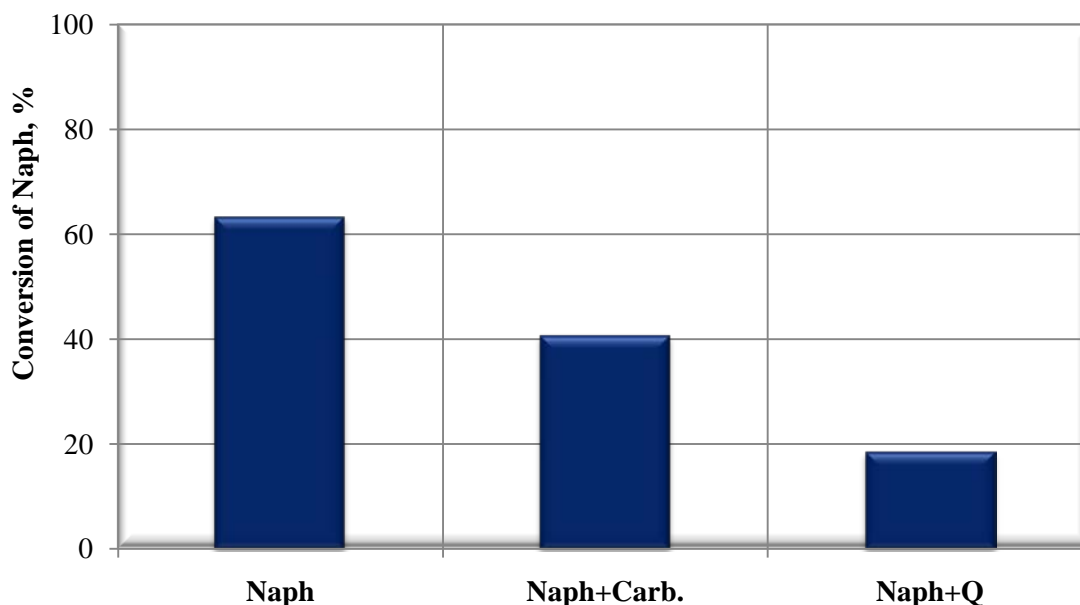


Fig. 7 - 3 Effect of the nitrogen-containing compounds on the hydrogenation of naphthalene over a dispersed Mo sulfide catalyst using *in-situ* hydrogen. 590 psi of CO and 10 psi of H₂S (at room temperature), 500 ppmw Mo, 380°C

Comparing the two nitrogen-containing compounds, non-basic carbazole was less harmful to the HDS of both refractory sulfur compounds. Turaga *et al.* used semi-empirical computational and molecular modeling data and correlated the activity towards hydrogenation to the highest bond order in the molecule to explain the difference in the inhibitive effect caused by quinoline and carbazole on HDS^{13b}. They found that the highest bond order in the molecules decreased in the order of quinoline > carbazole ~ 4,6-DMDBT and hence resulted in the preferential adsorption of quinoline on the hydrogenation active sites and caused a stronger inhibitive effect on the

hydrogenation of 4,6-DMDBT than that of carbazole. Their finding is in agreement with our experimental result on the hydrogenation of naphthalene in the presence of quinoline or carbazole.

It is also important to note that the concentration of the isomerized products of 4,6-DMDBT was lower in the experiments with nitrogen-containing compounds, especially in the experiment with quinoline. Isomerization during the HDS reactions is beneficial for the HDS of 4,6-DMDBT by transforming it into more reactive isomers⁴⁵⁻⁴⁶. The isomerization of the 4,6-DMDBT is acid catalyzed⁴⁵. The basicity of the nitrogen-containing compounds, especially the strongly basic quinoline, decreases the acidity of the Mo sulfide catalyst, therefore, resulting in a decrease in the concentration of the isomerized products of 4,6-DMDBT which contributed to a more severe inhibiting effect of the nitrogen-containing compounds on the HDS of 4,6-DMDBT.

7.3.2 HDS in the presence of N-containing compounds using molecular H₂

The use of *in-situ* H₂ is the key point in the design of our one-step bitumen emulsion upgrading technology. The previous chapters has shown that

- The unsupported Mo sulfide catalyst prepared in *in-situ* hydrogen dispersed in smaller particles with shorter and more curved slabs stacked in lower degree (Chapter 4).
- *In-situ* H₂ was more efficient than molecular H₂ in the HDS reactions of both DBT and 4,6-DMDBT over the dispersed Mo sulfide catalyst (Chapter 5).

In this section, the comparison between these two sources of hydrogen will be continued in the HDS experiments in the presence of N-containing compounds. The experiment results were illustrated in Fig. 7-4. With the presence of carbazole, the conversion and desulfurization of DBT and 4,6-DMDBT obtained using *in-situ* H₂ were 4~5% and 2~4 mol%, respectively, lower than the numbers obtained using molecular H₂. With the presence of quinoline, the conversion and desulfurization were slightly higher using *in-situ* H₂ in the HDS of DBT, and slightly lower in the HDS of 4,6-DMDBT than using molecular H₂. The difference of 5% in the experiment result is within the experimental error range of a batch reactor. Therefore, comparative HDS results of DBT and 4,6-DMDBT were obtained using the two different sources of hydrogen.

Considering the HDS of 4,6-DMDBT, the molar ratio between the two reaction pathways, DDS/HYDD, was almost the same when using the two different hydrogen reaction atmospheres in the experiments with quinoline or carbazole (Fig. 7-5). In the HDS of DBT with the presence of quinoline, the sulfur-removal was almost the same, 0.9% in difference, when using the two hydrogen sources. However, the ratio of DDS/HYDD obtained in *in-situ* H₂ was significantly higher than the number observed in the molecular H₂. Therefore, in the HDS of DBT with the presence of quinoline, the *in-situ* H₂ had higher selectivity towards the direct desulfurization route.

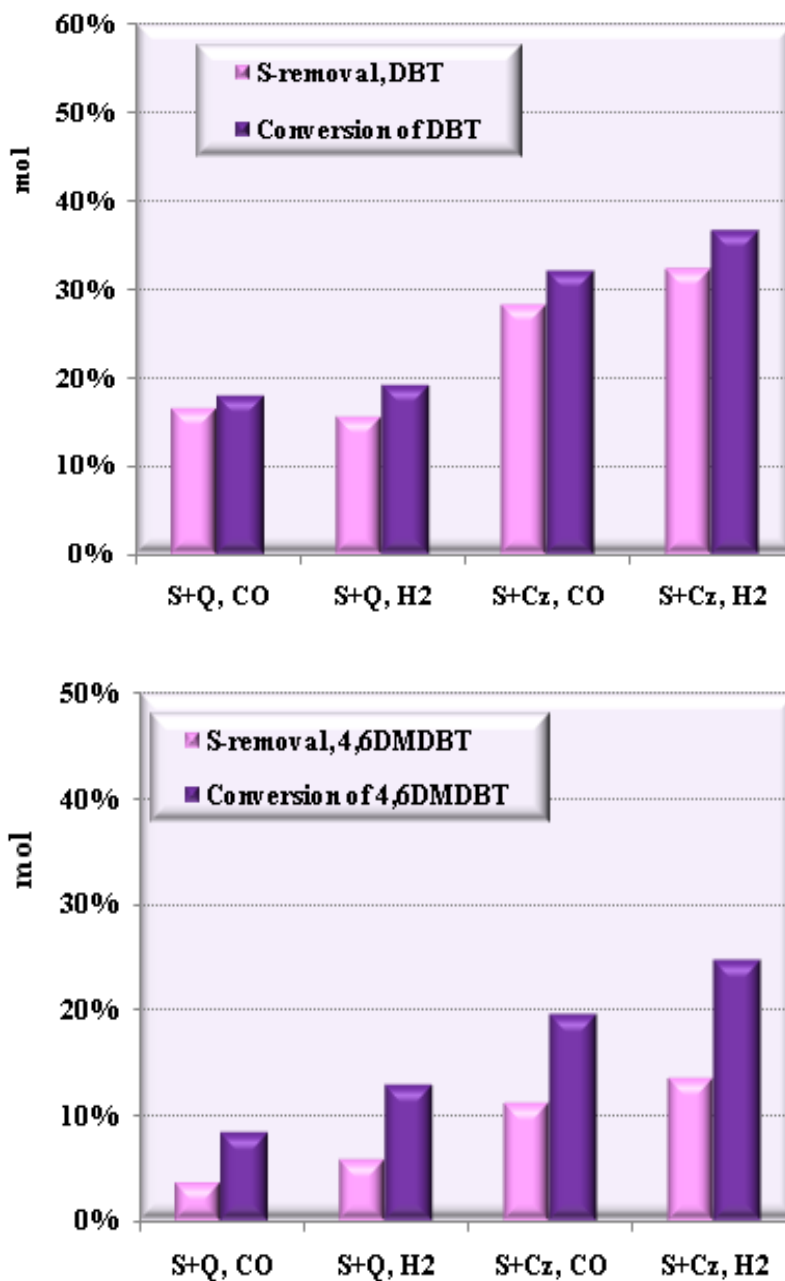


Fig. 7 - 4 HDS of DBT and 4,6-DMDBT in over dispersed Mo sulfide catalyst obtained at different reaction conditions: *In-situ* H₂/molecular H₂, with/without quinoline or carbazole, 590 psi of CO(or H₂) and 10 psi of H₂S (the pressure at room temperature), 400~500 ppmw Mo, 380°C, 3hr

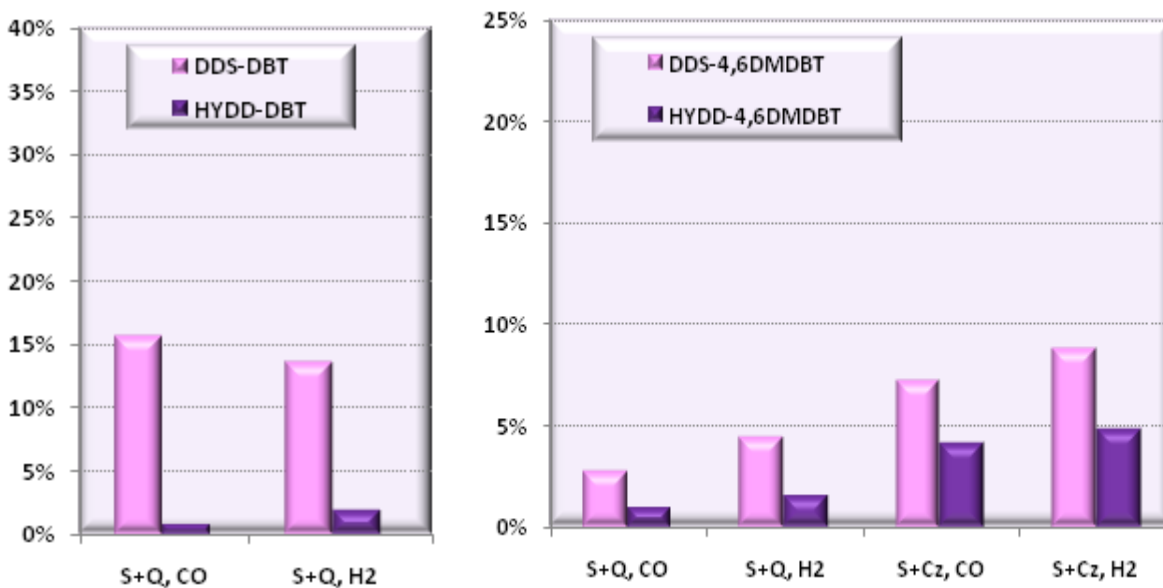


Fig. 7 - 5 Selectivity between HDS reaction pathways of DBT and 4,6-DMDBT obtained at different reaction conditions: *In-situ* H₂/molecular H₂, with/without quinoline or carbazole, 590 psi of CO(or H₂) and 10 psi of H₂S (the pressure at room temperature), 400~500 ppmw Mo, 380°C, 3hr

7.4 Conclusions

- (1) Severe inhibitive effect of the two nitrogen-containing model compounds on the HDS of sulfur species was observed. Basic quinoline was a much stronger inhibitor than non-basic carbazole for HDS reactions over the dispersed Mo sulfide catalyst.
- (2) The HDS of 4,6-DMDBT was more inhibited than that of DBT with the addition of nitrogen-containing compounds.
- (3) The desulfurization from the HYD route was more influenced than from the DDS route in the presence of quinoline or carbazole.

(4) In the presence of nitrogen species, comparable HDS activities were observed when using the two different sources of hydrogen, *in-situ* hydrogen or external provided molecular hydrogen.

Chapter 8 Hydrodenitrogenation of Refractory Heterocyclic N-Containing Compound of Carbazole

8.1 Introduction

The N-containing compounds detected in petroleum or synthetic oils generally could be divided into two groups: heterocycles or nonheterocycles. The latter group consists of anilines and aliphatic amines. The present study will be only focused on the HDN of heterocyclic N-containing compounds due to their much lower HDN reactivity of than aliphatic amines during hydro-treating processes. Heterocyclic nitrogen-containing compounds fall into two types: those having a six-membered pyridinic ring and those having a five-membered pyrrolic ring. The different electron configuration of these two types of heterocyclic N-containing compounds results in the difference in their basic properties. The extra lone pair of electrons in the nitrogen atom of the five-numbered N-containing hetero-aromatics is involved in the π -cloud of aromatic ring, and hence, it is not available to interact with acids. In this case, five-membered N-containing heterocyclic compounds were regarded as non-basic or neutral species. For example, the pKa value of pyrrole, indole, and carbazole were found to be 0.4, -3.6, and -6.0, respectively²¹. Conversely, in the six-membered ring compounds, the lone pair of electrons in the nitrogen atom is not tied up in the π -cloud and resulted in the basicity of this group of cyclic N-containing compounds, such as pyridine (pKa of 5.2²¹) and quinoline (pKa of 4.9²¹).

Among basic heterocyclic N-containing compounds, quinoline is a widely used model compounds in HDN studies. The mechanism for the HDN of quinoline has been well documented, which included C-N bond cleavage, hydrogenation of aromatic heterocyclic rings, and hydrogenation of benzenic rings (Fig. 8-1). In previous study in our group done by Lee^{42, 88}, the HDN of quinoline over the dispersed Mo sulfide catalyst using *in-situ* H₂ generated *via* the WGS reaction was studied. Lee observed that⁴²:

- Higher than 99% of quinoline was converted at 2 hr over dispersed Mo sulfide (1500 ppmw Mo) catalyst using *in-situ* H₂ at a low reaction temperature, 340⁰C. With increasing the reaction temperature to 415⁰C, the N-removal from quinoline increased significantly, indicating that C-N bond cleavage was the rate-controlling step in the HDN of quinoline⁴².
- The amount of water used in the HDN reaction should be optimized. At a low level of water concentration, the addition of more water promoted the denitrogenation of quinoline *via* generating more active catalysts and providing acidic functions⁴².
- Appropriate amount of H₂S in the reaction system would promote the N-elimination step, while blocking the hydrogenation of aromatic rings⁴².
- Ni had shown significant promotional effect on the HDN activity of the dispersed Mo sulfide catalysts; while no evident promotional effect of Co was observed. The optimized ratio between Ni/Mo was found to be 0.5⁴².
- At optimized conditions, more effective HDN results were obtained using *in-situ* H₂ than molecular H₂⁴².

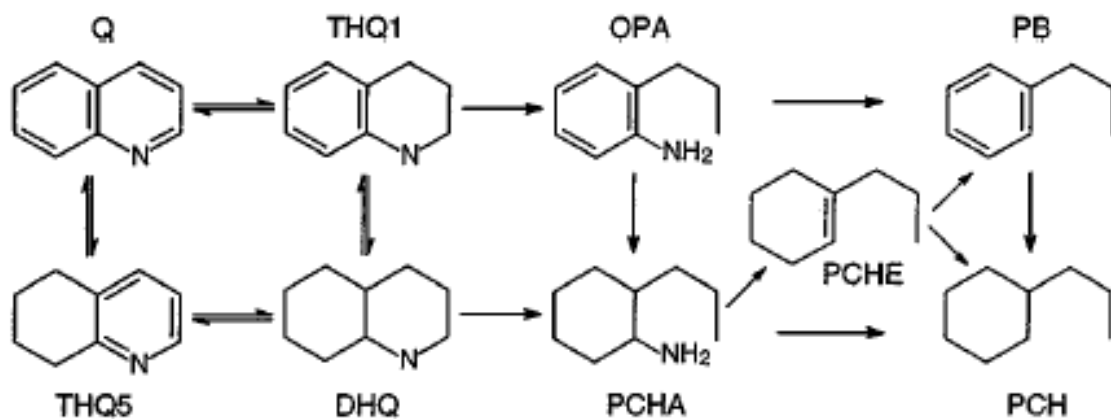


Fig. 8 - 1 HDN reaction network of quinoline⁸⁹. Where, Q is quinoline, THQ1, 1,2,3,4-tetrahydroquinoline, THQ5, 5,6,7,8-tetrahydroquinoline, DHQ, decahydroquinoline, OPA, ortho-propylaniline, PCHA, 2-propylcyclohexylamine, PCHE, propylcyclohexene, PCH, propylcyclohexane, PB, propylbenzene. License number for reusing this figure from Elsevier: 2531650864304

Unlike the HDN of quinoline, the HDN reaction network and product identification of carbazole have not reached to an agreement. Tetrahydro-carbazole (TH-Cz) was a commonly detected partially hydrogenated intermediate of carbazole during HDN reactions^{79,54a-90}. The detection of further hydrogenated intermediates of hexahydro-carbazole, octahydro-carbazole, and dodecahydro-carbazole were also reported^{54a, 91}. Besides these nitrogen-containing partially hydrogenated intermediates in the HDN products of carbazole, there was no other N-containing product, such as aniline- or amine-type products, reported in literatures. The product of direct denitrogenation (DDN), i.e. biphenyl (BP) was not observed after the HDN of carbazole in any literatures^{54a, 79, 90-92}. Hence, N-removal from the molecules took place only after the aromatic rings were hydrogenated, and the cleavage of the two C-N bonds occurred simultaneously from hydrogenated intermediates in the HDN of carbazole.

The bicyclic-six-membered-ring products such as cyclohexylbenzene (CHB), dicyclohexyl (DCH), and cyclohexyl-cyclohexene (CHCHE) were reported as major N-removed products of carbazole^{54a, 79, 85, 92}, while the contribution of each bicyclic-ring N-removed product to the total denitrogenation of carbazole was different in separate studies. A bicyclic-ring product having one six-membered-ring and one five-membered-ring, i.e. methylcyclopentylcyclohexane (MeCPCH), was reported by Lewandowski *et al*⁸⁵ as the final product of carbazole conversions *via* the isomerisation of DCH. Some ring-opened products, such as phenylhexane (PHA), hexylcyclohexane (HCHA), were detected by Yamamoto *et al* over a phosphoric acid-promoted Mn₂O₃-NiO catalyst⁹¹.

Based on the identification of HDN products, several different HDN reaction network of carbazole have been suggested in literatures, as shown in Fig.8-2 to Fig.8-4. Although the reported HDN reaction networks of carbazole were not in agreement, it was clear that three types of reactions occurred leading to N-removal from carbazole molecules: (1) hydrogenation of aromatic rings, (2) ring-opening *via* hydro-cracking, and (3) C-N bond cleavage *via* hydrogenolysis. Therefore, bifunctional catalysts with both hydrogenation and hydrogenolysis active centers are desirable.

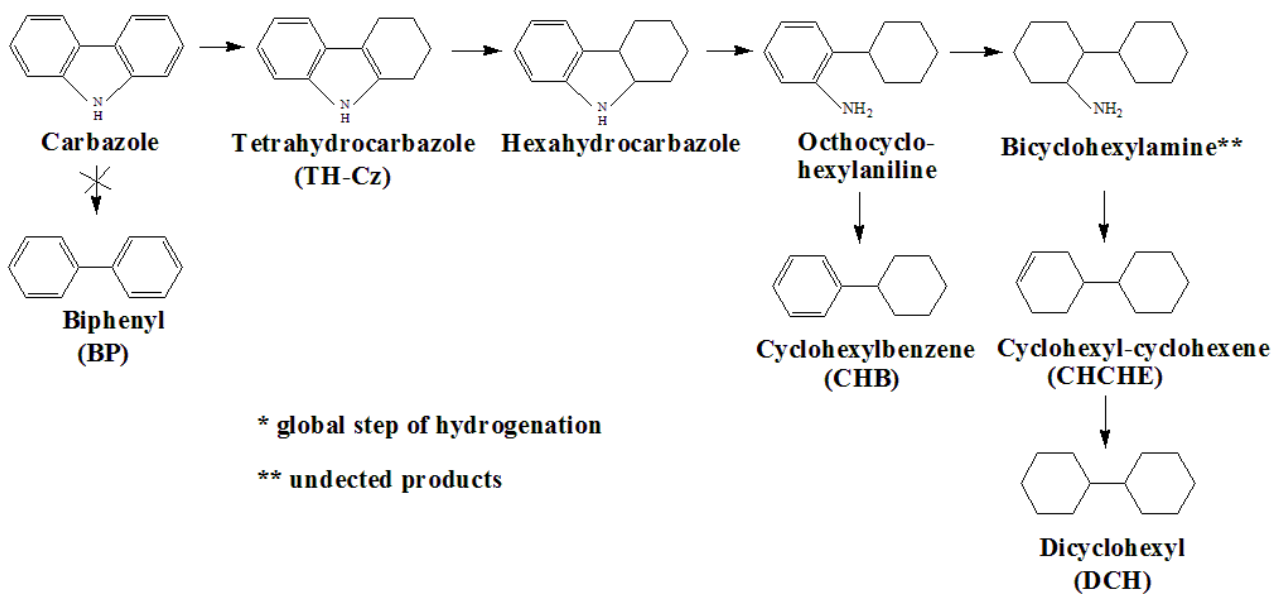


Fig. 8 - 2 HDN reaction network of carbazole presented by Szymanska *et al*^{54a} over bulk β - Mo_2C

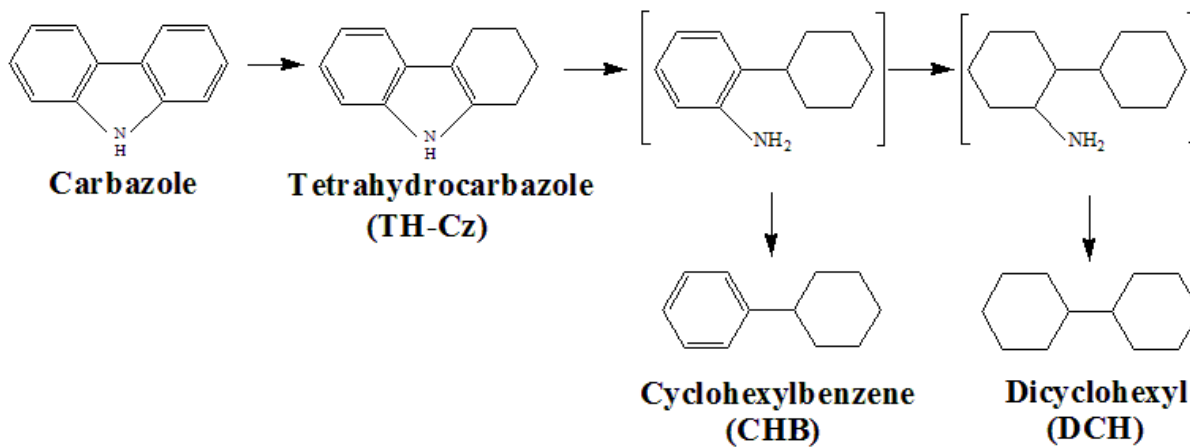


Fig. 8 - 3 HDN reaction network of carbazole suggested by F. Sanchez-Minero *et al*,⁹²

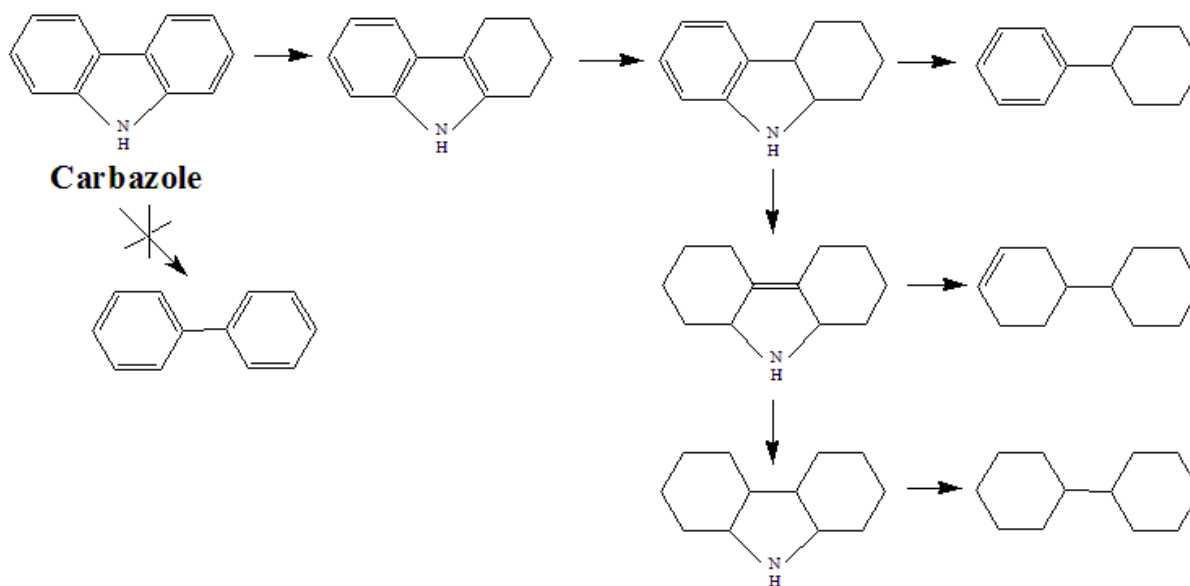


Fig. 8 - 4 HDN reaction network of carbazole suggested in literatures^{54c-49c}

This chapter would be the first to study the HDN of carbazole over dispersed Mo sulfide catalyst using *in-situ* hydrogen. An HDN reaction network of carbazole will be proposed on the basis of the identification of HDN products. Therefore, in the present chapter, we will study:

- HDN mechanism of carbazole
- WGS reaction with the presence of carbazole
- Pseudo-first-order rate constant of carbazole at 380⁰C over dispersed Mo sulfide catalyst using *in-situ* H₂
- Comparison of *in-situ* H₂ versus molecular H₂ for the HDN of carbazole
- Effect of 4,6-DMDBT on the HDN of carbazole.

8.2 Experimental

Detailed experiment process has been described in Chapter 2 and will not be repeated here. The detailed conditions of experiments involved in the present chapter are listed in Table 8-1.

Table 8 - 1 Detailed reaction conditions of the experiments involved in Chapter 8*

Experiment ID	Model compounds	Reaction temp., °C	Reactant gases, psi		
			CO	H ₂	H ₂ S
Cz0901 [†]	Cz	380	600	0	10
Cz0902 [†]	Cz	340	600	0	10
Cz0903	Cz	360	600	0	10
Cz0904 [†]	Cz	380	0	600	10
Cz0905 [†]	Cz	380	600	0	10
NS0901	Cz and 4,6DMDBT	380	600	0	10
N-01 ^{††}	Q	380	600	0	10
N-05 [‡]	Cz	380	600	0	10
DS0909	Q, Cz, DBT, 4,6-DMDBT, Naph	380	600	0	10

* Other conditions (except DS0909): 10 ml H₂O, 100ml toluene, 0.365g carbazole (2.2 mmol, 4200 ppmw), 340~350 ppmw N, 430~500ppmw Mo (PMA as the precursor), HC reactor

Other conditions (DS0909): 590 psi CO, 10 psi H₂S, equi-mol of each component (about 1.2 mmol of each), 100 ml toluene, 10 ml PMA solution, 430 ppmw Mo

[†] Repeated 2 times

^{††} Quinoline was used as the model compound instead of carbazole (equi-molar as carbazole used in other experiments). Reaction time: 60min, SS reactor

[‡] Reaction time: 60min, SS reactor

8.3 Identification of HDN products of carbazole

Fig.8-5 shows GC chromatographs of carbazole denitrogenation product obtained using the detectors of FID and TSD. Since TSD only responds to N-containing species, the two peaks in the time range of 36.5~38.0 min belong to the compounds with the hetero atom. They have been identified as tetrahydrocarbazole (TH-Cz, 36.9 min) and carbazole (Cz, 37.7 min) *via* GC-MS (Varian GC-CP3800/Saturn 2000) and the injection of standard reagent. The peaks shown in the FID chromatograph between the retention times of 12.0 min and 16.0 min are N-removed products derived from the hydrodenitrogenation of carbazole. Among these peaks (12.0 - 16.0 min), hexyl-cyclo-hexane (HCHA), 1-phenylhexane (PHA), di-cyclo-hexyl (DCH), and cyclo-hexyl-benzene (CHB) have been identified *via* using standard reagents (purchased from Aldrich). The peak at 14.9 min was identified as cyclohexyl-cyclohexene (CHCHE) as suggested by GC-MS.

The identification of peaks at 13.94 min and 14.24 min was the most difficult part. These two products were only detected by GC-FID. The specific detector for N-containing compounds, TSD, did not detect the presence of these two products. This indicated that they were nitrogen removed products of carbazole. The GC-MS analysis suggested the molecular weights of the two products were 166 g/mol, which was the same as DCH. (cyclopentylmethyl)-cyclohexyl was suggested as a N-removed product as suggested by literatures^{54a, 85, 93}, and it was assumed to be derived from the isomerization of the HDN products of carbazole. MS spectra of the two unidentified products are shown in Fig. 8-6. The proposed molecular structures of these two products by GC-MS processed in the present study were listed in Tables 8-2 and 8-3.

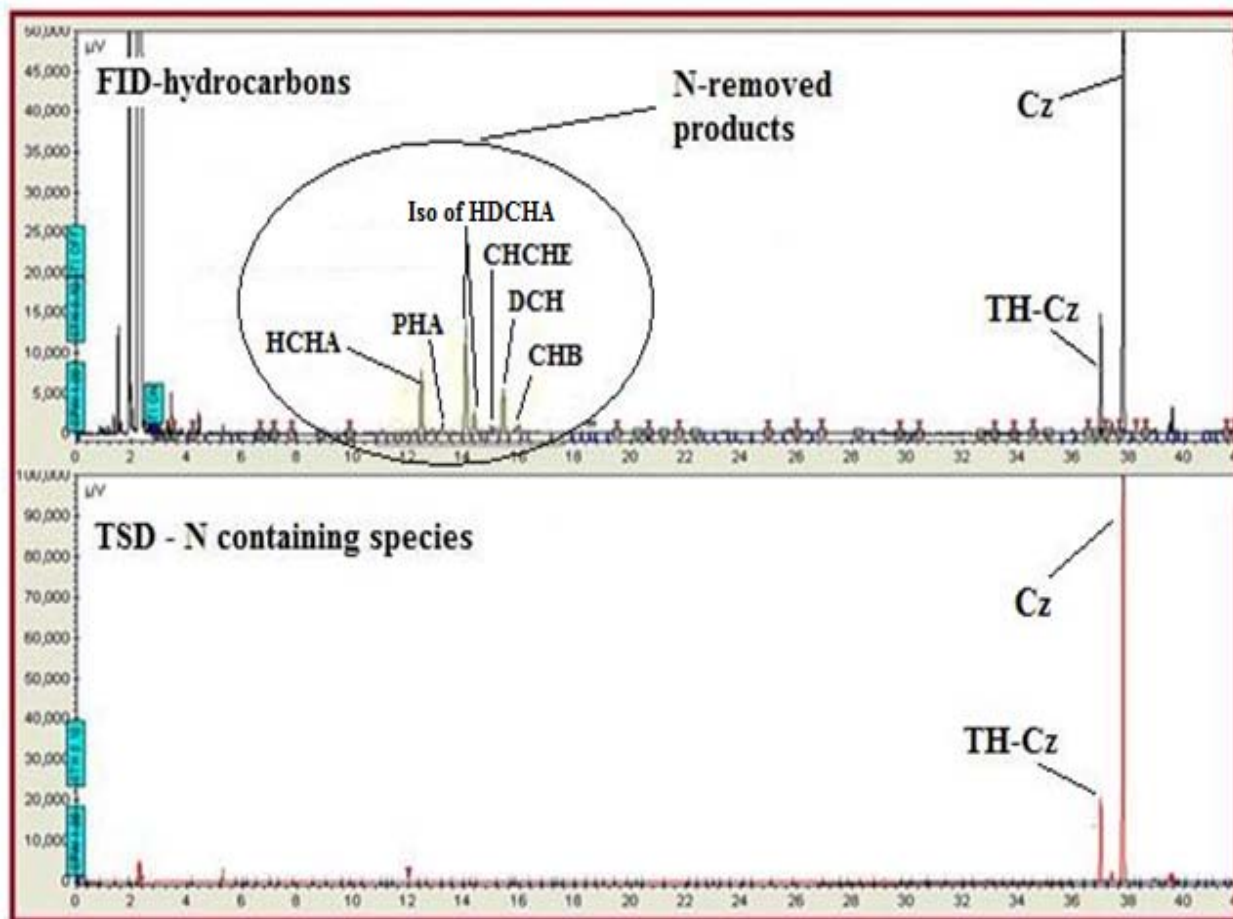


Fig. 8 - 5 GC Chromatographs of carbazole HDN products obtained *via* FID and TSD detectors (Reaction conditions: 380°C, *in situ* hydrogen, Mo sulfide catalyst)

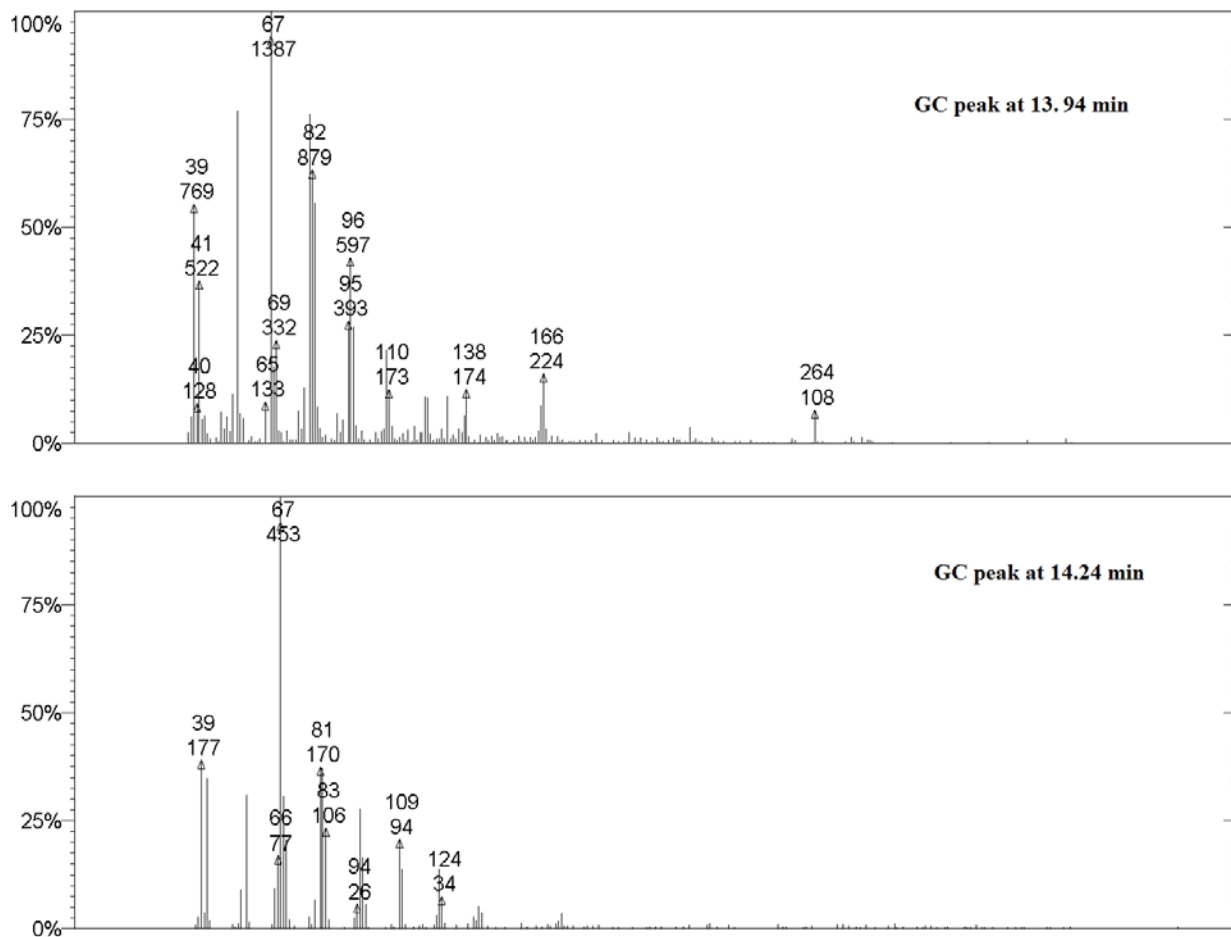
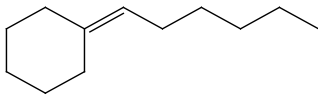
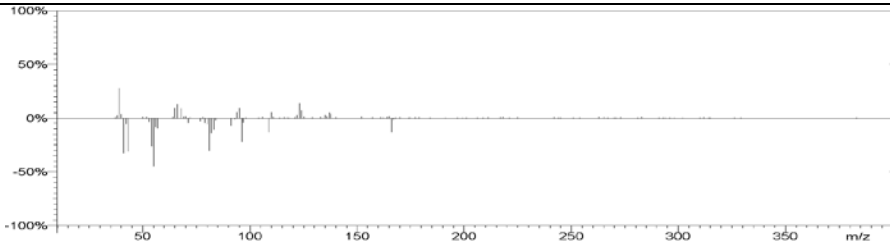
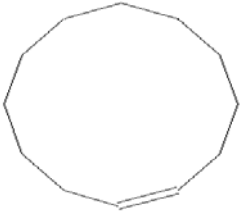
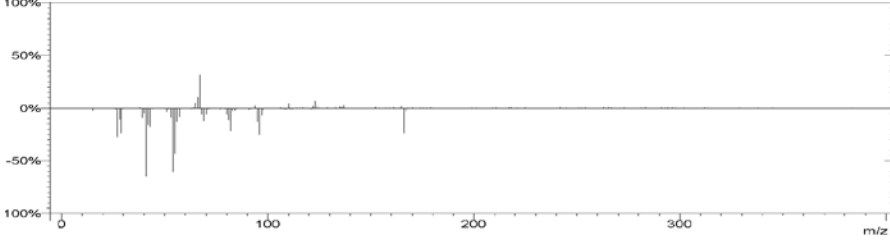


Fig. 8 - 6 MS spectra of the N-removed products of carbazole with the GC retention times of 13.94 min and 14.24 min.

Table 8 - 2 Suggested molecular structures (GC-MS results) of the N-removed product at the retention time of 13.94 min

Suggested chemicals via GC-MS	Molecular Structure (2D)	R. Match	Difference between MS spectra (the suggested structure to the real one)
Hexylidencyclohexane		880	
Cyclopentylmethyl- Cyclohexane		811	
(4-methyl-pent-3- enyl)-cyclohexane		805	
(E)-Cyclododecene		800	
1-Hexyl-cyclohexene		755	

Table 8 - 3 Suggested molecular structures (GC-MS results) of the N-removed product at the retention time of 14.24 min

Suggested chemicals via GC-MS	Molecular Structure (2D)	R. Match	Difference between MS spectra (the suggested structure to the real one)
Hexyliden- Cyclohexane		794	
Cyclododecene		748	

A mixture of trans- and cis-cyclododecene was purchased from Sigma-Aldrich (product No. 28780) and their GC retention times were different from the two un-identified products. So the two unknown product could not be isomers of cyclo-dodecene. According to the HDN mechanism proposed by Prins⁹⁴, removal of the nitrogen atom from an aliphatic C-N bond fragment in a propylaniline molecule took place via Hofmann elimination. In the Hofmann elimination reaction, an acidic site helps in quaternizing the nitrogen atom and thereby creating a leaving group, while a basic site promotes the elimination by removal of a β -H atom. Therefore, based on this HDN mechanism, hexyl-cyclohexene (HCHE) is the most possible structure of the unknown N-removed product with the GC retention time of 13.94 min and the other unknown product is probably an isomer of HCHE with the double bond located at different positions.

Identified HDN products of carbazole are listed in Table 8-4.

A typical HDN product distribution of carbazole is shown in Fig. 8-7, obtained using *in situ* H₂ over dispersed Mo sulfide catalyst at 380°C. The concentrations of N-removed products decreased in the order of: Isomers of HCHE>CHCHE>CHB>HCHA~DCH>PHA. Among them, isomers of HCHE were clearly the major denitrogenation products of carbazole under the experimental conditions of the present study. The molar ratio between ring-opened products and two-ring products was 1.40 at 180min. Hence, the nitrogen removal from carbazole was predominantly processed from the ring-opening reaction pathway.

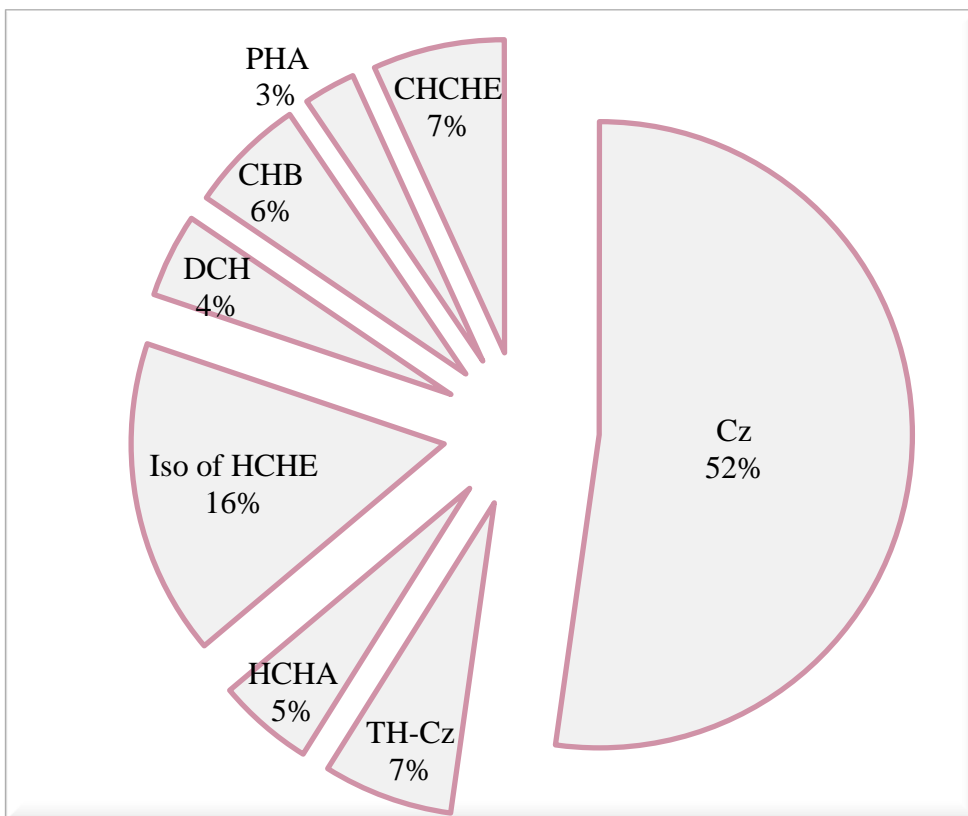
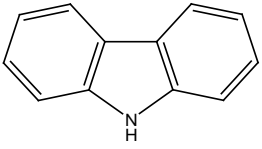

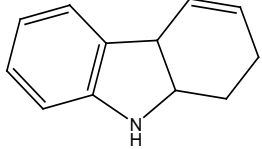
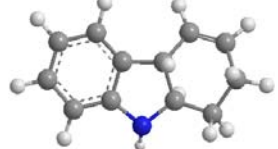
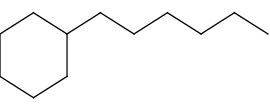
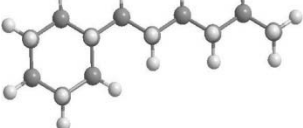
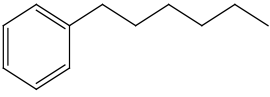
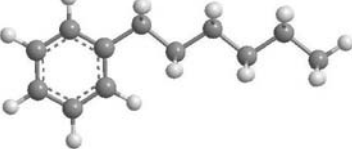
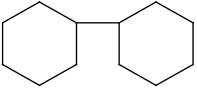
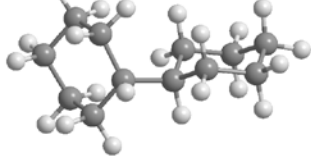
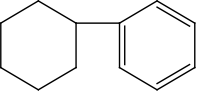

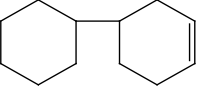
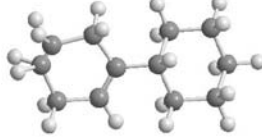
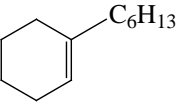
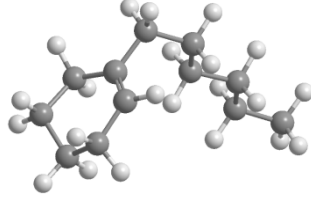


Fig. 8 - 7 HDN products distribution of carbazole (Cz0901-380°C, *in situ* H₂, 180 min)

The reactions of the hydrogenation of aromatic rings, the C-N bond cleavage, and the ring-opening happened during the HDN of carbazole over the dispersed Mo sulfide catalyst using *in situ* H₂. The N-removed products of carbazole could be grouped as two-ring products, including CHCHE, CHB, and DCH, and ring-opened products, including HCHA, PHA and isomers of HCHE. In the present study, biphenyl was not detected in the HDN product, indicating that direct denitrogenation did not occur during the HDN reaction of carbazole under the present experimental conditions, dispersed Mo sulfide catalyst and *in situ* H₂. The absence of biphenyl was in accordance with literature reports^{54a, 79, 90-92}.

Table 8 - 4 GC retention time and identification of hydrotreating products derived from HDN of carbazole

Products	Molecular weight	Molecular structure (2D)	Molecular structure (3D)	GC retention time, min	Identification
Carbazole (Cz)	167			37.71	GC-MS Standard compound
Tetrahydrocarbazole (TH-Cz)	171			36.89	GC-MS
Hexylcyclohexane (HCHA) [†]	168			12.31	GC-MS Standard compound
Phenylhexane (PHA) [†]	162			14.98	GC-MS
Dicyclohexyl (DCH) [†]	166			15.26	GC-MS Standard compound
Cyclohexylbenzene (CHB) [†]	160			15.82	GC-MS Standard compound
CycloHexylCycloHexEne (CHCHE) [†]	164			14.92	GC-MS GC-FID
Isomers of Hexyl-CycloHexene (HCHE)	166			13.94 14.24	GC-MS GC-FID

[†]: N-removed or denitrogenated products of carbazole

Clearly, the reaction mechanisms reported in literatures as shown in Figs. 8-2~8-4 could not be used to describe the HDN reaction of carbazole occurred in this study, hence a new HDN reaction network of carbazole over the dispersed Mo sulfide catalyst using *in situ* H₂ was proposed on the basis of our HDN product identification and with the consideration of literature reports, as shown in Fig. 8-8.

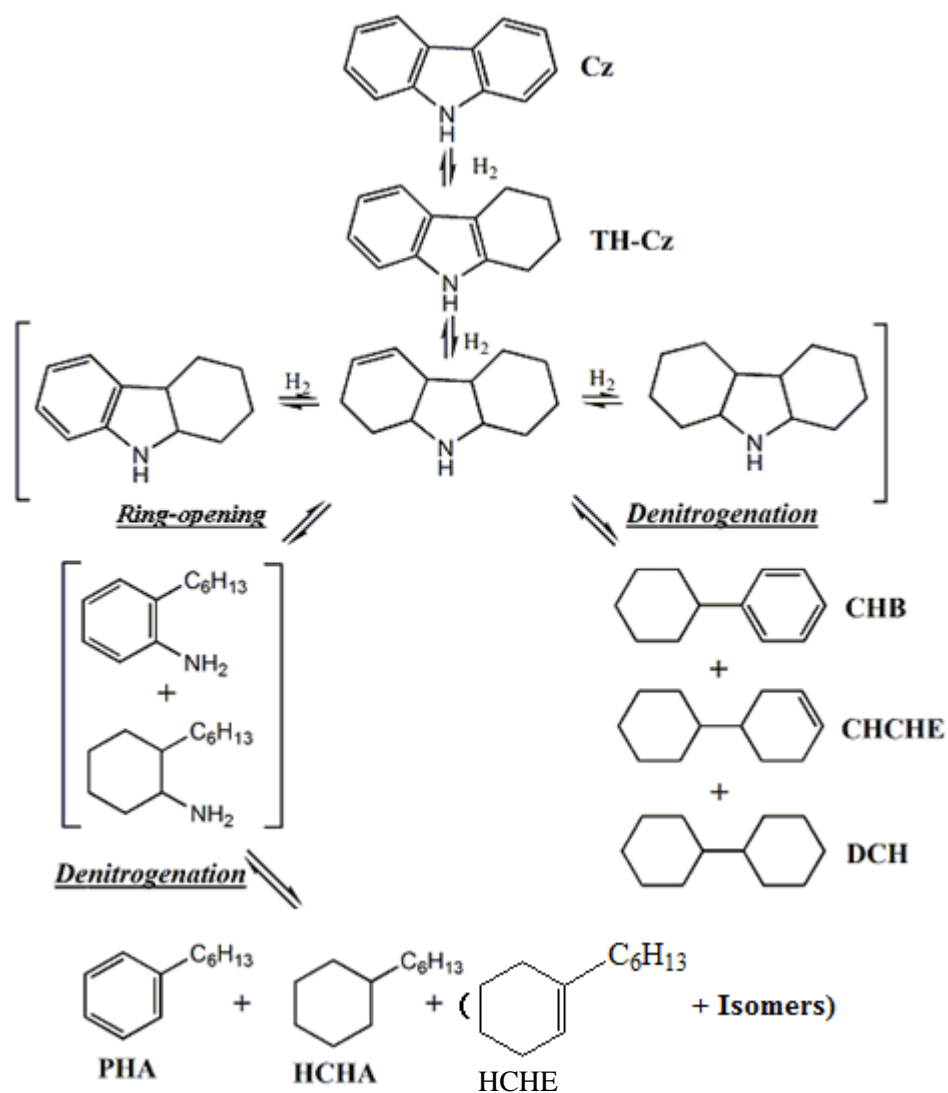


Fig. 8 - 8 Proposed HDN reaction network of carbazole over the dispersed Mo catalyst using *in situ* H₂ (the products blanketed were not detected by GC)

In this carbazole HDN reaction network, we proposed the presence of intermediates of aromatic amines derived from the hydrocracking of one benzene ring before nitrogen was removed. The hydro-treating of the two-ring products, CHB and DCH, was also run under the same conditions and no ring-opened product was detected. In the HDS of DBT, although DCH and CHB were detected, no ring-opened products were found under the same conditions as in the HDN of carbazole. Therefore, the reaction pathway (*via* ring-opened amine) was considered as the reaction pathway contributing to the ring-opened products of PHA, HCHA and isomers of HCHE.

However, why carbazole has ring-opened hydrotreated products, while the sulfur compound, DBT, have none of them? This may be due to the difference in the molecular structure of carbazole and DBT. In carbazole, the nitrogen atom is sp^3 hybridized and it is bonded with two aromatic rings and one hydrogen atom. In the most accepted hydrocracking reaction mechanism⁹⁵, cracking of hydrocarbon molecules proceeds through a carboniumion mechanism, wherein the hydrocarbon molecules lose a hydride ion to form a high reactive carboniumion and heteromolecules by a radical mechanism. The HDN of carbazole under the present experimental conditions possibly followed this hydrocracking mechanism and generated a carboniumion by losing a hydride ion from the $-NH$ group and then hydrocracked one aromatic ring and then removed the nitrogen atom from the molecules.

Due to the nitrogen-removal of carbazole occurred from a partially hydrogenated intermediate and the HYDD products of DBT were also derived from such a kind of intermediate, bond lengths and orders in molecules of TH-Cz and TH-DBT were compared

in Fig. 8-9. First of all, in the both molecules, the C-C bond lengths in the aromatic ring were shorter than in the hydrogenated ring. Secondly, the C-S bond lengths were calculated to be 1.8115Å and 1.9585Å in the molecule of TH-DBT, which were much longer than C-C bonds in the same molecule. Differently, the C-N bond lengths in the TH-Cz molecule were observed to be 1.4305Å and 1.4775Å, which were longer than those C-C bonds in the aromatic ring but shorter than those C-C bonds in the hydrogenated ring. Therefore, the occurrence of C-S bond cleavage from the TH-DBT molecule to produce two-ring sulfur removed products should be much easier than the C-N bond cleavage from the TH-Cz molecule. Thirdly, the C-C bond lengths in the hydrogenated ring were shorter in the TH-Cz molecule than in the TH-DBT one, except the C-C bond between the five-membered ring and the hydrogenated six-membered ring. This C-C bond was significantly longer than all the other C-C bonds and also C-N bonds in the TH-Cz molecule. The longer bond length indicates weaker bond strength. This suggested that it was highly possible to break this C-C bond and produce ring-opened products.

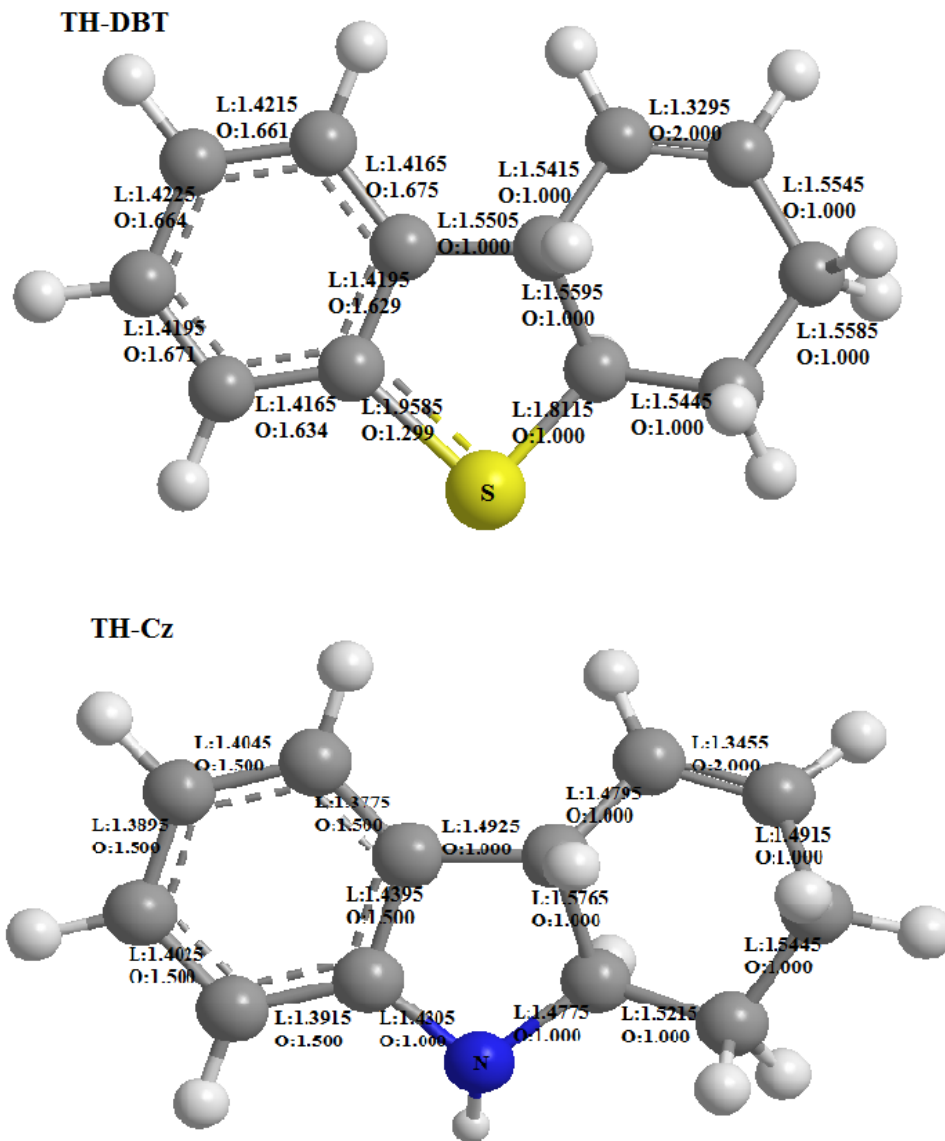


Fig. 8 - 9 Bond length and bond order of C-C, C-N/C-S bonds in molecules of intermediates of DBT and carbazole (MM2 calculation results). L: bond length, O: bond order.

8.4 Kinetics of the HDN of Carbazole

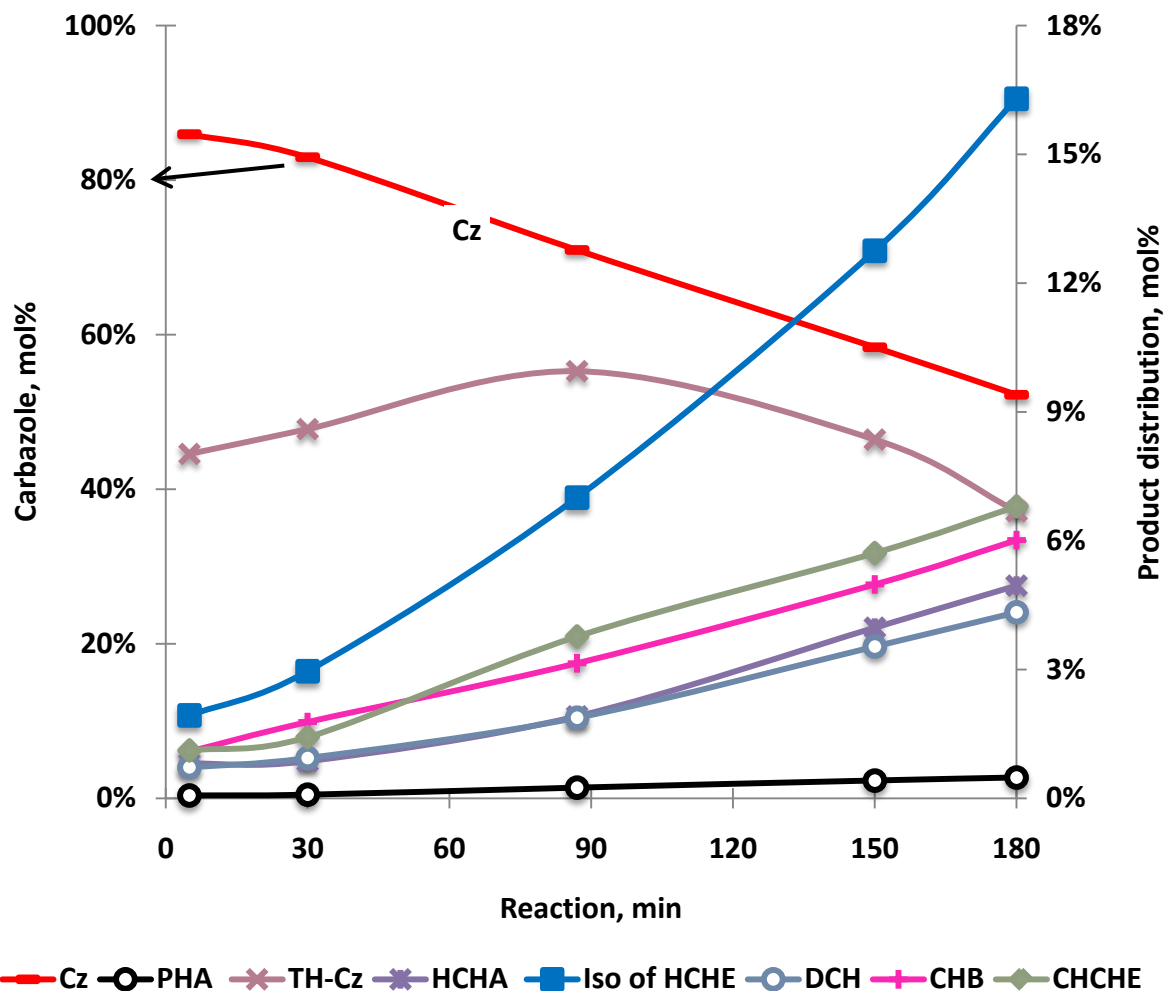


Fig. 8 - 10 Distribution of HDN products of carbazole over dispersed Mo sulfide catalyst using *in situ* H₂.

Other conditions: 590 psi CO and 10 psi H₂S (at room temperature), 430 ppmw Mo, 380 °C, 3hr, 10 ml H₂O

Fig. 8-10 shows the distribution of HDN products of carbazole as a function of reaction time, observed at 380°C using *in situ* H₂ over the dispersed Mo sulfide catalyst (detailed reaction

conditions given under the figure). At the beginning of the HDN reaction at 380⁰C, partially hydrogenated TH-Cz was the major product and its concentration increased in the first 90 minutes and then decreased gradually. This suggested that TH-Cz was an intermediate during the HDN of carbazole and the concentration decreased to produce nitrogen-removed products. As suggested in literatures, the first step in the HDN reaction of N-containing heterocyclic compounds was the hydrogenation of the aromatic rings adjacent to the nitrogen atom^{8, 54a, 79}, producing partially hydrogenated intermediates, such as TH-Cz. With extending the reaction time, the concentration of N-removed products increased gradually producing ring-opened products mainly. The absence of direct denitrogenated product, BP, indicated that the C-N bond cleavage required ring hydrogenation prior to removing the nitrogen atom from the molecules.

Assuming the concentration of hydrogen as a constant, the pseudo first order rate constant for the conversion of carbazole in the HDN reaction over the dispersed Mo sulfide catalyst using *in situ* H₂ was calculated according to (Eq.(8-1&8-2)).

$$r = -\frac{dC_{Cz}}{dt} = k' \cdot C_{Cz} \quad (8 - 1)$$

Where $k' = k \cdot p_{H_2}$

Upon integrating Eq. (7-1) one obtains:

$$\ln\left(\frac{C_t}{C_0}\right) = -k' \cdot t \quad (8 - 2)$$

Where: r is the reaction rate, $M \cdot s^{-1}$, k the pseudo first order reaction rate constant, s^{-1} , C_t the concentration of carbazole at time t , M , C_0 the initial concentration of carbazole, M .

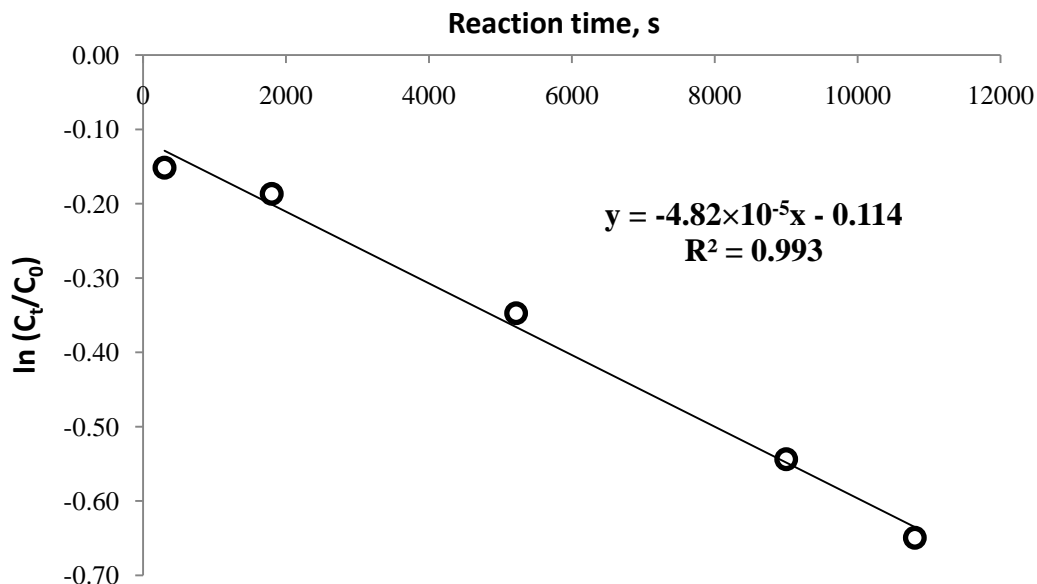


Fig. 8 - 11 Pseudo first order plots of carbazole at 380^oC

Other conditions: 590 psi CO and 10 psi H₂S (at room temperature), 380 ^oC, 430 ppmw Mo, 10 ml H₂O

The pseudo first order plots for the conversion of carbazole in the HDN reaction were shown in Fig.8-11. The R squared value, R^2 , in Fig.8-11 is 0.993, indicating that the conversion of carbazole followed the first order rate law using *in-situ* H₂. If assuming that all Mo was converted to MoS₂, the rate constant for the conversion of carbazole was found to be $7.7 \times 10^{-4} \text{ s}^{-1} \cdot \text{gcat}^{-1}$ under our experimental conditions. This value will be used as a reference for the results obtained in the following discussions.

Reproducibility is a key parameter of the batch reactor in our study. Therefore, some experiments were repeated and the repeatability was determined. The experiment of Cz0901 (detailed exp. conditions are shown in Table 8-1), wherein the HDN of carbazole was carried

out in *in situ* hydrogen at 380°C over the dispersed MoS catalyst, was repeated and the two experimental results were compared in Fig. 8-12. The conversions of carbazole were shown in Fig.8-12(A) and the numbers obtained were close. The molar concentration of each N-removed product group was also close as shown in Fig. 8-12 (B&C). The pseudo-first-order rate constant for the conversion of carbazole in the repeating run was calculated as $k'_{Cz} = 4.3 \times 10^{-5} s^{-1}$, which was 8% lower than the number obtained in the repeated experiment run. This difference is acceptable in a batch autoclave reactor. Therefore, the repeatability of the experiment Cz0901 is acceptable.

HDN of carbazole was also run at 340°C, 360°C and 380°C. Fig. 8-13 shows conversions of carbazole and concentrations of the intermediate, TH-Cz, obtained at different reaction temperatures, 340°C, 360°C, and 380°C. Obviously, the conversion of carbazole increased with increasing the reaction temperature. The concentration of TH-Cz started to decrease after 90 min at 380 °C and after 120 min at 360 °C, while at 340 °C, the concentration of TH-Cz kept increasing over the total duration of the run (3 hours). It was also observed that the concentrations of TH-Cz were very similar at different reaction temperatures. However, the difference between the nitrogen removals obtained at different reaction temperatures was much more significant, as shown in Fig. 8-14. So, the conversion of the intermediate of TH-Cz to further nitrogen-removed products was faster at higher temperatures than the first hydrogenation step of carbazole to TH-Cz. It has been suggested that the rate-limiting step in the HDN of carbazole may be the initial hydrogenation of carbazole⁹⁶. Therefore, for removing nitrogen from carbazole, it is important to improve the hydrogenation activity of the catalyst.

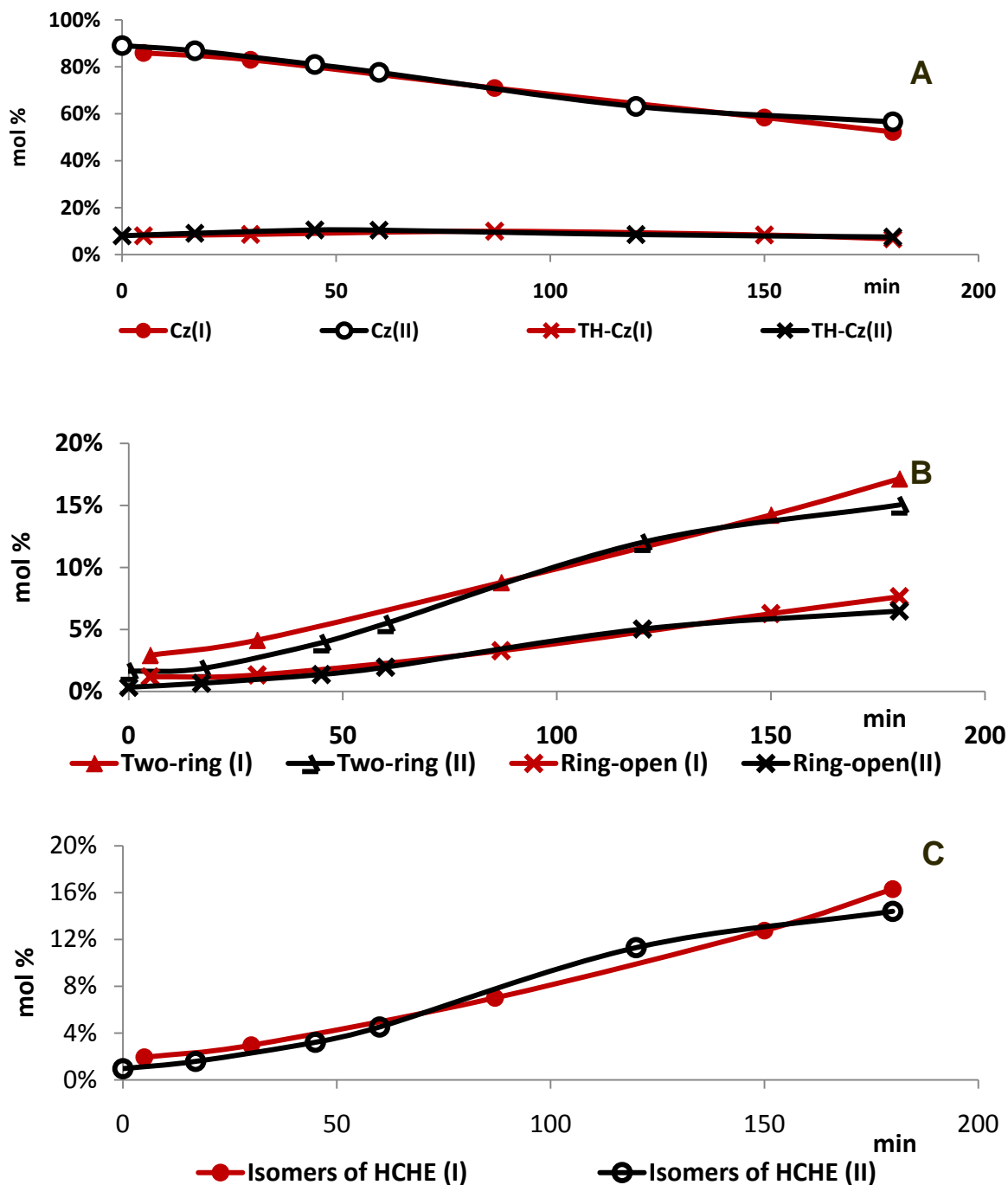


Fig. 8 - 12 Repeatability of the experiment, Cz0901, (380°C, *in situ* hydrogen). A: N-containing species, including carbazole and TH-carbazole; B: Two-ring and ring-opened products; C: Isomers of HCHE

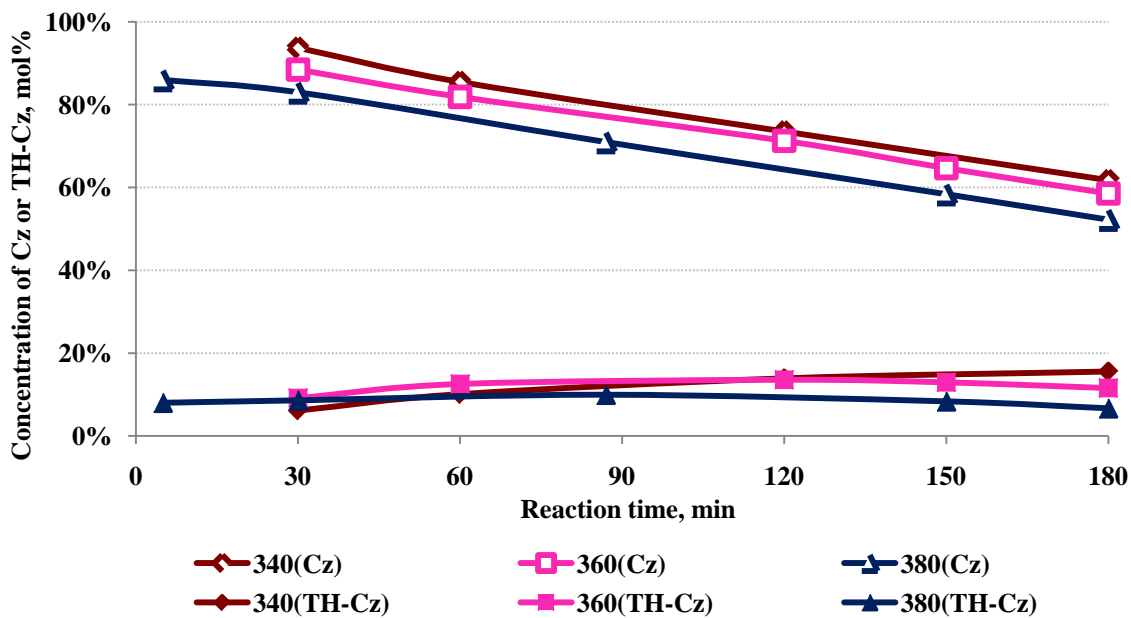


Fig. 8 - 13 Concentrations of carbazole and TH-Cz as a function of reaction time at different reaction temperatures, 340~380 °C.

Other conditions: 590 psi CO and 10 psi H₂S (at room temperature), 430 ppmw Mo, 380 °C, 3hr, 10 ml H₂O

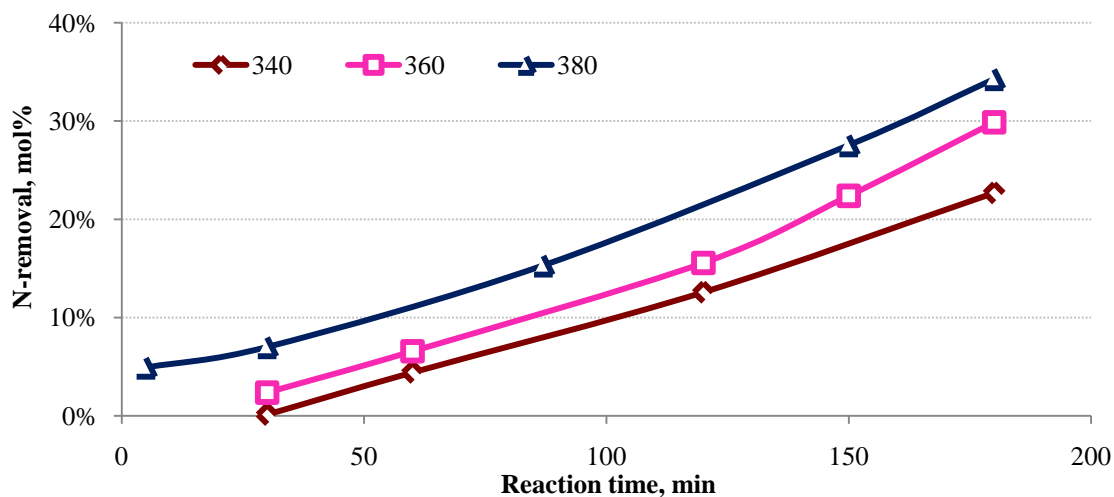


Fig. 8 - 14 Denitrogenation of carbazole as a function of reaction time at different reaction temperatures, 340~380 °C.

Other conditions: 590 psi CO and 10 psi H₂S (at room temperature), 430 ppmw Mo, 380 °C, 3hr, 10 ml H₂O

8.5 WGS reaction in the presence of carbazole

The *in situ* H₂ used for the current HDN study was generated from CO and H₂O *via* the water gas shift reaction. According to (Eq. (1-1)), CO reacts with water and converts to *in situ* H₂. CO₂ was generated as a side-product. So CO, H₂, and CO₂ are major gases present in the reaction system. Small amounts of H₂S and COS were also detected during the reaction, which was introduced as the sulfidation gas and was the intermediate of the WGS reaction, respectively. One blank WGS reaction experiment, wherein carbazole or 4,6-DMDBT was not introduced into the reaction system, was carried out to compare the CO conversion *via* the WGS reaction and the concentration of *in situ* H₂ generated for the HDN experiment. As shown in Fig. 8-15, the concentration of *in situ* H₂ in the WGS gas mixture was around 30 mol% at the beginning of the reaction at 380⁰C. This indicated that the WGS reaction started before reaching to the reaction temperature of 380⁰C. The concentrations of *in situ* H₂ detected at different reaction times in the HDN run were almost the same as what observed in the blank WGS experiment, and the conversions of CO in the HDN run were even a little higher than those in the blank WGS run. Therefore, the presence of non-basic carbazole did not inhibit the WGS reaction. This suggested that the adsorption of carbazole occurred on different active sites than CO during the HDN reaction.

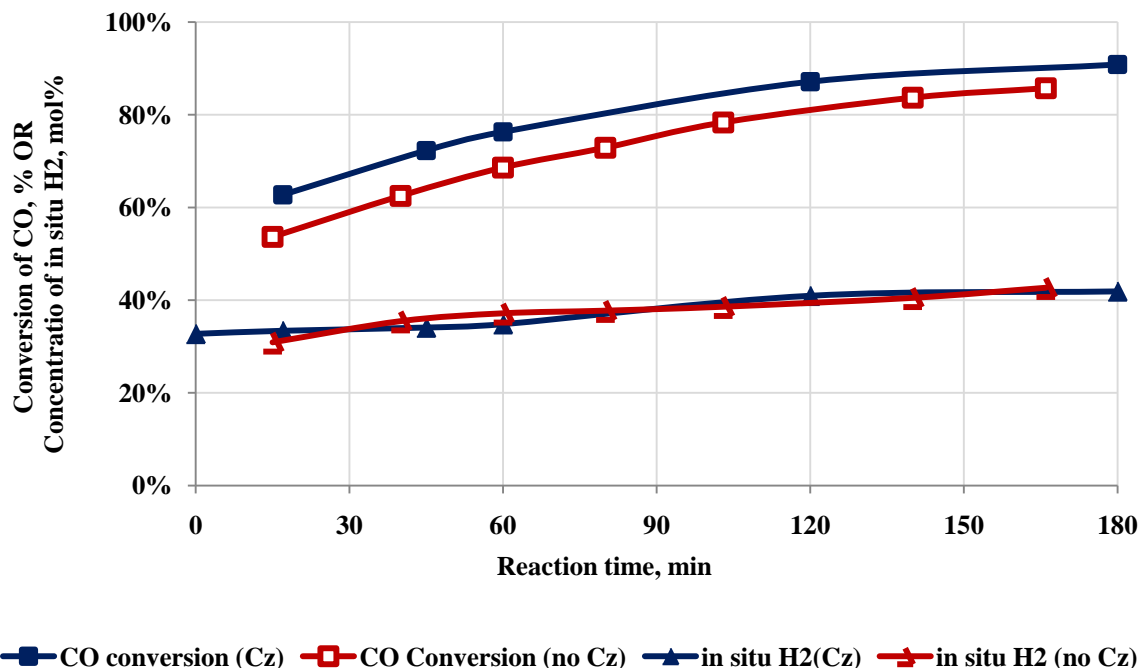


Fig. 8 - 15 CO conversions *via* the WGS reaction and the concentrations of *in situ* H₂ generated as a function of reaction time.

Other conditions: 590 psi CO and 10 psi H₂S (at room temperature), 380 °C, 430 ppmw Mo, 10 ml H₂O

8.6 *In-situ* H₂ versus molecular H₂ in the HDN of carbazole over the dispersed Mo sulfide catalyst

In Chapter 5, the *in-situ* hydrogen reaction system had been found to be more effective in the simultaneous HDS of DBT and 4,6-DMDBT. Furthermore, the dispersed Mo sulfide catalyst prepared in *in-situ* hydrogen was significantly active towards HDS reactions than the one *in-situ* prepared in molecular hydrogen, and this contributed to the higher efficiency of the *in-situ* hydrogen reaction system in HDS reactions. In this section, the reactivity of *in situ*

hydrogen (CO) *versus* molecular hydrogen (H₂) was compared in HDN of carbazole at 380°C over the dispersed MoS catalyst.

Comparing Fig. 8-16 to Fig. 8-10, the conversion of carbazole obtained using *in situ* H₂ was slightly higher than using molecular H₂. The pseudo first order reaction rate constant for the conversion of carbazole using molecular H₂, $6.7 \times 10^{-4} \text{ s}^{-1} \cdot \text{gcat}^{-1}$ was 13% lower than the number obtained using *in-situ* H₂, $7.7 \times 10^{-4} \text{ s}^{-1} \cdot \text{gcat}^{-1}$.

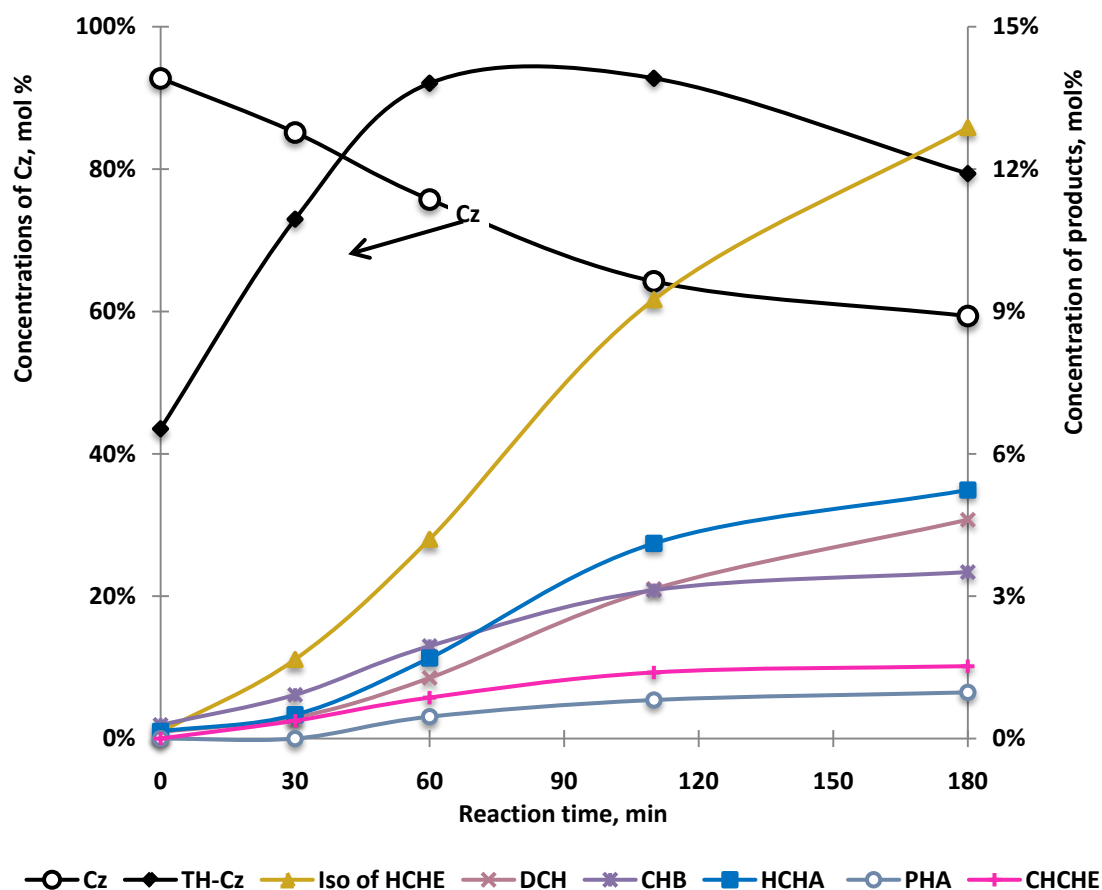


Fig. 8 - 16 Distribution of HDN products of carbazole over dispersed Mo sulfide catalyst using molecular H₂.

Other conditions: 590 psi CO and 10 psi H₂S (at room temperature), 430 ppmw Mo, 380 °C, 3hr, 10 ml H₂O

For comparing the denitrogenation activity of the catalyst under different reaction conditions, a factor α (Eq.(8-3)) was introduced and defined as the molar ratio between the concentrations of the N-containing intermediate of TH-Cz and those of N-removed products. If $\alpha > 1$, N-containing intermediate, TH-Cz, is the major product. If $\alpha < 1$, nitrogen-removed products are predominant, indicating that denitrogenation from partially hydrogenated intermediate is faster than the initial hydrogenation reaction step, in which carbazole was converted to TH-Cz.

$$\alpha = \frac{TH - Cz}{N - removed\ Products}, molar$$

$$= \frac{TH-Cz, mol\%}{(UKN1+UKN2+DCH+CHB+PHA+CHCHE+HCHA), mol\%} \quad (8 - 3)$$

In the molecular H₂ experiment (Fig.8-16), the concentration of nitrogen-containing intermediate, TH-Cz, was significantly higher, and the concentration of nitrogen-removed products was lower than what observed in the *in situ* H₂ experiment. The value of α (Fig. 8-17) decreased to 1.0 at 30 min in the *in-situ* H₂ experiment and at around 75 min in the molecular H₂ experiment. Hence apparently, the reaction step of nitrogen-removal from nitrogen-containing intermediate was significantly faster when using *in-situ* H₂. Hence, using *in-situ* H₂ has advantages in removing nitrogen from the refractory nitrogen-containing compound, carbazole, over molecular H₂.

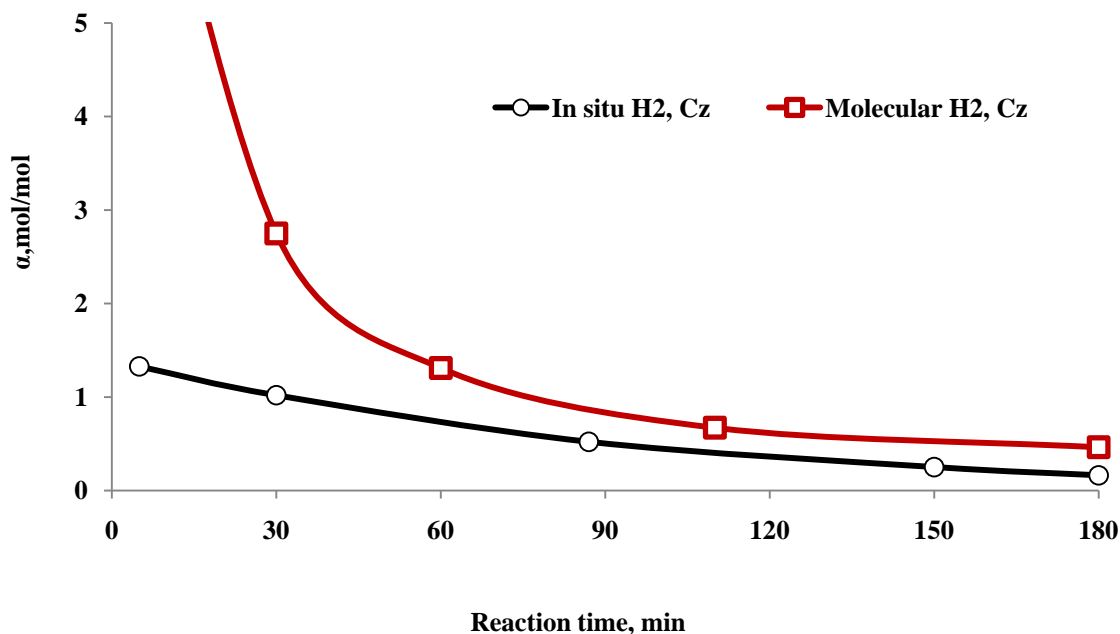


Fig. 8 - 17 Values of α as a function of reaction time obtained under different reaction conditions, using in situ H₂ or molecular H₂.

Other conditions: 590 psi CO (or H₂) and 10 psi H₂S (at room temperature), 430 ppmw Mo, 380 °C, 3hr, 10 ml H₂O

In the *in-situ* H₂ experiment, active hydrogen atoms were generated on the catalyst surface first and could participate in the hydro-treating reaction immediately before desorbed from the catalyst surface and then dispersed into the gas phase. However, in the molecular H₂ experiment, hydrogen molecules have to disperse into the liquid phase from the gas phase before having chance to adsorb on the catalyst surface to be involved in hydro-treating reactions. The higher access of the active hydrogen in the *in situ* H₂ experiment may be one reason for observed faster nitrogen removal from TH-Cz than in the molecular H₂ experiment.

As concluded in Chapter 6, the catalyst prepared in *in-situ* hydrogen had higher hydrogenation activity than the other one prepared in molecular hydrogen and this may play an important role in the HDN of carbazole. It is suggested that in the future, the use of *ex-situ* prepared catalyst could be extended into the HDN study to compare the role of the hydrogen source (CO or molecular hydrogen) in the HDN activity of the dispersed Mo sulfide catalyst.

As discussed, the presence of water would have inhibitive effect on the HDN reactions. In the molecular H₂ experiment, the amount of water was kept in a constant level, while in the *in-situ* H₂ experiment, the amount of water kept decreasing due to the consumption in WGS reaction. Therefore, the inhibitive effect of water on HDN reactions was reduced when using *in-situ* H₂. This may be one more reason for higher HDN results obtained in the *in-situ* H₂ experiment.

8.7 HDN of carbazole *versus* HDN of quinoline

Although the HDN of quinoline has been studied in details previously in our group^{42, 88} and previous results were summarized in the introduction section of this chapter, some experiments on the HDN of quinoline were also run in the present study to compare the HDN results between the two nitrogen-containing model species, carbazole and quinoline, and investigate the effect of quinoline/carbazole on the HDS of DBT and 4,6-DMDBT. The effect of nitrogen-containing compounds on HDS reactions will be reported and discussed in

the following section. In this section, the HDN of carbazole will be compared with the HDN of quinoline over dispersed Mo sulfide catalyst using *in-situ* H₂.

Both HDN reactions were run under 380°C for 1 hour in a batch Autoclave reactor (detailed experimental conditions refer to Table 8-1). It needs to be noted that the HDN reaction of quinoline was carried out in the SS reactor, while the HDN of carbazole was carried out in the HC reactor. Therefore, in this section, the relative HDN reactivity of both reactants will not be compared.

Table 8 - 5 HDN product distribution of quinoline and carbazole over nano-dispersed Mo sulfide catalyst in *in-situ* H₂ at 380°C for 1 hr (2.2 mmol N, 350 ppmw N, 430-500 ppmw Mo, SS reactor, 60min, 590 psi CO, 10 psi H₂S)

	HDN of Quinoline (N-01)		HDN of Carbazole (N-05)	
Starting material, mol%	Q	1.3	Carbazole	77.5
N-containing products, mol%	THQ-1	43.0	TH-Cz	10.3
	THQ-5	40.9		
	DHQ	0.1		
	OPA	6.5		
	PCHA	0.4		
N-removed Products, mol%	PCH	3.4	HCHA	1.0
			Isomers of HDCHA	4.7
	PCHE	0.5	DCH	1.1
			CHB	2.1
	PB	3.7	PHA	1.0
			CHCHE	2.3
$\frac{N - \text{containing products}}{N - \text{removed products}}$, molar	12.0		0.8	

A well-accepted HDN mechanism of quinoline suggested by Jian and Prins⁸⁹ is shown in Fig. 8-1, and a proposed carbazole reaction network in HDN based on the present study results is illustrated in Fig. 8-8. Clearly, there are three major reaction steps involved in HDN reactions, hydrogenation of aromatic rings, opening hydrogenated ring, and cleavage of C-N bond. The HDN products of each model compound could be grouped as starting material, nitrogen-containing products, and nitrogen-removed products. Table 8-5 and Fig. 8-18 show the HDN product distributions of quinoline and carbazole in separate 1-hr runs.

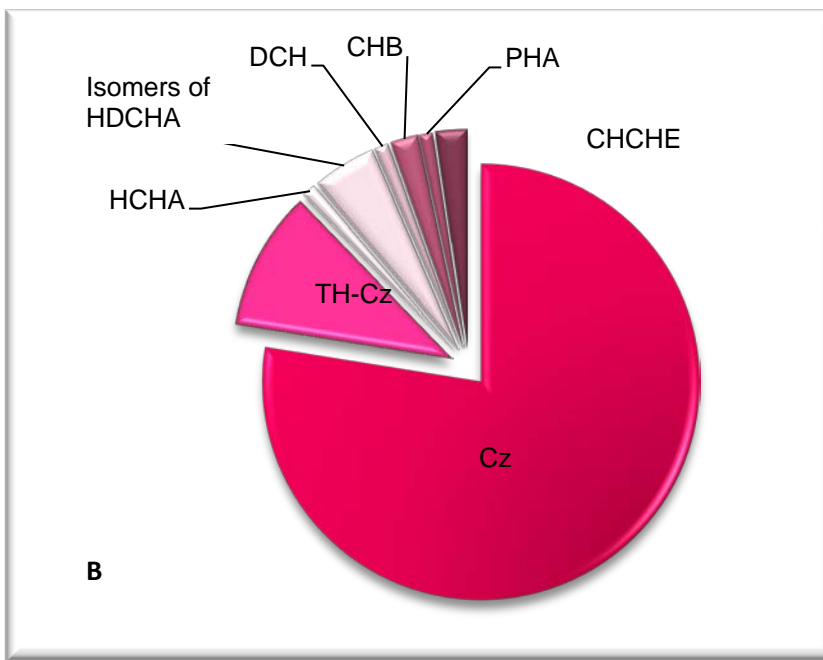
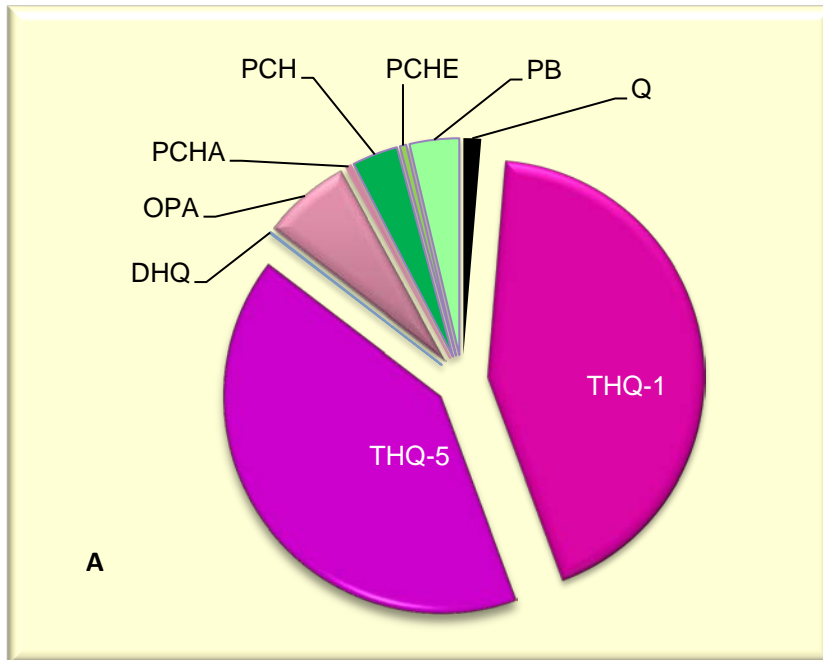


Fig. 8 - 18 HDN product distribution of quinoline and carbazole obtained in separate runs. Other conditions: 380°C, 1 hr, 2.2 mmol N, 350 ppmw N, 430-500 ppmw Mo, SS reactor, 60min, 590 psi CO, 10 psi H₂S

Quinoline was observed to be very reactive in HDN reactions and the conversion of quinoline was as high as 99% at 60 min. The hydrogenated products of tetrahydro-quinolines, THQ-5 and THQ-1, were predominant products of quinoline. Compared with the total concentration of nitrogen-removed products of quinoline, the total concentration of nitrogen-containing products was 11 times higher (Table 8-5). This indicated that the first step, hydrogenation of the benzenic ring (producing THQ-5) or the hydrogenation of the heterocyclic aromatic ring (producing THQ-1), was very fast and much faster than the following reaction step of C-N bond cleavage in the HDN of quinoline. This phenomenon was also observed and reported by other researchers^{89,97,98}.

As shown in Fig. 8-18B, less than one quarter carbazole was converted when at 60 min over the dispersed Mo sulfide catalyst in *in-situ* H₂. The only nitrogen-containing product, tetrahydro-carbazole, was the major product of carbazole and contributed to 46% in the HDN product mixture (Table 8-3). The total concentration of nitrogen-removed products was 1.25 times as high as that of the nitrogen-containing product, TH-Cz. Therefore, compared with the HDN of quinoline, the reaction step of C-N bond cleavage from hydrogenated nitrogen-containing products occurred relatively faster in the HDN of carbazole. As observed and suggested by Ho⁹⁹, in the HDN of quinoline, hydrogenolysis was the rate-limiting step, while in the HDN of 3-ethylcarbazole, hydrogenation was the rate-limiting step.

Yang and Satterfield¹⁰⁰ suggested that the surface Mo vacancy was responsible for hydrogenation reaction. H₂S adsorbed on such Mo vacancy and transferred it into a Brønsted acid site which was active in the cleavage of an aliphatic C-N bond. Mo sites at the edges in

the layered structure of MoS₂ was considered to be responsible for the C_{sp2}-N bond hydrogenolysis reaction¹⁰¹. The ratio between the two HDN product groups may depend on the access of the nitrogen-containing compound on active sites of the catalyst surface. Additionally, it also may be influenced by adsorption modes of reactant on the catalyst surface. The initial adsorption of quinoline on the active sites was proposed to be through the nitrogen heteroatom, either by donating its unpaired electron to a Lewis site or by the interaction with the proton of a Brønsted site^{8,50a,102}, while the carbazole molecule favored to adsorb on the catalytically active sites *via* aromatic rings in a parallel way because the lone pair of electrons in the nitrogen atom are not available in the end-on adsorption way on the catalyst surface⁵³.

Turaga *et al*^{13b} used bond order to explain the relative reactivity of quinoline and carbazole.. According to their calculation results, the highest bond order was 1.652 in the molecule of quinoline and was 1.449 in the carbazole molecule. The adsorption of quinoline molecules on the catalyst surface was considered to be stronger than carbazole molecules on the catalyst surface and may contribute to the higher initial hydrogenation.

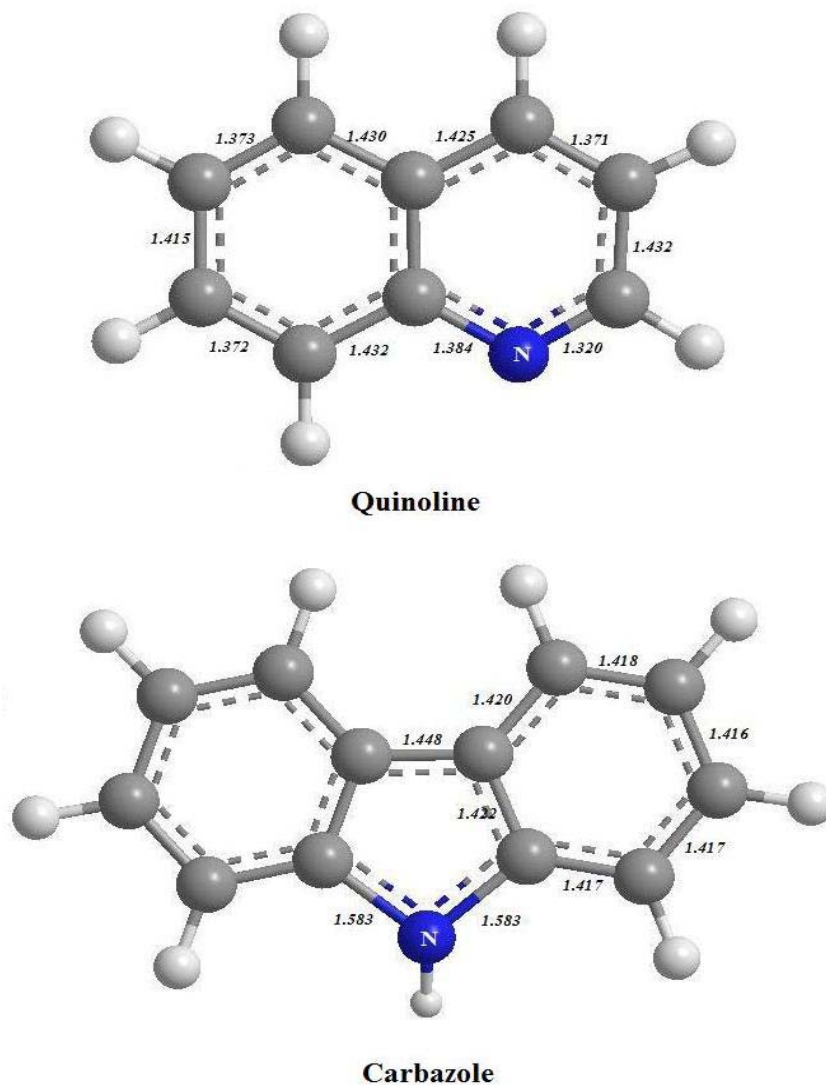


Fig. 8 - 19 Length of C-C and C-N bonds in molecules of Quinoline and carbazole (Molecular Mechanics (MM2) Calculations, MINIMIZED ENERGY, CHEM OFFICE)

However, the higher degree in denitrogenation (higher ratio between the concentrations of nitrogen-containing products and nitrogen-removed products) observed in the HDN of carbazole than in the HDN of quinoline (Table 8-5) indicated that the C-N bond cleavage from hydrogenated quinoline products seems relatively more difficult than from hydrogenated carbazole intermediate. This may be due to the different C-N bond length in

the two kinds of molecules. The lengths of C-C and C-N bonds in the molecules of quinoline and carbazole were calculated *via* the Molecular Mechanics (MM2) Calculation method processed using the software of Chem3D[®] Ultra Molecular Modeling and Analysis (Cambridgesoft). The numbers are listed beside each bond as shown in Fig. 8-19. The calculated C-N bond lengths in the quinoline molecule were 1.320 and 1.384, and the C-N bond length in the carbazole molecule was 1.583. The shorter of the bond length means the stronger of the bond. Hence, the shorter C-N bond length in the quinoline molecules will result in higher difficulty in removing the nitrogen atom.

8.8 Effect of 4,6-DMDBT on the HDN of Carbazole

The inhibitive effect of N-containing heterocyclic compounds on the HDS of refractory sulfur compounds had been studied and reported intensively^{8, 13c, 92, 103}, while the effect of sulfur-containing compounds on HDN reactions was rarely reported. In the present study, one of the most refractory sulfur-containing compounds, 4,6-DMDBT, was introduced into the reactant mixture according to the molar ratio of N:S equal to 1:1. Comparing the HDN product distributions of carbazole (shown in Fig. 8-10 *vs.* Fig. 8-20) obtained with and without adding 4,6-DMDBT, strong inhibitive effect of 4,6-DMDBT on the HDN of carbazole using *in-situ* H₂ was observed. With the presence of 4,6-DMDBT, the pseudo first order rate constant for the conversion of carbazole decreased from $7.7 \times 10^{-4} \text{ s}^{-1} \cdot \text{gcat}^{-1}$ to $4.1 \times 10^{-4} \text{ s}^{-1} \cdot \text{gcat}^{-1}$ (Table 8-6), which is equivalent to a decrease of 47%. The nitrogen removal at 180 min from carbazole decreased from 41 mol% to 18 mol%, which is equivalent to a decrease of 56%. Slight inhibitive effect of DBT on the HDN of carbazole

was observed by Laredo *et al*^{86b} over a NiMoP/ γ -Al₂O₃ commercial catalyst. They reported an estimated 12% inhibition on HDN caused by the presence of DBT. The inhibitive effect on the HDN of carbazole caused by the presence of 4,6-DMDBT observed in the present study was much stronger. This may be due to the difference between supported and dispersed catalysts. In any case, the inhibitive effect is due to the competitive adsorption of sulfur-containing compound, DBT or 4,6-DMDBT, on the catalyst surface in hydro-treating reactions. As reported, the DBT molecule adsorbed mainly in the mode of σ -adsorption *via* the sulfur atom, while the 4,6-DMDBT molecule preferred to adsorb on the catalyst surface *via* the π -orbital of aromatic rings with the molecule lying flat on the catalyst surface^{8, 13a, 44}. Literature reports suggested the molecules of carbazole preferred to adsorb on the catalyst surface in the same way as 4,6-DMDBT molecules^{44, 53}. This could account for the stronger inhibitive effect on the HDN of carbazole caused by 4,6-DMDBT than DBT.

Table 8 - 6 Pseudo first order rate constants for the conversion of carbazole and 4,6-DMDBT under different experimental conditions: (a) using *in-situ* H₂, without the addition of 4,6-DMDBT, or (b) using *in-situ* H₂, with adding 4,6-DMDBT*.

Experimental conditions	<i>In-situ</i> H ₂	<i>In-situ</i> H ₂
	(Cz) ^a	(Cz+4,6DMDBT) ^b
Conversion of carbazole at 180 min, %	48	29
Denitrogenation of carbazole at 180 min, mol%	41	18
Pseudo first order rate constants		
$k'_{Cz}, s^{-1} \cdot gcat^{-1}$	7.7×10^{-4}	4.1×10^{-4}
R^2_{Cz}	0.99	0.97
$k'_{4,6DMDBT}, s^{-1} \cdot gcat^{-1}$	---	1.5×10^{-4}
$R^2_{4,6DMDBT}$	---	0.97

*: Other conditions: 590 psi CO (H₂ used in b) and 10 psi H₂S (at room temperature), 430 ppmw Mo, 380 °C, 3hr, 10 ml H₂O, (b) S:N=1:1

As shown in Fig. 8-21, after introducing 4,6-DMDBT into the reaction system, the value of α (defined in Eq.(8-3)) was much higher than what observed in the carbazole experiment, and it decreased to less than 1.0 after reacting for longer than 130 min. Therefore, 4,6-DMDBT affected HDN of carbazole in two ways:

(i) 4,6-DMDBT molecules competed with carbazole molecules in the initial adsorption on the catalyst surface with carbazole, resulting in the decrease in the conversion of carbazole;

(ii) The denitrogenation active sites were partially occupied by 4,6-DMDBT, resulting in the lower denitrogenation degree of carbazole.

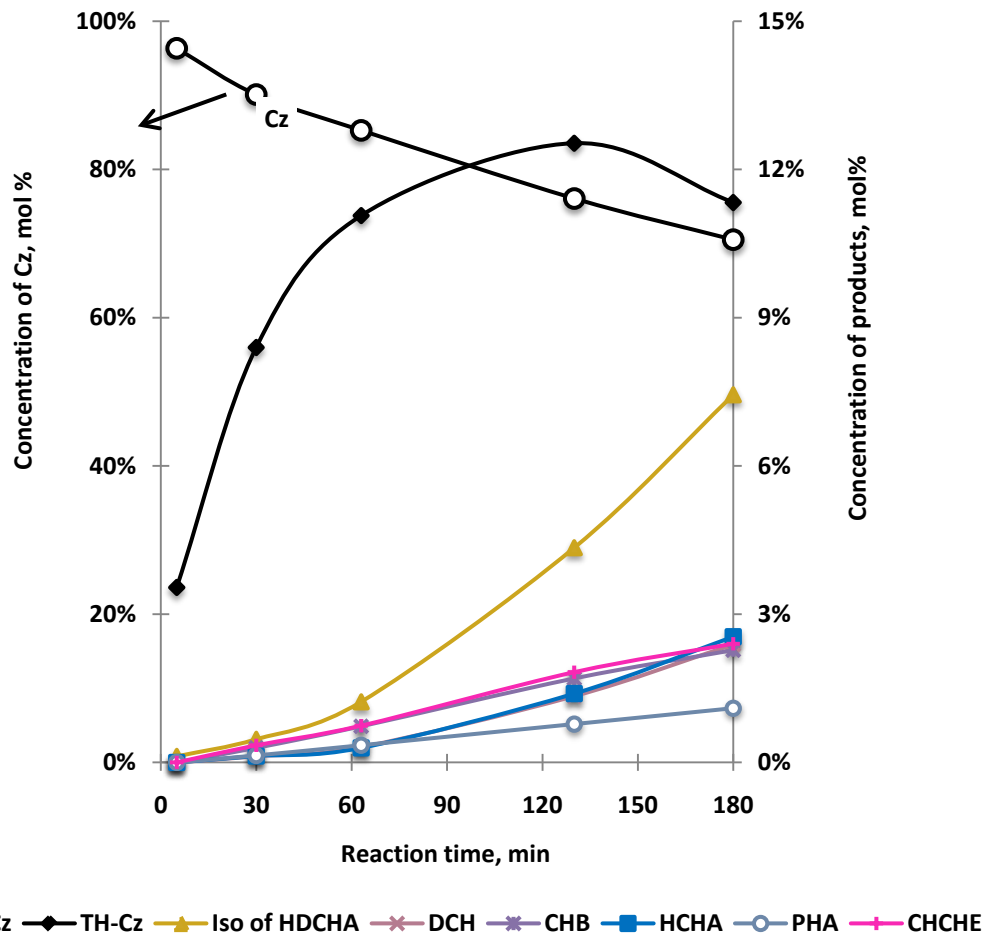


Fig. 8 - 20 Distribution of HDN products of carbazole under different reaction conditions over dispersed Mo sulfide catalyst with adding 4,6-DMDBT.

Other conditions: 590 psi CO and 10 psi H₂S (at room temperature), 430 ppmw Mo, 380 °C, 3hr, 10 ml H₂O, S:N=1:1

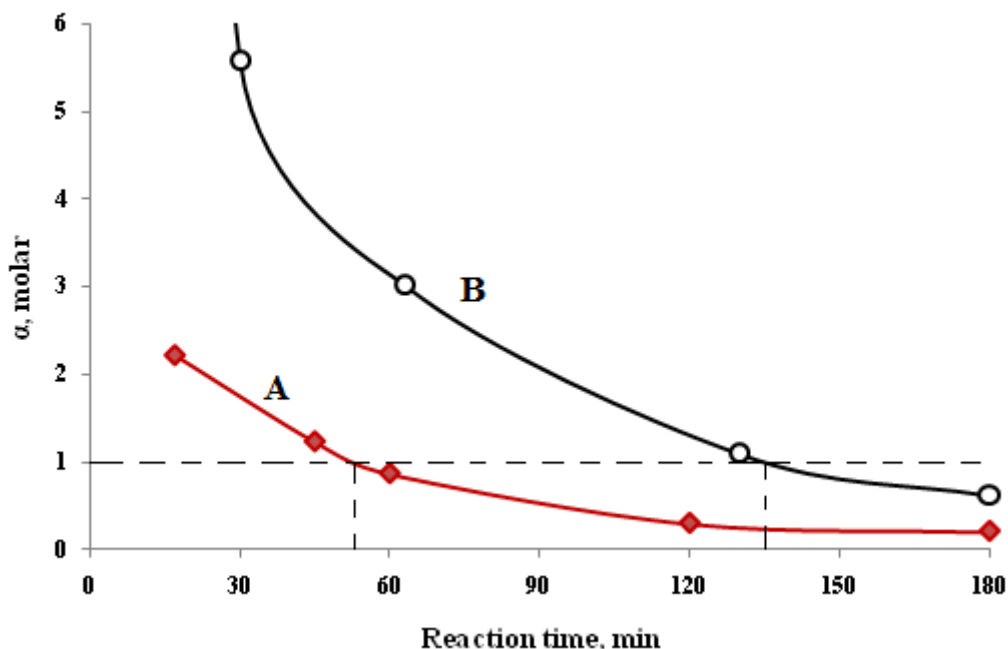


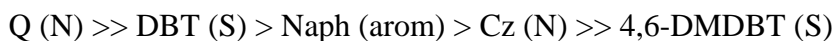
Fig. 8 - 21 Values of α as a function of reaction time obtained under different reaction conditions, (A) without the addition of 4,6-DMDBT, or (B) with adding 4,6-DMDBT.

Other conditions: 590 psi CO and 10 psi H₂S (at room temperature), 430 ppmw Mo, 380 °C, 3hr, 10 ml H₂O, (B) S:N=1:1

In Chapter 6, a significant inhibitive effect of carbazole on the HDS of 4,6-DMDBT was reported. The hydrogenation desulfurization reaction pathway in the HDS of 4,6-DMDBT was much more inhibited than the direct desulfurization route by carbazole, due to the competitive adsorption on the catalyst surface. So, in the present reaction system using *in-situ* H₂, the refractory N- and S-containing compounds have competitive inhibitive effect on hydrogenation and heteroatom removal. In the mixture of carbazole and 4,6-DMDBT, carbazole showed higher reactivity than 4,6-DMDBT (Table 8-4). The pseudo first order rate constants for the conversions of carbazole and 4,6-DMDBT were $4.1 \times 10^{-4} s^{-1} \cdot gcat^{-1}$ and $1.5 \times 10^{-4} s^{-1} \cdot gcat^{-1}$, respectively. The reactivity of 4,6-DMDBT was 1.7 times

lower than that of carbazole under the present reaction conditions. Hence, the dispersed Mo sulfide catalyst had higher selectivity towards the HDN of carbazole than the HDS of 4,6-DMDBT. This suggested that non-basic carbazole adsorbed preferentially on the active sites over the refractory sulfur-containing compound 4,6-DMDBT.

One hydro-treating experiment in the presence of all model compounds used in this study, including DBT, 4,6-DMDBT, quinoline, carbazole, and naphthalene, was carried out to compare their hydro-treating reactivity in an equi-molar mixture over the dispersed Mo sulfide catalyst using *in-situ* hydrogen. Detailed reaction conditions are given in Fig. 8-22. At the beginning of the reaction at 380°C, the conversion of quinoline had reached 100%, while significant conversion of 4,6-DMDBT was observed at 60 min. The conversions of the other three model compounds increased gradually with extending the reaction time. The pseudo-first-order of each component, except quinoline and 4,6-DMDBT, is listed in Table 8-7. The rate constant of DBT was found to be almost 10 times as high as that of carbazole, and the rate constant of carbazole was slightly lower than that of naphthalene. Therefore, over the dispersed Mo sulfide catalyst using *in-situ* hydrogen, an order of the relative reactivity of model sulfur-/nitrogen-containing compounds and aromatic component in a mixture of all of them could be obtained:



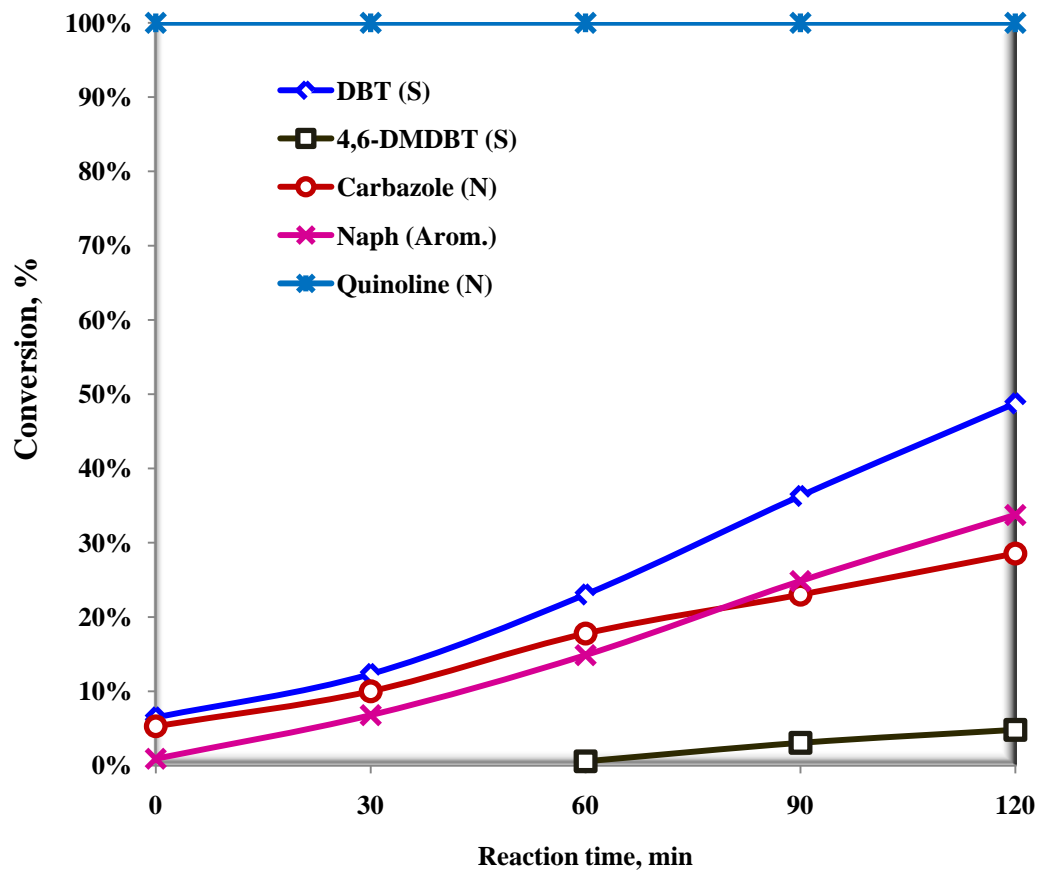


Fig. 8 - 22 Conversions of DBT, 4,6-DMDBT, quinoline, carbazole and naphthalene over dispersed Mo sulfide catalyst in in-situ hydrogen at 380°C.

Other conditions: 590 psi CO, 10 psi H₂S, equi-mol of each component (about 1.2 mmol of each), 100 ml toluene, 10 ml PMA solution, 430 ppmw Mo

Table 8 - 7 Pseudo-first-order rate constant of each component in the hydro-treating reaction of the mixture*.

	<i>k'</i> (for the conversion)
DBT (S)	36.0×10^{-5}
4,6-DMDBT (S)[†]	N/A
Carbazole (N)	3.6×10^{-5}
Quinoline (N)[‡]	N/A
Naphthalene (Arom.)	5.7×10^{-5}

* Other conditions: 590 psi CO, 10 psi H₂S, equi-mol of each component (about 1.2 mmol of each), 100 ml toluene, 10 ml PMA solution, 430 ppmw Mo

† The conversion of 4,6-DMDBT was too low for the calculation

‡ The conversion of Quinoline was 100% when heated the reactor up to the reaction temperature.

8.9 Conclusions

In this chapter, the effect of molecular hydrogen and in-situ hydrogen for the HDN of carbazole over dispersed Mo sulfide catalyst with or without the presence of sulfur-containing species was elucidated.

- (1) The conversion of CO *via* the WGS reaction or the concentration of *in-situ* generated hydrogen was not inhibited in the presence of non-basic carbazole.
- (2) One HDN reaction network was proposed. In this mechanism, reactions of hydrogenation, C-N bond cleavage, and ring-opening were involved. As a result, the HDN products of carbazole could be divided into three groups: partially

hydrogenated intermediate, bicyclic nitrogen removed products, and ring-opened nitrogen removed products. Among these products, HCHE was found to be the predominant denitrogenation product. The proposed HDN reaction network of carbazole and the predominant concentration of ring-opened product in the mixture of N-removed products have not been observed or reported by other researchers.

- (3) In the mixture with 4,6-DMDBT, carbazole had shown higher reactivity in hydro-treating reactions over dispersed Mo sulfide catalyst in *in-situ* H₂ at 380°C.
- (4) The presence of 4,6-DMDBT also had significant inhibitive effect on the HDN of carbazole.

Chapter 9 Conclusions and Recommendations

9.1 Conclusions

9.1.1 *In-situ* H₂ versus molecular H₂ in the preparation of dispersed catalyst

XRD and HRTEM-EDX characterization results confirmed the preparation of MoS₂ via the hydro-thermal decomposition of the aqueous Mo precursor, PMA. Nano-dispersed Mo sulfide catalysts with high surface area (>200m²/g) were prepared in *in-situ* hydrogen or molecular hydrogen. The catalyst made in *in-situ* hydrogen was found to have higher BET surface area, shorter and more curved MoS₂ slabs, and lower stacking degree than the one made in molecular hydrogen under the same conditions. SEM images suggested the size of MoS₂ poly-crystallines was also smaller when prepared in *in-situ* hydrogen.

9.1.2 Simultaneous HDS of DBT and 4,6-DMDBT using *in-situ* hydrogen

The simultaneous HDS of DBT and 4,6-DMDBT was carried out in *in-situ* hydrogen from 330°C to 400°C. DDS was the major reaction pathway in the HDS of DBT, whereas HYD was the predominant HDS pathway of 4,6-DMDBT. The relative reactivity of the more refractory sulfur-containing compound, 4,6-DMDBT, to DBT obtained over dispersed Mo sulfide catalyst using *in-situ* hydrogen was found to be much higher than the number reported in literatures obtained over supported catalysts using molecular hydrogen. The DDS reaction pathway was more preferred at high reaction temperature.

9.1.3 *In-situ* H₂ versus molecular H₂ in HDS

The *in-situ* hydrogen reaction system, including *in-situ* prepared catalyst and *in-situ* generated hydrogen, was found to be more efficient in the simultaneous HDS of DBT and 4,6-DMDBT. The HDS study carried out over *ex-situ* prepared dispersed Mo sulfide catalysts suggested that the one prepared in *in-situ* hydrogen had higher hydrogenation activity than the other one made in molecular hydrogen. The high hydrogenation activity of the catalyst prepared in *in-situ* hydrogen was attributed to the morphology of the catalyst. The experiment results also suggested that *in-situ* hydrogen had comparable reactivity to molecular hydrogen in the simultaneous HDS of DBT and 4,6-DMDBT. The competitive adsorption of DBT and 4,6-DMDBT molecules on HYD active sites resulted in the higher selectivity of the DDS pathway in the HDS of DBT carried out in the *in-situ* reaction system.

9.1.4 Effect of promoters on the simultaneous HDS of DBT and 4,6-DMDBT

The promotional effect of Ni on the HDS of DBT was more significant than on the HDS of 4,6-DMDBT. The low promotional effect of Ni observed in the present study was attributed to the low sulfidation of NiMo catalyst and to the separate dispersion of Ni to bulky Mo in the reaction system. To improve the HDS efficiency of Ni promoted Mo sulfide catalyst, the preparation conditions need to be optimized. Significant improvement in the WGS reaction was observed after adding potassium into the Mo sulfide catalyst, whereas, the HDS activity of KMo sulfide catalyst decreased dramatically. Therefore, potassium could not be used as a promoter for hydro-treating reactions.

9.1.5 Effect of nitrogen-containing compounds on HDS

Strong inhibitive effect of either basic or non-basic nitrogen-containing compound on the simultaneous HDS of DBT and 4,6-DMDBT was observed over dispersed Mo sulfide catalyst using *in-situ* hydrogen. Compared to the DDS route, the desulfurization from the HYD route was inhibited more severely by nitrogen-containing compounds due to the competitive adsorption on HYD active sites. The *in-situ* reaction system exhibited comparable HDS activity as molecular hydrogen in the presence of nitrogen-containing compounds.

9.1.6 HDN of carbazole

HDN products of carbazole were identified *via* GC-MS and an HDN reaction network was proposed. There were three groups of products detected in the HDN of carbazole: partially hydrogenated nitrogen-containing intermediate, bicyclic ring nitrogen-removed products, and ring-opened nitrogen-removed products. The presence of carbazole did not show inhibitive effect on the WGS reaction. The *in-situ* hydrogen system was comparatively effective in the conversion of carbazole as the molecular hydrogen reaction system.

9.2 Recommendations

9.2.1 Optimizing the preparation conditions of dispersed catalyst

In this thesis, the activities of dispersed Mo sulfide based catalysts were investigated and discussed, but the preparation conditions were not optimized. To improve the efficiency of

the dispersed catalyst, the preparation conditions could be optimized *via* modifying the oil/water ratio, the partial pressure of H₂S, stirring speed, preparation temperature and pressure, and so on. Additionally, based on personal experimental experience, the Mo sulfide catalyst dispersed better in acetone and ethanol than in toluene. So in the future, the composition of the organic phase may be modified to optimize the catalyst preparation conditions. Finally, surfactants may also be introduced into the catalyst preparation system to improve the dispersion of precursor in the organic phase to increase the activity of the candidate catalysts.

9.2.2 Extend the use of *ex-situ* prepared catalysts for hydro-treating gas oil and upgrading bitumen emulsions

In this thesis, *ex-situ* catalyst studies allowed us to investigate the effect of the sources of hydrogen on catalyst preparation and on HDS reactions. In the future, this study could be extended to hydro-treating light gas oils and upgrading bitumen emulsions.

9.2.3 Investigate the HDN activity of Ni promoted Mo sulfide catalysts

Once the preparation conditions of Ni promoted Mo sulfide catalyst were optimized, the promotional effect of Ni on the HDN activity of Mo sulfide catalyst could be studied.

References

1. <http://www.canadasoilsands.ca/en/overview/>.
2. Ng, F. T. T., Tsakiri, S.K., US Patent 5,5055,175. **1991**.
3. NG, F. T. T. C., TSAKIRI, SOPHIA K. (Canada), UPGRADING CRUDE OIL EMULSIONS *Canadian Patent* **1993**.
4. Ng, F. T. T.; Tsakiri, S. K., Activation of water in emulsion for catalytic desulphurization of benzothiophene. *Fuel* **1992**, *71* (11), 1309-1314.
5. Moll, J. K.; Li, Z.; Ng, F. T. T., Activity of alternative hydrogen sources for the hydrodesulfurization of diesel and bitumen in the presence of water using dispersed Mo-based catalyst. **2000**, *45* (4), 599-602.
6. Moll, J., Feasibility study on desulfurization of bitumen emulsion using hydrogen from the water gas shift reaction. *Master Thesis, University of Waterloo* **1999**.
7. Rana, M. S.; Sámano, V.; Ancheyta, J.; Diaz, J. A. I., A review of recent advances on process technologies for upgrading of heavy oils and residua. *Fuel* **2007**, *86* (9), 1216-1231.
8. Prins, R.; Egorova, M.; Röhlisberger, A.; Zhao, Y.; Sivasankar, N.; Kukula, P., Mechanisms of hydrodesulfurization and hydrodenitrogenation. *Catalysis Today* **2006**, *111* (1-2), 84-93.
9. Girgis, M. J.; Gates, B. C., Reactivities, reaction networks, and kinetics in high-pressure catalytic hydroprocessing. *Industrial & Engineering Chemistry Research* **1991**, *30* (9), 2021-2058.
10. Laredo S, G. C.; De los Reyes H, J. A.; Luis Cano D, J.; Jesús Castillo M, J., Inhibition effects of nitrogen compounds on the hydrodesulfurization of dibenzothiophene. *Applied Catalysis A: General* **2001**, *207* (1-2), 103-112.
11. Laredo, G. C.; Leyva, S.; Alvarez, R.; Mares, M. T.; Castillo, J.; Cano, J. L., Nitrogen compounds characterization in atmospheric gas oil and light cycle oil from a blend of Mexican crudes. *Fuel* **2002**, *81* (10), 1341-1350.
12. Zeuthen, P.; Knudsen, K. G.; Whitehurst, D. D., Organic nitrogen compounds in gas oil blends, their hydrotreated products and the importance to hydrotreatment. *Catalysis Today* **2001**, *65* (2-4), 307-314.

13. (a) van Looij, F.; van der Laan, P.; Stork, W. H. J.; DiCamillo, D. J.; Swain, J., Key parameters in deep hydrodesulfurization of diesel fuel. *Applied Catalysis A: General* **1998**, *170* (1), 1-12;
- (b) Turaga, U. T.; Ma, X.; Song, C., Influence of nitrogen compounds on deep hydrodesulfurization of 4,6-dimethyldibenzothiophene over Al₂O₃- and MCM-41-supported Co-Mo sulfide catalysts. *Effects of Support in Hydrotreating Catalysis for Ultra-clean Fuels* **2003**, *86* (1-4), 265-275;
- (c) Egorova, M.; Prins, R., Competitive hydrodesulfurization of 4,6-dimethyldibenzothiophene, hydrodenitrogenation of 2-methylpyridine, and hydrogenation of naphthalene over sulfided NiMo/[gamma]-Al₂O₃. *Journal of Catalysis* **2004**, *224* (2), 278-287.
14. Bearden, R.; Aldridge, C. L., Novel catalyst and process to upgrade heavy oils. **1981**, *1* (1-4), 44-8.
15. Siewe, C. N.; Ng, F. T. T., Hydrodesulfurization of Cold Lake Diesel Fraction Using Dispersed Catalysts: Influence of Hydroprocessing Medium and Sources of H₂. *Energy & Fuels* **1998**, *12* (3), 598-606.
16. Tian, K. P.; Mohamed, A. R.; Bhatia, S., Catalytic upgrading of petroleum residual oil by hydrotreating catalysts: a comparison between dispersed and supported catalysts. *Fuel* **1998**, *77* (11), 1221-1227.
17. Bataille, F.; Lemberon, J.-L.; Michaud, P.; Pérot, G.; Vrinat, M.; Lemaire, M.; Schulz, E.; Breyse, M.; Kasztelan, S., Alkyldibenzothiophenes Hydrodesulfurization-Promoter Effect, Reactivity, and Reaction Mechanism. *Journal of Catalysis* **2000**, *191* (2), 409-422.
18. Nikolova, D.; Edreva-Kardjieva, R.; Gouliev, G.; Grozeva, T.; Tzvetkov, P., The state of (K)(Ni)Mo/[gamma]- Al₂O₃ catalysts after water-gas shift reaction in the presence of sulfur in the feed: XPS and EPR study. *Applied Catalysis A: General* **2006**, *297* (2), 135-144.
19. Newsome, D. S., Kellogg, P., Houston, The water-gas shift reaction. *Catal. Rev.-Sci. Eng.* **1980**, *21* (2), 275-318.
20. Nikolova, D.; Edreva-Kardjieva, R.; Giurginca, M.; Meghea, A.; Vakros, J.; Voyiatzis, G. A.; Kordulis, C., The effect of potassium addition on the state of the components in the oxide precursor of the (Ni)(Mo)/[gamma]- Al₂O₃ water-gas shift catalysts:

FT-IR, diffuse reflectance and Raman spectroscopic studies. *Vibrational Spectroscopy* **2007**, *44* (2), 343-350.

21. Ho, T. C., Hydrodenitrogenation Catalysis. *Catalysis Reviews* **1988**, *30* (1), 117-160.
22. Laredo, G. C.; Altamirano, E.; De los Reyes, J. A., Inhibition effects of nitrogen compounds on the hydrodesulfurization of dibenzothiophene: Part 2. *Applied Catalysis A: General* **2003**, *243* (2), 207-214.
23. Sánchez-Delgado, R. A.; Robert, H. C.; Mingos, D. M. P., Hydrodesulfurization and Hydrodenitrogenation. In *Comprehensive Organometallic Chemistry III*, Elsevier: Oxford, 2007; pp 759-800.
24. Le, Z.; Afanasiev, P.; Li, D.; Long, X.; Vrinat, M., Solution synthesis of the unsupported Ni-W sulfide hydrotreating catalysts. *Catalysis Today* **2008**, *130* (1), 24-31.
25. Yoneyama, Y.; Song, C., A new method for preparing highly active unsupported Mo sulfide. Catalytic activity for hydrogenolysis of 4-(1-naphthylmethyl)biphenyl. *Catalysis Today* **1999**, *50* (1), 19-27.
26. Iwata, Y.; Araki, Y.; Honna, K.; Miki, Y.; Sato, K.; Shimada, H., Hydrogenation active sites of unsupported molybdenum sulfide catalysts for hydroprocessing heavy oils. *Catalysis Today* **2001**, *65* (2-4), 335-341.
27. Iwata, Y.; Sato, K.; Yoneda, T.; Miki, Y.; Sugimoto, Y.; Nishijima, A.; Shimada, H., Catalytic functionality of unsupported molybdenum sulfide catalysts prepared with different methods. *Catalysis Today* **1998**, *45* (1-4), 353-359.
28. Alonso, G.; Berhault, G.; Aguilar, A.; Collins, V.; Ornelas, C.; Fuentes, S.; Chianelli, R. R., Characterization and HDS Activity of Mesoporous MoS₂ Catalysts Prepared by in Situ Activation of Tetraalkylammonium Thiomolybdates. *Journal of Catalysis* **2002**, *208* (2), 359-369.
29. Nava, H.; Espino, J.; Berhault, G.; Alonso-Nuñez, G., Effect of phosphorus addition on unsupported Ni-Mo-W sulfide catalysts prepared by the in situ activation of nickel/tetramethylammonium thiomolybdotungstate. *Applied Catalysis A: General* **2006**, *302* (2), 177-184.
30. Nava, H.; Pedraza, F.; Alonso, G., Nickel-Molybdenum-Tungsten Sulfide catalysts prepared by in situ activation of tri-metallic (Ni-Mo-W) alkylthiomolybdotungstates. *Catalysis Letters* **2005**, *99* (1), 65-71.

31. Eijsbouts, S.; Mayo, S. W.; Fujita, K., Unsupported transition metal sulfide catalysts: From fundamentals to industrial application. *Applied Catalysis A: General* **2007**, *322*, 58-66.
32. Daage, M.; Chianelli, R. R., Structure-Function Relations in Molybdenum Sulfide Catalysts: The "Rim-Edge" Model. *Journal of Catalysis* **1994**, *149* (2), 414-427.
33. Lauritsen, J. V.; Kibsgaard, J.; Helveg, S.; Topsøe, H.; Clausen, B. S.; Lægsgaard, E.; Besenbacher, F., Size-dependent structure of MoS₂ nanocrystals. *Nature Nanotechnology* **2007**, *2* (1), 53-58.
34. Lauritsen, J. V.; Bollinger, M. V.; Lægsgaard, E.; Jacobsen, K. W.; Nørskov, J. K.; Clausen, B. S.; Topsøe, H.; Besenbacher, F., Atomic-scale insight into structure and morphology changes of MoS₂ nanoclusters in hydrotreating catalysts. *Journal of Catalysis* **2004**, *221* (2), 510-522.
35. Lauritsen, J. V.; Besenbacher, F.; Bruce, C. G.; Helmut, K., Model Catalyst Surfaces Investigated by Scanning Tunneling Microscopy. In *Advances in Catalysis*, Academic Press: 2006; Vol. Volume 50, pp 97-147.
36. Lee, R. Z.; Ng, F. T. T., Effect of water on HDS of DBT over a dispersed Mo catalyst using in situ generated hydrogen. *Catalysis Today* **2006**, *116* (4), 505-511.
37. Wang, H.; Liang, C.; Prins, R., Hydrodenitrogenation of 2-methylpyridine and its intermediates 2-methylpiperidine and tetrahydro-methylpyridine over sulfided NiMo/Î³-Al₂O₃. *Journal of Catalysis* **2007**, *251* (2), 295-306.
38. Devers, E.; Afanasiev, P.; Jouguet, B.; Vrinat, M., Hydrothermal Syntheses and Catalytic Properties of Dispersed Molybdenum Sulfides. *Catalysis Letters* **2002**, *82* (1), 13-17.
39. Furimsky, E.; Massoth, F. E., Deactivation of hydroprocessing catalysts. *Catalysis Today* **1999**, *52* (4), 381-495.
40. Satterfield, C. N.; Smith, C. M.; Ingalls, M., Catalytic hydrodenitrogenation of quinoline. Effect of water and hydrogen sulfide. *Industrial & Engineering Chemistry Process Design and Development* **2002**, *24* (4), 1000-1004.
41. Song, C.; Saini, A. K.; Yoneyama, Y., A new process for catalytic liquefaction of coal using dispersed MoS₂ catalyst generated in situ with added H₂O. *Fuel* **2000**, *79* (3-4), 249-261.

42. R.Z., L., Investigation of hydrodesulfurization of dibenzothiophene and hydrodenitrogenation of quinoline using in situ H₂ generated via water gas shift reaction over dispersed Mo based catalysts. *Ph.D thesis, University of Waterloo* **2004**.
43. Song, C., An overview of new approaches to deep desulfurization for ultra-clean gasoline, diesel fuel and jet fuel. *Catalysis Today* **2003**, 86 (1-4), 211-263.
44. Liu, K.; Ng, F. T. T., Effect of the nitrogen heterocyclic compounds on hydrodesulfurization using in situ hydrogen and a dispersed Mo catalyst. *Catalysis Today In Press, Corrected Proof*.
45. Michaud, P.; Lemberton, J. L.; Pérot, G., Hydrodesulfurization of dibenzothiophene and 4,6-dimethyldibenzothiophene: Effect of an acid component on the activity of a sulfided NiMo on alumina catalyst. *Applied Catalysis A: General* **1998**, 169 (2), 343-353.
46. Ma, X.; Sakanishi, K.; Mochida, I., Hydrodesulfurization reactivities of various sulfur compounds in diesel fuel. *Industrial & Engineering Chemistry Research* **1994**, 33 (2), 218-222.
47. Egorova, M.; Prins, R., Mutual influence of the HDS of dibenzothiophene and HDN of 2-methylpyridine. *Journal of Catalysis* **2004**, 221 (1), 11-19.
48. Jae Hyung Kim, X. M., Chunshan Song, Yong-kul Lee and S. Ted Oyama, Kinetics of two pathways for 4,6-dimethyldibenzothiophene hydrodesulfurization over NiMo, CoMo sulfide, and nickel phosphide catalysts. *Energy & Fuels* **2005**, 19, 12.
49. (a) Ng, F. T. T.; Milad, I. K., Catalytic desulphurization of benzothiophene in an emulsion via in situ generated H₂. *Applied Catalysis A: General* **2000**, 200 (1-2), 243-254;
(b) C. Liu, F. T. T. N., *Chin. J. Catal.* **1999**, 20 (6);
(c) M. Kumar, A. A., R. Anthony, *Ind. Eng. Chem. Res* **1984**, 23;
(d) Y. Takemura, H. I., K. Ouchi, *J. Jpn. Petrol. Inst.* **1981**, 24 (6), 357.
50. (a) La Vopa, V.; Satterfield, C. N., Poisoning of thiophene hydrodesulfurization by nitrogen compounds. *Journal of Catalysis* **1988**, 110 (2), 375-387;
(b) Nagai, M.; Sato, T.; Aiba, A., Poisoning effect of nitrogen compounds on dibenzothiophene hydrodesulfurization on sulfided NiMo/Al₂O₃ catalysts and relation to gas-phase basicity. *Journal of Catalysis* **1986**, 97 (1), 52-58;

(c) Nagai, M.; Kabe, T., Selectivity of molybdenum catalyst in hydrodesulfurization, hydrodenitrogenation, and hydrodeoxygenation: Effect of additives on dibenzothiophene hydrodesulfurization. *Journal of Catalysis* **1983**, *81* (2), 440-449.

51. (a) Shin, S.; Sakanishi, K.; Mochida, I.; Grudoski, D. A.; Shinn, J. H., Identification and Reactivity of Nitrogen Molecular Species in Gas Oils. *Energy & Fuels* **2000**, *14* (3), 539-544;

(b) Sumbogo Murti, S. D.; Yang, H.; Choi, K.-H.; Korai, Y.; Mochida, I., Influences of nitrogen species on the hydrodesulfurization reactivity of a gas oil over sulfide catalysts of variable activity. *Applied Catalysis A: General* **2003**, *252* (2), 331-346.

52. Ho, T. C.; Markley, G. E., Property-reactivity correlation for hydrodesulfurization of prehydrotreated distillates. *Applied Catalysis A: General* **2004**, *267* (1-2), 245-250.

53. Ho, T. C., Deep HDS of diesel fuel: chemistry and catalysis. *Catalysis Today* **2004**, *98* (1-2), 3-18.

54. (a) Szymanska, A.; Lewandowski, M.; Sayag, C.; Djega-Mariadassou, G., Kinetic study of the hydrodenitrogenation of carbazole over bulk molybdenum carbide. *Journal of Catalysis* **2003**, *218* (1), 24-31;

(b) Sánchez-Minero, F.; Ramírez, J.; Gutiérrez-Alejandre, A.; Fernández-Vargas, C.; Torres-Mancera, P.; Cuevas-García, R., Analysis of the HDS of 4,6-DMDBT in the presence of naphthalene and carbazole over NiMo/Al₂O₃-SiO₂(x) catalysts. *Catalysis Today* *133-135*, 267-276;

(c) Abu, I. I.; Smith, K. J., Hydrodenitrogenation of carbazole over a series of bulk Ni_xMoP catalysts. *Catalysis Today* **2007**, *125* (3-4), 248-255.

55. (a) Szymanska, A.; Lewandowski, M.; Sayag, C.; Djéga-Mariadassou, G., Kinetic study of the hydrodenitrogenation of carbazole over bulk molybdenum carbide. *Journal of Catalysis* **2003**, *218* (1), 24-31;

(b) Katzer, J. R.; Sivasubramanian, R., Process and Catalyst Needs for Hydrodenitrogenation. *Catalysis Reviews: Science and Engineering* **1979**, *20* (2), 155 - 208.

56. Pérot, G., The reactions involved in hydrodenitrogenation. *Catalysis Today* **1991**, *10* (4), 447-472.

57. Ledoux, M. J.; Bouassida, A.; Benazouz, R., The use of pyridine and piperidine hdn as probe for activity of molybdenum-based hydrotreatment catalysts. The role of the nickel (part II). *Applied Catalysis* **1984**, *9* (1), 41-52.
58. Wang, H.; Fan, Y.; Shi, G.; Liu, Z.; Liu, H.; Bao, X., Highly dispersed NiW/[gamma]-Al₂O₃ catalyst prepared by hydrothermal deposition method. *Catalysis Today* **2007**, *125* (3-4), 149-154.
59. Roxlo, C. B.; Daage, M.; Ruppert, A. F.; Chianelli, R. R., Optical absorption and catalytic activity of molybdenum sulfide edge surfaces. *Journal of Catalysis* **1986**, *100* (1), 176-184.
60. Topsøe, H.; Clausen, B. S., Active sites and support effects in hydrodesulfurization catalysts. *Applied Catalysis* **1986**, *25* (1-2), 273-293.
61. Liu, C.; Zhou, J.; Que, G.; Liang, W.; Zhu, Y., Hydrocracking of Gudao residue with dispersed-phase Mo catalyst. *Fuel* **1994**, *73* (9), 1544-1550.
62. Afanasiev, P., Synthetic approaches to the molybdenum sulfide materials. *Comptes Rendus Chimie II* (1-2), 159-182.
63. Russell R. Chianelli, M. H. S., Myriam Perez De la Rosa, Gilles Berhault, Jess P. Wilcoxon, Roby Bearden, Jr., Billie L. Abrams, Catalytic properties of single layers of transition metal sulfide catalytic materials. *Catalysis Reviews* **2006**, *48*, 41.
64. Johnston, D. C.; Jacobson, A. J.; Silbernagel, B. G.; Frysinger, S. P.; Rich, S. M.; Gebhard, L. A., Magnetic susceptibility and electron spin resonance as probes of different magnetic species in MoS₃. *Journal of Catalysis* **1984**, *89* (2), 244-249.
65. Johnston, D. C., Silbernagel, B.G., Daage, M., Chianelli, R.R., *Prepr.Am. Chem. Soc., Div. Pet. Chem.* **1985**, *30* (1).
66. Besenbacher, F.; Brorson, M.; Clausen, B. S.; Helveg, S.; Hinnemann, B.; Kibsgaard, J.; Lauritsen, J. V.; Moses, P. G.; Nørskov, J. K.; Topsøe, H., Recent STM, DFT and HAADF-STEM studies of sulfide-based hydrotreating catalysts: Insight into mechanistic, structural and particle size effects. *Catalysis Today* **2008**, *130* (1), 86-96.
67. Lauritsen, J. V.; Nyberg, M.; Nørskov, J. K.; Clausen, B. S.; Topsøe, H.; Lægsgaard, E.; Besenbacher, F., Hydrodesulfurization reaction pathways on MoS₂ nanoclusters revealed by scanning tunneling microscopy. *Journal of Catalysis* **2004**, *224* (1), 94-106.

68. Eijsbouts, S.; Heinerman, J. J. L.; Elzerman, H. J. W., MoS₂ structures in high-activity hydrotreating catalysts: I. Semi-quantitative method for evaluation of transmission electron microscopy results. Correlations between hydrodesulfurization and hydrodenitrogenation activities and MoS₂ dispersion. *Applied Catalysis A: General* **1993**, *105* (1), 53-68.
69. Genuit, D.; Afanasiev, P.; Vrinat, M., Solution syntheses of unsupported Co(Ni)-Mo-S hydrotreating catalysts. *Journal of Catalysis* **2005**, *235* (2), 302-317.
70. Vogelaar, B. M.; Steiner, P.; van der Zijden, T. F.; van Langeveld, A. D.; Eijsbouts, S.; Moulijn, J. A., Catalyst deactivation during thiophene HDS: The role of structural sulfur. *Applied Catalysis A: General* **2007**, *318*, 28-36.
71. Dong, D.; Jeong, S.; Massoth, F. E., Effect of nitrogen compounds on deactivation of hydrotreating catalysts by coke. *Catalysis Today* **1997**, *37* (3), 267-275.
72. Furimsky, E., Chemical Origin of Coke Deposited on Catalyst Surface. *Industrial & Engineering Chemistry Product Research and Development* **1978**, *17* (4), 329-331.
73. Satterfield, C. N.; Modell, M.; Hites, R. A.; Declerck, C. J., Intermediate Reactions in the Catalytic Hydrodenitrogenation of Quinoline. *Industrial & Engineering Chemistry Process Design and Development* **1978**, *17* (2), 141-148.
74. Koltai, T.; Macaud, M.; Guevara, A.; Schulz, E.; Lemaire, M.; Bacaud, R.; Vrinat, M., Comparative inhibiting effect of polycondensed aromatics and nitrogen compounds on the hydrodesulfurization of alkyldibenzothiophenes. *Applied Catalysis A: General* **2002**, *231* (1-2), 253-261.
75. Topsøe, H., Clausen, B.S., Massoth, F.E., *Hydrotreating Catalysis, Science and Technology* **1996**, *11*.
76. Besenbacher, F.; Lauritsen, J. V.; Linderoth, T. R.; Lægsgaard, E.; Vang, R. T.; Wendt, S., Atomic-scale surface science phenomena studied by scanning tunneling microscopy. *Surface Science* **2009**, *603* (10-12), 1315-1327.
77. (a) Kantschewa, M.; Delannay, F.; Jeziorowski, H.; Delgado, E.; Eder, S.; Ertl, G.; Knözinger, H., Nature and properties of a potassium-promoted NiMo/Al₂O₃ water gas shift catalyst. *Journal of Catalysis* **1984**, *87* (2), 482-496;
- (b) Hou, P.; Meeker, D.; Wise, H., Kinetic studies with a sulfur-tolerant water gas shift catalyst. *Journal of Catalysis* **1983**, *80* (2), 280-285.

78. Yoosuk, B.; Kim, J. H.; Song, C.; Ngamcharussrivichai, C.; Prasassarakich, P., Highly active MoS₂, CoMoS₂ and NiMoS₂ unsupported catalysts prepared by hydrothermal synthesis for hydrodesulfurization of 4,6-dimethyldibenzothiophene. *New developments in sulfide catalysis: Linking industrial needs to fundamental challenges - Proceedings of the 4th International Symposium on Molecular Aspects of Catalysis by Sulfides (MACS-IV)* **2008**, 130 (1), 14-23.
79. Abu, I. I.; Smith, K. J., HDN and HDS of model compounds and light gas oil derived from Athabasca bitumen using supported metal phosphide catalysts. *Applied Catalysis A: General* **2007**, 328 (1), 58-67.
80. Egorova, M.; Prins, R., Hydrodesulfurization of dibenzothiophene and 4,6-dimethyldibenzothiophene over sulfided NiMo/[gamma]-Al₂O₃, CoMo/[gamma]-Al₂O₃, and Mo/[gamma]-Al₂O₃ catalysts. *Journal of Catalysis* **2004**, 225 (2), 417-427.
81. Wang, H.; Prins, R., Hydrodesulfurization of dibenzothiophene, 4,6-dimethyldibenzothiophene, and their hydrogenated intermediates over Ni-MoS₂/[gamma]-Al₂O₃. *Journal of Catalysis In Press, Corrected Proof*.
82. Alghamdi, A., Hydrodesulphurization of Light Gas Oil using Hydrogen from the Water Gas Shift Reaction. *MSc Thesis, University of Waterloo* **2009**.
83. Liu, K., Use of Nano-Dispersed Molybdenum for Upgrading Bitumen Emulsions. *Ph.d Proposal, University of Waterloo* **2007**.
84. Andreev, A. A.; Kafedjiysky, V. J.; Edreva-Kardjieva, R. M., Active forms for water-gas shift reaction on NiMo-sulfide catalysts. *Applied Catalysis A: General* **1999**, 179 (1-2), 223-228.
85. Lewandowski, M.; Sarbak, Z., Simultaneous HDS and HDN over supported PtSn catalysts in comparison to commercial NiMo/Al₂O₃. *Applied Catalysis B: Environmental* **2008**, 79 (4), 313-322.
86. (a) Ho, T. C., Inhibiting effects in hydrodesulfurization of 4,6-diethyldibenzothiophene. *Journal of Catalysis* **2003**, 219 (2), 442-451;
- (b) Laredo, G. C.; Montesinos, A.; De los Reyes, J. A., Inhibition effects observed between dibenzothiophene and carbazole during the hydrotreating process. *Applied Catalysis A: General* **2004**, 265 (2), 171-183.

87. Logadóttir, Á.; Moses, P. G.; Hinnemann, B.; Topsøe, N.-Y.; Knudsen, K. G.; Topsøe, H.; Nørskov, J. K., A density functional study of inhibition of the HDS hydrogenation pathway by pyridine, benzene, and H₂S on MoS₂-based catalysts. *Catalysis Today* **2006**, *111* (1-2), 44-51.
88. Lee, R.; Zhang, M.; Ng, F., Hydrodenitrogenation of Quinoline Over a Dispersed Molybdenum Catalyst Using in situ Hydrogen. *Topics in Catalysis* **2006**, *37* (2), 121-127.
89. M, J., R. Prins, Mechanism of the hydrodenitrogenation of quinoline over NiMo(P)/Al₂O₃ catalysts. *J. Catalysis* **1998**, *179*, 10.
90. Nagai, M.; Goto, Y.; Miyata, A.; Kiyoshi, M.; Hada, K.; Oshikawa, K.; Omi, S., Temperature-Programmed Reduction and XRD Studies of Ammonia-Treated Molybdenum Oxide and Its Activity for Carbazole Hydrodenitrogenation. *Journal of Catalysis* **1999**, *182* (2), 292-301.
91. Yamamoto, M.; Nishimura, O.; Kotanigawa, T., Heteroatom removals from aromatic hydrocarbons over a phosphoric acid-promoted Mn₂O₃-NiO catalyst. *Applied Catalysis A: General* **1998**, *174* (1-2), 41-50.
92. Sánchez-Minero, F.; Ramírez, J.; Gutiérrez-Alejandre, A.; Fernández-Vargas, C.; Torres-Mancera, P.; Cuevas-García, R., Analysis of the HDS of 4,6-DMDBT in the presence of naphthalene and carbazole over NiMo/ Al₂O₃-SiO₂(x) catalysts. *Catalysis Today* **2008**, *133-135*, 267-276.
93. Wiwel, P.; Knudsen, K.; Zeuthen, P.; Whitehurst, D., Assessing Compositional Changes of Nitrogen Compounds during Hydrotreating of Typical Diesel Range Gas Oils Using a Novel Preconcentration Technique Coupled with Gas Chromatography and Atomic Emission Detection. *Industrial & Engineering Chemistry Research* **2000**, *39* (2), 533-540.
94. R. Prins, M. J., M. Flechsenhar, Mechanism and kinetics of hydrodenitrogenation. *Polyhedron* **1997**, *16* (18), 10.
95. Qader, S. A.; Hill, G. R., Catalytic Hydrocracking. Mechanism of Hydrocracking of Low Temperature Coal Tar. *Industrial & Engineering Chemistry Process Design and Development* **1969**, *8* (4), 456-461.
96. Ho, T. C.; Nguyen, D., Poisoning effect of ethylcarbazole on hydrodesulfurization of 4,6-diethyldibenzothiophene. *Journal of Catalysis* **2004**, *222* (2), 450-460.

97. Aboul-Gheit, A. K., Comparison of the hydrodenitrogenation of the petroleum model nitrogen compounds quinoline and indole. *Applied Catalysis* **1985**, *16* (1), 39-47.
98. Kozai, S.; Kabashima, H.; Hattori, H., Participation of acidic sites on catalyst in hydrodenitrogenation of quinoline. *Fuel* **2000**, *79* (3-4), 305-310.
99. Ho, T. C., Hydroprocessing catalysis on metal sulfides prepared from molecular complexes. *Catalysis Today* **2008**, *130* (1), 206-220.
100. Yang, S. H.; Satterfield, C. N., Catalytic hydrodenitrogenation of quinoline in a trickle-bed reactor. Effect of hydrogen sulfide. *Industrial & Engineering Chemistry Process Design and Development* **2002**, *23* (1), 20-25.
101. Jian, M.; Prins, R., Existence of different catalytic sites in HDN catalysts. *Catalysis Today* **1996**, *30* (1-3), 127-134.
102. Nagai, M.; Masunaga, T.; Hana-oka, N., Selectivity of molybdenum catalyst in hydrodenitrogenation, hydrodesulfurization and hydrodeoxygenation: Effects of sulfur and oxygen compounds on acridine hydrodenitrogenation. *Journal of Catalysis* **1986**, *101* (2), 284-292.
103. Xiang, C.; Chai, Y.-m.; Liu, Y.; Liu, C., Mutual influences of hydrodesulfurization of dibenzothiophene and hydrodenitrogenation of indole over NiMoS/γ-Al₂O₃ catalyst. *Journal of Fuel Chemistry and Technology* **2008**, *36* (6), 684-690.

APPENDIX A --- Mass Balance Sample Calculations

A1. Concentrations of reactants (listed in Table 3-2)

- **Weights:**

$$W_{DBT} = 0.42g, W_{4,6DMDBT} = 0.50,$$

$$W_{toluene} = d_{toluene} \times V_{toluene} = \frac{0.8669g}{ml} \times 100ml = 86.69g$$

- **Concentrations of model compounds:**

$$C_{DBT} = \frac{n_{DBT, mol}}{V_{Org.Phase, l}} = \frac{W_{DBT, g}}{M_{DBT, \frac{g}{mol}}} \times \frac{1}{V_{Org.Phase, l}} = \frac{0.42 \times 98\%, g}{184.26 g/mol} \times \frac{1}{0.1 l} = 0.022 mol/l$$

$$C_{4,6DMDBT} = \frac{n_{4,6DMDBT, mol}}{V_{Org.Phase, l}} = \frac{W_{4,6DMDBT, g}}{M_{4,6DMDBT, \frac{g}{mol}}} \times \frac{1}{V_{Org.Phase, l}} = \frac{0.50 \times 97\%, g}{212.31 g/mol} \times \frac{1}{0.1 l} \\ = 0.023 mol/l$$

- **Concentrations of S:**

$$C_S, \frac{mol}{l} = C_{DBT} + C_{4,6DMDBT}, \frac{mol}{l} = 0.022 + 0.023, \frac{mol}{l} = 0.045, \frac{mol}{l}$$

$$n_S, mol = C_S, mol/l \times V_{Org.phase, l} = 0.045 \times 0.1, mol = 0.0045 mol = 4.5 mmol$$

$$C_S, ppmw = \frac{n_S, mol \times M_S, g/mol}{W_{Org.Phase}} = \frac{0.0045 mol \times 32.06 g/mol}{86.69 g + 0.42 g + 0.50 g} = 1647 ppmw$$

- **Concentration of Mo**

To obtain accurate concentration of Mo in the aqueous phase, a condensed PMA aqueous solution was prepared and the exact concentration of Mo was detected by ICP.

Preparation of PMA aqueous solution: dissolved 3.3506g PMA in 100 ml DI water.

Calculated Mo concentration in the PMA aqueous solution:

$$W_{Mo, g} = \frac{W_{PMA, g}}{M_{PMA, g \cdot mol}} \times 12 \times M_{Mo, \frac{g}{mol}} = \frac{3.3506 g}{1825.24, g/mol} \times 12 \times 95.94, \frac{g}{mol} = 2.11 g$$

$$C_{Mo, ppmw} = \frac{W_{Mo, g}}{W_{aqu. solution, g}} = \frac{2.11, g}{(100 + 3.35), g} = 2.05 wt\% = 20500 ppmw$$

Mo concentration in the PMA aqueous solution quantified by ICP is **15553** ppmw.

The difference between the calculated and the quantified concentrations may be due to the presence of crystal water combined to PMA molecules. Therefore, it is necessary to quantify the concentration of Mo in the aqueous precursor solution. The ICP number will be used in further calculations.

In a typical experiment, 2.42ml of PMA aqueous solution was taken. So there was about

$$\begin{aligned} n_{Mo, mol} &= \frac{C_{Mo, ppmw} \times W_{PMA solution, g}}{M_{Mo, g/mol}} = \frac{15553 ppmw \times 2.42 g \times 10^{-6}}{95.94, g/mol} \\ &= 0.0004 mol = 0.4 mmol \end{aligned}$$

Concentration of Mo based on the weight of model sulfur compounds solution:

$$C_{Mo, ppmw} = \frac{W_{Mo, g}}{W_{Org.Phase, g}} \times 10^6 = \frac{15553 \times 2.42 \times 10^{-6}}{86.69 g + 0.42 g + 0.50 g} \times 10^6 \approx 430 ppmw$$

- **Ratio between S and Mo, S:Mo**

S here refers to the sulfur present in S-containing model compounds.

$$S:Mo, \frac{mol}{mol} = n_{S, mol} : n_{Mo, mol} = 0.0045 mol : 0.0004 mol = 11.5 \left(\frac{mol}{mol} \right)$$

- **Mol of CO/H₂S charged into the reactor**

The Ideal Gas Law is used to estimate the mass of gases charged or collected based on pressure, temperature and volume. At the beginning of the reaction, 590 psi CO and 10 psi H₂S were charged into the reactor at room temperature (25°C). The working volume of the SS reactor vessel is 249 ml.

$$n_{CO} = \frac{p_{CO} \times (V_{working} - V_{liquie})}{R \times T} = \frac{590 \text{ psi} \times 6.895 \text{ kPa} \times (249 - 100 - 10) \text{ ml}}{298.2 \text{ K} \times 8.314 \text{ kPa} \cdot \text{L} \times 1000 \text{ ml/l}} = 0.228 \text{ mol}$$

$$n_{H_2S} = \frac{p_{H_2S} \times (V_{working} - V_{liquie})}{R \times T} = \frac{10 \text{ psi} \times 6.895 \text{ kPa} \times (249 - 100 - 10) \text{ ml}}{298.2 \text{ K} \times 8.314 \text{ kPa} \cdot \text{l} \times 1000 \text{ ml/l}} = 0.004 \text{ mol}$$

$$H_2S:Mo, \frac{mol}{mol} = n_{H_2S, mol} : n_{Mo, mol} = 0.004 mol : 0.0004 mol = 10 \left(\frac{mol}{mol} \right)$$

The working volume of the HC reactor vessel is 300 ml. The mass/volume of reactants and solvents are the same as experiments run in the SS reactor. Amounts of gas reactants in the two reactors are different due to different working volumes. So in an experiment processed in the HC reactor:

$$n_{CO} = \frac{p_{CO} \times (V_{working} - V_{liquie})}{R \times T} = \frac{590 \text{ psi} \times 6.895 \text{ kPa} \times (300 - 100 - 10) \text{ ml}}{298.2 \text{ K} \times 8.314 \text{ kPa} \cdot \text{L} \times 1000 \text{ ml/l}} = 0.312 \text{ mol}$$

$$n_{H_2S} = \frac{p_{H_2S} \times (V_{working} - V_{liquie})}{R \times T} = \frac{10 \text{ psi} \times 6.895 \text{ kPa} \times (300 - 100 - 10) \text{ ml}}{298.2 \text{ K} \times 8.314 \text{ kPa} \cdot \text{l} \times 1000 \text{ ml/l}} = 0.005 \text{ mol}$$

$$H_2S: M_o, \frac{\text{mol}}{\text{mol}} = n_{H_2S, \text{mol}} : n_{M_o, \text{mol}} = 0.005 \text{ mol} : 0.0004 \text{ mol} = 12.5 \left(\frac{\text{mol}}{\text{mol}} \right)$$

A2. Mass balance of the gas phase (involved in a CO experiment)

In an experiment using in situ hydrogen for hydro-treating reactions, CO and H₂S are charged into the reaction system at the ratio of 59:1 at the total pressure of 600 psi at room temperature. Mol amounts of charged CO and H₂S have been given in the last section, A1. In this section, gas data of the experiment DM-65 will be used for the calculation example.

Reaction conditions for the experiment DM-65 are:

0.50g 4,6-DMDBT, 0.42g DBT, 590 psi CO, 10 psi H₂S, 380°C, 1hr, 900 rpm, SS reactor.

After the reaction, the reactor cooled down to room temperature. The gas phase was transferred and collected in a 30L gas sampling bag. The Perkin Elmer 8500 GC equipped with a TCD was used for analysis. The GC data of WGS gas components are:

Table A - 1 Composition of WGS gases in the final gas sample in the experiment DM-65 (590 psi CO, 10 psi H₂S, 380°C, 1hr)

Gas component	H ₂	CO ₂	CO	H ₂ S
GC Area	3.3991	191.8455	95.6387	1.467
Response factor	9.996	0.18	0.21	0.16
Normalized mol%	38.3	38.9	22.6	0.3
n, mol	0.107	0.109	0.063	0.001

Normalized mol percent of each WGS gas component was calculated according to the following equation:

$$M_j, \text{mol}\% = \frac{\text{Area}_j \times RF_j}{\sum_i (\text{Area}_i \times RF_i)}$$

For example:

$$\sum_i (\text{Area}_i \times RF_i) = 3.3991 \times 9.996 + 191.8455 \times 0.18 + 95.6387 \times 0.21 + 1.467 \times 0.3 = 88.8$$

$$M_{H_2}, \text{mol}\% = \frac{\text{Area}_{H_2} \times RF_{H_2}}{\sum_i (\text{Area}_i \times RF_i)} = \frac{3.3991 \times 9.996}{88.8} = 38.3 \text{ mol}\%$$

Total mol amount of final gases is estimated based on the final pressure and temperature according to the Ideal Gas Law.

$$P = 686 \text{ psi}, T = 25^\circ\text{C} = 298.15\text{K}, V_{org.} = 97 \text{ ml}, V_{aqu.} = 5 \text{ ml}$$

So, total mol of final gases:

$$n_{total}, \text{mol} = \frac{PV_{gas}}{RT} = \frac{686 \text{ psi} \times 6.895 \text{ kPa} \times (249 - 97 - 5) \text{ ml}}{298.2 \text{ K} \times 8.314 \text{ kPa} \cdot \text{L} \times 1000 \text{ ml/l}} = 0.280 \text{ mol}$$

Mol of each WGS gas component:

$$n_i, \text{mol} = M_i, \text{mol}\% \times n_{total}, \text{mol}$$

For example:

$$n_{H_2}, \text{mol} = M_{H_2}, \text{mol}\% \times n_{total}, \text{mol} = 38.3 \text{ mol}\% \times 0.280 \text{ mol} = 0.107 \text{ mol}$$

Reacted amount of CO:

$$n_{CO}^{reacted}, mol = n_{CO}^{charged} - n_{CO}^{collected} = 0.228 - 0.063 mol = 0.165 mol$$

Conversion of CO *via* the WGS reaction:

$$Conversion\ of\ CO, \% = \frac{(n_{CO}^{charged} - n_{CO}^{collected})}{n_{CO}^{charged}} \times 100\% = \frac{0.228 - 0.063}{0.228} \times 100\% = 72.4\%$$

A3. Mass balance of *in situ* H₂

In the experiment DM-65, *in situ* H₂ was generated from CO and H₂O and on the other hand, it was consumed in HDS of DBT and 4,6-DMDBT. Therefore, the concentration of *in situ* H₂ detected by GC was found to be lower than that of CO₂ as listed in Table A-1. The amount of consumed hydrogen in HDS reactions could be calculated from concentrations of HDS products of the two model-containing compounds, as shown in Table A-2.

Table A - 2 Concentrations of HDS products and the amount of consumed hydrogen in the experiment DM-65 (590 psi CO, 10 psi H₂S, 380°C, 1hr)

Component	Mol%	Mol*	Mol of H ₂ required to get 1 mol HDS product	Mol of consumed H ₂ , mol
DBT	37.32%	0.000821	0	0
TH-DBT	3.99%	8.78E-05	2	0.000176
DCH	1.16%	2.56E-05	7	0.000179
CHB	25.71%	0.000566	4	0.002263
BP	31.82%	0.0007	2	0.0014
4,6-DMDBT	43.0%	0.00099	0	0
Iso-DMDBT	5.3%	0.000121	0	0
HH-DMDBT	3.3%	7.65E-05	3	0.00023
TH-DMDBT	5.1%	0.000116	2	0.000233
DMBPs	15.1%	0.000347	2	0.000694
DMCHBs	28.2%	0.000649	4	0.002597
Sum=				0.0081

Mol of hydrogen collected after the reaction is 0.107 (Table A-1). Adding the amount of consumed hydrogen: 0.0081 mol, the amount of hydrogen would be 0.115 mol. According to the stoichiometry of the WGS reaction, mol of *in situ* H₂ or CO₂ generated from CO should be the same as mol of consumed CO. So there should be 0.165 mol H₂ and 0.165 mol CO₂. So the recovery of *in situ* hydrogen is:

$$\text{Recovery of in situ } H_2 = \frac{0.115}{0.165} \times 100\% = 69.7\%$$

The low recovery of *in-situ* hydrogen was due to the hydrogenation of the solvent, toluene.

A4. Mass balance of the aqueous phase

In the experiment DM-65, 10 ml of DI water added at the beginning of the reaction.

Water consumed at the CO conversion of 72.4%:

$$n_{H_2O} = n_{CO}^{charged} - n_{CO}^{collected} = 0.228 - 0.063 \text{ mol} = 0.165 \text{ mol}$$

Volume of consumed 0.165mol DI water is:

$$V_{H_2O}, ml = \frac{n_{H_2O} \times M_{H_2O}, g/mol}{d_{H_2O}} = 2.97 \text{ ml} \approx 3 \text{ ml}$$

So, there should be about 7 ml of water left after the reaction. Actually, 5 ml of aqueous phase was collected at the end. The recovery of the aqueous phase is 71.4%. The loss of water may be due to its evaporation and its adsorption on the catalyst surface.

A5. Mass balance of the organic phase

Mass balance of the organic phase is calculated based on the volume of the solvent. The presence of model compounds and their hydro-treating products does not affect the volume of the organic phase significantly.

In the experiment DM-65, 96 ml of organic phase was collected from the reactor vessel after the reaction. About one more ml of liquid product came out with the final gas sample. So:

Volume of the organic phase before reaction	100 ml
Volume of the organic phase collected from the reactor vessel after reaction	96 ml
Volume of organic liquid product coming out with the final gas sample	1 ml
Recovery	97 %

APPENDIX B --- GC Analytic Methods

B-1 Liquid Sample Analysis – GC method

The liquid products of HDS of DBT and 4,6-DMDBT were analyzed by GC-FID, TCD, and PFPD (Varian CP-3800) equipped with a VF-05MS capillary column ($30m \times 0.30mm \times 1.0\mu m$). Ultra high purity helium is used as the carrier gas.

B-1.1 Control method:

Injector: Middle (1177 split/splitless)

Split event talbe	Time, min Initial	Split state On	Split ratio 15
-------------------	----------------------	-------------------	-------------------

Heater: ON; Set point: 250°C; Stabilization time: 0.50 min

Column oven zone:

Temperature program:

Rate, °C/min	Step, °C	Time, min
Initial	80	0.00
5.0	120	0.00
2.0	170	0.00
10.0	240	5.00
	Total time	45.00

Column:

Carrier gas	He
Length	30.00 m
Inside diameter	320 um
Constant flow	Enabled
Column flow	6.0 ml/l
Pressure pulse	Disabled

Detectors:

• **Front (FID)**

He makeup flow	H ₂ flow	Air flow
28 ml/min	30 ml/min	300 ml/min

FID event table:

Time, min	Range	Autozero
Initial	12	Yes

Heater: ON; Set point: 300°C

• **Middle (TSD)**

He makeup flow	H ₂ flow	Air flow
10 ml/min	0 ml/min	0 ml/min

Bead current: 3.300 A

TSD event table:

Time, min	Range	Autozero	Bead power
Initial	12	Yes	ON

Heater: ON; Set point: 300°C

• **Rear (PFPD)**

Air 1 flow	H ₂ flow	Air flow
17 ml/min	13 ml/min	10 ml/min

Bead current: 3.300 A

Square root mode	OFF
Trigger level	200 mV
Tube voltage	550 V
Sampling delay	6.0 ms
Sampling width	20.0 ms
Use gain factor	Yes
Gain factor	2

PFPD event table:

	Time, min	Range	Autozero
	Initial	10	Yes

Heater: ON; Set point: 300°C

B-1.2 Integration event

Active	Time	Event	On	Value
Yes	0.00	Set peak width		0.1
Yes	0.00	Set threshold		0.1
Yes	0.00	Turn integration	Off	
Yes	2.80	Turn integration	On	

B-1.3 Calibration Method

Method type: External Standard

Response: Area (for FID), Square root of Height (for PFPD)

Standard Unit: ppm-comp.

Calibration curves of calibrated starting materials were shown in Fig. B-1.

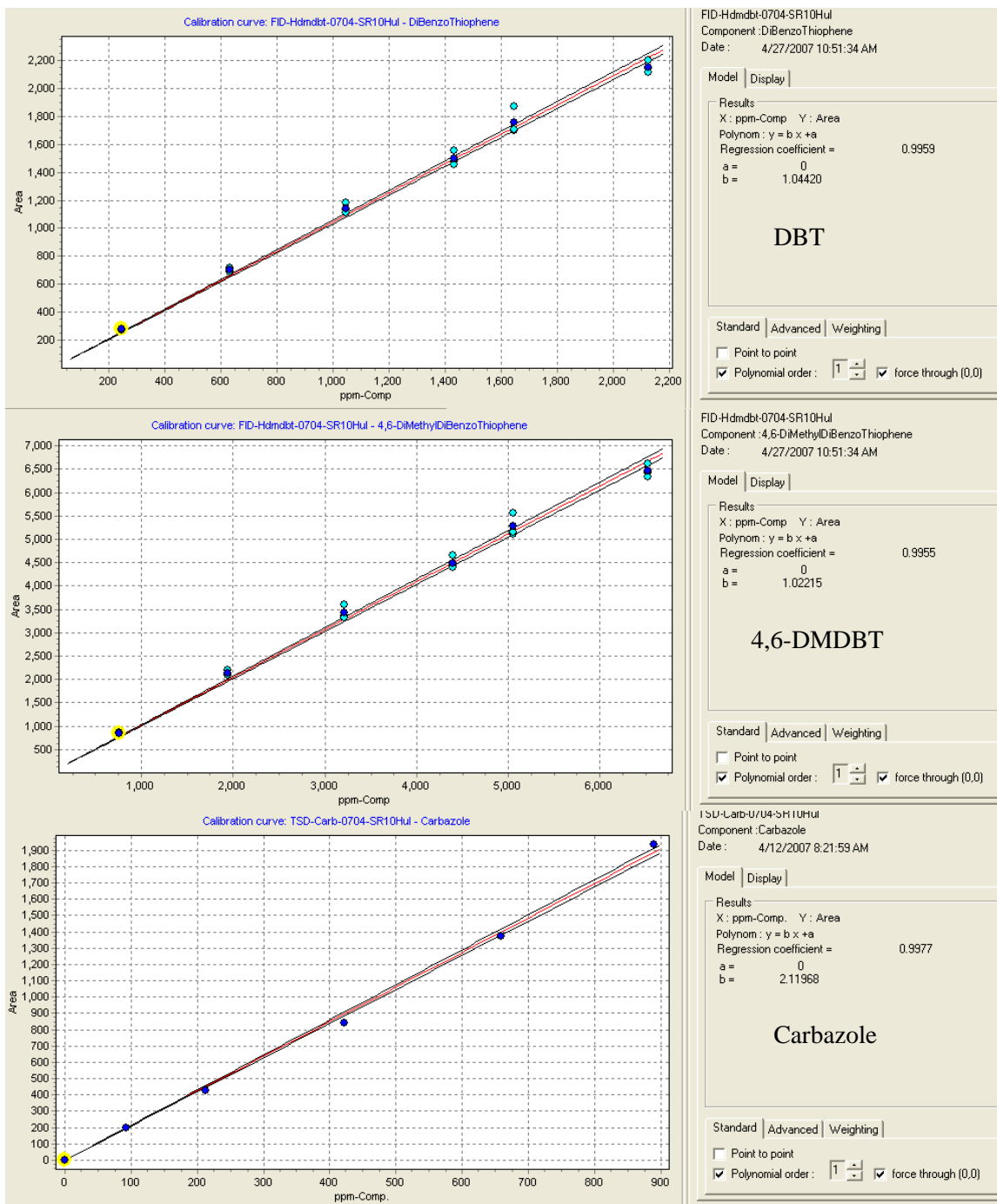


Fig. B - 1 GC calibration curves of starting reactants, DBT, 4,6-DMDBT, and carbazole.

B-2 GC Calculation Processes

- **Calculation of product component concentrations in liquid product samples:**

1. Concentration of starting reagents (DBT, 4,6-DMDBT, quinoline, or carbazole) in the feedstock:

$$C_j^{inFeed}, ppmw \cdot mol \cdot g^{-1} = \frac{R_j^{inFeed}, ppmw}{MW_R, g \cdot mol^{-1}}$$

2. Concentration of HDS products and starting reagents in liquid product samples:

$$C_i, ppmw = \frac{Area^{GC}}{Rf_i}, \text{ Rf: Response factor}$$

$$C_i, ppmw \cdot mol \cdot g^{-1} = \frac{C_i, ppmw}{MW_i, g \cdot mol^{-1}}$$

3. Normalized concentration of the component i based on the composition:

$$C_i, mol\% = \frac{C_i, ppmw \cdot mol \cdot g^{-1}}{\sum_i C_i, ppmw \cdot mol \cdot g^{-1}} \times 100 mol\%$$

- **Conversion of starting reagents:**

$$Conv_j = \left(1 - \frac{C_j^{inProd}, ppmw \cdot mol \cdot g^{-1}}{C_j^{inFeed}, ppmw \cdot mol \cdot g^{-1}} \right) \times 100 mol\% \quad \text{---applied in the}$$

calculation of the conversion of 4,6-DMDBT

Or

$Conv_j = 1 - \sum_{i(i \neq j)} C_i, mol\%$ ---applied in the calculation of conversions of DBT, quinoline and carbazole

- **S-removal or N-removal of starting reagents:**

$$S - removal_j, mol\% = 1 - \sum_{i(j'sHDSprod)} C_i^{S-removed}, mol\%$$

$$N - removal_j, mol\% = 1 - \sum_{i(j'sHDNprod)} C_i^{N-removed}, mol\%$$

- **Selectivity between HDS reaction pathways**

In the HDS of DBT:

DDS product --- BP

HYDD products --- DCH and CHB

HYD products --- TH-DBT and HYDD products

In the HDS of 4,6-DMDBT:

DDS products --- 3,3'-DMBP and its isomers

HYDD products --- DMCHB and its isomers

HYD products --- DM-TH-DBT (and its isomers), DM-HH-DBT (and its isomers), and HYDD products

So the selectivity between reactions pathways can be obtained *via* following equations:

$$\frac{DDS}{HYDD_j}, molar = \frac{\sum_{i \neq j} C_i^{j'sDDS-prod}, ppmw \cdot mol \cdot g^{-1}}{\sum_{i \neq j} C_i^{j'sHYDD-prod}, ppmw \cdot mol \cdot g^{-1}}$$

B-3 RGA Analytic Method

B-3.1 Configuration of the RGA

3000 GC Configuration	A	B	C	D
Injector Type	Backflush	Backflush	Backflush	Backflush
Carrier Gas	Argon	Helium	Helium	Helium
Column Type	Molecular Sieve	Plot U	Alumina	OV-1
Detector Type	TCD	TCD	TCD	TCD
Inlet Type	Heated	Heated	Heated	Heated

RGA set points:

3000 GC Configuration	A	B	C	D
Sample Inlet Temp., °C	100 [ON]	100 [ON]	100 [ON]	100 [ON]
Inlet Temp., °C	100 [ON]	100 [ON]	100 [ON]	100 [ON]
Column Temp., °C	110 [ON]	100 [ON]	140 [ON]	90 [ON]
Sampling Time, S	30 [ON]	30 [ON]	30 [ON]	30 [ON]
Inject Time, ms	20	20	20	20
Run Time, s	240	240	240	240
Post Run Time, s	10	10	10	10
Pressure Equilibration Time, s	10	10	10	10
Column Pressure, psi	40.00 [ON]	36.00 [ON]	40.00 [ON]	36.00 [ON]
Post Run Pressure, psi	40.00 [ON]	36.00 [ON]	40.00 [ON]	36.00 [ON]
Detector Filament	Enabled	Enabled	Enabled	Enabled
Detector Sensitivity	Standard	Standard	Standard	Standard
Detector Data Rate, Hz	50	50	50	50
Baseline Offset, mV	0	0	0	0
Backflush Time, s	11.0	6.5	8.0	N/A

Integrator settings and times events:

- Signal 1

Initial Setting	Value
Slope Sensitivity	2000,000
Peak Width	0.020
Area Reject	1.000
Height Reject	1.000
Shoulders	OFF
Advanced Baseline	OFF

Time	Event	Value
0.000	Integration	OFF
0.500	Integration	ON
1.350	Slope Sensitivity	1000,000

- Signal 2

Initial Setting	Value
Slope Sensitivity	10000,000
Peak Width	0.020
Area Reject	1.000
Height Reject	1.000
Shoulders	OFF
Advanced Baseline	OFF

Time	Event	Value
0.000	Integration	OFF
0.500	Baseline Now	
0.260	Integration	ON

- Signal 3

Initial Setting	Value
Slope Sensitivity	5000,000
Peak Width	0.040
Area Reject	1.000
Height Reject	1.000
Shoulders	OFF
Advanced Baseline	OFF

Time	Event	Value
0.000	Integration	OFF
0.480	Integration	ON
2.200	Slope Sensitivity	1000,000

- Signal 4

Initial Setting	Value
Slope Sensitivity	5000,000
Peak Width	0.040
Area Reject	1.000
Height Reject	1.000
Shoulders	OFF
Advanced Baseline	OFF

Time	Event	Value
0.000	Integration	OFF
0.420	Integration	ON
0.460	Integration	OFF
0.800	Integration	ON

Calibration Table:

Retention Time [min]	Sig	Lvl	Amount	Area	Amt/Area	Ref	Multiplier	Peak Name
0.000	2	1	1.00000	1.00000	1.00000e+000		1.00000	Peak32
0.347	2	1	2.99000	4.1296e+004	7.24041e-005		1.00000	CO2
0.409	2	1	2.00000	2.8415e+004	7.03854e-005		1.00000	C2H4
0.440	4	1	0.29900	1.2195e+004	2.45182e-005		1.00000	i-C4
0.449	2	1	3.99000	6.0647e+004	6.57906e-005		1.00000	C2H6
0.523	3	1	1.00000	1.0960e+004	9.12409e-005		1.00000	Propylene
0.548	2	1	1.00000	1.1746e+004	8.51354e-005		1.00000	C2H2
0.652	3	1	2.01000	1.9693e+004	1.02067e-004		1.00000	C3
0.665	1	1	12.10000	1.1501e+005	1.05208e-004		1.00000	Hydrogen
0.689	3	1	0.29900	3907.00000	7.65293e-005		1.00000	NC4
0.698	2	1	2.53000	3.2878e+004	7.69512e-005		1.00000	H2S
0.763	1	1	20.86000	1.9621e+004	1.06315e-003		1.00000	Oxygen
0.864	1	1	78.47200	6.2608e+004	1.25339e-003		1.00000	Nitrogen
0.872	2	1	5.02000	8.1948e+004	6.12584e-005		1.00000	COS
0.939	3	1	0.30000	3698.00000	8.11249e-005		1.00000	t-2 C4=
0.990	3	1	0.29900	3677.00000	8.13163e-005		1.00000	i-C4=
1.052	3	1	0.29900	3600.00000	8.30556e-005		1.00000	1-C4=
1.064	1	1	5.00000	9981.24000	5.00940e-004		1.00000	CH4
1.092	4	1	0.04990	2446.82000	2.03938e-005		1.00000	n-C6
1.126	3	1	0.29900	3603.00000	8.29864e-005		1.00000	c-2-C4=
1.218	2	1	0.96800	5.2089e+004	1.85836e-005		1.00000	1-2 prop=
1.289	1	1	1.02000	818.26000	1.24655e-003		1.00000	CO
1.399	3	1	0.10000	1326.91000	7.53631e-005		1.00000	i-C5
1.525	3	1	0.09980	1330.78900	7.49931e-005		1.00000	n-C5
1.684	3	1	0.30000	3000.50300	9.99832e-005		1.00000	1-3 butadiene
1.895	2	1	0.66800	1.2391e+004	5.39101e-005		1.00000	Water
2.064	2	1	0.98800	8573.95000	1.15233e-004		1.00000	MetyAcetylene
2.203	3	1	0.09970	1319.95000	7.55332e-005		1.00000	t-2-C5=
2.406	3	1	0.04850	623.18000	7.78266e-005		1.00000	2-meth-2-C4=
2.532	3	1	0.09990	1286.44000	7.76562e-005		1.00000	1-C5=
2.775	3	1	0.09500	1230.04000	7.72333e-005		1.00000	c-2-C5=
3.726	4	1	0.04990	2149.26200	2.32173e-005		1.00000	n-C8

B-4 Calculation of gas component concentrations based on GC analytic results

Interested WGS gases include CO, CO₂, H₂, H₂S, and COS. The concentration of each component is calculated according to the following equation:

$$C_{i, mol\%} = \frac{Area_i^{GC} \times Rf_i}{\sum_j Area_j^{GC} \times Rf_j}, mol\%$$

B-5 Compare of calculation methods for conversions

Method 1:

$$\text{Conversion of DBT} = 100\% - \frac{A_{DBT}^P}{A_{DBT}^F} \times 100\%$$

Where: A_{DBT}^P --- percentage area of the GC peak for DBT in product;

A_{DBT}^F --- percentage area of the GC peak for DBT in feed.

$$\text{Conversion of DMDBT} = 100\% - \frac{A_{DMDBT}^P}{A_{DMDBT}^F} \times 100\%$$

Where: A_{DMDBT}^P --- percentage area of the GC peak for DMDBT in product;

A_{DMDBT}^F --- percentage area of the GC peak for DMDBT in feed.

Method 2:

$$\text{Conversion of DBT} = \frac{(4H - DBT),\% + BP,\% + (CHB + DCH),\%}{DBT,\% + (4H - DBT),\% + BP,\% + (CHB + DCH),\%} * 100\%$$

Method 3:

$$\text{Conversion of DBT} = 100\% - \frac{S - DBT(\text{left-in-prod.}), \text{ppm}}{S - DBT(\text{added-in-feed}), \text{ppm}} \times 100\%$$

$$S - DBT(\text{left-in-prod.}), \text{ppm} = 0.0007 \times A_{GC-DBT}$$

$$S - DBT(\text{added-in-feed}), \text{ppm} = \frac{32.06 \times \frac{W_{DBT} \times 98\%}{184.26}}{W_{FEED}} \times 10^6$$

$$\text{Conversion of DMDBT} = 100\% - \frac{S - DMDBT(\text{left-in-prod.}), \text{ppm}}{S - DMDBT(\text{added-in-feed}), \text{ppm}} \times 100\%$$

$$S - DMDBT(\text{left-in-prod.}), \text{ppm} = 0.0006 \times A_{GC-DMDBT} - 3.4344$$

$$S - DMDBT(\text{added-in-feed}), \text{ppm} = \frac{32.06 \times \frac{W_{DMDBT} \times 97\%}{212.32}}{W_{FEED}} \times 10^6$$

Comparison:

Pooled standard deviation, $s_p=0.6595$ (degree of freedom = 3)

$$T_{CRITICAL} = T_{0.025,3} = 3.18 \text{ and } T_{OBS} = \frac{|(\bar{X}_1 - \bar{X}_2) - H_0|}{s \sqrt{1/n_1 + 1/n_2}}$$

Hypothesis: There is not significant difference between the two compared calculation methods. $H_0 : \bar{X}_1 - \bar{X}_2 = 0, H_1 : \bar{X}_1 - \bar{X}_2 \neq 0$

Conclusion: If $T_{OBS} > T_{CRITICAL}$, then reject the hypothesis, which means that there is significant difference between the two compared calculation methods.

If $T_{OBS} < T_{CRITICAL}$, then accept the hypothesis and interested methods are not significantly different.

Method 1 vs Method 3

Example 1: DM-73

	Method 1	Method 3		Method 1	Method 3
Conv.of DBT	75.19	59.30	Conv.of DMDBT	71.20	51.00
	76.79	58.10		72.72	51.80
	AVE.=75.99	AVE.=58.70		AVE.=71.96	AVE.=51.40
	N ₁ =2	N ₂ =2		N ₁ =2	N ₂ =2
	$T_{OBS} = 26.22 > T_{CRITICAL} = 3.18$			$T_{OBS} = 31.17 > T_{CRITICAL} = 3.18$	
Conclusion	Method 1 and method 3 are significant different.				

Example 2: DM-74

	Method 1	Method 3		Method 1	Method 3
Conv.of DBT	93.70	96.60	Conv.of DMDBT	88.40	93.50
		97.00			92.60
	AVE.=93.70	AVE.=96.80		AVE.=88.40	AVE.=93.05
	N ₁ =1	N ₂ =2		N ₁ =1	N ₂ =2
	$T_{OBS} = 3.84 > T_{CRITICAL} = 3.18$			$T_{OBS} = 6.31 > T_{CRITICAL} = 3.18$	
Conclusion	Method 1 and method 3 are significant different.				

Method 2 vs Method 3

Example 1: DM-73

	Method 3	Method 2
Conv.of DBT	59.30	58.13
	58.10	57.26
	AVE.=58.70	AVE.=57.70
	N ₁ =2	N ₂ =2
	$T_{OBS} = 1.52 < T_{CRITICAL} = 3.18$	
Conclusion	Method 2 and method 3 are not significant different.	

	Method 3	Method 2
Conv.of DBT	96.60	96.52
	97.00	96.58
	AVE.=96.80	AVE.=96.55
	$N_1=2$	$N_2=2$
	$T_{OBS} = 1.52 < T_{CRITICAL} = 3.18$	
Conclusion	Method 2 and method 3 are not significant different.	

Conclusions:

Results calculated by method 1 are different from those by method 2 or 3, so the calculation method 1 should not be applied in the future.

APPENDIX C --- HREM Statistic Results and EDX Spectra

C-1. EDX spectra for MoCO340, MoH340, and SMOCO340

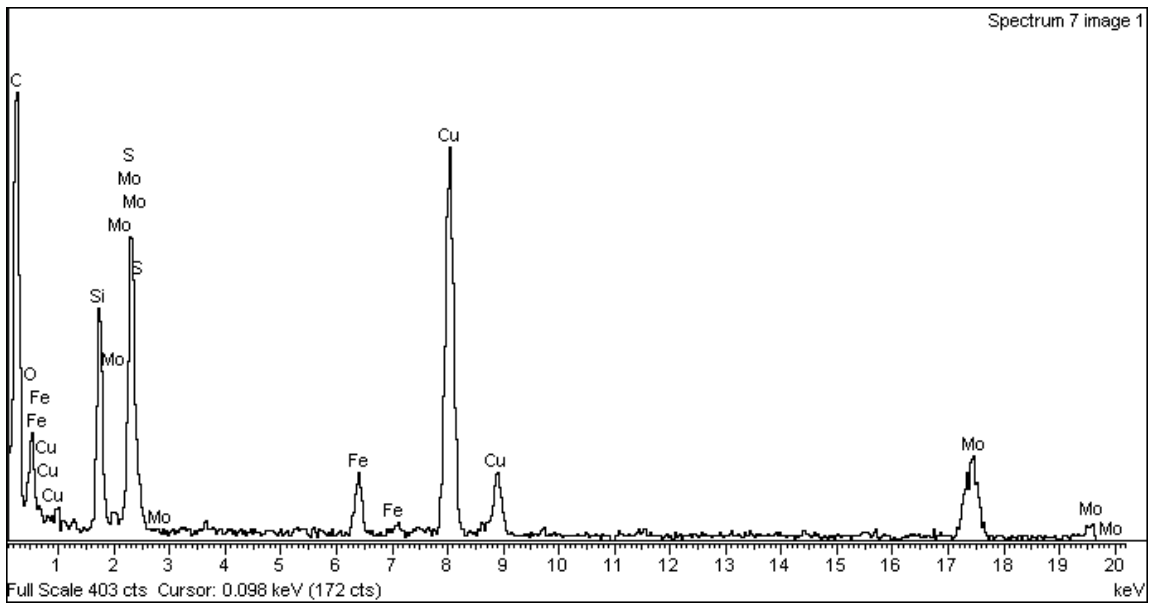


Fig. C - 1 EDX spectra of MoCO340-org

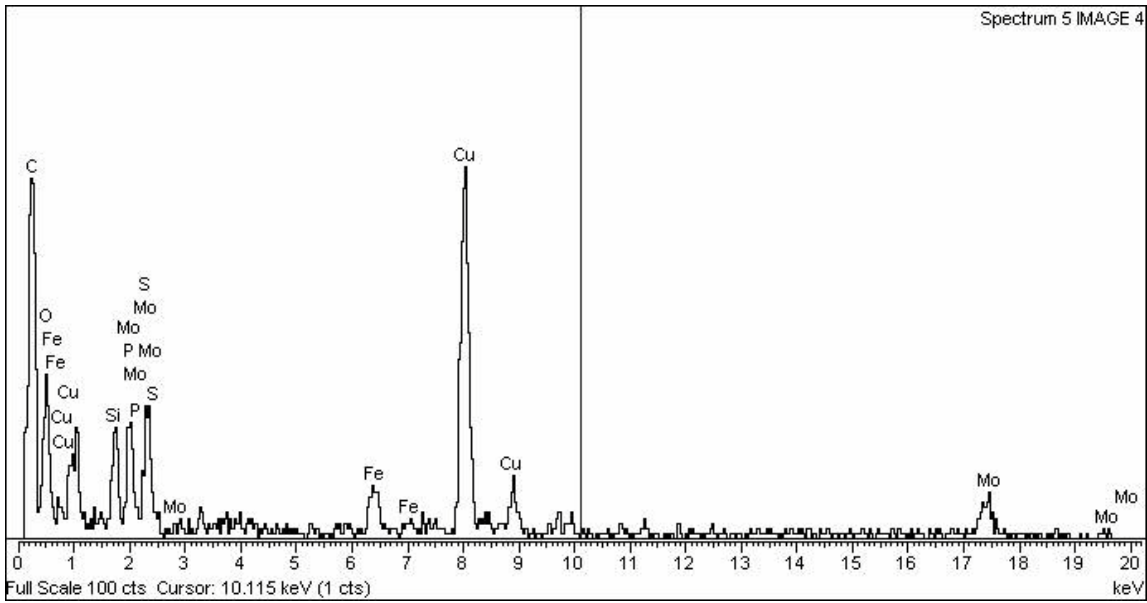


Fig. C - 2 EDX spectra of MoCO340-Baq

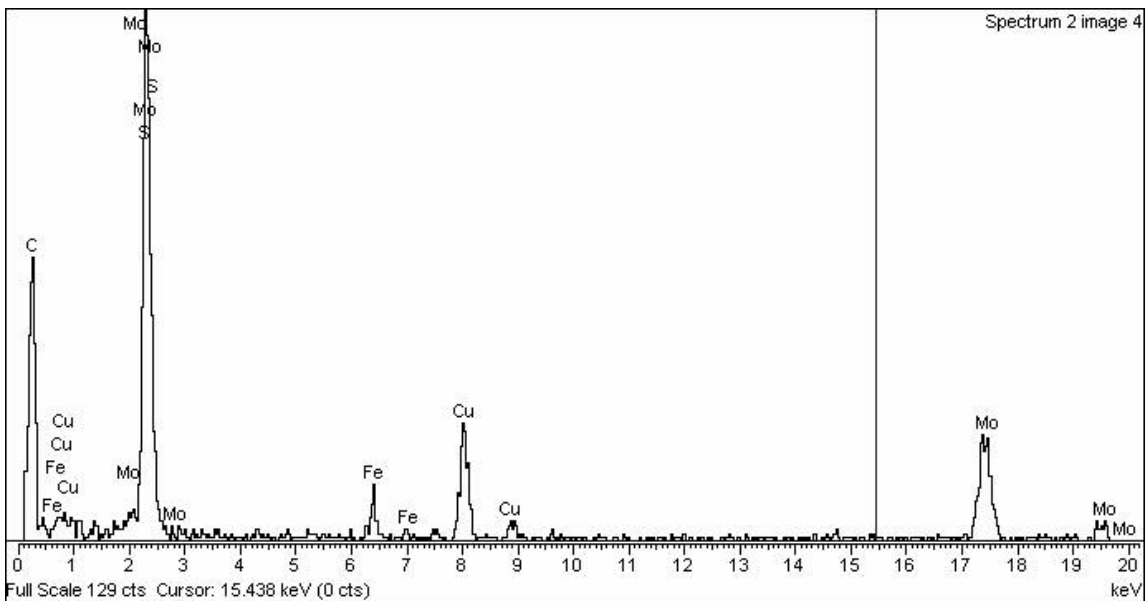


Fig. C - 3 EDX spectra of MoH340-org

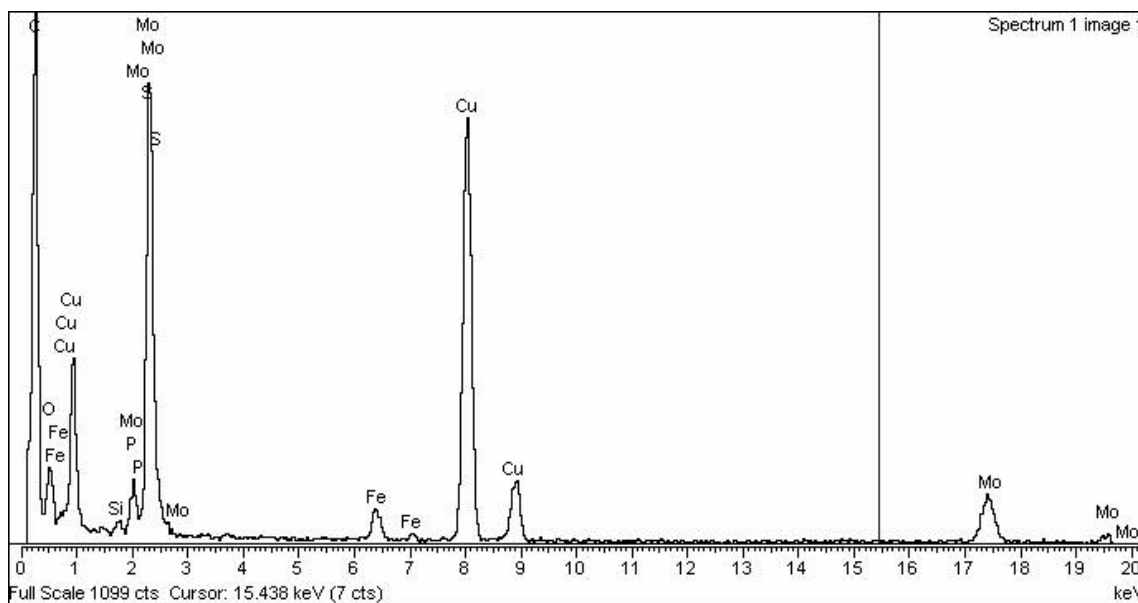


Fig. C - 4 EDX spectra of MoH340-Aqu

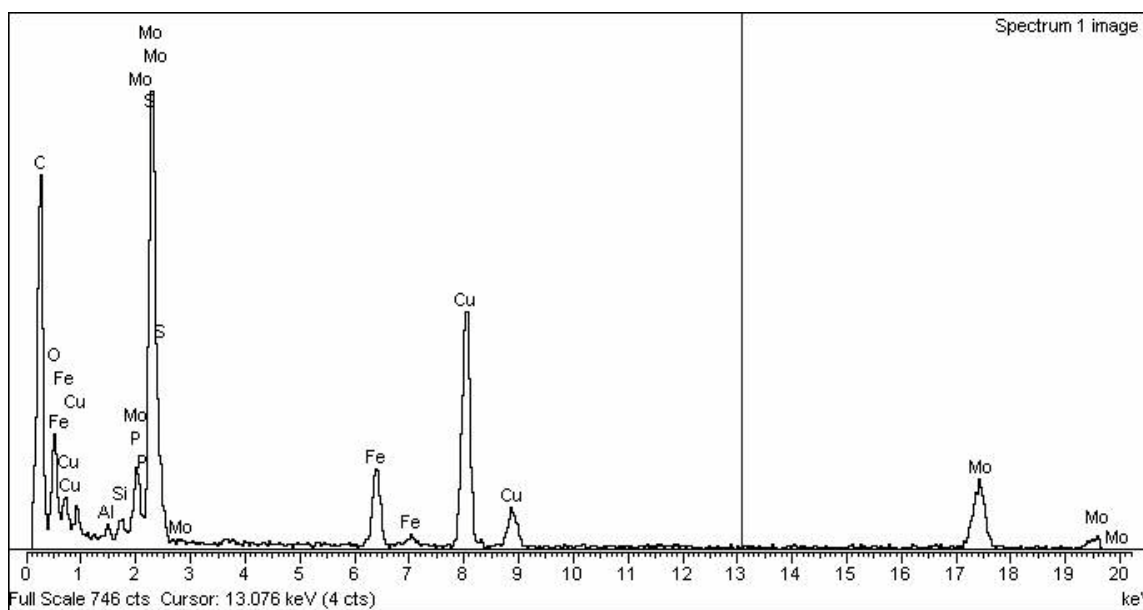


Fig. C - 5 EDX spectra of MoH340-Baq

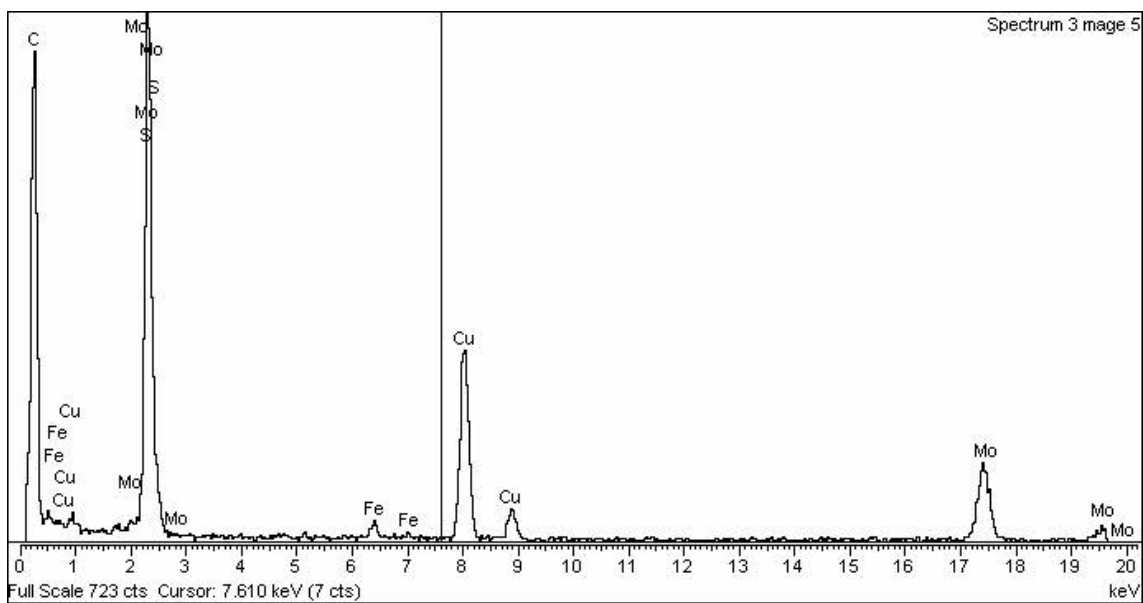


Fig. C - 6 EDX spectra of MoH340-O/W

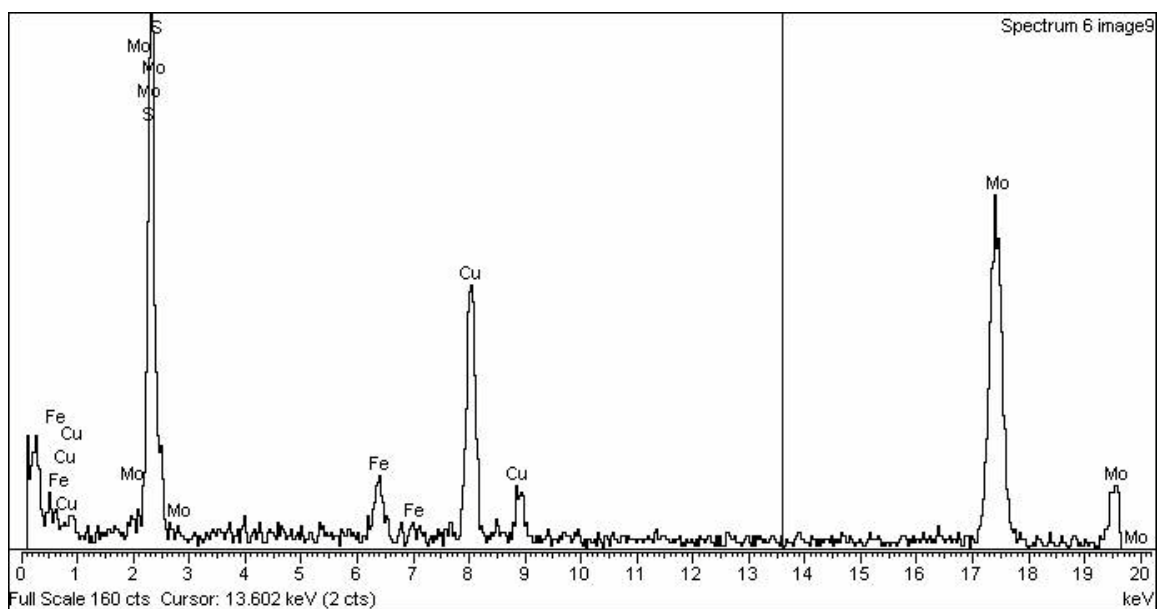


Fig. C - 7 EDX spectra of MoH340-Wcat

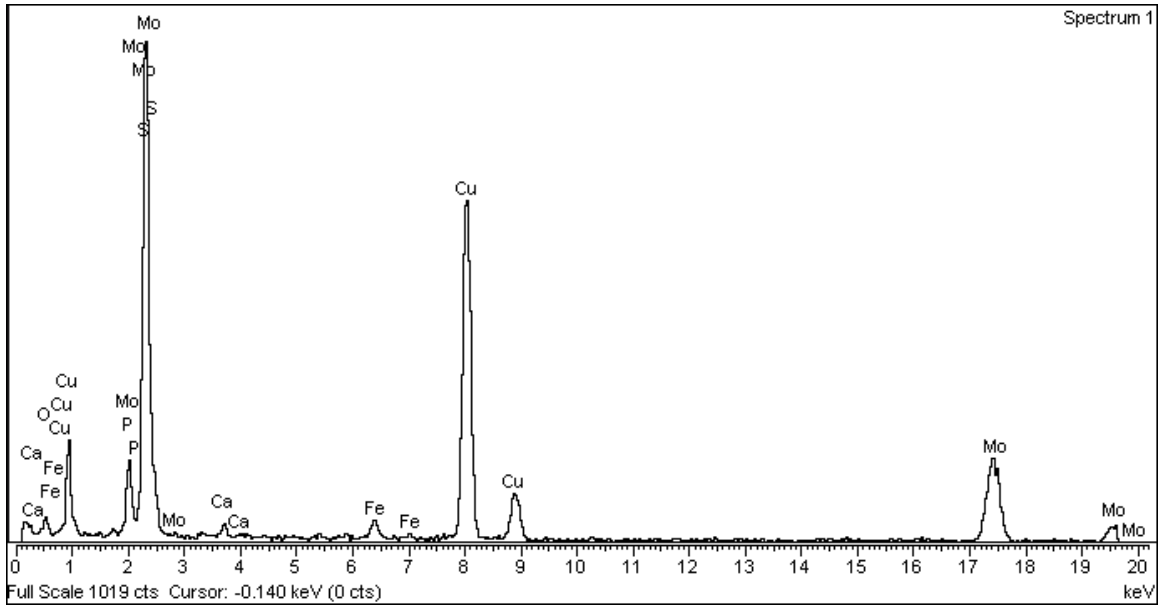


Fig. C - 8 EDX spectra of SMOCO340-O/W

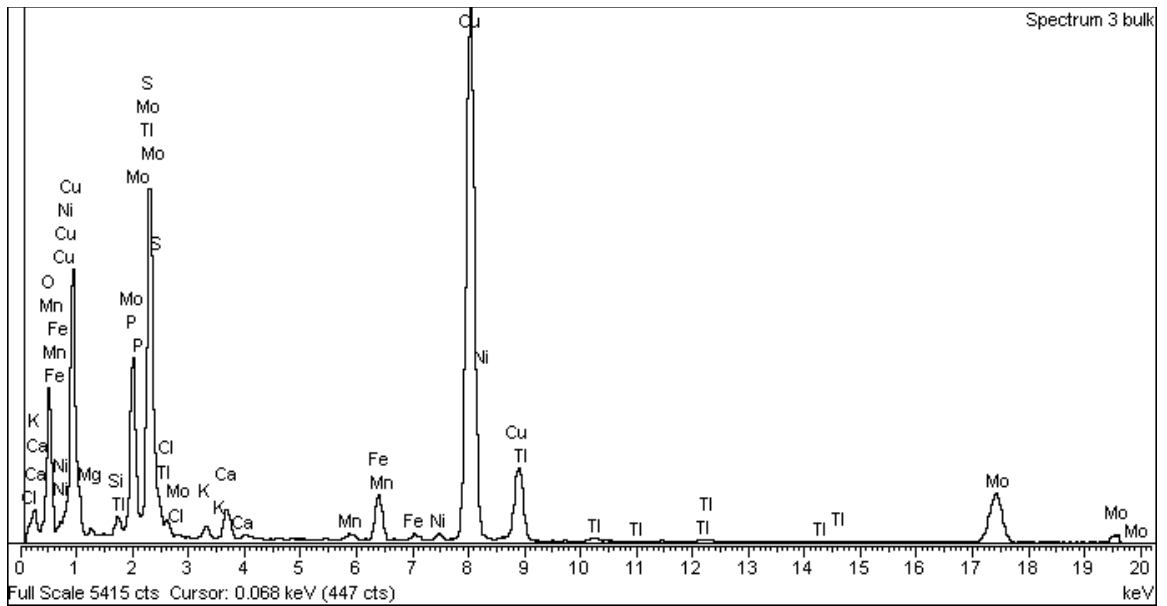


Fig. C - 9 EDX spectra of SMOCO340-Baq

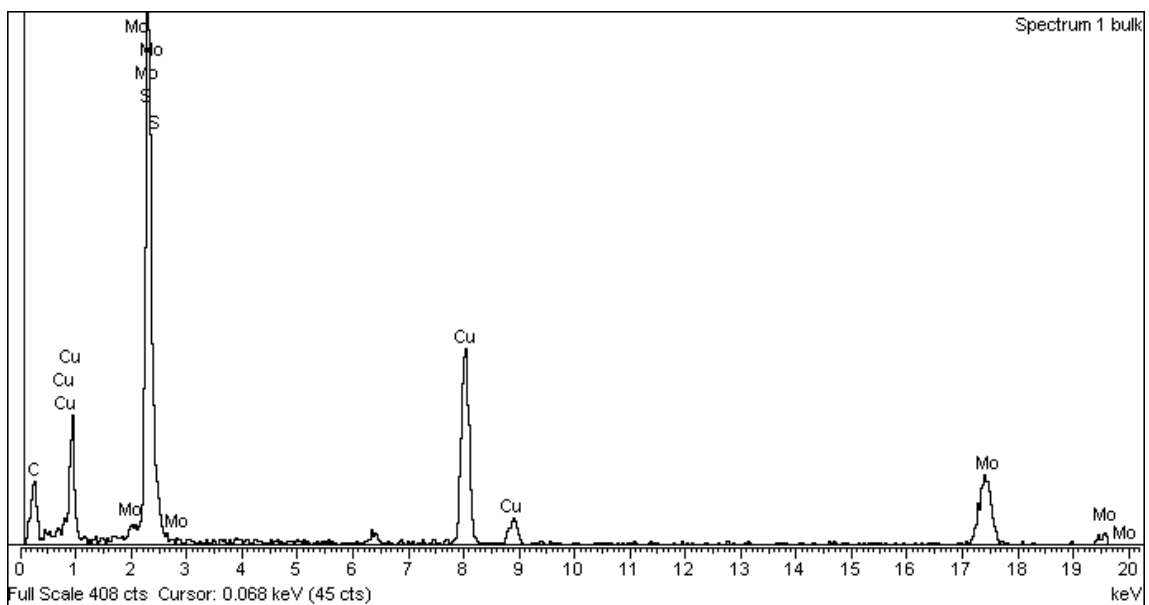


Fig. C - 10 EDX spectra of sMoCO340-org

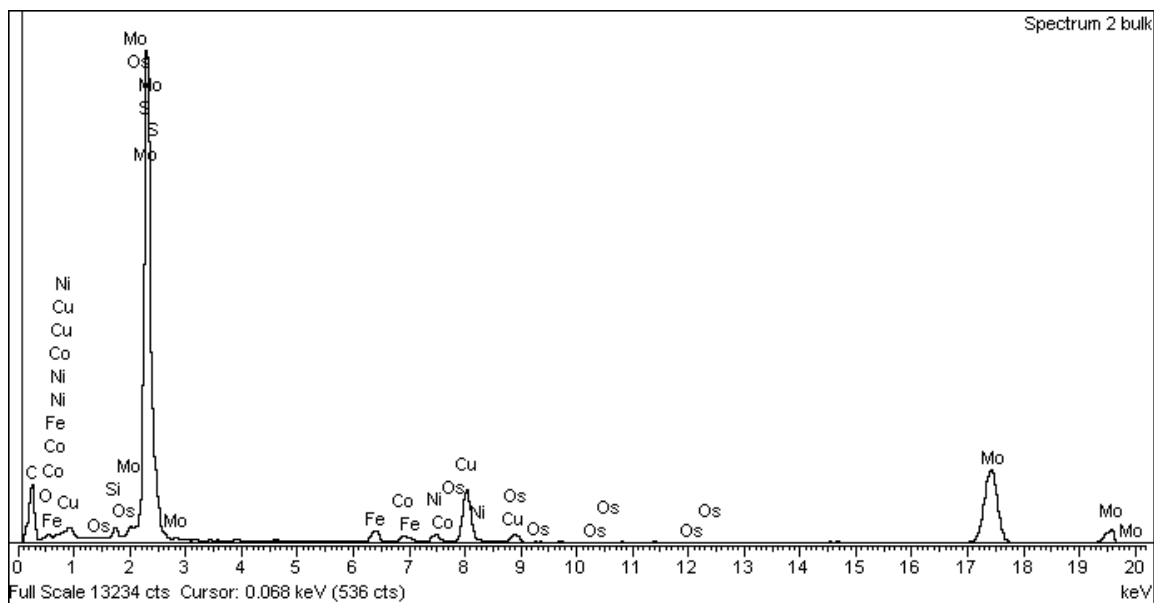


Fig. C - 11 EDX spectra of SMOCO340-Aqu

C-2. HRTEM statistic results

- **MoCO340**

Table C - 1 Distribution of MoS₂ slab length, catalyst sample of MoCO340

Length, nm	Org.	Aqu.	O/W	Wcat.	Baq.
<0.99	1.15	0.73	0	0.91	0
1.00~1.99	5.75	2.9	9.23	6.35	5.88
2.00~2.99	12.64	20.29	23.08	19.09	11.76
3.00~3.99	21.84	7.97	28.46	19.09	35.29
4.00~4.99	26.44	14.49	20.77	17.27	23.53
5.00~5.99	12.64	23.19	10	10	11.76
6.00~6.99	12.64	4.35	4.62	10.91	0
7.00~7.99	2.3	10.9	0.77	10	11.76
8.00~8.99	4.6	5.07	0.77	4.55	0
9.00~9.99	0	1.45	0.77	0	0
10.00~10.99	0	4.35	0.77	0.91	0
11.00~11.99	0	2.9	0.77	0	0
12.00~12.99	0	0.73	0	0	0
13.00~13.99	0	0.73	0	0	0
>=14.00	0	0	0	0.91	0

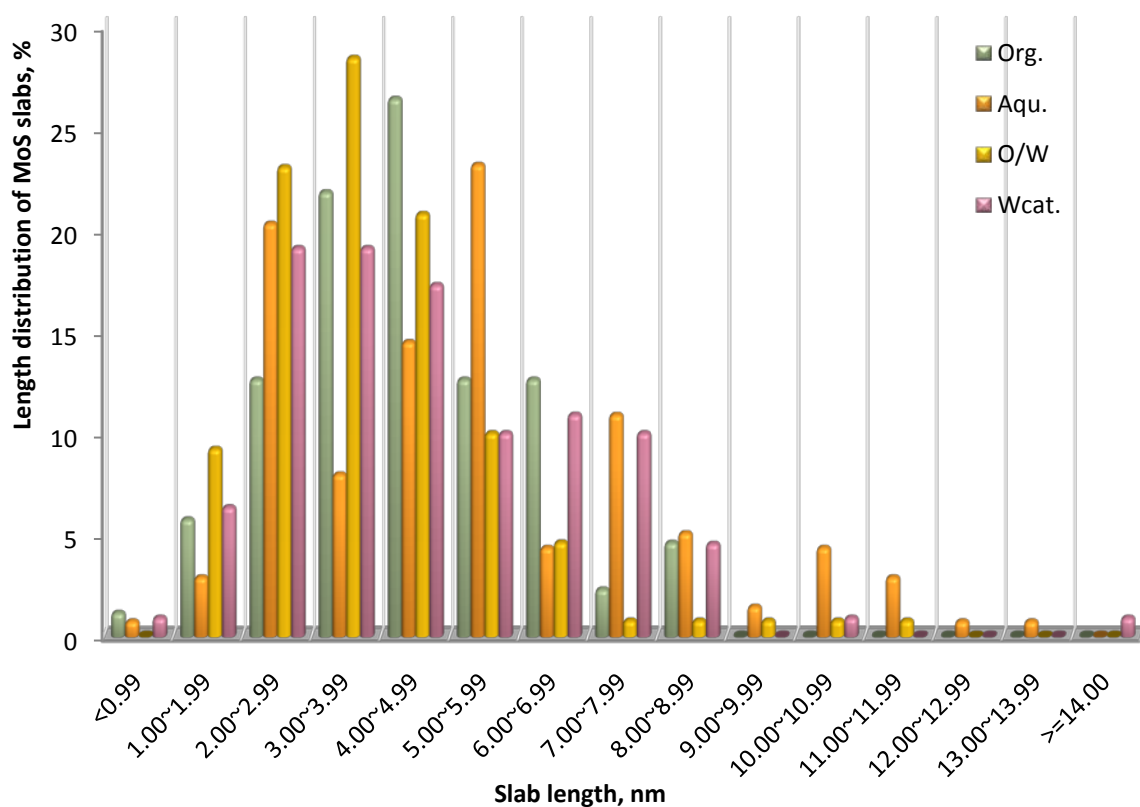


Fig. C - 12 Distribution of MoS₂ slab length, catalyst sample of MoCO340, prepared at 340 C in CO derived from PMA

Table C - 2 Stacking degree distribution of MoCO340

Stacking number	Org.	Wcat.	Aqu.	O/W
1	9.2%	6.7%	5.6%	7.3%
2	29.2%	30.0%	32.4%	31.7%
3	33.8%	41.7%	34.3%	34.1%
4	16.9%	15.0%	16.7%	19.5%
5	4.6%	6.7%	8.3%	4.9%
6	3.1%	0.0%	2.8%	0.0%
7	1.5%	0.0%	0.0%	0.0%
8	1.5%	0.0%	0.0%	2.4%

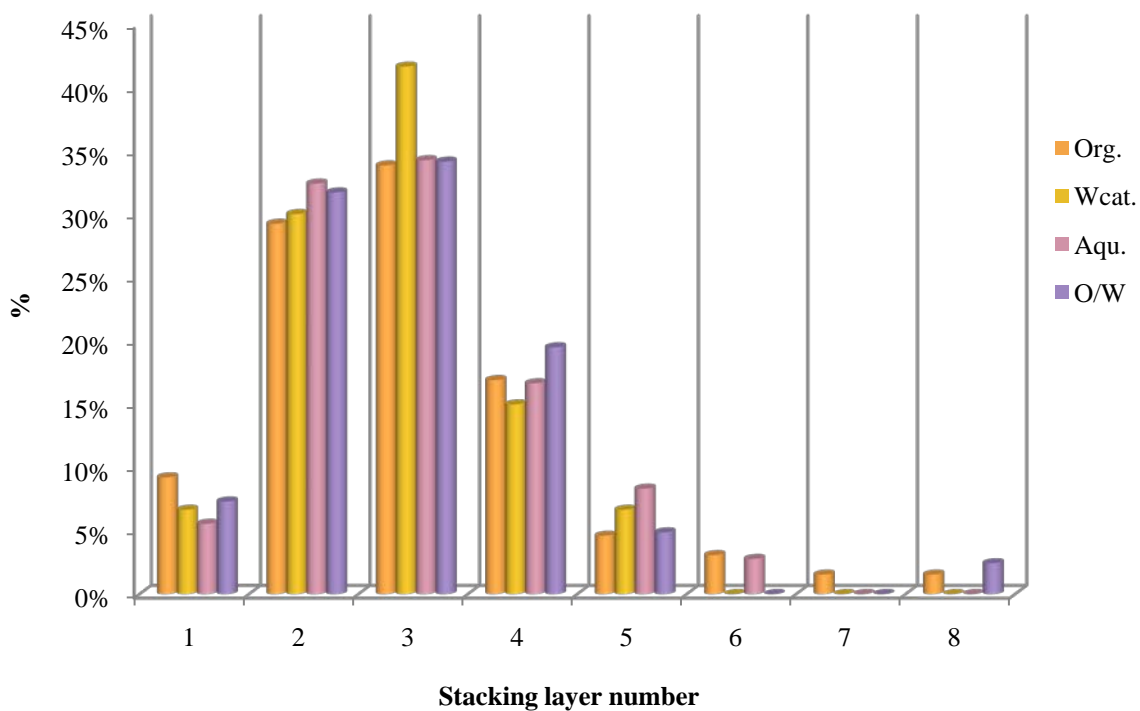


Fig. C - 13 Distribution of MoS₂ slab stacking degree, catalyst sample of MoCO340, prepared at 340 C in CO derived from PMA

- **MoH340**

Table C - 3 Distribution of MoS₂ slab length, catalyst sample of MoH340

Length, nm	Org.	Aqu.	O/W	Wcat.	Baq.
<0.99	0	0	0	0	0
1.00~1.99	0	0	0	0	1.87
2.00~2.99	6.52	14.71	3.81	8.33	9.35
3.00~3.99	8.7	13.97	10.48	16.67	18.69
4.00~4.99	13.04	19.12	9.52	23.21	15.89
5.00~5.99	15.22	9.56	16.19	15.48	10.28
6.00~6.99	13.04	11.77	24.76	11.31	23.36
7.00~7.99	2.17	5.88	10.48	2.38	4.67
8.00~8.99	8.7	7.35	4.76	11.31	4.67
9.00~9.99	4.35	2.94	12.38	5.36	4.67
10.00~10.99	2.17	5.88	0.95	2.98	0.94
11.00~11.99	10.87	5.15	2.86	0.6	0.94
12.00~12.99	2.17	2.21	0.95	0.6	0.94
13.00~13.99	0	0.74	2.85	0	0
>=14.00	13.04	0.74	0	1.79	3.74

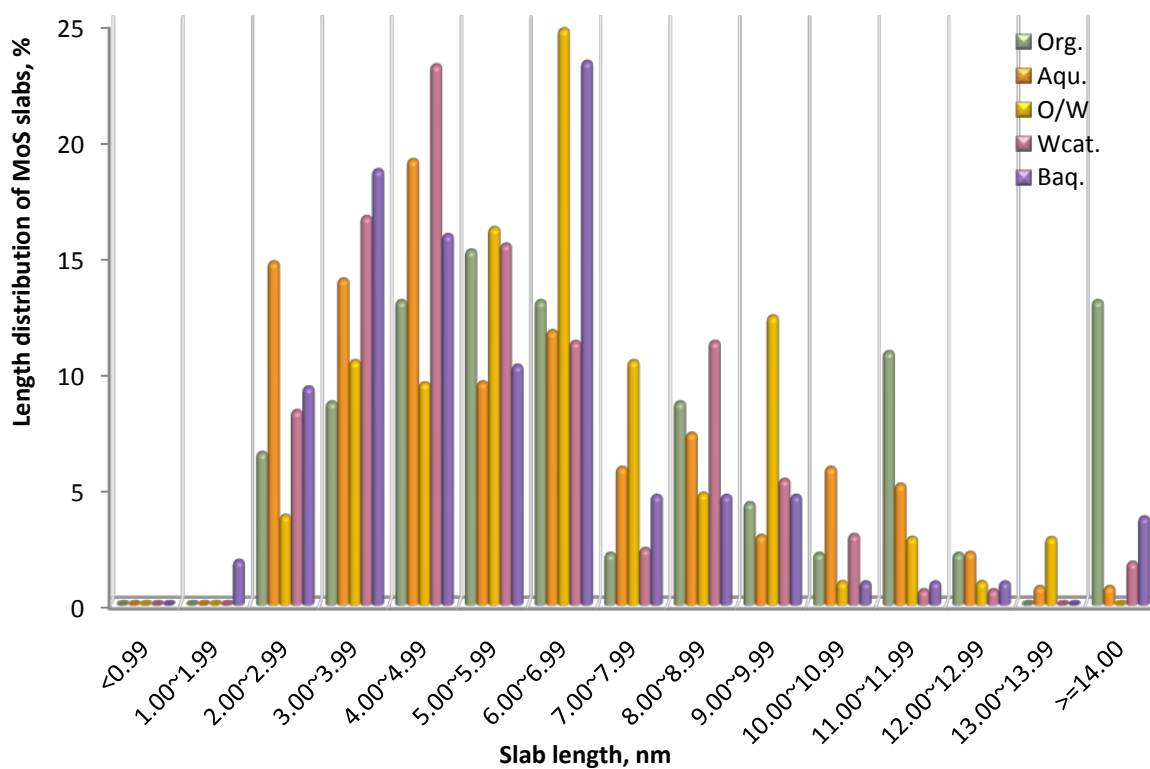


Fig. C - 14 Distribution of MoS₂ slabs, catalyst sample of MoH340, prepared at 340 C in H₂ derived from PMA

Table C - 4 Stacking degree distribution of MoH340

Stacking number	Org.	Aqu.	O/W	Wcat.	Baq.
2	2.4%	5.0%	0.0%	8.9%	10.5%
3	23.8%	30.0%	29.2%	16.5%	13.2%
4	11.9%	17.5%	38.5%	31.6%	34.2%
5	11.9%	27.5%	16.9%	25.3%	21.1%
6	23.8%	10.0%	7.7%	7.6%	18.4%
7	9.5%	7.5%	3.1%	6.3%	2.6%
8	2.4%	2.5%	1.5%	1.3%	0.0%
9	0.0%	0.0%	1.5%	2.5%	0.0%
10	4.8%	0.0%	1.5%	0.0%	0.0%
11	2.4%	0.0%	0.0%	0.0%	0.0%
12	0.0%	0.0%	0.0%	0.0%	0.0%
13	4.8%	0.0%	0.0%	0.0%	0.0%
14	2.4%	0.0%	0.0%	0.0%	0.0%

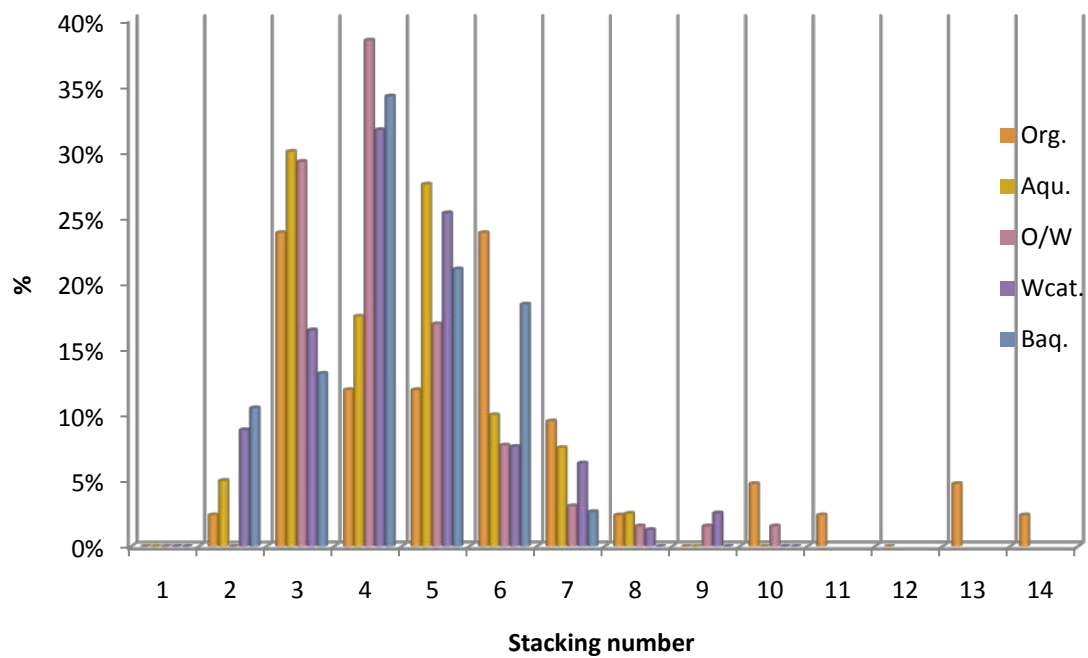


Fig. C - 15 Distribution of MoS₂ slab stacking degree, catalyst sample of MoH340, prepared at 340 C in H₂ derived from PMA

- **SMoCO340**

Table C - 5 Distribution of MoS₂ slab length, catalyst sample of SMOCO340

Length, nm	Org.	Aqu.	O/W	Wcat.	Baq.
<0.99	0	0	0	0	0
1.00~1.99	6.65	2.6	1.2	0	2.5
2.00~2.99	21.88	5.3	12.3	13.21	16.5
3.00~3.99	23.82	13.2	17.2	9.4	29.8
4.00~4.99	15.79	13.2	23.3	28.3	9.9
5.00~5.99	8.86	7.9	15.3	13.2	20.7
6.00~6.99	11.91	21.1	12.9	9.4	11.6
7.00~7.99	1.94	5.3	3.7	17	1.7
8.00~8.99	2.77	5.3	2.5	1.9	2.5
9.00~9.99	3.6	6.6	3.7	7.6	3.3
10.00~10.99	0.83	2.63	1.8	0	0.8
11.00~11.99	1.39	3.95	3.1	0	0
12.00~12.99	0	3.95	0	0	0
13.00~13.99	0.28	1.32	0	0	0.8
>=14.00	0.28	7.91	3.1	0	0

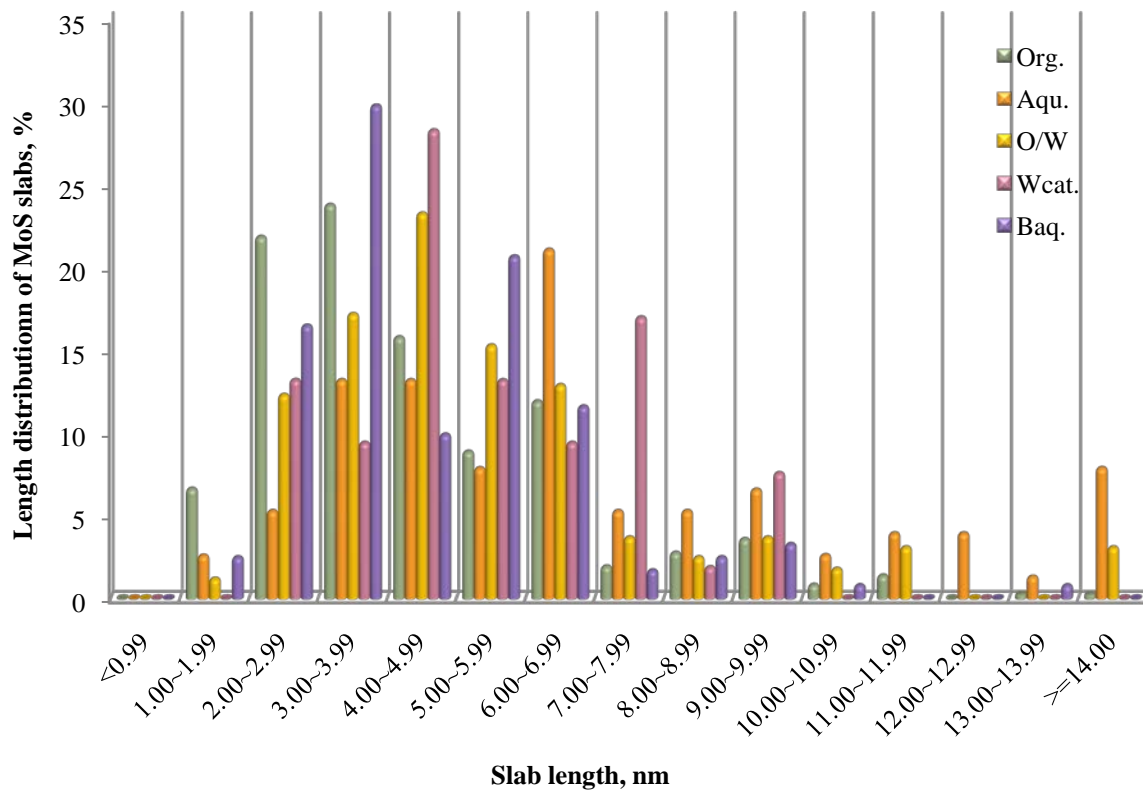


Fig. C - 16 Distribution of MoS₂ slabs, catalyst sample of SMOCO340, prepared at 340 C in CO derived from PMA

Table C - 6 Stacking degree distribution of SMOCO340

layer number	Org. (N=3.3)	Aqu. (N=4.0)	O/W (N=3.3)	Wcat. (N=3.7)	Baq. (N=3.2)
1	0.8%	0.0%	5.2%	0.0%	6.8%
2	28.9%	10.7%	26.7%	15.0%	27.3%
3	28.9%	32.1%	31.0%	30.0%	29.5%
4	23.1%	21.4%	19.8%	25.0%	20.5%
5	15.7%	25.0%	11.2%	30.0%	11.4%
6	1.7%	7.1%	2.6%	0.0%	2.3%
7	0.0%	3.6%	0.0%	0.0%	0.0%
8	0.8%	0.0%	2.6%	0.0%	0.0%
9	0.0%	0.0%	0.9%	0.0%	2.3%

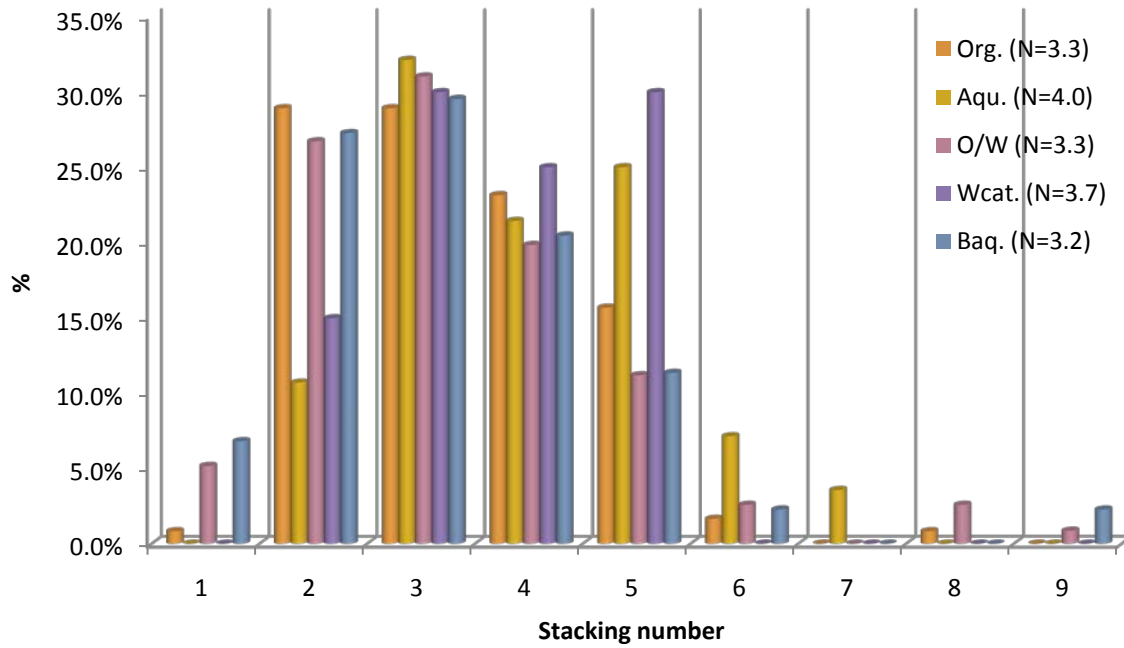


Fig. C - 17 Distribution of MoS₂ slab stacking degree, catalyst sample of SMOCO340, prepared at 340 C in CO derived from PMA

- **NMoCO340**

Table C - 7 Distribution of MoS₂ slab length, catalyst sample of NMoCO340

Length, nm	Org.	Aqu.	O/W	Wcat.	Baq.
<0.99	0	0	0	0	0
1.00~1.99	0.85	0.54	0	0.55	1.5
2.00~2.99	3.39	3.76	7.09	5.48	12.28
3.00~3.99	11.02	7.53	16.42	13.97	18.26
4.00~4.99	22.88	20.97	17.54	19.18	21.56
5.00~5.99	22.88	25.81	19.4	22.74	15.27
6.00~6.99	14.41	12.37	10.82	10.96	10.48
7.00~7.99	9.32	13.44	7.84	13.15	8.98
8.00~8.99	2.54	4.3	4.85	5.21	5.39
9.00~9.99	3.39	4.3	3.36	3.29	2.69
10.00~10.99	4.24	3.23	3.36	3.29	1.8
11.00~11.99	2.54	2.69	1.49	0.82	0.3
12.00~12.99	1.69	0.54	2.24	0.55	0.9
13.00~13.99	0.85	0.54	0.37	0.55	0.3
>=14.00	0	0	5.22	0.27	0.3

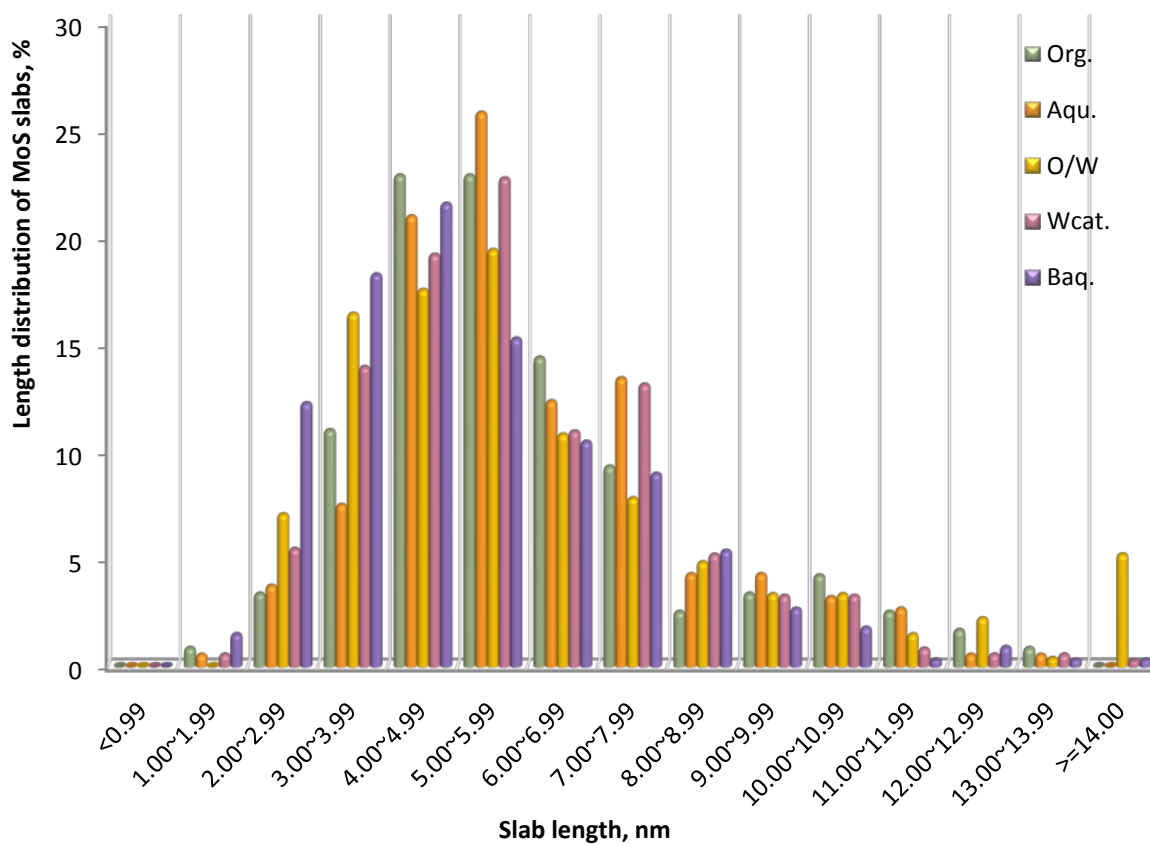


Fig. C - 18 Distribution of MoS₂ slabs, catalyst sample of NMoCO340, prepared at 340 C in CO derived from PMA

Table C - 8 Stacking degree distribution of NMoCO340

Stacking number	Org. (N=3.8)	Aqu. (N=3.3)	O/W (N=3.3)	Wcat. (N=3.8)	Baq. (N=3.8)
1	4.9%	4.3%	8.8%	0.0%	0.0%
2	19.5%	28.6%	22.1%	18.4%	11.9%
3	24.4%	32.9%	30.9%	32.9%	37.3%
4	17.1%	17.1%	19.1%	23.7%	28.8%
5	17.1%	8.6%	10.3%	11.8%	13.6%
6	12.2%	5.7%	5.9%	6.6%	5.1%
7	2.4%	1.4%	1.5%	5.3%	1.7%
8	2.4%	1.4%	1.5%	1.3%	1.7%
9	0.0%	0.0%	0.0%	0.0%	0.0%

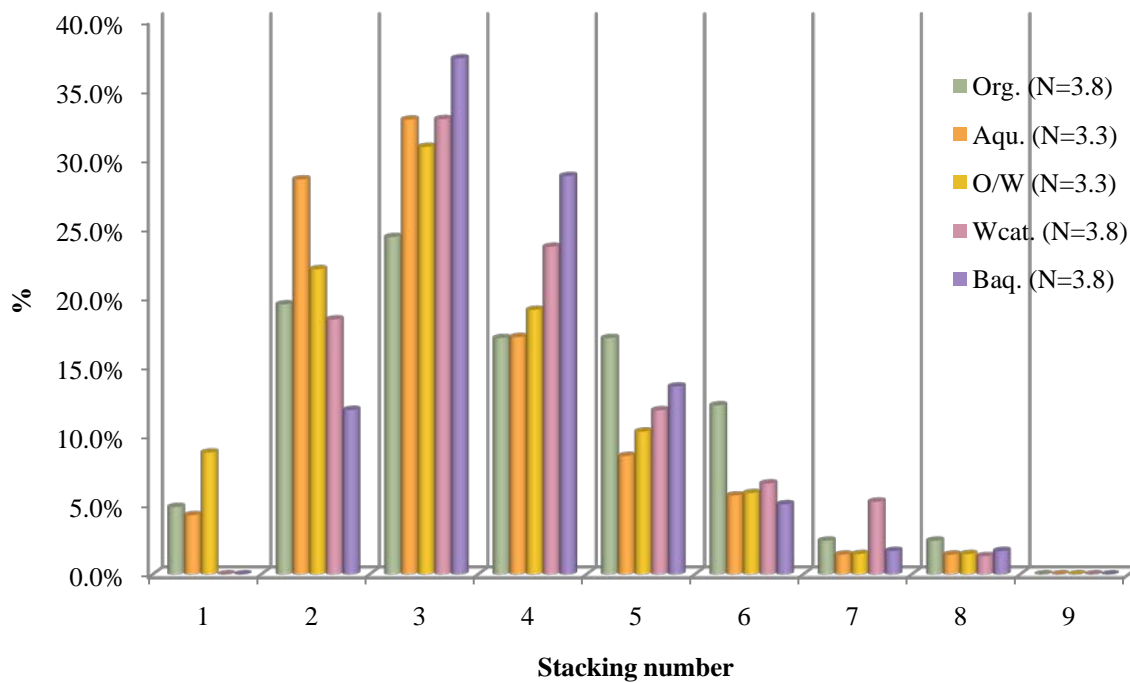


Fig. C - 19 Distribution of MoS₂ slab stacking degree, catalyst sample of NMoCO340, prepared at 340 C in CO derived from PMA

APPENDIX D --- Example Calculation of Average MoS₂ Slab Length

Size of MoS₂ slabs observed on HRTEM images is described via average slab length and average stacking degree. They are calculated according to equations (3-1) and (3-2), which are also given in Chapter 3.

$$\bar{L} = \frac{\sum_{i=1}^n n_i L_i}{\sum_{i=1}^n n_i}, \quad (3-1)$$

Wherein:

\bar{L} --- is the average length of the MoS slabs

L_i --- is the length of the i^{th} MoS slab

n_i --- is the number of the slabs with the length of L_i

An example will be given in this section. Fig. D-1. In this image, 33 MoS₂ slabs were measured. Length of each MoS₂ slab is listed in Table C-1. The originally measured length is in the unit of centimetre on the HRTEM image. On this picture, 10 nm is 5.38 cm long. This ratio is used to convert measured length to real MoS₂ slab length in nanometre (Table D-1).

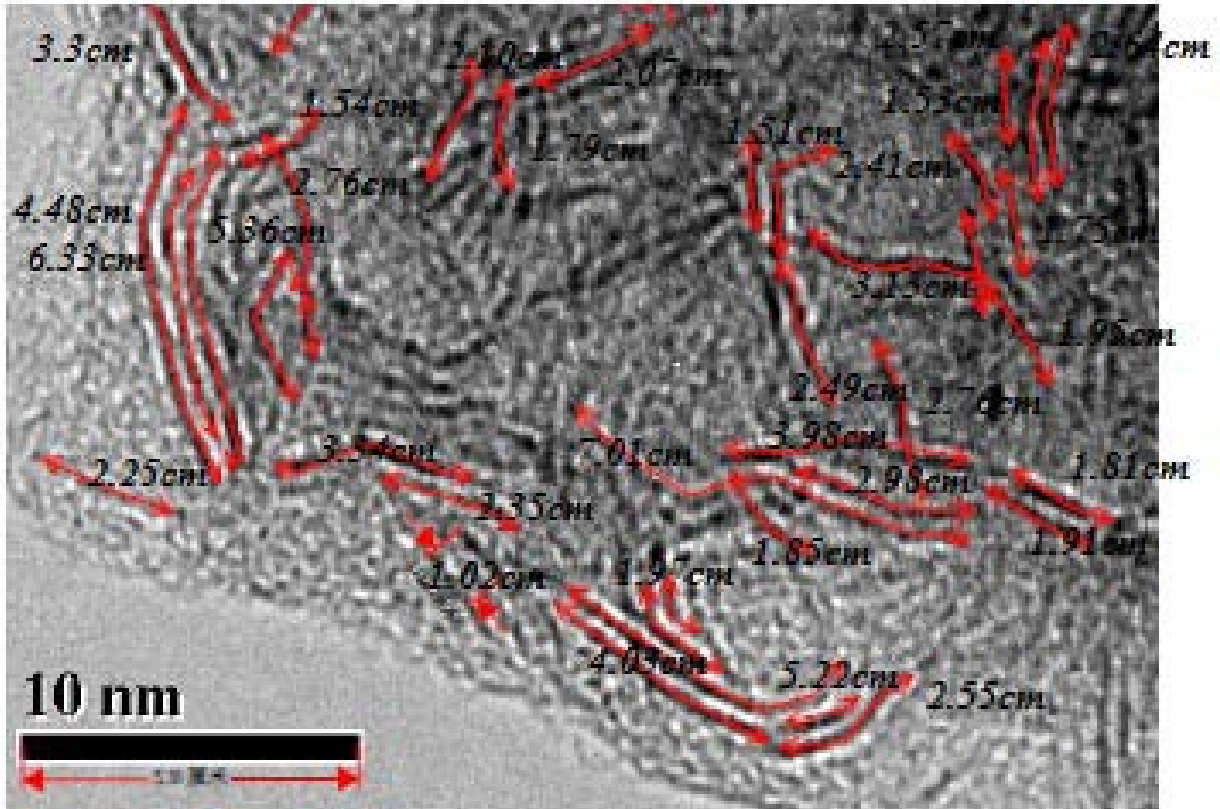


Fig. D - 1 An HRTEM picture of the catalyst sample, SMOCO340, with measurement marked

In Table D-1, numbers of “length on the picture” were measured on the HRTEM image.

Numbers of “length of slab” were obtained from:

$$\text{Length of slab, nm} = \text{Length on the picture, cm} \times \frac{10 \text{ nm}}{5.38 \text{ cm}}$$

Average slab length of MoS₂ slabs shown in Fig. D-1 was calculated according to equation

(3-1):

$$\bar{L} = \frac{\sum_i n_i L_i}{\sum_i n_i} = \frac{1 \times 1.90 + 1 \times 2.82 + \dots + 1 \times 11.81 + 1 \times 13.08}{1 + 1 + \dots + 1 + 1} \text{ nm} = 5.36 \text{ nm}$$

Table D - 1 Table of MoS₂ slab length and distribution (sorted from maximum to minimum)

number	Length on the picture, cm	Length of slab, nm	Distribution
1	1.02	1.90	1 (1.00-1.99)
1	1.51	2.82	
1	1.53	2.85	3
1	1.54	2.87	(2.00-2.99)
1	1.75	3.26	
1	1.79	3.34	
1	1.81	3.38	
1	1.85	3.45	
1	1.91	3.56	
1	1.95	3.64	
1	1.97	3.68	
1	2.07	3.86	9
1	2.1	3.92	(3.00-3.99)
1	2.25	4.20	
1	2.35	4.38	
1	2.41	4.50	
1	2.49	4.65	
1	2.55	4.76	
1	2.57	4.79	7
1	2.64	4.93	(4.00-4.99)
1	2.76	5.15	
1	2.76	5.15	
1	2.98	5.56	4
1	3.13	5.84	(5.00-5.99)
1	3.3	6.16	2
1	3.34	6.23	(6.00-6.99)
1	3.98	7.43	2
1	4.03	7.52	(7.00-7.99)
1	4.48	8.36	1 (8.00-8.99)
1	5.22	9.74	1 (9.00-9.99)
1	5.36	10.00	1 (10.00-10.99)
1	6.33	11.81	1 (11.00-11.99)
1	7.01	13.08	1 (13.00-13.99)

Distribution of MoS₂ slab length in each nanometre is shown in Fig. D-2.

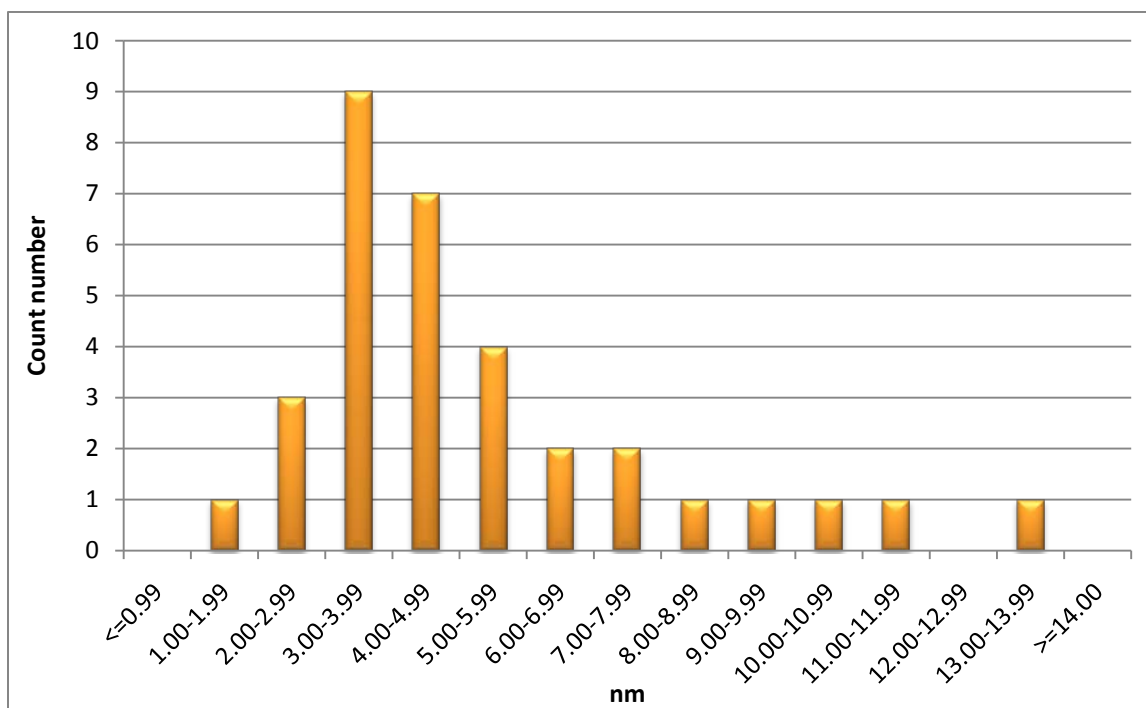


Fig. D - 2 Distribution of MoS₂ slab length

APPENDIX E --- Experimental raw data for Chapter 5

E.1 Experimental data of HDS over Mo sulfide at different reaction temperatures and regression figures / ANOVA tables

- Experiment DS0905

Reaction conditions: 330°C, HC reactor, equi-molar DBT and 4,6-DMDBT, 1600-1800 ppmw S in total, 400-450 ppmw Mo, S/Mo: ~10/1, 10 ml H₂O, 100 ml toluene, 590 psi CO mixed with 10 psi H₂S

Table E - 1 Experiment DS0905, 330 °C

Reaction time, min	1	10	22	45	60	84	160	175
DCH	0.00%	0.00%	0.00%	0.00%	0.00%	0.00%	0.17%	0.18%
CHB	0.23%	0.00%	0.00%	0.28%	0.65%	1.42%	7.75%	8.90%
BP	2.52%	2.17%	2.69%	4.61%	6.40%	8.59%	19.45%	20.67%
TH-DBT	0.12%	0.21%	0.62%	1.51%	2.24%	2.97%	4.20%	4.24%
DBT	97.12%	97.63%	96.69%	93.60%	90.71%	87.02%	68.43%	66.01%
DMCHB	1.15%	0.00%	0.45%	2.48%	4.61%	8.08%	19.13%	18.96%
ISO-DMBP	0.82%	0.51%	1.94%	1.23%	1.36%	1.61%	1.88%	1.96%
DMBP	2.55%	2.40%	2.28%	0.66%	0.64%	0.88%	1.41%	1.33%
TH-DMDBT	0.35%	0.72%	1.16%	1.22%	1.45%	1.84%	1.78%	2.09%
HH-DMDBT	0.63%	2.21%	1.59%	0.73%	0.78%	0.78%	0.94%	0.97%
ISO-DMDBT	0.23%	0.58%	0.85%	0.56%	0.58%	0.65%	0.70%	0.78%
4,6-DMDBT	94.28%	93.58%	91.73%	93.11%	90.58%	86.17%	74.16%	73.91%

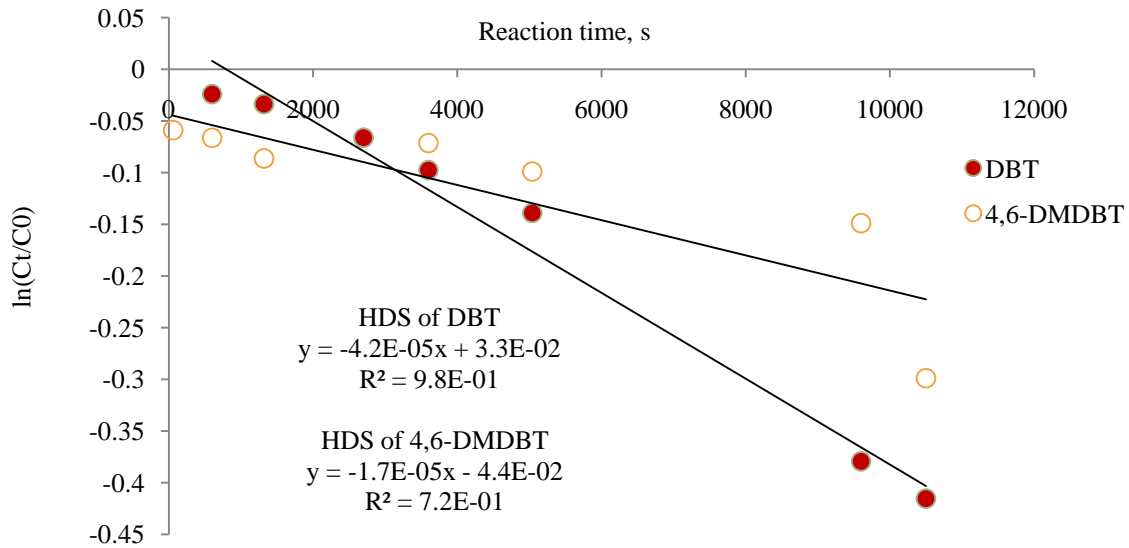


Fig. E - 1 Pseudo-first order plots for the conversions of DBT and 4,6-DMDBT in HDS, DS0905, 330°C

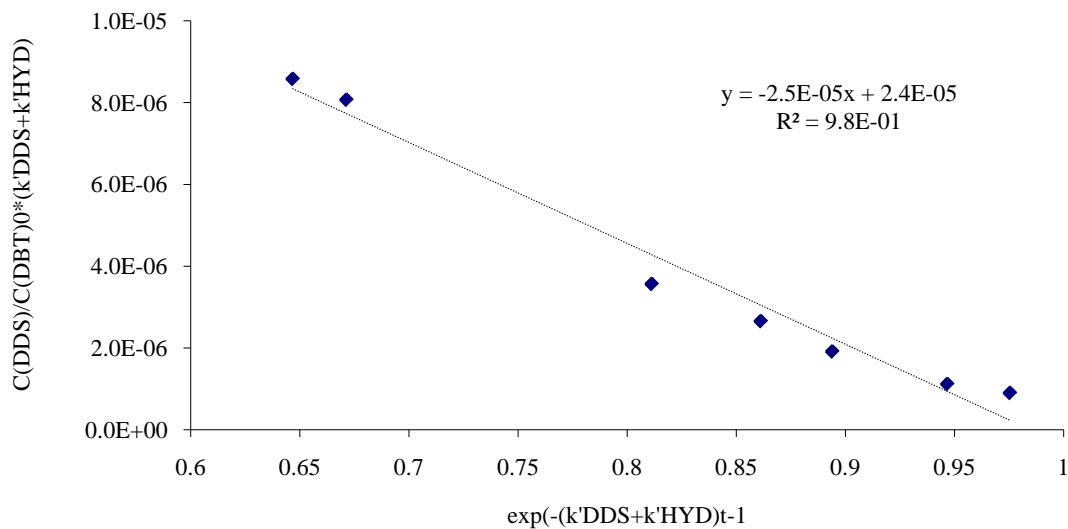


Fig. E - 2 Regression for k'_{DDS} in the HDS of DBT, DS0905, 330°C

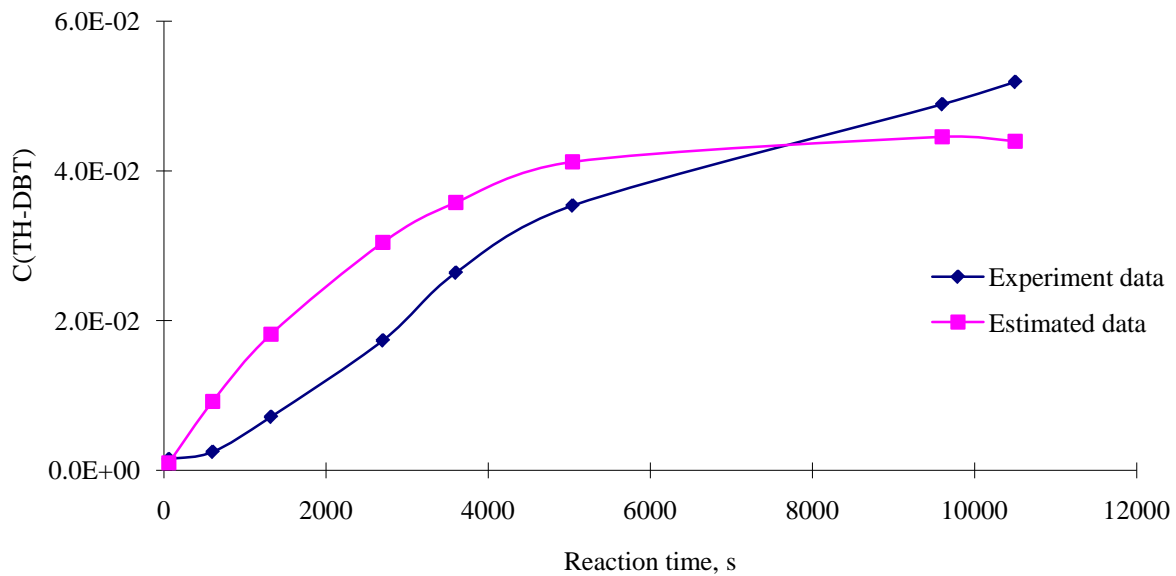


Fig. E - 3 Regression for k'_{HYDD} in the HDS of DBT, DS0905, 330°C

Table E - 2 ANOVA table of $k'_{(DBT\ HYDD)}$, DS0905, 330°C,

Source	SS	Df	MS	F _{OBS}
Regression	SSR	p-1=1	1.23E-03	10
Error	SSE	n-p=6	1.29E-04	
Total	SST	n-1=7		

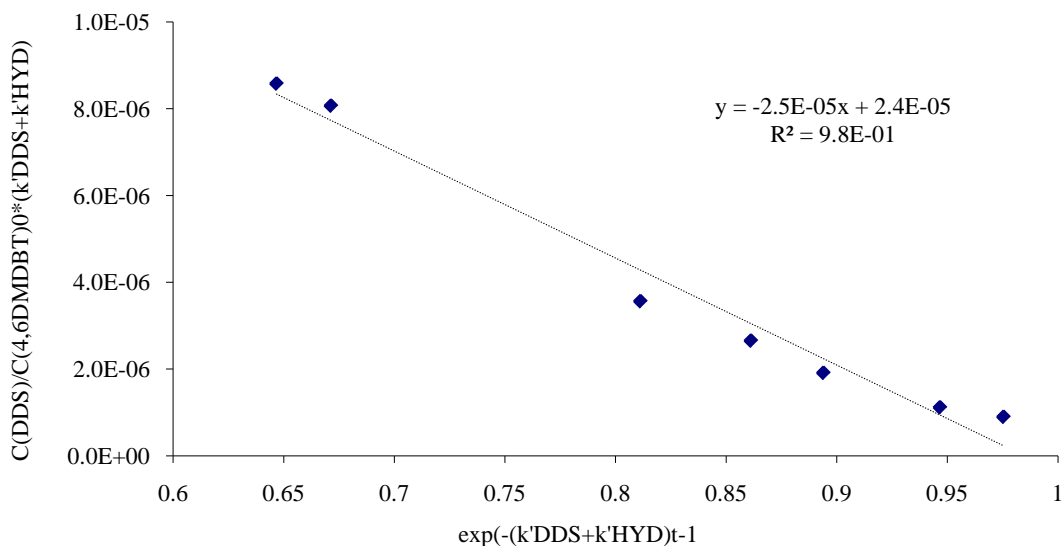


Fig. E - 4 Regression for k'_{DDS} in the HDS of 4,6-DMDBT, DS0905, 330°C

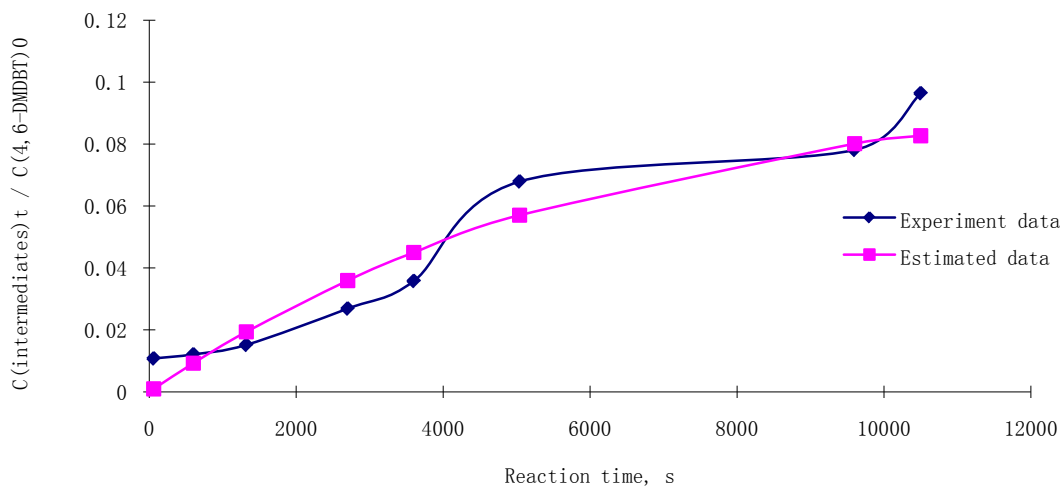


Fig. E - 5 Regression for k'_{HYDD} in the HDS of 4,6-DMDBT, DS0905, 330°C

Table E - 3 ANOVA table of $k'_{(4,6DMDBT\ HYDD)}$, DS0905, 330°C

Source	SS	Df	MS	F _{OBS}
Regression	SSR	p-1=1	6.70E-03	142
Error	SSE	n-p=6	4.72E-05	
Total	SST	n-1=7		

- Experiment DS0906

Reaction conditions: 355°C, HC reactor, equi-molar DBT and 4,6-DMDBT, 1600-1800 ppmw S in total, 400-450 ppmw Mo, S/Mo: ~10/1, 10 ml H₂O, 100 ml toluene, 590 psi CO mixed with 10 psi H₂S

Table E - 4 Experiment DS0906, 355 °C

Reaction time, min	1	9	32	40	63	90	135	180
DCH	0.00%	0.00%	0.00%	0.00%	0.00%	0.12%	0.21%	0.30%
CHB	0.30%	0.21%	1.06%	2.04%	3.36%	7.78%	13.06%	17.27%
BP	2.63%	3.89%	10.06%	13.37%	17.69%	28.29%	39.34%	47.63%
TH-DBT	0.37%	0.84%	2.50%	2.97%	3.41%	3.31%	2.77%	2.09%
DBT	96.70%	95.06%	86.38%	81.62%	75.54%	60.50%	44.61%	32.72%
DMCHB	4.31%	3.33%	3.52%	8.61%	10.62%	19.57%	27.80%	32.76%
ISO-DMBP	2.80%	4.74%	2.12%	2.98%	3.06%	4.04%	4.63%	5.20%
DMBP	1.03%	0.81%	0.49%	0.93%	1.07%	1.73%	2.35%	2.86%
TH-DMDBT	1.77%	1.93%	0.91%	1.22%	1.15%	1.30%	1.15%	0.93%
HH-DMDBT	1.43%	1.16%	0.33%	0.54%	0.61%	0.76%	0.91%	0.91%
ISO-DMDBT	1.33%	0.95%	0.36%	0.53%	0.59%	0.89%	1.09%	1.20%
4,6-DMDBT	87.33%	87.08%	92.27%	85.19%	82.90%	71.72%	62.07%	56.15%

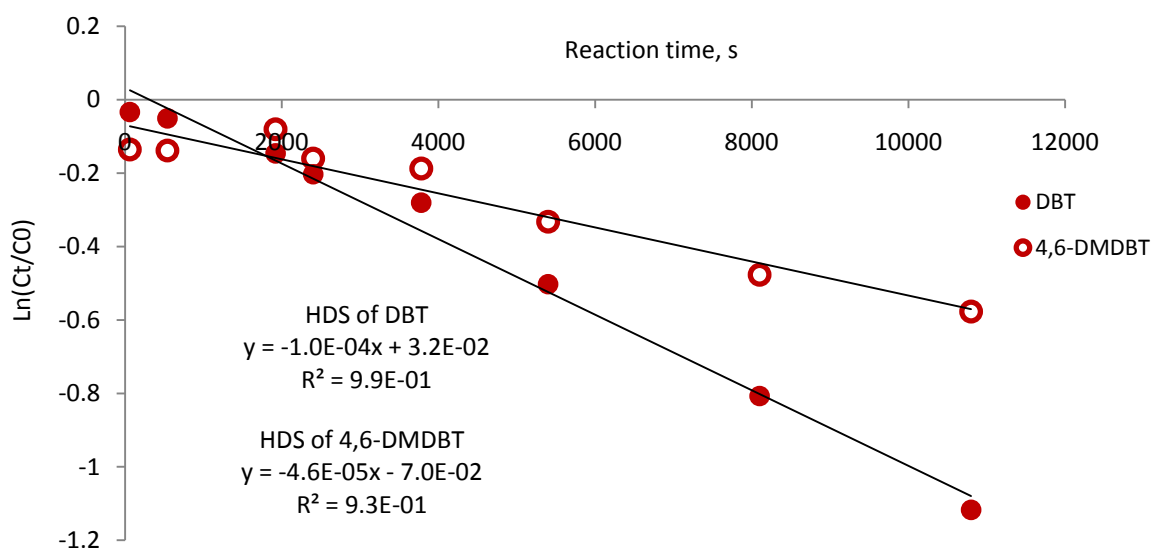


Fig. E - 6 Pseudo-first order plots for the conversions of DBT and 4,6-DMDBT in HDS, DS0906, 355°C

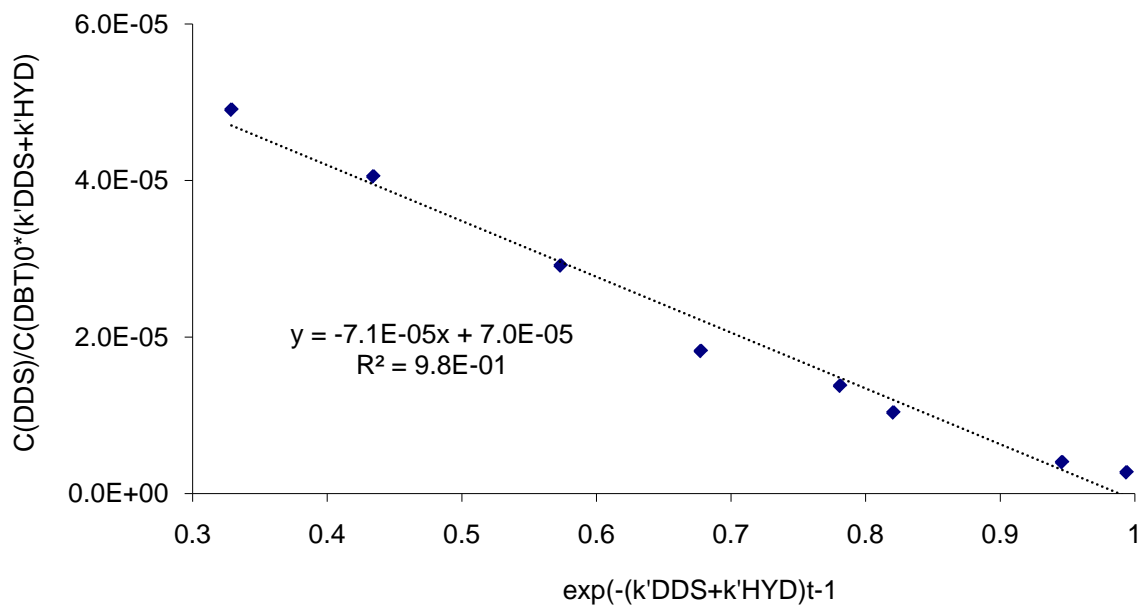


Fig. E - 7 Regression for k'_{DDS} in the HDS of DBT, DS0906, 355°C

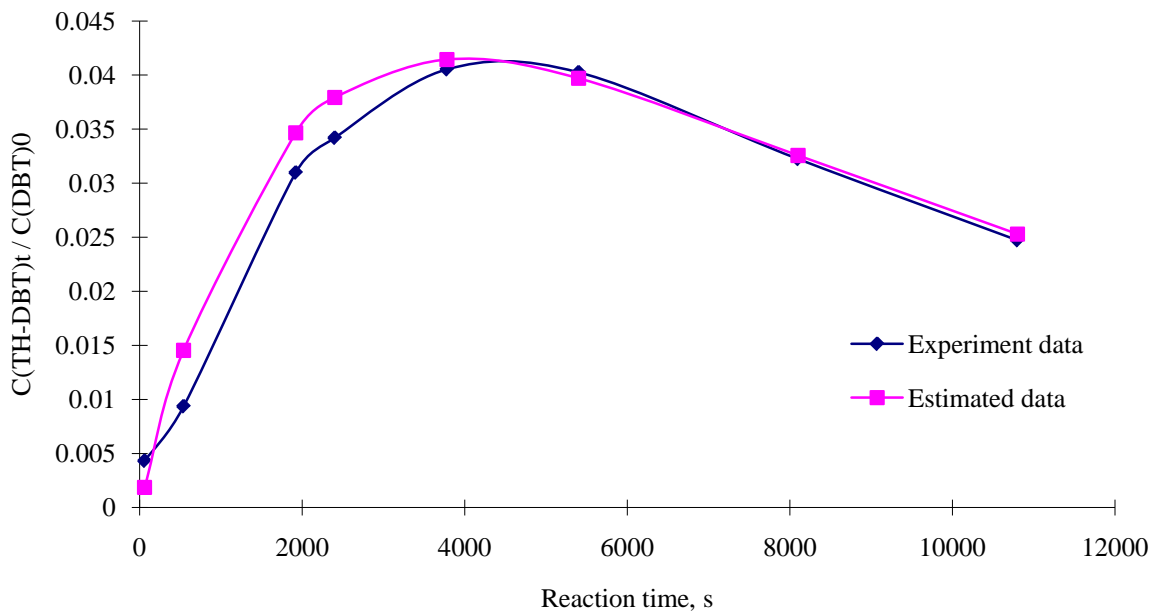


Fig. E - 8 Regression for k'_{HYDD} in the HDS of DBT, DS0906, 355°C

Table E - 5 ANOVA table of $k'_{DBT HYDD}$ at 355°C

Source	SS	Df	MS	F _{OBS}
Regression	SSR	p-1=1	1.27E-03	137
Error	SSE	n-p=6	9.28E-06	
Total	SST	n-1=7		

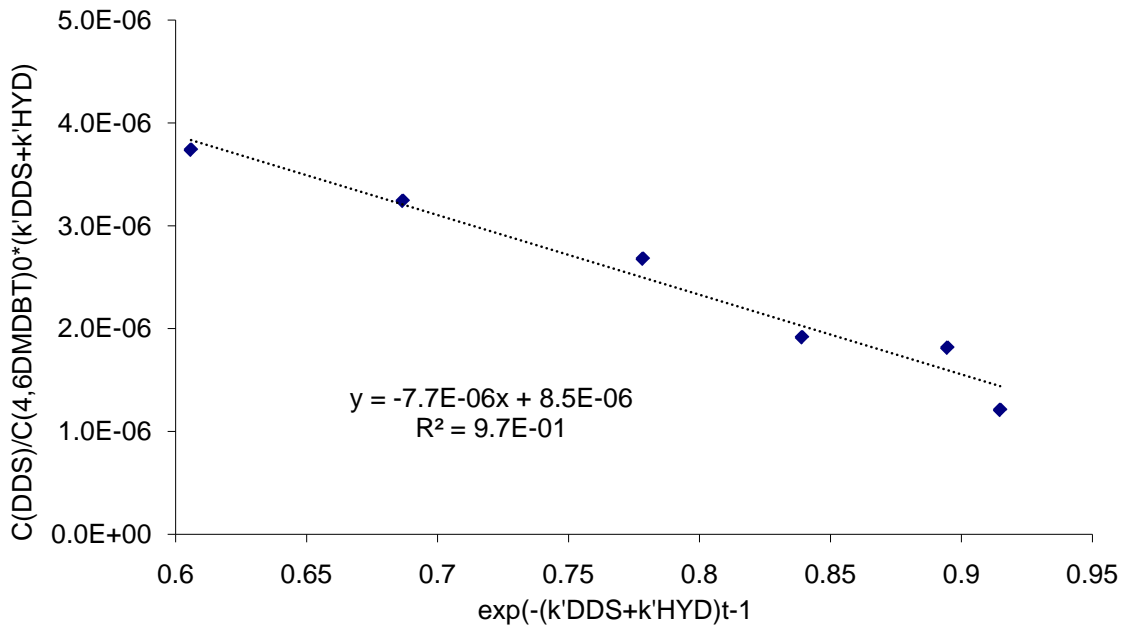


Fig. E - 9 Regression for k'_{DDS} in the HDS of 4,6-DMDBT, DS0906, 355°C

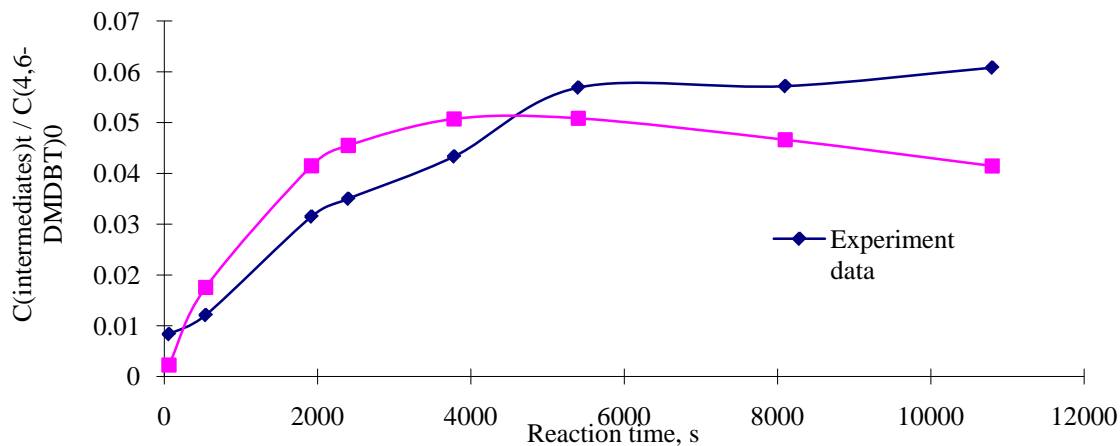


Fig. E - 10 Regression for k'_{HYDD} of 4,6-DMDBT, DS0906, 355°C

Table E - 6 ANOVA $k'_{4,6\text{DMDBT HYDD}}$ at 355°C

Source	SS	Df	MS	F _{OBS}
Regression	SSR	p-1=1	5.51E-03	28
Error	SSE	n-p=6	2.00E-04	
Total	SST	n-1=7		

- Experiment DS0907

Reaction conditions: 380°C, HC reactor, equi-molar DBT and 4,6-DMDBT, 1600-1800 ppmw S in total, 400-450 ppmw Mo, S/Mo: ~10/1, 10 ml H₂O, 100 ml toluene, 590 psi CO mixed with 10 psi H₂S

Table E - 7 Experiment DS0907, 380C

Reaction time, min	0	10	28	60	98	120	146	180
DCH	0.00%	0.00%	0.00%	0.00%	0.17%	0.21%	0.23%	0.29%
CHB	0.94%	1.11%	3.00%	7.14%	12.51%	15.06%	15.78%	17.31%
BP	6.54%	12.36%	22.73%	37.77%	54.28%	62.41%	65.68%	72.16%
TH-DBT	1.33%	2.67%	3.54%	3.29%	2.14%	1.44%	1.18%	0.65%
DBT	91.19%	83.86%	70.73%	51.80%	30.91%	20.88%	17.13%	9.58%
DMCHB	8.00%	5.57%	14.06%	20.75%	33.73%	38.67%	39.09%	40.92%
ISO-DMBP	4.41%	4.19%	7.40%	7.89%	4.80%	5.81%	5.80%	11.17%
DMBP	1.08%	0.86%	1.74%	2.40%	3.78%	4.52%	5.10%	5.97%
TH-DMDBT	1.20%	0.66%	0.99%	0.86%	0.72%	0.50%	0.44%	0.26%
HH-DMDBT	0.75%	0.52%	0.90%	1.06%	1.13%	1.12%	1.11%	1.05%
ISO-DMDBT	0.60%	0.41%	0.78%	1.00%	1.32%	1.35%	1.30%	1.11%
4,6-DMDBT	83.96%	87.79%	74.13%	66.04%	54.52%	48.03%	47.14%	39.52%

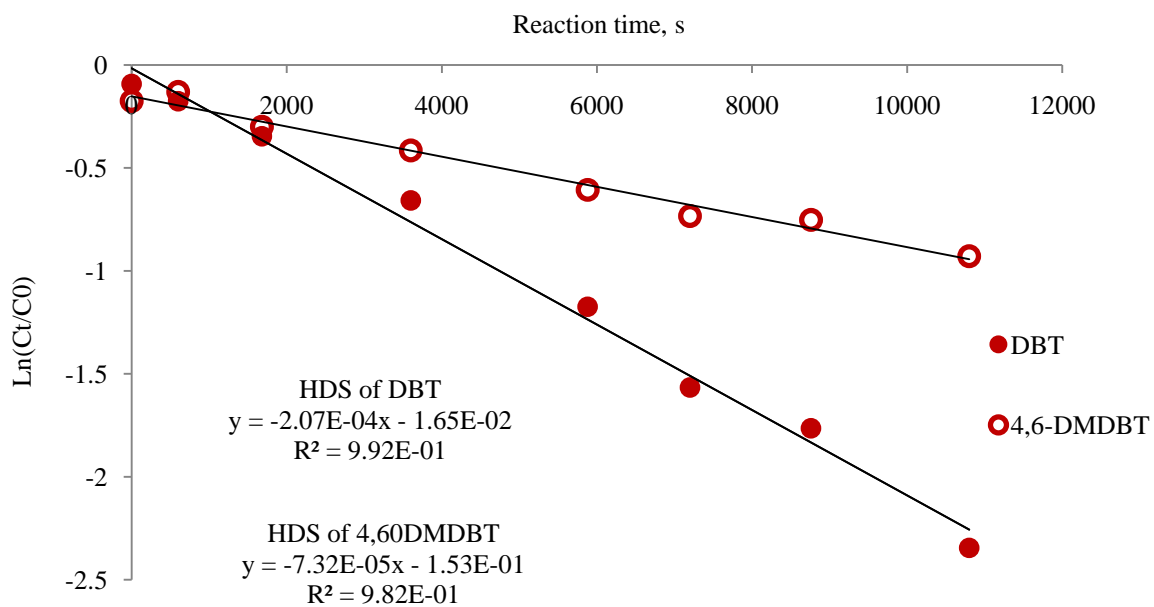


Fig. E - 11 Pseudo-first order plots for the conversions of DBT and 4,6-DMDBT in HDS, DS0907, 380°C

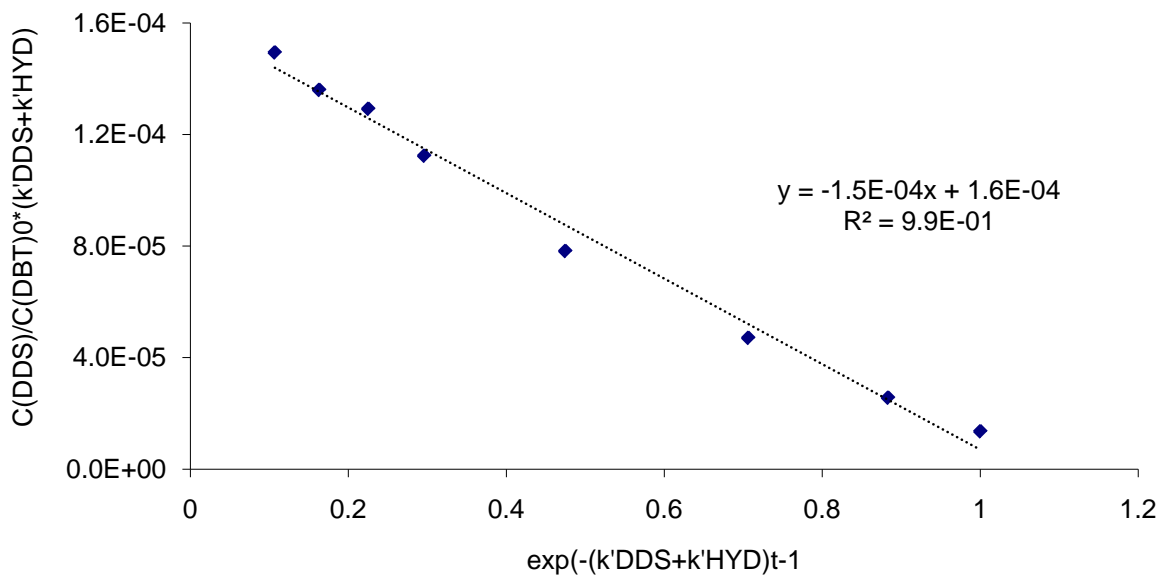


Fig. E - 12 Regression for k'_{DDS} in the HDS of DBT, DS0907, 380°C

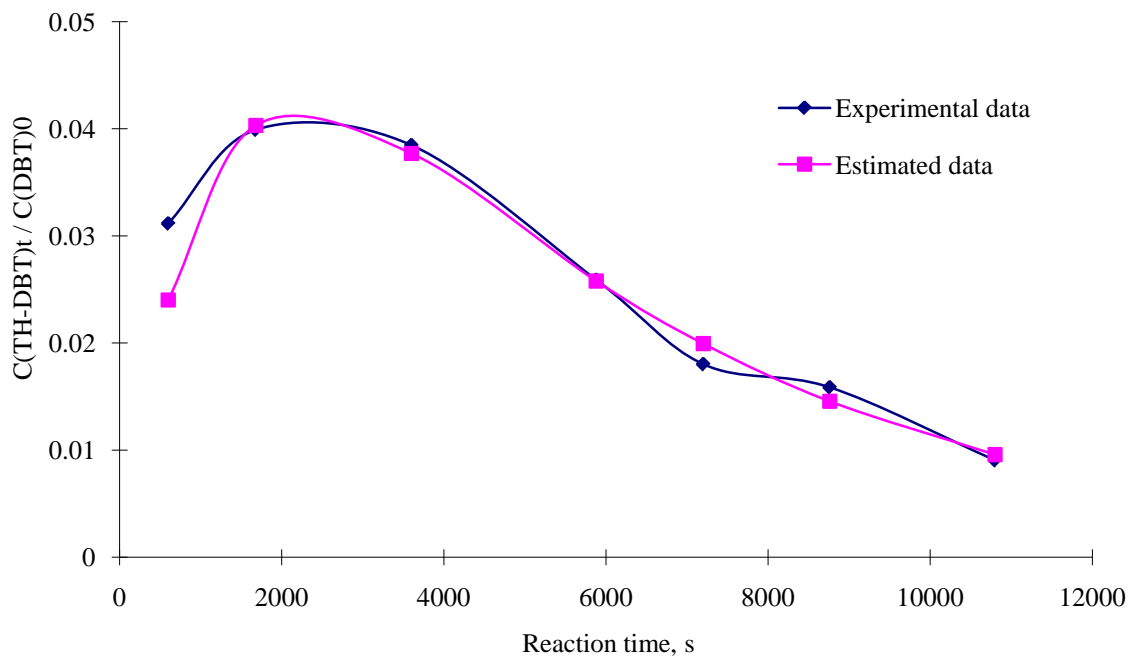


Fig. E - 13 Regression for k'_{HYDD} in the HDS of DBT, DS0907, 380°C, ... k_{HYDD}

Table E - 8 ANOVA $k'_{(DBT\ HYDD)}$, 380°C

Source	SS	Df	MS	F _{OBS}
Regression	SSR	p-1=1	5.08E-03	533
Error	SSE	n-p=6	4.58E-05	
Total	SST	n-1=7		

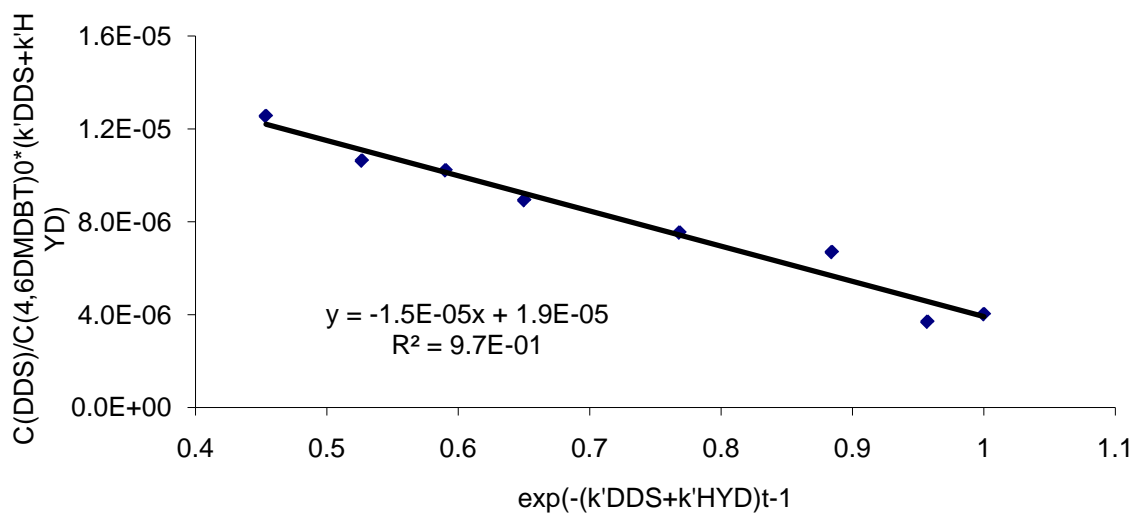


Fig. E - 14 Regression for k'_{DDS} in the HDS of 4,6-DMDBT, DS0907, 380°C

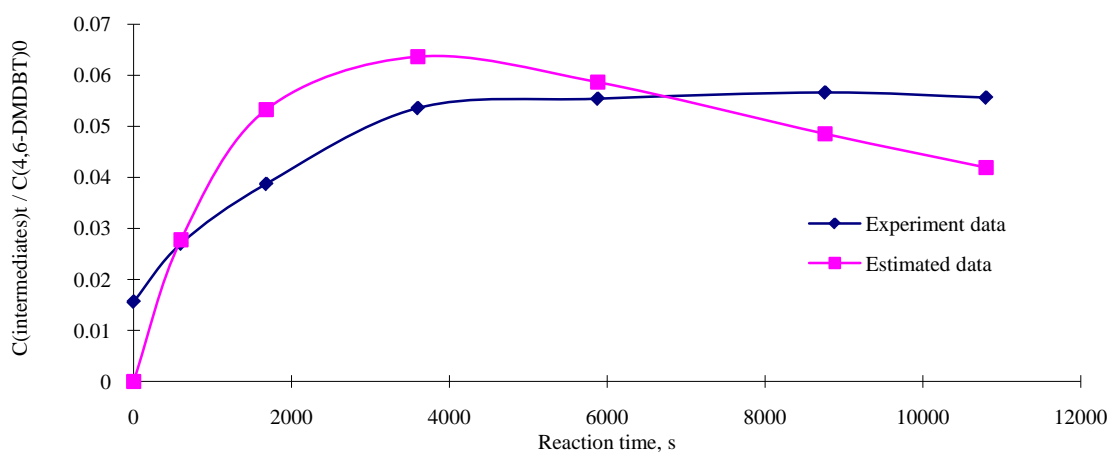


Fig. E - 15 Regression of k'_{HYDD} of 4,6-DMDBT, DS0907, 380°C

Table E - 9 ANOVA $k'_{(4,6DMDBT HYDD)}$, 380°C

Source	SS	Df	MS	F _{OBS}
Regression	SSR	p-1=1	5.61E-03	16
Error	SSE	n-p=6	3.56E-04	
Total	SST	n-1=7		

- Experiment DS0908

Reaction conditions: 400°C, HC reactor, equi-molar DBT and 4,6-DMDBT, 1600-1800 ppmw S in total, 400-450 ppmw Mo, S/Mo: ~10/1, 10 ml H₂O, 100 ml toluene, 590 psi CO mixed with 10 psi H₂S

Table E - 10 Experiment DS0908, 400 C

Reaction time, min	0	10	30	44	60	90	120	180
DCH	0.00%	0.00%	0.00%	0.00%	0.00%	0.15%	0.18%	0.22%
CHB	1.38%	2.04%	5.46%	7.85%	9.09%	11.81%	12.58%	13.26%
BP	12.39%	19.81%	39.43%	50.91%	57.13%	71.99%	77.71%	83.04%
TH-DBT	1.92%	2.35%	2.25%	1.75%	1.43%	0.74%	0.51%	0.37%
DBT	84.31%	75.80%	52.86%	39.49%	32.35%	15.32%	9.02%	3.11%
DMCHB	8.00%	5.57%	14.06%	20.75%	33.73%	38.67%	39.45%	41.00%
ISO-DMBP	4.41%	4.19%	7.40%	7.89%	4.80%	5.81%	5.65%	11.12%
DMBP	1.08%	0.86%	1.74%	2.40%	3.78%	4.52%	4.97%	5.95%
TH-DMDBT	1.20%	0.66%	0.99%	0.86%	0.72%	0.50%	0.43%	0.26%
HH-DMDBT	0.75%	0.52%	0.90%	1.06%	1.13%	1.12%	1.08%	1.05%
ISO-DMDBT	0.60%	0.41%	0.78%	1.00%	1.32%	1.35%	1.27%	1.10%
4,6-DMDBT	90.46%	90.68%	83.49%	77.67%	67.62%	46.54%	43.29%	25.24%

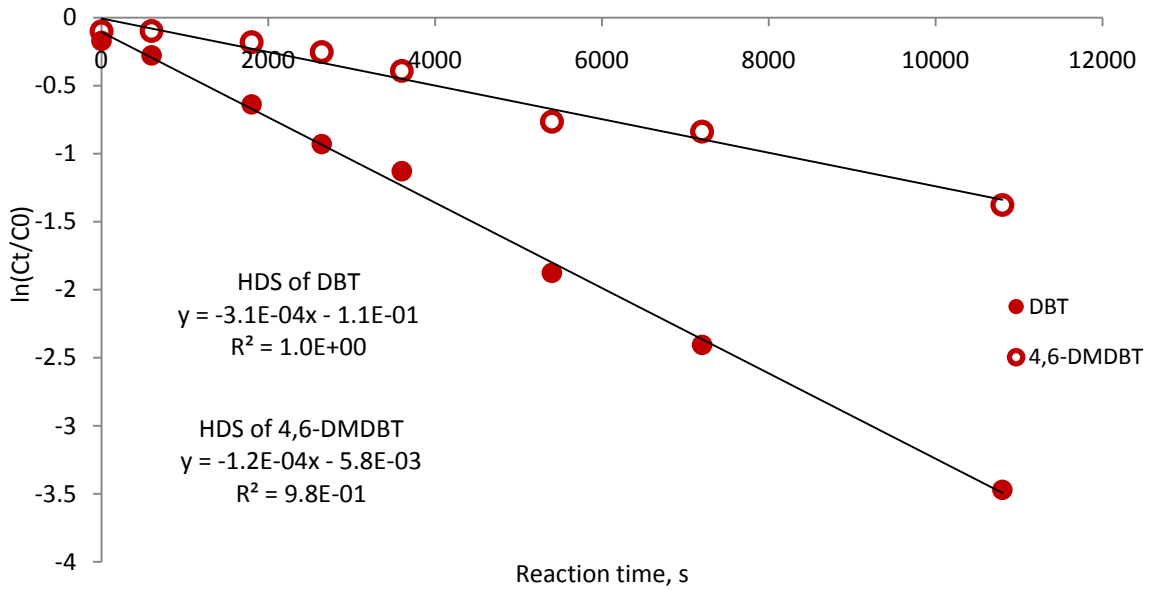


Fig. E - 16 Pseudo-first order plots for the conversions of DBT and 4,6-DMDBT in HDS, DS0908, 400°C

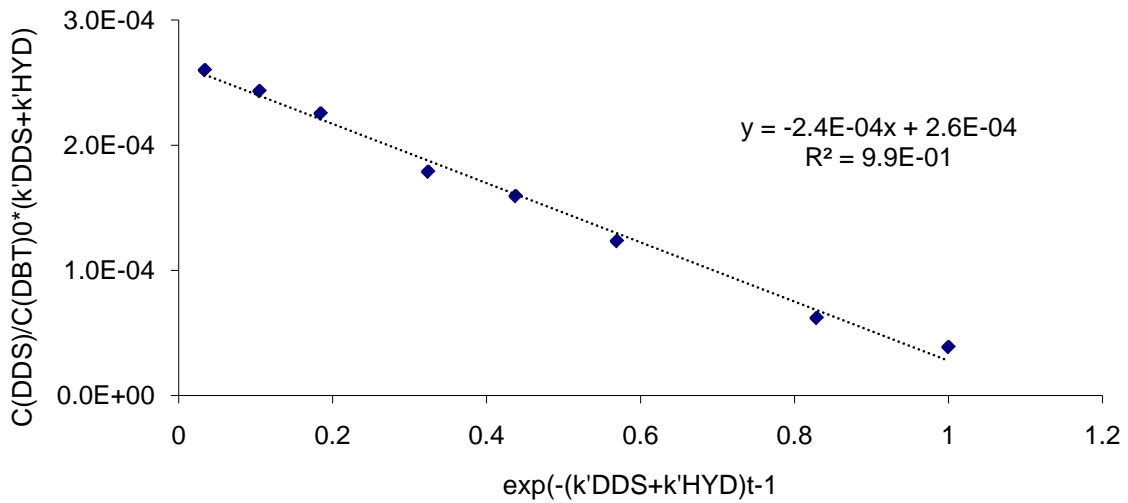


Fig. E - 17 Regression for k'_{DDS} in the HDS of DBT, DS0908, 400°C

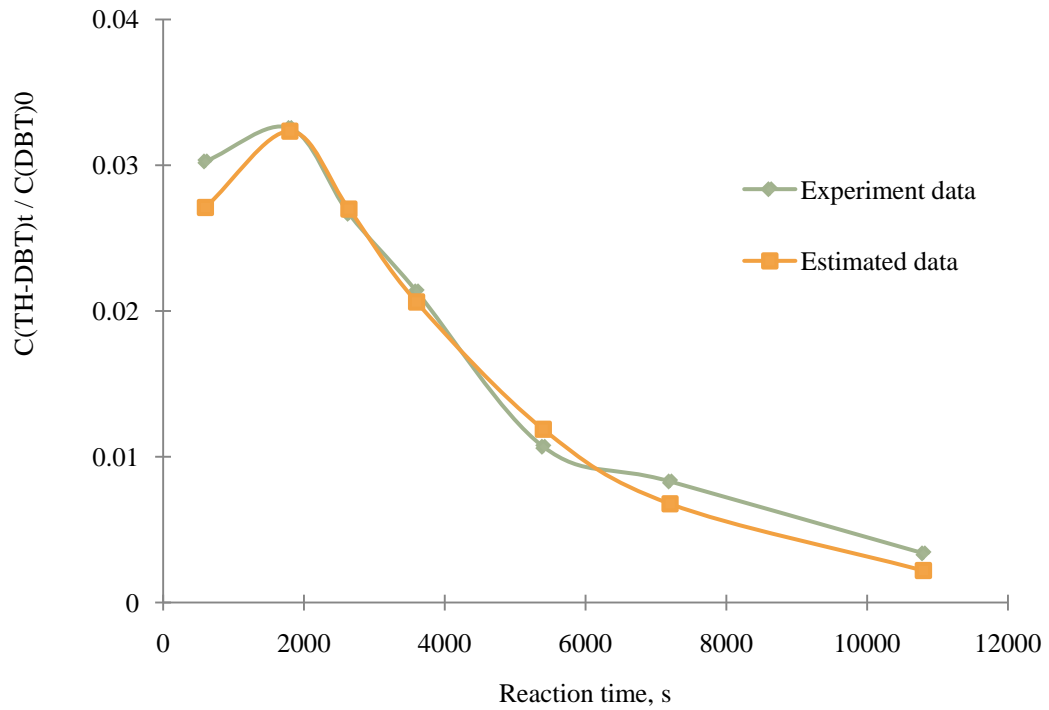


Fig. E - 18 Regression for k'_{HYDD} in the HDS of DBT, DS0908, 400°C

Table E - 11 ANOVA $k'_{(DBT\ HYDD)}$, 400°C

Source	SS	Df	MS	F _{OBS}
Regression	SSR	p-1=1	1.21E-03	333
Error	SSE	n-p=6	9.62E-05	
Total	SST	n-1=7		

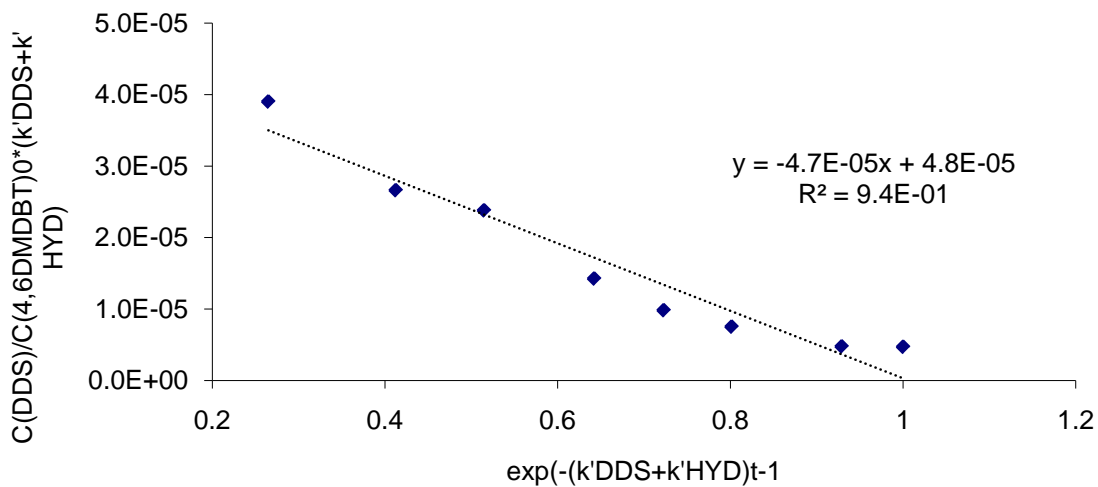


Fig. E - 19 Regression for k'_{DDS} in the HDS of 4,6-DMDBT, DS0908, 400°C

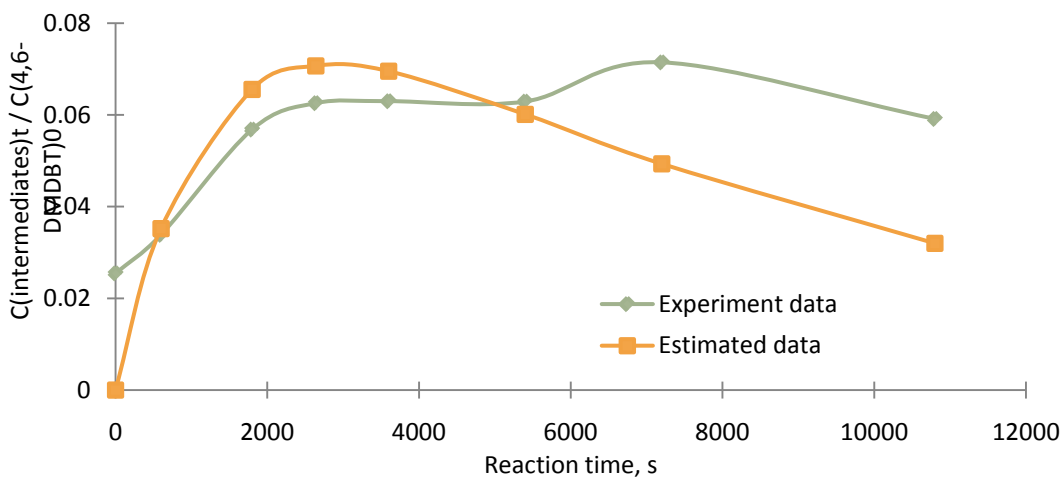


Fig. E - 20 Regression for k'_{HYDD} of 4,6-DMDBT, DS0908, 400 C

Table E - 12 ANOVA $k'_{(4,6DMDBT\ HYDD)}$, 400°C

Source	SS	Df	MS	F _{OBS}
Regression	SSR	p-1=1	8.09E-03	14
Error	SSE	n-p=6	5.96E-04	
Total	SST	n-1=7		

E.2 Experiment data for HDS over promoted (Ni or K) Mo sulfide catalysts

Table E - 13 HDS of DBT and 4,6-DMDBT over the dispersed MoNi catalysts

	Base080401 (Mo)	NiS-01' (Ni/Mo=0.5)	NiS-2 (15 psi H ₂ S)
DBT	82.74%	72.45%	64.21%
TH-DBT	4.23%	3.05%	4.50%
BP	11.74%	20.83%	25.70%
DCH	1.11%	3.16%	4.65%
CHB	0.18%	0.51%	0.93%
Conversion of DBT, w/w	17.26%	27.55%	35.79%
Desulfurization of DBT, mol%	13.03%	24.50%	31.29%
4,6-DMDBT	83.31%	83.72%	73.3%
ISO-DMDBT	0.90%	0.67%	1.2%
HH-DMDBT	1.53%	0.99%	1.5%
TH-DMDBT	1.41%	0.65%	1.1%
3,3'-DMBP	1.76%	1.76%	2.3%
ISO-DMBP	4.42%	4.62%	7.6%
DMCHB	6.67%	7.58%	12.9%
Conversion of 4,6-DMDBT, w/w	16.69%	16.28%	26.7%
Desulfurization of 4,6-DMDBT, mol%	12.85%	13.96%	15.3%

Table E - 14 HDS results of DBT and 4,6-DMDBT over KMo catalyst using *in-situ* H₂.

		K/Mo=0.4	Mo
Feed	DBT	95.9%	68.6%
Intermediate	TH-DBT	0.6%	8.9%
DDS	BP	3.2%	16.7%
HYDD	CHB	0.3%	4.9%
	DCH	0	0.9%
Feed	4,6-DMDBT	91.0%	69.7%
Intermediate	ISO-DMDBT	1.4%	2.5%
	HH-DMDBT	2.2%	2.3%
	TH-DMDBT	1.5%	2.4%
DDS	DMBP	1.9%	2.6%
HYDD	DMCHB	2.0%	20.5%

E.3 EDX spectra for NiMo catalyst after consumed in HDS

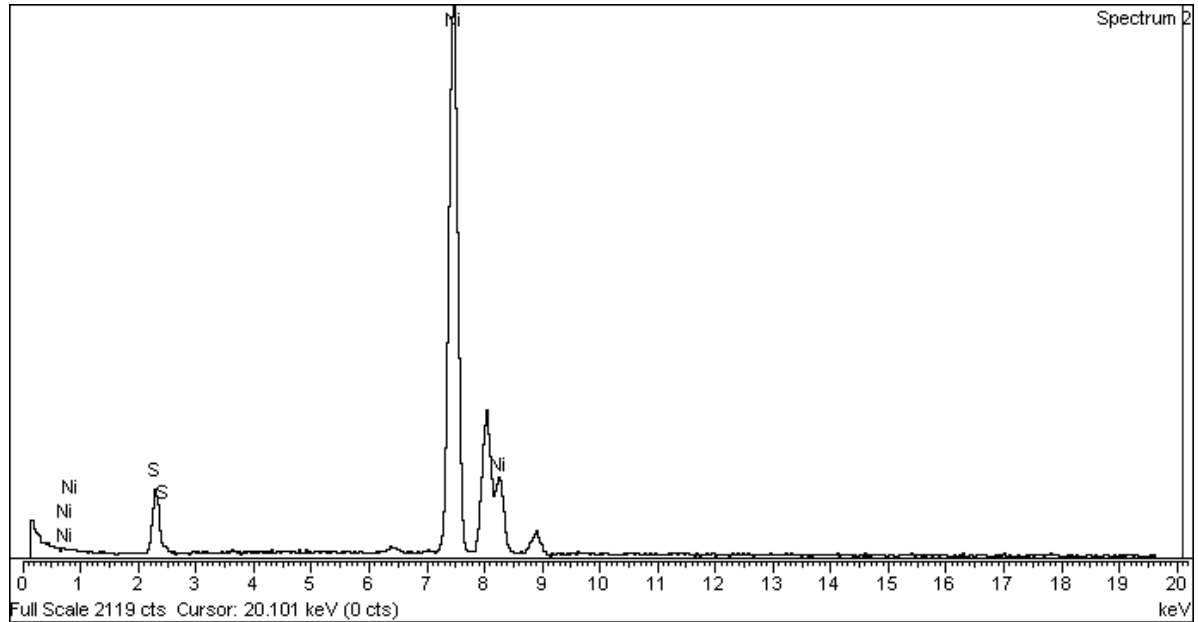


Fig. E - 21 EDX of NiMo(after HDS) sulfide, organic phase

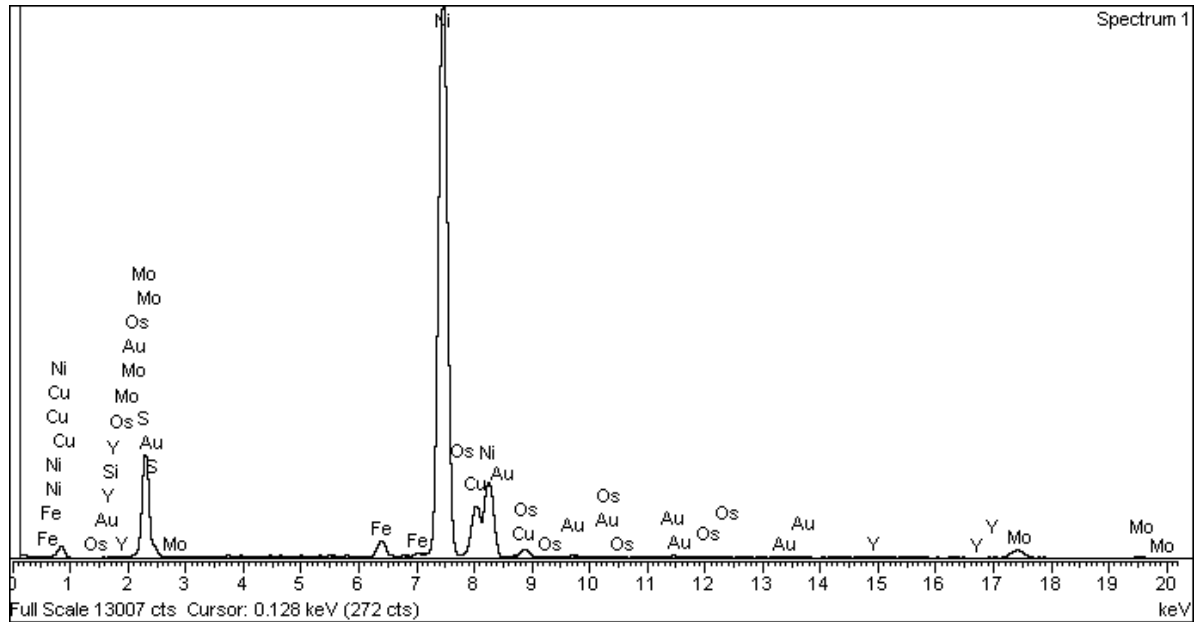


Fig. E - 22 EDX of NiMo(after HDS) sulfide, Wcat phase Sp1-Fig. 5-12

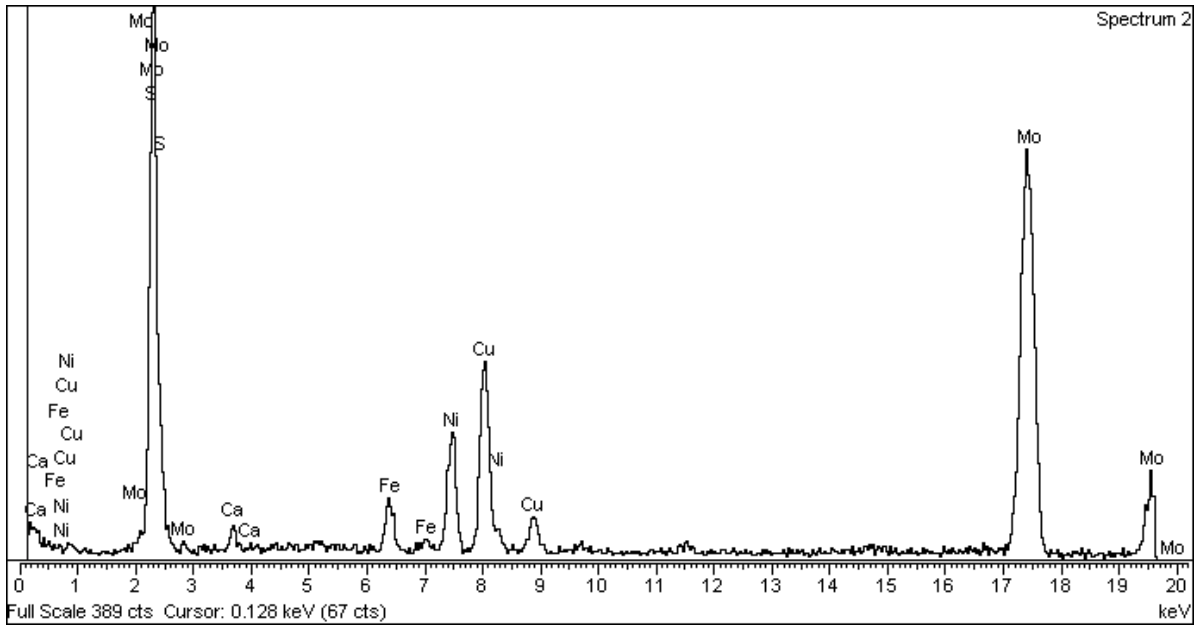


Fig. E - 23 EDX of NiMo(after HDS) sulfide, Wcat phase Sp2-Fig. 5-12

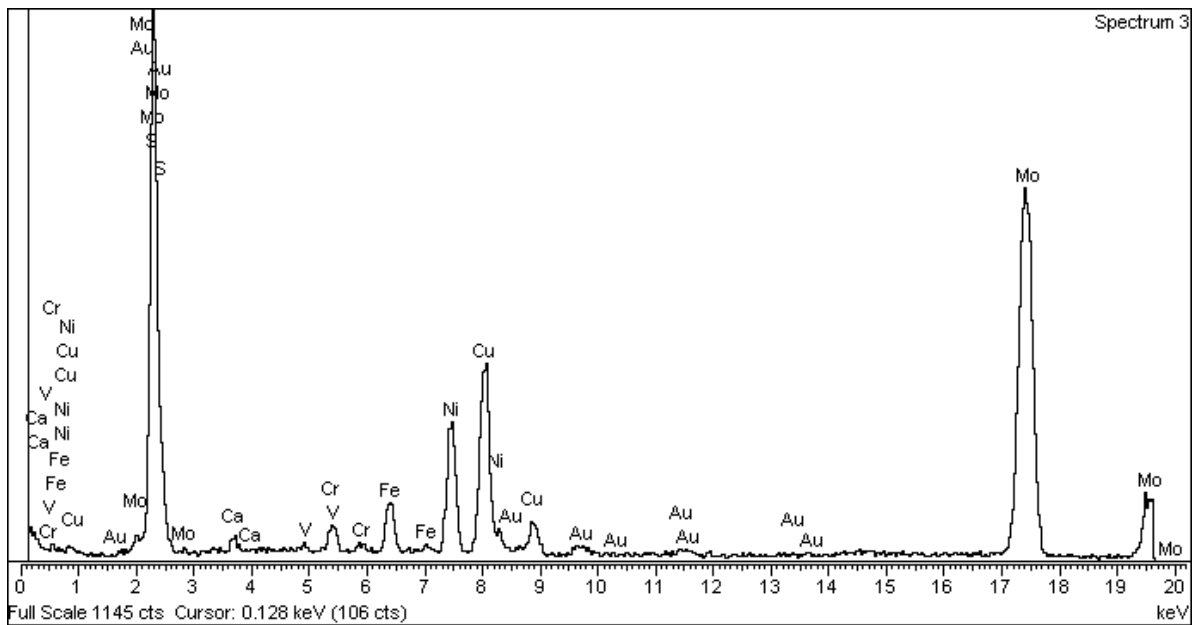


Fig. E - 24 EDX of NiMo(after HDS) sulfide, Wcat phase Sp3-Fig. 5-12

APPENDIX F --- Experimental raw data for the Chapter 6

Table F - 1 Experiment raw data of DS1001-PMA, H₂

Reaction time, min	10	30	65	93	119	150
DCH+CHCHE	0.6%	1.3%	2.7%	3.4%	4.1%	5.1%
CHB	3.1%	8.0%	15.2%	18.0%	20.0%	22.5%
BP	12.2%	21.4%	34.6%	40.4%	45.1%	53.1%
TH-DBT	4.6%	4.9%	3.9%	3.0%	2.4%	1.3%
DBT	79.5%	64.4%	43.6%	35.2%	28.4%	18.0%
S-removal	15.9%	30.7%	52.5%	61.8%	69.2%	80.7%
DMBP	1.1%	1.5%	2.8%	4.2%	5.7%	8.9%
DMCHB	2.0%	4.4%	8.5%	13.0%	16.2%	21.0%
TH-DMDBT+HH-DMDBT	0.9%	1.0%	1.0%	1.1%	1.2%	1.2%
4,6-DMDBT	96.0%	92.8%	87.1%	81.0%	75.9%	67.6%
Iso-DMDBT	0.1%	0.3%	0.6%	0.8%	1.0%	1.3%

Table F - 2 Experiment raw data of DS1002-PMA, CO

Reaction time, min	9	31	60	90	120	150
DCH	0.3%	0.7%	1.8%	3.0%	4.0%	4.9%
CHB	1.4%	3.5%	9.0%	13.8%	17.0%	18.9%
BP	8.8%	15.5%	30.1%	42.4%	51.4%	58.1%
TH-DBT	3.4%	3.8%	3.3%	2.4%	1.5%	0.9%
DBT	86.1%	76.5%	55.7%	38.5%	26.0%	17.1%
DMBP	0.88%	2.68%	5.54%	8.57%	11.59%	14.93%
DMCHB	1.37%	5.13%	13.68%	22.77%	29.76%	34.52%
TH-DMDBT+HH-DMDBT	0.31%	0.79%	1.26%	1.50%	1.53%	1.31%
4,6-DMDBT	97.34%	91.05%	78.79%	66.10%	55.89%	48.03%
Iso-DMDBT	0.11%	0.35%	0.73%	1.05%	1.22%	1.21%

Table F - 3 Experiment raw data of ATTM, syngas

mol%	DM57	DM60	DM54
	CO	CO+H ₂	H ₂
CO/(CO+H ₂)	1	0.5	0
DCH	4.38%	2.62%	0.19%
CHB	21.34%	18.78%	12.82%
BP	65.27%	55.95%	52.58%
TH-DBT	0.71%	1.66%	1.95%
DBT	8.30%	20.99%	32.46%
DMBP	22.21%	18.84%	17.07%
DMCHB	46.55%	30.61%	24.69%
TH-DMDBT	0.73%	2.17%	2.90%
HH-DMDBT	0.98%	0.81%	1.19%
Iso-DMDBT	1.50%	2.38%	2.00%
4,6-DMDBT	28.03%	45.20%	52.15%

Table F - 4 Experiment raw data of ExCO0901

Reaction time, min	2	10	30	69	92	133	180
DCH	0.5%	0.8%	1.2%	2.0%	2.4%	2.7%	2.9%
CHB	5.7%	13.0%	23.2%	32.6%	35.8%	35.6%	35.1%
BP	8.2%	16.0%	28.6%	44.1%	50.6%	57.2%	59.6%
TH-DBT	5.5%	7.5%	5.1%	2.4%	1.3%	0.6%	0.4%
DBT	80.2%	62.6%	41.8%	19.0%	10.0%	3.9%	1.9%
S-removal	14.3%	29.8%	53.1%	78.7%	88.8%	95.5%	97.7%
DMBP	3.8%	6.1%	6.4%	12.8%	17.2%	20.3%	25.5%
DMCHB	10.3%	18.7%	29.1%	38.6%	45.8%	54.7%	56.7%
TH-DMDBT	1.0%	3.4%	2.0%	0.9%	0.6%	0.3%	0.2%
HH-DMDBT	2.4%	1.5%	1.2%	0.9%	0.5%	0.6%	0.5%
4,6-DMDBT	81.8%	68.3%	59.0%	45.0%	34.4%	23.0%	16.2%
Iso-DMDBT	0.8%	1.9%	2.3%	1.8%	1.6%	1.1%	0.8%
S-removal	14.1%	24.9%	35.5%	51.5%	62.9%	75.0%	82.2%

Table F - 5 Experiment raw data of ExH0901

Reaction time, min	0	10	30	60	120	182
DCH	0.5%	0.6%	1.2%	1.4%	2.4%	2.8%
CHB	6.0%	11.3%	20.5%	24.7%	35.9%	36.8%
BP	10.8%	14.7%	25.0%	30.1%	48.7%	54.1%
TH-DBT	2.2%	7.7%	6.1%	5.0%	1.5%	0.7%
DBT	80.5%	65.7%	47.2%	38.7%	11.6%	5.6%
S-removal	17.3%	26.6%	46.7%	56.3%	87.0%	93.7%
DMBP	5.2%	6.3%	7.5%	6.7%	18.6%	22.7%
DMCHB	9.8%	15.1%	20.6%	26.0%	40.6%	46.5%
TH-DMDBT	0.7%	2.7%	1.5%	1.4%	0.6%	0.4%
HH-DMDBT	0.4%	1.5%	1.1%	1.1%	0.9%	0.5%
4,6-DMDBT	83.4%	72.7%	67.1%	62.5%	37.4%	28.6%
Iso-DMDBT	0.3%	1.7%	2.1%	2.2%	1.9%	1.4%
Iso-DMDBT	15.1%	21.4%	28.1%	32.7%	59.2%	69.2%

Table F - 6 Experiment raw data of ExCO1001

Reaction time, min	0	10	30	60	90	120
DCH	0.3%	0.7%	1.2%	2.4%	3.7%	3.6%
CHB	2.5%	5.6%	9.2%	16.2%	23.2%	23.9%
BP	5.3%	9.7%	12.9%	17.4%	21.7%	20.6%
TH-DBT	2.3%	4.7%	5.4%	5.8%	5.7%	5.9%
DBT	89.7%	79.9%	72.3%	59.9%	48.2%	48.4%

Table F - 7 Experiment raw data of ExH1001

Reaction time, min	1	10	30	60	90	120
DCH	1.0%	0.6%	1.0%	2.0%	2.6%	4.5%
CHB	6.6%	4.9%	8.1%	14.2%	17.8%	27.4%
BP	8.5%	8.2%	11.1%	15.1%	17.2%	24.1%
TH-DBT	3.1%	4.7%	5.5%	6.4%	6.4%	5.4%
DBT	81.5%	82.1%	74.9%	63.7%	57.8%	41.7%

Table F - 8 Experiment raw data of ExCO0902

Reaction time, min	0	30	60	90	140	180
DCH	0.3%	0.2%	0.1%	0.3%	0.2%	0.2%
CHB	1.5%	3.0%	5.6%	8.2%	9.7%	11.2%
BP	8.6%	28.3%	45.6%	56.5%	65.7%	74.0%
TH-DBT	1.7%	2.0%	1.6%	1.2%	0.6%	0.0%
DBT	87.8%	66.5%	47.0%	33.9%	23.7%	14.6%
S-removal	10.4%	31.5%	51.4%	64.9%	75.7%	85.4%
DMBP	4.4%	9.6%	14.8%	19.2%	23.4%	28.2%
DMCHB	3.1%	5.6%	10.1%	14.4%	16.6%	19.0%
TH-DMDBT	0.2%	0.3%	0.3%	0.3%	0.3%	0.2%
HH-DMDBT	0.5%	0.9%	1.3%	1.5%	1.6%	1.7%
4,6-DMDBT	91.5%	83.0%	72.6%	63.5%	56.9%	49.6%
Iso-DMDBT	0.3%	0.6%	0.9%	1.1%	1.2%	1.2%
S-removal	7.5%	15.3%	24.9%	33.6%	40.0%	47.2%

Table F - 9 Experiment raw data of ExCO0903

Reaction time, min	0	30	60	108	180
DCH	0.4%	0.5%	0.6%	0.8%	1.0%
CHB	3.0%	10.2%	17.0%	23.0%	29.3%
BP	11.6%	25.0%	34.4%	43.6%	55.2%
TH-DBT	3.6%	4.3%	4.0%	2.8%	1.3%
DBT	81.3%	60.1%	44.1%	29.9%	13.3%
S-removal	15.1%	35.7%	52.0%	67.3%	85.4%
DMBP	-10.2%	4.4%	6.4%	8.3%	13.1%
DMCHB	-15.8%	10.2%	18.0%	23.5%	32.1%
TH-DMDBT	-5.1%	1.3%	1.2%	0.9%	0.7%
HH-DMDBT	-3.4%	0.6%	0.6%	0.6%	0.8%
4,6-DMDBT	135.3%	82.9%	72.6%	65.4%	51.7%
Iso-DMDBT	-0.8%	0.6%	1.2%	1.4%	1.6%
S-removal	-26.0%	14.6%	24.3%	31.8%	45.2%

APPENDIX G --- Raw Data for Chapter 7

Table G - 1 HDS of DBT and 4,6-DMDBT with the presence of N-containing compounds

Exp. ID	NS-20	NS-21	NS-19	NS-18	DM-90	DM-91
Conditions	S+Q, CO	S+Q, H2	S+Cz, CO	S+Cz, H2	CO	H2
DBT	81.93%	80.88%	67.84%	63.37%	54.28%	48.32%
TH-DBT	1.54%	3.52%	3.81%	4.35%	4.86%	4.29%
BP	15.73%	13.65%	18.18%	20.07%	29.30%	34.66%
CHB	0.80%	1.95%	6.71%	7.09%	11.14%	12.34%
DCH	0.00%	0.00%	3.47%	5.12%	0.42%	0.39%
<i>DDS/HYDD</i>	<i>19.71</i>	<i>7.02</i>	<i>1.79</i>	<i>1.64</i>	<i>2.54</i>	<i>2.72</i>
<i>HDS of DBT</i>	<i>16.53%</i>	<i>15.60%</i>	<i>28.35%</i>	<i>32.28%</i>	<i>40.86%</i>	<i>47.39%</i>
<i>Conversion of DBT</i>	<i>18.07%</i>	<i>19.12%</i>	<i>32.16%</i>	<i>36.63%</i>	<i>45.72%</i>	<i>51.68%</i>
4,6-DMDBT	91.46%	86.93%	80.41%	75.18%	55.67%	58.32%
ISO-DMDBT	0.54%	0.63%	1.06%	1.51%	2.16%	2.34%
HH-DMDBT	2.09%	2.47%	4.76%	5.72%	2.07%	1.95%
TH-DMDBT	2.19%	3.98%	2.43%	3.92%	2.24%	2.96%
3,3'-DMBP	2.16%	3.57%	4.66%	6.53%	6.50%	7.10%
ISO-DMBP	0.57%	0.86%	2.52%	2.32%	9.68%	8.88%
DMCHB	0.99%	1.56%	4.16%	4.83%	21.68%	18.45%
<i>DDS/HYDD</i>	<i>2.77</i>	<i>2.85</i>	<i>1.73</i>	<i>1.83</i>	<i>0.75</i>	<i>0.87</i>
<i>HDS of DMDBT</i>	<i>3.72%</i>	<i>5.99%</i>	<i>11.34%</i>	<i>13.67%</i>	<i>37.85%</i>	<i>34.43%</i>
<i>Conversion of DMDBT</i>	<i>8.54%</i>	<i>13.07%</i>	<i>19.59%</i>	<i>24.82%</i>	<i>44.33%</i>	<i>41.68%</i>

APPENDIX H --- Raw Data for Chapter 8

Table H - 2 HDN carbazole at 380 °C, Cz0901

Reaction time, min	5	30	87	150	180
Cz	85.94%	82.97%	70.96%	58.38%	52.23%
TH-Cz	8.02%	8.60%	9.95%	8.36%	6.69%
HCHA	0.81%	0.86%	1.91%	3.97%	4.95%
Iso of HDCHA	1.93%	2.96%	7.01%	12.76%	16.30%
DCH	0.72%	0.94%	1.88%	3.54%	4.33%
CHB	1.09%	1.78%	3.15%	4.98%	6.01%
PHA	0.38%	0.47%	1.38%	2.30%	2.69%
CHCHE	1.11%	1.42%	3.77%	5.71%	6.80%

Table H - 2 HDN carbazole at 330 °C, Cz0902

Reaction time, min	5	30	60	103	150	180
Cz	94.89%	93.32%	88.28%	80.12%	70.47%	66.37%
TH-Cz	2.96%	6.12%	10.53%	13.82%	15.50%	15.33%
HCHA	0.26%	0.00%	0.00%	0.64%	1.77%	2.64%
Iso of HDCHA	0.94%	0.35%	1.18%	2.51%	6.26%	7.69%
DCH	0.29%	0.10%	0.00%	0.66%	1.95%	2.90%
CHB	0.46%	0.00%	0.00%	1.28%	2.25%	2.97%
PHA	0.00%	0.00%	0.00%	0.30%	0.53%	0.64%
CHCHE	0.19%	0.11%	0.00%	0.68%	1.26%	1.47%

Table H - 3 HDN carbazole at 360 °C, Cz0903

Reaction time, min	0	30	60	120	150	180
Cz	91.78%	88.46%	81.87%	72.27%	64.66%	58.56%
TH-Cz	4.69%	9.17%	12.56%	13.58%	12.95%	11.58%
HCHA	0.37%	0.12%	0.36%	1.39%	2.57%	3.72%
Iso of HDCHA	1.24%	0.71%	2.05%	5.63%	9.24%	12.89%
DCH	0.42%	0.15%	0.42%	1.51%	2.61%	3.78%
CHB	0.42%	0.45%	1.10%	2.18%	3.01%	3.73%
PHA	0.53%	0.25%	0.49%	0.97%	1.34%	1.66%
CHCHE	0.56%	0.69%	1.15%	2.47%	3.62%	4.09%

Table H - 4 HDN carbazole at 380 °C, Cz0904, molecular H₂

Reaction time, min	0	30	60	110	180
Cz	92.75%	85.14%	75.74%	64.23%	59.36%
TH-Cz	6.53%	10.95%	13.81%	13.92%	11.91%
HCHA	0.15%	0.50%	1.70%	4.11%	5.24%
Iso of HDCHA	0.14%	1.67%	4.20%	9.25%	12.88%
DCH	0.14%	0.44%	1.28%	3.15%	4.61%
CHB	0.29%	0.92%	1.95%	3.13%	3.51%
PHA	0.00%	0.00%	0.46%	0.81%	0.97%
CHCHE	0.00%	0.37%	0.86%	1.39%	1.53%